

Scanning electron micrograph (SEM) of a porous, interconnected scaffold structure. The scaffold consists of thick, cylindrical struts forming a grid-like pattern. Numerous bright green spots are scattered across the surface of the struts, representing the presence of a thin film or coating. The background is dark, highlighting the 3D structure of the scaffold.

**MULTILAYERED THIN FILMS
FROM POLY(AMIDO AMINE)S
FOR CONTROLLED DELIVERY**

Sry Dewi Hujaya

MULTILAYERED THIN FILMS
FROM POLY(AMIDO AMINE)S
FOR CONTROLLED DELIVERY

DISSERTATION

to obtain
the degree of doctor at the University of Twente,
on the authority of the rector magnificus,
Prof. Dr. H. Brinksma,
on account of the decision of the graduation committee,
to be publicly defended
on Thursday, November 20th, 2014 at 14:45

by

Sry Dewi Hujaya

born on October 23rd, 1986
in Medan, Indonesia

This dissertation has been approved by:

Supervisor : Prof. Dr. J.F.J. Engbersen
Co-Supervisor : Dr. J.M.J. Paulusse

Committee

Chairman:	Prof. Dr. Ir. J.W.M. Hilgenkamp	University of Twente, TNW
Secretary:	Prof. Dr. Ir. J.W.M. Hilgenkamp	University of Twente, TNW
Supervisor:	Prof. Dr. J.F.J. Engbersen	University of Twente, TNW
Co-Supervisor:	Dr. J.M.J. Paulusse	University of Twente, TNW
Members:	Prof. Dr. Ir. J. Huskens	University of Twente, TNW
	Prof. Dr. H.B.J. Karperien	University of Twente, TNW
	Prof. Dr. W.E. Hennink	Utrecht University
	Prof. Dr. B.J. Ravoo	University of Münster
	Prof. Dr. G. Storm	Utrecht University
Referee:	Dr. Ing. A.A. Apeldoorn	University of Twente, TNW

The research described in this thesis was carried out from 2010 until 2014 in the research group BioMedical Chemistry / Controlled Drug Delivery of the MIRA Institute for Biomedical Technology and Technical Medicine, University of Twente, Enschede, The Netherlands.

UNIVERSITY OF TWENTE.

The research is financially supported by Netherlands Institute of Regenerative Medicine (NIRM), which is part of the Netherlands Organization for Scientific Research (NWO).



The printing of this thesis was sponsored by the Dutch Society for Biomaterials and Tissue Engineering (NBTE).



Nederlandse vereniging voor Biomaterialen en Tissue Engineering
Netherlands society for Biomaterials and Tissue Engineering

Multilayered thin films from poly(amido amine)s for controlled delivery

Sry Dewi Hujaya
PhD Thesis with references; with summary in English and Dutch
University of Twente, Enschede, the Netherlands, 2014.

Copyright © by Sry Dewi Hujaya, 2014. All rights reserved.

Cover design by Sry Dewi Hujaya
Printed by Ipskamp Drukkers B.V.

ISBN: 978-90-365-3770-4
DOI: 10.3990/1.9789036537704
URL: <http://dx.doi.org/10.3990/1.9789036537704>

CONTENTS

Chapter 1	General Introduction	1
Chapter 2	Responsive Layer-by-Layer Films	5
Chapter 3	Multilayered Thin Films from Classic Poly(amido amine)s and DNA	33
Chapter 4	Physical and Chemical Crosslinking for Improved Stability of Poly(amido amine)-based Multilayered Thin Films	55
Chapter 5	Multilayered Thin Films from Boronic Acid-Functionalized Poly(amido amine)s with Poly(vinyl alcohol) and Chondroitin Sulfate	75
Chapter 6	Multilayered Thin Films from Boronic Acid-Functionalized Poly(amido amine)s and Chondroitin Sulfate as Drug-Releasing Surfaces	105
Chapter 7	Multilayered Thin Films from Boronic Acid-Functionalized Poly(amido amine)s and Poly(Vinyl Alcohol) for Surface-Controlled Bortezomib Delivery	125
Chapter 8	Optimization of Poly(amido amine)-Based Multilayered Thin Films for Surface-Mediated Cell Transfection	141
Summary		161
Samenvatting		163
Acknowledgement		165
Curriculum Vitae		167

1.1 LAYER-BY-LAYER ASSEMBLY

Along with the vast growth in material science, the medical field obtains a tremendous boost through the introduction of novel materials aimed to increase therapeutic efficacy of any medical treatments. It is apparent now that how a drug is delivered into its site of action is as important as its therapeutic effect. Thus, a delivery system is born with the aim of assisting a drug in exerting its maximum therapeutic effect while keeping the patient as comfortable as possible through reduced side effects and longer treatment intervals. The plethora of research dedicated to delivery systems also drives further interest in the more risky area of gene therapy. With the ability to design delivery systems that can target the specific pathological organs or tissues, and release drugs on demand, many of the biological barriers can be circumvented.

In the hospital settings, development in material science manifests in the emergence of safer and biodegradable medical devices such as surgical sutures, adhesives, and various implants. Together with the enormous advances in tissue engineering, limitless amount of biomaterials are fabricated in all specified sizes and shapes to perform different specialized medical tasks.

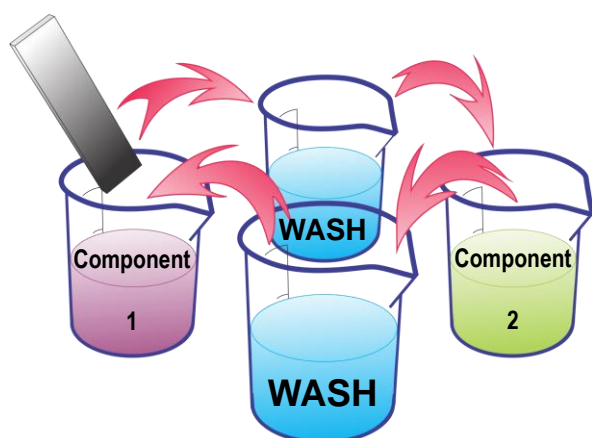


Figure 1.1 The schematic illustration of dip-coating layer-by-layer assembly.

As much as the property of the bulk of a biomaterial is important, its surface also plays a crucial role in interacting with a biological environment [1]. In that respect, surface functionalization offers a way not only to modify an existing surface for better performance, but also add functionality such as stimuli-responsive drug release, controlled cellular differentiation, and transfection.

Layer-by-layer (LbL) assembly through dip coating is a surface modification technique consisting of alternate incubation in two deposition solutions of complementary macromolecules (Figure 1.1) [2, 3]. The resulting multilayer conforms to any size and shape of the

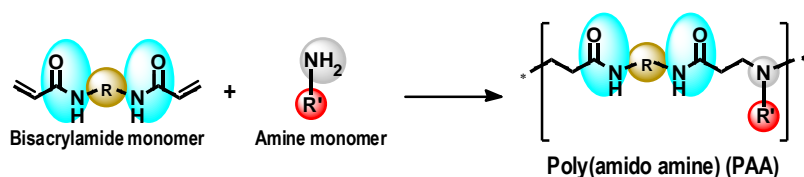
substrate and is controllable in both material amount and thickness through the repetition of deposition cycles. Moreover, the mild deposition condition with main components dissolved in aqueous conditions at ambient temperature preserves the native conformation of many important functional biomolecules.

1.2 POLY(AMIDO AMINE)S

Poly(amido amine)s (PAA) are a class of water soluble biomaterials that have had profound accomplishments as drug and gene delivery systems. They are easy to synthesize via Michael type polymerization as depicted in Scheme 1.1. By choosing the appropriate amine and bisacrylamide monomers, as well as varying their molar ratio, linear or branched structures can be obtained that contain specific side groups and hence functionality.

Their peptidomimetic structure renders them biodegradable via hydrolysis of the amide bond in the main chain, while the tertiary amines render them positively charged under physiological conditions to interact with various biological macromolecules such as nucleic acids, proteins, carbohydrates, and other synthetic polymers [4]. As

such, they have shown promise as nanoparticle-based gene delivery systems [5-7], protein delivery systems [8], and hydrogel for drug delivery applications [9].



Scheme 1.1 Poly(amido amine) synthetic scheme.

1.3 AIM OF THE STUDY

The aim of the study reported in this thesis is to incorporate poly(amido amine)s (PAA) into functional multilayered systems via dip coating LbL technique. The multilayers will be characterized based on the properties of the PAA, their biocompatibility as surfaces for cell culture, and the ability to provide surface mediated gene delivery and drug releasing surfaces aimed at surface functionalization of various biomaterials.

1.4 OUTLINE OF THE THESIS


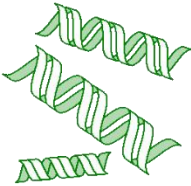

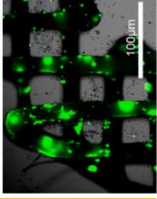
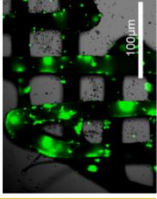
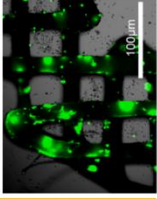



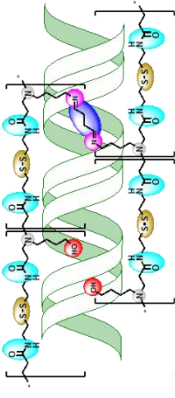




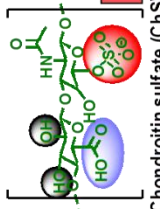

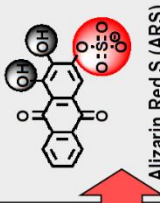

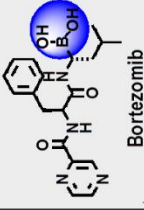
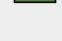
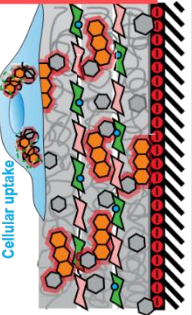
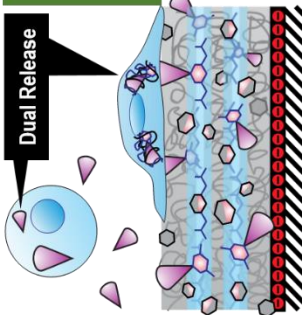
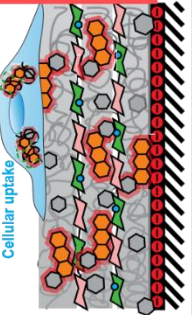
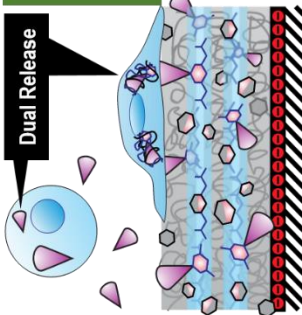
The thesis is outlined as follows. **Chapter 2** describes a literature overview of the general physicochemical aspects of LbL assembly and recent development in their research for biomedical applications.

Chapter 3 presents a study on structure–function relationship of a series of linear homopolymers of PAAs for their ability to form multilayers with DNA via electrostatic interactions. A preliminary *in vitro* cell culture study is also shown to briefly demonstrate the ability of the multilayers to provide surface-mediated gene delivery. In **Chapter 4**, a series of linear copolymers of PAAs described in Chapter 3 are studied for their structure-function relationship in forming stable multilayers with DNA. The best performing copolymer is further used to study the effect of glutaraldehyde interlayer crosslinking on improving the stability of the multilayers against physiological salt concentration. The effect of the physical and chemical crosslinks is also studied with respect to the multilayers' transfection capabilities.

In **Chapter 5**, randomly branched copolymers of boronic acid-functionalized PAAs (BA-PAAs) are studied for their properties in forming multilayers with two macromolecules containing diol functional groups, poly(vinyl alcohol) (PVA) and chondroitin sulfate (ChS). The two possible driving forces (boronic ester formation and electrostatic interaction) for multilayer formation with both PVA and ChS are studied based on the multilayers' responsiveness to glucose and pH. The *in vitro* biocompatibility of the multilayers as surfaces for cell culture are also studied. In **Chapter 6**, the ChS-based multilayers from Chapter 5 are studied for their ability to incorporate and release alizarin red S (ARS) as a model compound for small catechol-containing drugs. *In vitro* cellular uptake of ARS is studied based on the fluorescence characteristics of the boronic ester of BA-PAAs and ARS through flow cytometry and confocal microscopy. In **Chapter 7**, the PVA-based multilayers from Chapter 5 are studied for their ability to incorporate and release bortezomib, a proteasome inhibitor used for treatment of multiple myeloma. The therapeutic efficacy of bortezomib-loaded multilayers is studied in relation to bortezomib loading concentrations, number of layers, and spatial aspects of the target cells.

In **Chapter 8**, the multilayers developed in Chapter 3 for surface-mediated gene delivery is optimized on cell seeding density, types of PAA carrier, and the number of layers. The optimal conditions are applied to coat selected biomaterials in both 2D and 3D to demonstrate the possibility of achieving cell transfecting scaffolds for tissue engineering.

The schematic overview of the different concepts and respective chapters presented in this thesis is illustrated below.

Poly(Amido Amine)s	Counter Macromolecule	(Model) Drugs	Surface Functionality
<p> $\text{pCABOL, R} = \text{---OH}$ $\text{pCHIS, R} = \text{---NH---}$ $\text{pCDAB, R} = \text{---NH}_2$ </p> <p> $\text{Poly(amido amine) (PAA)}$ $\text{---[NH---C(=O)---S---S---C(=O)---NH---R]}_n$ </p>	<p>  </p> <p>  </p> <p>  </p>	<p>  </p> <p> Chapter 3 </p> <p>  </p> <p> Surface-mediated transfection </p>	<p>  </p> <p> Chapter 8 </p>
<p> $\text{p(CBA-ABOL-x\%/DAB)}_{(100-X)\%}$ $\text{---[NH---C(=O)---S---S---C(=O)---NH---(HO)X\%---(H2N)100-X\%]}_n$ </p> <p>  </p>	<p>  </p> <p> Therapeutic DNA </p>	<p>  </p>	<p>  </p> <p> Chapter 4 </p> <p> Covalently-crosslinked 90%ABOL-(DNA)90%ABOL_n </p>
<p> $\text{p(CBA-50\%/4AMPBA50\%)(X-BA-PAA)}$ $\text{---[NH---C(=O)---S---S---C(=O)---NH---(HO)50\%---(X)50\%]}_n$ </p> <p> $\text{X} = \text{NH} \rightarrow \text{DAB}$ $\text{X} = \text{OH} \rightarrow \text{ABOL}$ </p> <p>     </p>	<p>  </p> <p> Chondroitin sulfate (ChS) </p> <p>  </p> <p>  </p> <p> Alizarin Red S (ARS) </p> <p>  </p> <p>  </p> <p> Bortezomib </p> <p>  </p>	<p>  </p> <p> Cellular uptake </p> <p> Chapter 6 </p> <p>  </p> <p> Dual Release </p> <p> Chapter 7 </p>	<p>  </p> <p> Chapter 6 </p> <p>  </p> <p> Chapter 7 </p>

1.5 REFERENCES

- [1] J.S. Hayes, E.M. Czekanska, R.G. Richards, The Cell–Surface Interaction, in: C. Kasper, F. Witte, R. Pörtner (Eds.) *Tissue Engineering III: Cell - Surface Interactions for Tissue Culture*, Springer Berlin Heidelberg, 2012, pp. 1-31.
- [2] B.M. Wohl, J.F.J. Engbersen, Responsive layer-by-layer materials for drug delivery, *J Control Release*, 158 (2012) 2-14.
- [3] P.T. Hammond, Building biomedical materials layer-by-layer, *Mater Today*, 15 (2012) 196-206.
- [4] P. Ferruti, M.A. Marchisio, R. Duncan, Poly(amido-amine)s: Biomedical Applications, *Macromol Rapid Comm*, 23 (2002) 332-355.
- [5] C. Lin, Z. Zhong, M.C. Lok, X. Jiang, W.E. Hennink, J. Feijen, J.F.J. Engbersen, Novel Bioreducible Poly(amido amine)s for Highly Efficient Gene Delivery, *Bioconjugate Chem.*, 18 (2006) 138-145.
- [6] L.J. van der Aa, P. Vader, G. Storm, R.M. Schiffelers, J.F.J. Engbersen, Optimization of poly(amido amine)s as vectors for siRNA delivery, *J Control Release*, 150 (2011) 177-186.
- [7] M. Piest, M. Ankoné, J.F.J. Engbersen, Carbohydrate-interactive pDNA and siRNA gene vectors based on boronic acid functionalized poly(amido amine)s, *J Control Release*, 169 (2013) 266-275.
- [8] G. Coué, C. Freese, R.E. Unger, C. James Kirkpatrick, J.F.J. Engbersen, Bioresponsive poly(amidoamine)s designed for intracellular protein delivery, *Acta Biomater*, 9 (2013) 6062-6074.
- [9] M. Piest, X. Zhang, J. Trinidad, J.F.J. Engbersen, pH-responsive, dynamically restructuring hydrogels formed by reversible crosslinking of PVA with phenylboronic acid functionalised PPO-PEO-PPO spacers (Jeffamines[registered sign]), *Soft Matter*, 7 (2011) 11111-11118.

CHAPTER 2

Responsive Layer-by-Layer Films*

ABSTRACT

Layer-by-layer (LbL) assembly has been under extensive research as a versatile method to produce smart coatings and capsules with a distinct multilayered structure. This specific fabrication technique provides ways to induce responsiveness not only through the chemically engineered macromolecular components, but also through the way the multilayers are built up. This chapter is dedicated to LbL fabrication-specific responsiveness, as well as to the recent developments in multilayers composed of specifically-tailored polymers. This chapter further focuses on chemically- and biologically-responsive LbL systems, with main applications in the biomedical field. In the introduction, general aspects of LbL assembly as a fabrication technique are described, along with physicochemical aspects of the assemblies. The second part describes the physicochemical aspects in more detail with examples on how variation in deposition conditions, such as pH and ionic strength, can be used to induce responsiveness upon the resulting multilayers. This section also highlights several reports on the fabrication of compartmentalized multilayered coatings for tunable disassembly or release of incorporated materials. The third part describes recent examples of multilayers fabricated with chemically-tailored biomaterials for various chemical and biological responsiveness. More specifically, the multilayer disassembly can be triggered through inherent responsiveness of one of the multilayer components, through chemically- or biologically-triggered degradation of one of the multilayer components, or through disruption of the interlayer interaction between two or more components of the multilayers.

2

* Sry D. Hujaya, Benjamin M. Wohl, Johan F.J. Engbersen, Jos M.J. Paulusse, Responsive Layer-by-Layer Films, in: Hans.-J. Schneider (Eds.), Smart Materials for Chemical and Biological Stimulation, RSC Publishing.

2.1 LIST OF ABBREVIATIONS

Alg = alginate	pDNA = plasmid DNA
BCM = block copolymer micelles	PDPA = poly(2-diisopropylaminoethyl methacrylate)
BSM = bovine submaxillary mucin	PEG = poly(ethylene glycol)
CHI = chitosan	PEI = poly(ethylene imine)
CLSM = confocal laser scanning microscopy	PGA = poly(L-glutamic acid)
DS = dextran sulfate	PLAA = poly(L-aspartic acid)
FITC = fluorescein isothiocyanate	PLGA = poly(lactic-co-glycolic acid)
HA = hyaluronic acid	PLL = poly(L-lysine)
HCEC = human corneal epithelial cells	PMAAc = poly(methacrylic acid)
HEP = heparin	PNIPAM = poly(N-isopropylacrylamide)
JAC = lectin jacalin	polymer 1 = (poly(β -amino ester))
LbL = Layer-by-layer	PSS = poly(styrenesulfonate)
MF = melamine formaldehyde	PVA = poly(vinyl alcohol)
MNP = magnetic nanoparticle	PVCL = poly(N-vinylcaprolactam)
PAAc = poly(acrylic acid)	PVPON = poly(N-vinylpyrrolidone)
PAH = poly(allylamine hydrochloride)	RB = rhodamine B
PBA = phenyl boronic acid	RHB = reducible hyperbranched poly(amido amine)
PDADMAC = poly(diallyldimethylammonium chloride)	SMC = smooth muscle cells
PDMAEMA = poly(2-(dimethylamino)ethyl methacrylate)	TA = tannic acid
PDMAEMA-b-PDEAEMA = poly(2-(dimethylamino)ethyl methacrylate)-block-poly(2-(diethylamino)ethyl methacrylate)	TR = Texas red

2.2 INTRODUCTION

Thin multilayers, often referred to as polyelectrolyte multilayers, multilayer films, multilayered thin films, multilayered capsules (free-standing nano- or micro-sized), or simply multilayers, are a class of smart materials distinguished by the layer-by-layer (LbL) fabrication technique, i.e. they are built up one layer at a time. As illustrated in Figure 2.1, fabrication involves incubating a substrate alternately in two or more aqueous deposition solutions of complementary macromolecules. This results in formation of self-assembled layers with intricate architectures on the molecular level. The properties of each layer can be tuned by the deposition solution, and/or deposition technique. Factors such as pH, ionic strength, and temperature affect how macromolecules in solution interact with macromolecules on the surface and hence determine the layer properties and architecture. In addition to conventional dip-coating techniques, multilayers have been fabricated in various other ways such as alternate [1, 2] or simultaneous [3] spraying, spin coating [4, 5], agitation [6], de-wetting [7], inkjet printing [8], microfluidic [9], and flexible roll coating [10] endowing different properties to the multilayer products. The resulting multilayers can also be treated post-assembly in various ways to further alter their properties and functionalities.

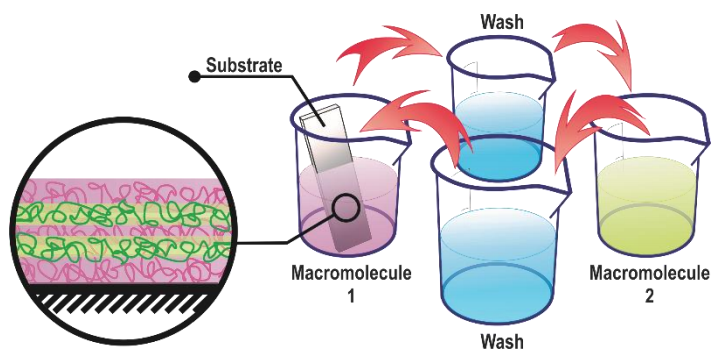


Figure 2.1 Schematic illustration of layer-by-layer assembly via alternate dipping in two complementary macromolecule solutions and an illustration of the resulting multilayers.

The versatility of the LbL fabrication technique allows for incorporation of a wide choice of materials to be used as both multilayer components and substrates on which layer build-up occur. Multilayers have been built not only on inorganic solids (e.g. glass [11], gold electrodes [12], metal stents [13], etc.), but also on organic templates (ionic liquids [14], polymeric membranes [15], plastics [16, 17], 3D tissue engineering scaffolds [18], polymeric microneedles [19-21]) and even biological objects (living cells [22, 23], or as sacrificial template [24]), in all shapes and sizes. Likewise for multilayer components, it is possible to combine polymers with inorganic materials and render the multilayers magnetically responsive [25, 26], electroconductive [27, 28] or optically active [29]. Smaller molecules, such as therapeutic compounds may be incorporated through conjugation to one of the polymeric components or through physical entrapment within the multilayer [30], while the all-aqueous deposition conditions are ideally suited to fragile biomacromolecules such as enzymes. Multilayers may also be constructed based on different driving forces. In addition to conventional electrostatic interactions, multilayers have been built through hydrogen bonding interactions [31, 32], van der Waals interactions [33], hydrophobic interactions [34, 35], stereocomplexation [36-38], charge transfer [39-41], host-guest [42, 43], specific biorecognition [44, 45] (including DNA hybridization [46, 47]), and covalent bonding [48-50]. Due to these versatilities, multilayers have found application in a wide range of fields such as nanoelectronics and sensors [51-54], separation membranes [55-57], mechanical enhancing [58], superhydrophobic [59, 60], scratch resistant [61], antireflection [62], anticorrosion [63], and anti-fouling [64] coatings, bioreactors [65, 66], and tissue engineering and biomedical applications [31, 67-70].

The intricate architecture of a multilayered system sets it apart from other smart systems such as hydrogels and other coatings, which can be considered as homogenous media. A multilayer is divided into regions with distinct differences in material composition. These unique physicochemical characteristics of multilayers will be briefly explained in the first part of this chapter, followed by examples of their chemical and biological responsiveness. In the following sections responsiveness attributed to the use of specifically tailored polymers is described. The final section discusses conclusions, challenges and prospects of the future development of chemically and biologically responsive multilayered systems.

2.3 LBL FABRICATION-SPECIFIC RESPONSIVENESS

The physicochemical aspects of multilayers have been mostly investigated for those built through electrostatic interactions as classic examples dating back to the early reports on LbL assembly first reported on poly(styrenesulfonate) (PSS) and poly(allylamine hydrochloride) (PAH) by Decher et al. in the early 1990s [71]. Stratification and the molecular growth mechanism have been matter of continuous debate. As indicated previously, the multilayer architecture is a unique property that can be potentially exploited to induce responsiveness. In this respect, the build-up profile is an exclusive characteristic of multilayers, which is known to have direct correlation to its architectural aspects. Most multilayers can be classified into two distinct build-up profiles: linear and supralinear or exponential, with some exceptions described as combination of two linear functions due to the influence of underlying substrates and electrostatic interactions [72-74]. The different build-up profiles, experimental findings, and proposed molecular mechanisms reported to date are briefly described here in relation to the possible responsiveness.

The multilayer growth mechanism is generally described as originating from overcompensation of surface functionality (i.e. the driving force for layer deposition) thereby facilitating the formation of the next layer. The process is driven by entropy increases through the liberation of polymer-associated water and ions. More specific molecular phenomena, however, determine whether build-up follows a linear or exponential profiles. This build-up is usually followed by the incremental increases in either mass or thickness as a function of deposition cycle or layer number. For example, while a 10-bilayered linearly growing multilayer may reach ~100 nm in thickness, exponentially growing multilayers easily reach micro- or even millimeter range thicknesses at the same number of layers [75].

Multilayers with linear build-up profiles make up most of the early reports on LbL assembly together with electrostatic driving force. Architecturally, these multilayers possess stratification with interpenetration between neighboring layers [76]. The polymer chains within the multilayer are described to be frozen and immobilized, and the overall layer is 'fuzzy' and highly disordered despite observable stratification [77]. The proposed molecular mechanism for these systems involves the assumption that incoming polymer chains form complex only with the topmost layer [78] and thus 1:1 deposition and overcompensation are maintained in every cycle of deposition. In 2000, Decher and co-workers proposed a three-zone model consisting of a charged zone closest to the substrate whose nature is influenced by the substrate, a zone at the interface with air or solution which is charged to facilitate new layer deposition, and a neutral "bulk" zone in-between, which grows along with the addition of new layers (Figure 2.2) [79].

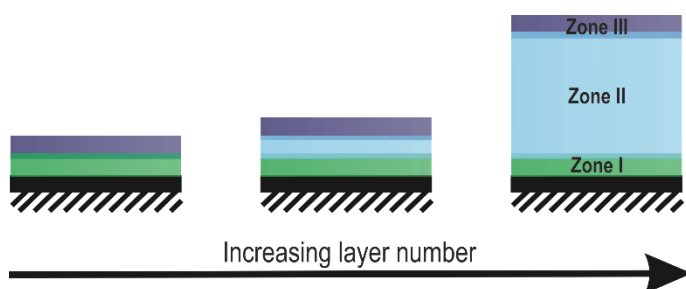


Figure 2.2 A schematic illustration of the three zone model as proposed by Decher and co-workers (adapted from [79, 80]).

Exponentially growing multilayers were first discovered by Hubbel and co-workers in 1999 on ((poly(L-lysine) (PLL) # alginate (Alg)) multilayers [81]. Laugel et al. found through isothermal titration microcalorimetry that higher exothermic electrostatic interactions tend to lead to linearly growing multilayer while weaker exothermic or endothermic interactions tend to lead to exponentially growing multilayers [82]. Thus, it was found that linearly growing multilayers can be rendered into exponentially growing layers by increasing the deposition temperature and/or increasing ionic strength of the deposition solutions to mask the strong electrostatic interactions between

the polyelectrolytes [82]. Two models have been proposed for the molecular mechanism of exponentially growing multilayers. The first model proposed that exponential profiles are a result of accumulation of surface roughness with increasing layer number [83-85]. The increase in surface roughness is attributed to the more globular conformation of polyelectrolytes when no significant charge repulsion takes place. This higher roughness leads to increases in surface area, resulting in the increased deposition of incoming polymers. This model is supported by the finding that multilayers that grow exponentially through dip-coating may be turned into linearly growing layers through spin coating, as was reported for hydrogen bonded (poly(ethylene glycol) (PEG) # poly(acrylic acid) (PAAc)) multilayers [16], and more recently for (PAH#PAAc) through application of high gravity fields [86], two deposition techniques that reduce potential surface roughness.

In an alternative model, Lavalle and co-workers proposed that incoming polyelectrolytes do not only interact with the outermost layer, but also diffuse into the core of the multilayer, through liberation of small counter ions from the multilayers [87]. The diffusion of the polyelectrolyte into the entire multilayer is accompanied by diffusion of smaller extents of the same polyelectrolyte out of the multilayer, which is limited by the presence of an electrostatic barrier at the film-solution interface. Diffusions halt when overcompensation is achieved by the polyelectrolytes complexating with the outermost layer, and the electrostatic barrier becoming too high for additional diffusion. As such, the amount of deposited polyelectrolyte depends not only on the fixed amount of outer polymer layers, but also on the relative thickness of the multilayer, resulting in an exponential increase with increasing layer number. This model is supported most notably by confocal laser scanning microscopy (CLSM) observation that fluorescein isothiocyanate (FITC)-labeled PLL diffuse through the entire multilayer consisting of unlabeled (PLL#hyaluronic acid (HA)). On the other hand, Texas red (TR)-labeled HA deposited into a distinct layer without diffusion, identifying PLL as the diffusing species (Figure 2.3) [88].

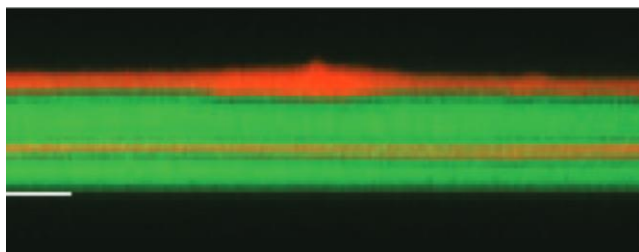


Figure 2.3 Vertical CLSM image of exponentially growing (PLL#HA)_{13.5}#HA^{TR}#(PLL#HA)₄#(PLL^{FITC}#HA^{TR}) with the glass substrate indicated by the white line. The green fluorescent layers emerged following the last deposition step of FITC-conjugated PLL. Reproduced with permission from [88].

Very interestingly, these findings indicate that compared to linearly growing multilayers, much higher mobility of polymers is observed for the exponentially growing layers, not only within the multilayer but also in the deposition solution where the two actively exchange during layer deposition [89-91]. In direct relation to chain mobility, it was found that faster growth was observed with polyelectrolytes of lower molecular weight [92], and higher polydispersity [93].

To maintain electroneutrality, multilayers also incorporate counter ions from solutions to compensate for excess charge of the polyelectrolytes. These multilayers are said to be extrinsically compensated and such compensation gives rise to Donnan potential [94, 95]. However, some multilayers have also been reported to display selectivity in ion incorporation. For example, Schlenoff et al. reported that no salt ions were present within a linearly growing (poly(diallyldimethylammonium chloride) (PDADMAC) # PSS) multilayer when the amount of positive and negative charges were approximately equal, indicating intrinsic charge compensation (i.e. charges of one polyelectrolyte are completely compensated by charges of the counter polyelectrolyte) [96]. The same research group further indicated the possibility to “dope” the intrinsically compensated multilayers with selected

ions by increasing the ionic strength of the incubation solution [97]. These features are highly beneficial for applications where high ion selectivity and permeability is required such as for separation and electronics applications.

For multilayer capsules, similar to liposomal or polymersome systems, multilayer capsules with weaker interactions undergo fusion [98, 99]. Sukhorukov and co-workers reported salt-induced fusion of (PDADMAC#PSS) upon slow increase in salt concentration [99], while Volodkin and co-workers reported fusion of (PAH#PSS) induced not by salt, but by elevated acidity ($[H^+] > 0.1 \text{ M}$) (Figure 2.4) [98]. The stronger interactions in the latter system were proposed to be the reason for its apparent non-responsiveness to salt. Fusion of two or more capsules upon contact is entropically driven by liberated water molecules, due to decreases in surface area. The kinetics of the fusion were found to be a function of layer number in relation to layer density, and the H^+ concentration. Thinner multilayers and elevated H^+ concentration increased the onset of the fusion. Volodkin and co-workers also identified that polymer exchange took place during fusion through the use of fluorescently-labeled PAH-containing multilayer capsules, which were mixed with non-fluorescently labeled capsules. The authors found that upon contact, non-fluorescently labeled capsules gradually became more fluorescent, depending on whether the final layers of the fusing capsules were of similar (enhanced) or opposing charges.

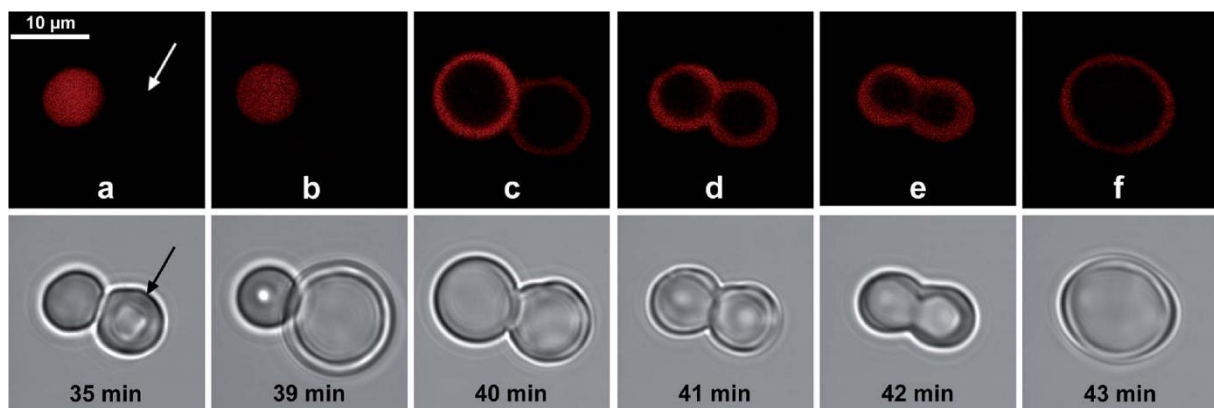


Figure 2.4 Fluorescence (top) and brightfield (bottom) images of rhodamine B (RB)-labeled (PAH^{RB}#PSS)₃ capsule during fusion with non-labeled (PAH#PSS)₃. Arrow shows the position of the non-labeled capsule before mixing of the multilayer components causes both capsules to be fluorescence. Reproduced with permission from [98].

These findings indicate that multilayer properties such as responsiveness can be introduced not only through the choice of the main multilayer components, but also through the physical deposition aspects.

2.3.1 PHYSICAL DEPOSITION ASPECTS

During LbL assembly, the presence of supporting components such as different types and concentrations of salt in the deposition solution, may exert detrimental features onto the resulting multilayers. In general, higher salt concentrations result in increased polymer entanglement due to screening of charges in the polyelectrolyte, which leads to increased material deposition, and increased surface roughness (Figure 2.5) [100]. Salt also increases the mobility of polyelectrolytes within the multilayer and therefore enhances multilayer stability by introducing higher degrees of entanglement through rearrangement. Multilayers built in the absence of salts are therefore much less stable and readily deconstruct upon introduction of salt or changes in pH [101]. However, when the salt concentration in the deposition solution is too high, polyelectrolytes tend to remain in solution and no multilayer build-up is observed.

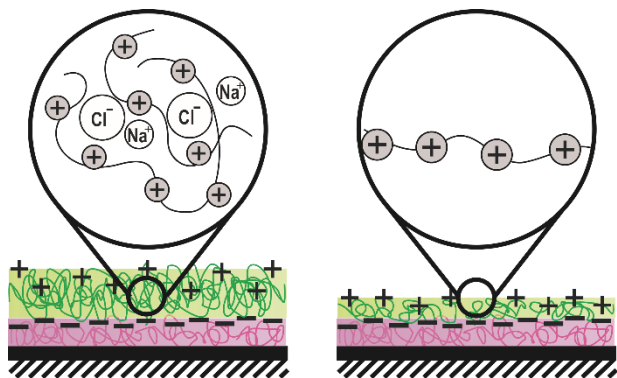


Figure 2.5 Schematic illustration of the effect of salt on polyelectrolyte multilayer build-up.

The type of salt influences multilayer thickness [102], porosity [103, 104], stiffness [105], as well as its swelling properties [106]. Stiffness and porosity are two surface characteristics known to play a role in cellular behavior [107, 108]. For example, by simply changing the pore size of (PAH#PAAc) multilayers to the nanometer range to mimic natural basement membranes, human corneal epithelial cells (HCEC) were found to proliferate and migrate at twice the speed, as compared to cells cultured on (PAH#PAAc) multilayers with sub-micron porosity [104].

In contrast to the usual trend of increasing thickness with increasing ionic strength, multilayers containing strong polyzwitterions (polymers are neutral over a wide range of pH) as one of the multilayer components display a reversed trend of decreasing deposition with increasing ionic strength [15]. For example, de Vos and co-workers studied the multilayer build-up characteristics of polysulfobetaine (a strong polyzwitterion) with PDADMAC and found that deposition was optimal at low salt concentration. This observation was explained as an effect of antipolyelectrolyte properties of polyzwitterions, where a more globular conformation of polyzwitterions is more readily attainable at low ionic strength as the internal charges in polyzwitterions are not screened (Figure 2.6). Thus, deposition onto a polycation layer is accompanied by relatively low entropic gain, leading to thicker layers. At higher ionic strength, screening of internal charges of polyzwitterions leads to higher entropic gain upon layer deposition resulting in thinner layers [96]. The authors further demonstrated that the multilayers can be fabricated on hollow fiber membranes to provide ionic strength responsiveness, where increased permeability is observed upon increases in NaCl concentration [15]. The reversed trend of decreased deposition with increasing salt concentration was also observed when NaBr instead of NaCl was used; this is attributed to the stronger interaction of bromide ion with the polycation in the multilayer [109].

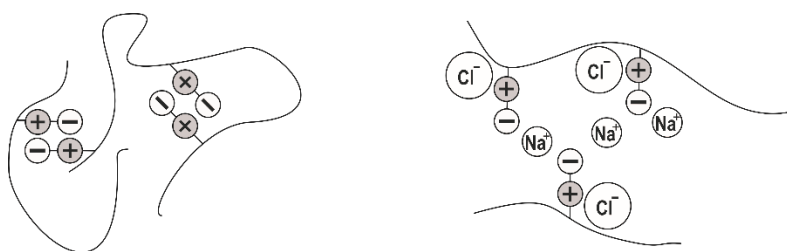


Figure 2.6 Schematic illustration of the antipolyelectrolyte properties of polyzwitterions in the absence (left) and presence (right) of salt.

The role of secondary substituents is not only limited to salts. Combining additional polymer in a blending fashion may help induce enhanced responsiveness. It was recently reported, that alginate (Alg) incorporation into (poly(ethylene imine) (PEI) # DNA) enhanced DNA release from the multilayer [110]. The effect was not only observed with alginate as additional layer (i.e. as (PEI#DNA#PEI#Alg)), but also when alginate was added separately into the incubation medium to provide an alginate-triggered release.

For weaker polyelectrolytes (e.g. those which contain carboxylic acid groups and amines), in addition to ionic strength, pH of deposition solutions also determines the growth behavior of multilayers, as well as their responsiveness. A classic example was reported by Shiratori and Rubner on (PAH#PAAc) multilayers [111]. In general, a deposition pH that results in increased proportions of charged groups will lead to decreased deposition [84, 101, 112]. Notably, the thickest films are obtained when pH is closest to the pKa of the ionizable groups [113]. These multilayers possess pH-responsiveness, which depends strongly on the deposition pH [101]. Multilayers fabricated at a pH that facilitates strong electrostatic interactions will be less likely to disassemble due to the stronger multivalent interactions, whereas multilayers that are fabricated at a pH that facilitates deposition of macromolecules of more globular conformation are significantly more sensitive to changes in pH. Likewise, multilayers that are fabricated at a pH at which most of the ionizable groups are not charged, will disassemble rapidly at a pH that ionizes the groups and causes charge repulsion.

Unlike multilayers based on electrostatic interactions, hydrogen bonded multilayers are characterized by a more limited pH range for deposition. Owing to this, these multilayers are able to readily disassemble at physiologically relevant pH, making them interesting for biomedical applications where pH responsiveness is desired. Some of the most commonly used hydrogen bond acceptor components are PEG, poly(*N*-vinylpyrrolidone) (PVPON), and the temperature-responsive poly(*N*-isopropylacrylamide) (PNIPAM), while the hydrogen bond donor components include poly(vinyl alcohol) (PVA), carboxylic acid-containing PAAc, and poly(methacrylic acid) (PMAAc). To obtain hydrogen bonded multilayers, assembly is carried out below the pKa of the carboxylic acid containing component. Subsequently, upon increase of pH above the pKa, a critical disintegration pH exists at which the hydrogen bonds are disrupted, leading to rapid multilayer disassembly [32, 114]. Higher salt concentrations may decrease the critical disintegration pH, as this increases the degree of ionization of the carboxylic acid groups [115]. By simply choosing the appropriate component, the stability of the multilayers can be maintained over a wider pH range, as was reported by Erel-Unal and Sukhishvili through the use of tannic acid (TA) with a pKa of 8.5 and a branched structure for enhanced multivalency [116].

To obtain prolonged and sustained release, Sakamoto and co-workers reported the use of plotted agarose scaffolds as substrate for hydrogen bonded multilayer fabrication of PEG, PAAc, and lysozyme [117]. They demonstrated sustained lysozyme release for up to four weeks with release kinetics dependent not only on the main multilayer components, but also on agarose concentration (i.e. porosity), and the type of precursor layer. This system also demonstrates the influence of the multilayer substrate on the multilayer properties.

The underlying substrates often only have a minor influence on the properties of the multilayer itself, and often persists only in the first few layers [118]. The substrate effect can be more pronounced when the type of interaction between polymer pair is different from that between the polymers and the substrate, or when the substrate possesses less functionality (e.g. lower charge density in the case of electrostatic interactions) [119]. To reduce the effect of the substrate, precursor layers from PEI, PSS, and PAH are sometimes deposited before the main multilayer components are deposited [120-123]. Especially when used for biomedical applications, the identity of the precursor layer has to be carefully considered, as most of the well-studied polyelectrolyte pairs are not biodegradable and may be cytotoxic. For example, high molecular weight PEI has been found to be potentially cytotoxic [124].

For multilayer capsules, sacrificial substrates based on CaCO₃ [125, 126], SiO₂ [99], or melamine formaldehyde (MF) [127] were found to lead to matrix-type, instead of shell-type multilayers, due to the incorporation of the multilayer components into the pores of the substrate during build-up. By choosing the appropriate core dissolution method, these matrix-type capsules can be forced into a shell-type, which retains gaseous hollow lumen [98]. Another example illustrating the influence of the substrate on multilayers was reported by Tsukruk and co-workers, who utilized cubic CdCO₃ as templates to be sacrificed for multilayer capsule preparation and

found that in comparison to capsules prepared using spherical SiO₂ template, the multilayer was softer and more permeable [128].

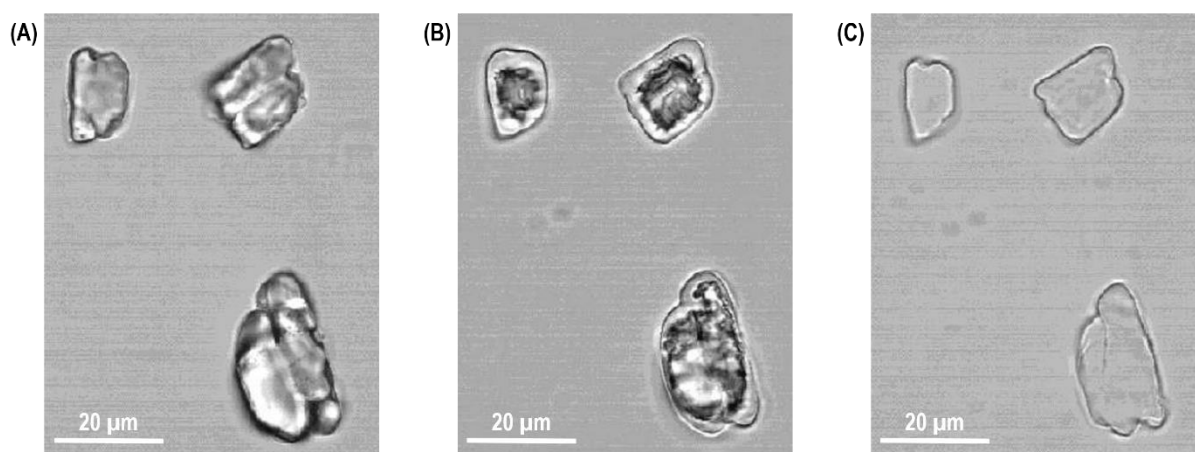


Figure 2.7 Transmission CLSM images of ibuprofen drug crystal coated with 15 bilayers of chitosan and dextran sulfate (A) before, (B) during, and (C) after complete ibuprofen core dissolution. Reproduced with permission from [129].

Drug crystals have also been used as substrates to automatically entrap the drug within the multilayer to achieve very high drug loading, and controlled release [129, 130]. Möhwald and co-workers encapsulated ibuprofen within multilayers of chitosan (CHI) and dextran sulfate (DS) by utilizing the limited solubility of ibuprofen at pH < 7 [129]. At pH 7.4, the ibuprofen crystals readily dissolved and diffused through the pores of the multilayers, leaving the empty multilayer shell intact (Figure 2.7). The release kinetics were found to depend on the size of the crystals (smaller crystals dissolved faster), number of layers (faster with thinner multilayers), and pH (much slower at pH 1.4 due to the low solubility of ibuprofen), but release kinetics were in all cases significantly slower than the dissolution rate of the uncoated drug crystals.

Almodóvar et al. found from their studies on carbohydrate-based multilayers, that hydrophilic multilayer surfaces are usually obtained from pairs of carbohydrates that are either both weak polyelectrolytes, or both strong polyelectrolytes, while multilayers from a combination of weak and strong polyelectrolytes tend to be hydrophobic [131]. This phenomenon was discussed based on the different predisposition of strong versus weak polyelectrolytes to ion pairing. This eventually leads to the ability of multilayers to swell and change hydrophilicity or hydrophobicity of the resulting surface.

2.3.2 POST-ASSEMBLY TREATMENT

Post-assembly treatments are aimed at addressing various needs. For tissue engineering applications, formation of additional fibronectin layers [132] or the tripeptide RGD [133, 134] is a straightforward way to promote protein adsorption and cell attachment. Treating (PDADMAC#PSS) multilayers with various NaCl concentration post-assembly has also been reported to result in different cell migration behavior [135]. Diffusion of multilayer components can be prevented by fabricating barrier layers which are impermeable to these components [136]. For example, for exponentially growing multilayers, addition of several bilayers of linearly growing multilayers may result in prevention of diffusion and offer a way to compartmentalize a multilayered construct. Examples of this approach are given in Section 2.3.3.

Depending on chain mobility within a multilayer, annealing steps can be carried out to smoothen the multilayer surface. In the case of weaker interactions, such as hydrogen bonding, this may be induced through simple incubation in deionized water [137], while in the case of stronger electrostatic interactions, exposure to high salt concentration is used to first weaken the interactions and induce rearrangement [138, 139]. However, some exponentially growing electrostatically-based multilayers were found to self-heal simply upon exposure to water

[140]. This swelling behavior may lead to disintegration as a function of time, salt concentration, and polymer molecular weight (slower with higher MW). For (PVPON#PAAc), it has been reported that such disintegration proceeds gradually from top to bottom [137], in contrast to the much more rapid responsiveness to pH where hydrogen bonding is directly affected. Quite recently, Voegel and co-workers reported that the restructuring of exponentially growing (PLL#HA) multilayers through increase or decrease in ionic strength may result in formation of holes within the multilayers [141].

Free-standing multilayers (both as macroscopic films or microscopic capsules) have also been prepared through post-assembly treatment. To obtain microscopic capsules, SiO₂, polystyrene, or CaCO₃ substrates that are already coated with multilayers are subjected to dissolution. These processes may often cause changes in the properties of the obtained capsules. For example, MF core removal has been associated with increased osmotic pressure, which may cause rupture of the multilayer capsule [142]. The use of organic solvent for PS core removal has been shown to affect the stability of the resulting capsule [143]. SiO₂ and MF removal is carried out at low pH with HF and HCl respectively and is therefore limited to multilayers with high stability at acidic pH [144].

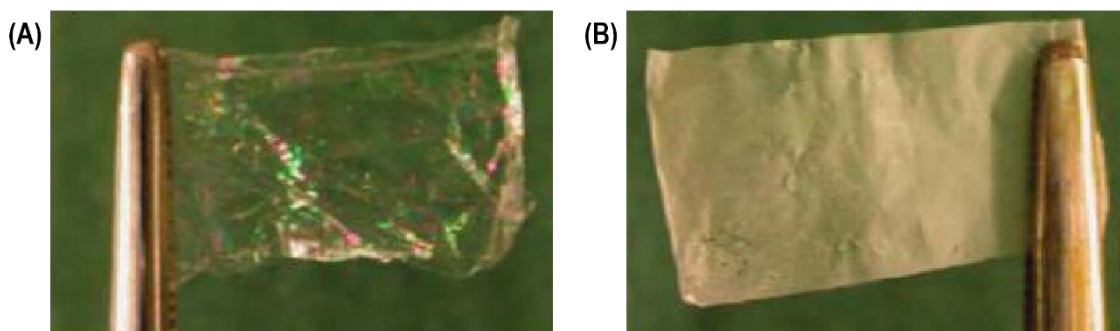


Figure 2.8 Digital photograph of hydrogen bonded (PEG#PAAc)₁₀₀ built through (A) spin and (B) dip-coated LbL assembly. Reproduced with permission from [16].

For macroscopic free-standing multilayers, hydrogen bonded multilayers serve as convenient sacrificial layers that are easily disassembled at mild pH. For example, (PEG#PAAc) disassembles at pH 5.6 – 6.3 [72]. In addition to the hydrogen bonded multilayers, polyelectrolyte-based multilayers have been utilized as sacrificial layer to obtain free-standing multilayers upon disassembly at pH \geq 12 [145]. Robust, defect-free mechanically detachable free-standing multilayers have also been reported for (CHI#HA) by choosing hydrophobic polypropylene as the multilayer substrate [17]. Similar attempts were reported for (PEG#PAAc) multilayers through the use of Teflon as substrate [16]. Interestingly, the free-standing (PEG#PAAc) multilayers differ depending on whether dip coating (linearly growing) or spin coating (exponentially growing) was used for their fabrication. The exponentially growing multilayers were found to result in opalescent films, while the linearly growing multilayers were transparent (Figure 2.8). Recently, Rubner and co-workers reported the fabrication of sacrificial multilayers from bovine submaxillary mucin (BSM) and lectin jacalin (JAC) which can be conveniently disassembled in the presence of melibiose (a sugar), which competes for binding with mucin [146]. The authors further demonstrated that such an on-demand disassembly may be used to release the free-standing multilayer to further perform as a drug-releasing “backpack” for cell monolayers *in vitro* (Figure 2.9). The multilayer segment containing magnetic nanoparticles serves as the model “backpack” in this study.

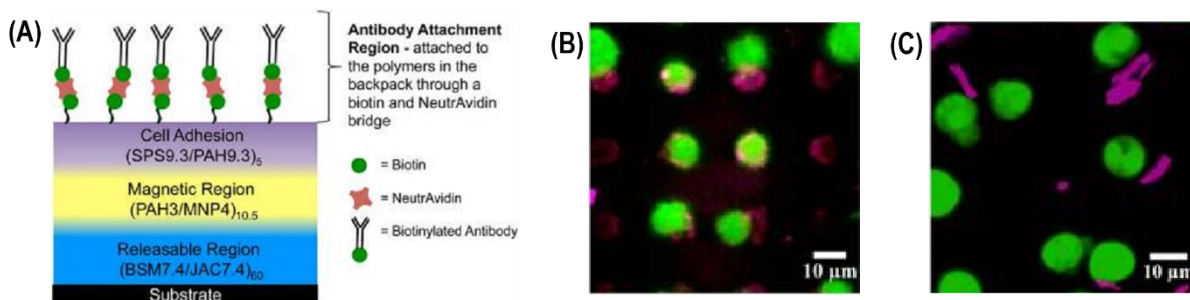


Figure 2.9 (A) Multilayer structure consisting of (BSM#JAC) base layer as sacrificial layer that can be disassembled upon introduction of melibiose. The magnetic region consists of (PAH# magnetic nanoparticle (MNP)) multilayer as backpack. The cell adhesion top layer consists of (PSS#PAH) multilayer for enhanced cell adhesion, further covalently coupled with IgG antibody for cell targeting. (B) Monocytes attaching to the backpack via IgG antibody prior to addition of melibiose. (C) Monocytes with attached backpack following sacrificial layer disassembly through addition of melibiose. Reproduced with permission from [146].

The majority of post-fabrication treatments is aimed at increasing mechanical strength and stability, especially for hydrogen bonded multilayers. Multivalent ion have for example been introduced to increase the stability of hydrogen bonded multilayers at pH 7.1 [147]. Heating is a popular way of forming amide crosslinks in (PAH#PAAc) multilayers [148-151]. Such crosslinks are therefore often introduced to act as barrier layer within a multilayered construct [148], to control release rate [150], and reduce permeability and increase ion-transport selectivity for separation membrane applications [151]. Other popular methods of forming covalent interlayer crosslinks include carbodiimide chemistry [152-154], click chemistry [2, 155, 156], thiol oxidation [157, 158], and glutaraldehyde crosslinking [17, 159]. Liu recently reviewed various stabilization techniques to enhance the stability of multilayer capsules [160]. Covalent crosslinking has been reported to increase multilayer stiffness. In a study by Picart and co-workers, increasing EDC concentration for crosslinking (PLL#HA) multilayers resulted in increased myoblast cell adhesion [161]. Additionally, crosslinks may also be introduced to add additional functionality and responsiveness. For example, Shu et al. prepared disulfide crosslinked (CHI#DS) multilayer capsules [158]. Compared to the non-crosslinked capsules, the disulfide-crosslinked capsules are more stable at the low pH encountered in the stomach, while being responsive to reducing enzymes and intracellular glutathione.

Controlled loading and release of small molecules, inorganic particles, and macromolecules has been achieved by utilizing pH as a trigger, when one of the multilayer components is a weak polyelectrolyte [162-165]. For example, the charge density within (PAH#HA) multilayers depends on pH, governing the ionization state of both amine groups of PAH, as well as carboxylic acid groups of HA. Thus, loading of chromotrope 2R, a dye containing two sulfonate groups is optimal when the pH is low due to the presence of excess positive charges in the multilayer [162], while its release is optimal at high pH where the decrease in PAH charge density weakens the electrostatic interactions with the dye. (PAH#PSS) multilayer capsules can also be “open” for incorporation of FITC-dextran at pH < 6 and “closed” from further incorporation at pH > 8 [163].

2.3.3 MULTILAYER ARCHITECTURE-SPECIFIC RESPONSIVENESS

Increasing the bilayer number of multilayers is associated with decreasing Young's modulus or stiffness due to more pronounced hydration [152, 166, 167]. As a consequence decrease in stiffness, substantially increased spreading of smooth muscle cells (SMC) cultured on top of (PLL#HA) was observed when the number of bilayers was 20 instead of 60 [152]. The same research group also reported that in addition to decreased chondrosarcoma cell adhesion on (PLL#poly(L-glutamic acid) (PGA)) with increasing bilayer number, cellular adherence may also be diminished entirely when the PGA layer is the topmost layer, due to the prevention of serum proteins adherence [168]. Interestingly, phenotypic properties of SaOS-2 (human osteoblast-like cells) and human periodontal ligament cells were reported to be maintained only when the multilayer topmost layer is negatively charged [169].

For the exponentially growing multilayers, the high mobility of polyelectrolytes in and out of the multilayer serves as a very convenient way to load additional materials homogeneously into the entire multilayered construct without the need for specific interactions between the materials to be loaded and the layer component. Lavalle and co-workers reported the loading of Oregon Green 488-labelled paclitaxel into exponentially growing (PLL#HA) multilayers [136]. By means of CLSM it was observed that paclitaxel was evenly distributed throughout the multilayer at an extent that was proportional to the concentration of paclitaxel in the loading solution and achieving up to 50 times higher concentration in the multilayer as compared to the concentration in the loading solution. The authors deposited (PAH#PSS) layers on top of the loaded multilayer and showed that this capping layer prevented release of paclitaxel from the multilayer, while facilitating good HT29 cell adhesion. As long as the capping layer was not thick enough for complete surface coverage, cells could still internalize paclitaxel. The authors further showed through another publication, that when a single poly(lactic-co-glycolic acid) (PLGA) layer was used instead of the nondegradable (PAH#PSS) layer, cells could degrade the PLGA layer and internalize the fluorescently-labeled PLL (Figure 2.10) [170].

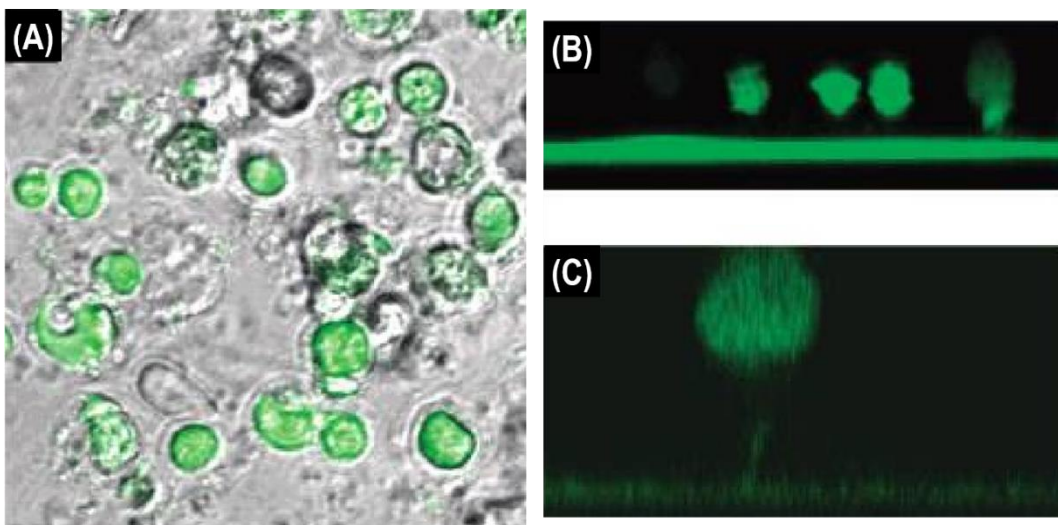


Figure 2.10 (A) Overlaid image of brightfield and green channel of bone marrow cells after 17 h of culture on exponentially growing (PLL#HA)₂₀#PLL^{FITC}#PLGA#PLL multilayers. The cells are green due to internalization of PLL^{FITC} from the multilayer. (B) CLSM images of the cross section of the multilayer with cells on top. (C) Higher magnification of the CLSM image showing the formation of pseudopod through the non-fluorescent, biodegradable PLGA layer. Reproduced with permission from [170].

Using a hydrolytically degradable polymer (poly(β -amino ester), here: polymer 1), Hammond and co-workers reported that different top-down film degradation profiles were observed depending on whether heparin (HEP) or dextran sulfate was used as the counter polyelectrolyte [148]. Build-up of (polymer 1#HEP) proceeded in an exponential manner with HEP as the diffusive species, while build-up of (polymer 1#DS) proceeded linearly. Erosion of the exponentially growing (polymer 1#HEP) proceeded in a linear manner, while that of (polymer 1#DS) proceeded through an early linear phase followed by leveling off of the erosion speed. The authors further demonstrated that by introducing one bilayer of thermally crosslinked (PAH#PAAc) in between (polymer 1#DS) bottom and (polymer 1#HEP) top, sequential erosion of the two hydrolyzable compartments could be achieved with a delay that depends on the crosslinking degree of the (PAH#PAAc) barrier layer (i.e. the length of thermal crosslinking duration). Crosslinking for over 1.5 h fully halted hydrolysis of the bottom region.

Another example on the influence of multilayer architecture on its responsiveness was given by Erel-Unal and Sukhishvili with their hydrogen bonded multilayers [115]. They showed that by combining (poly(N-vinylcaprolactam) (PVCL)#poly(L-aspartic acid) (PLAA)) having a critical disintegration pH of 3.3 with (PVCL#TA) having critical disintegration a pH of 9.5, it was possible to not only shift the disintegration profiles, but also introduce a two-step pH response [115].

2.4 POLYMER-SPECIFIC RESPONSIVENESS

A different approach to obtain responsive multilayers is by introducing polymer-specific responsiveness. This means that the responsiveness is not a consequence of the employed assembly methodology, but is inherent to the film components or due to the interaction between them. One approach that has been studied thoroughly is the incorporation of polymers with inherent responsiveness into the multilayers. When engineered in the right manner, these polymers will respond to specific stimuli by changing their properties (e.g. charge, hydrophobicity), leading to swelling or disassembly of the multilayer, which can be used to facilitate for example the release of a therapeutic cargo. A similar approach involves the incorporation of active components (e.g. enzymes, micelles, and liposomes) to achieve a responsive system. By retaining their activity within the multilayer, they can endow responsiveness on the entire assembly. In contrast, the incorporation of (bio)degradable polymers may result in films susceptible to hydrolytic and enzymatic degradation. Finally, multilayers may be assembled in a way that they require chemical stabilization through inter-layer bonds to remain stable. By engineering specific degradable or responsive linkages into the constructs these multilayers can be rendered responsive. In the following sections these different approaches will be reviewed and prominent and novel examples will be discussed to give the reader an overview of the available approaches found in the literature.

2.4.1 DISRUPTION OF MULTILAYERS WITH RESPONSIVE POLYMERS

The first reported multilayers were built up of alternating layers of polyanions and polycations. These systems are, especially in the case of weak polyelectrolytes, considered inherently responsive. Changes in pH can change the charge ratio of these polymers drastically around their pK_a and thus lead to uncompensated charges that destabilize the film. Similarly, (de)protonation of film components in multilayers stabilized through hydrogen bonding are susceptible to changes in pH. Increases in salt concentrations have similar effects by shielding the polymer charges. In both cases these effects can lead to enhanced permeability, but also complete film disassembly, depending on the precise circumstances (i.e. pH, salt concentration, employed film components) and importantly the presence of secondary chemical crosslinks between the layers. Assembly as well as disassembly of these films have been thoroughly studied by several authors and have been reviewed in greater detail elsewhere [114, 171-175].

A different approach to endow multilayers with responsiveness through charge-shifting polymers was first reported by De Geest et al. [176] By developing polymers with a side chain that flipped charge upon hydrolytic cleavage they were able to construct multilayers that slowly degraded over time depending on the pH (Figure 2.11). Other authors have subsequently reported similar systems with both positive and negative initial charges [177-179]. Degradation kinetics can be fine-tuned by small variations in the side chain chemistry as well as the degree of functionalization of the polymer [177, 178, 180].

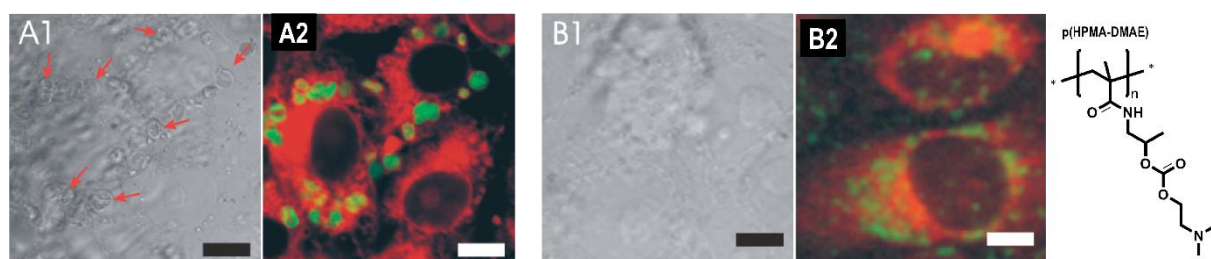


Figure 2.11 Brightfield (1) and overlaid fluorescence (2) images of VERO-1 cells after 60 h of culture with DS^{FITC} -filled nondegradable (PAH#PSS) (A) and charge shifting (p(HPMA-DMAE)#PSS) (B) microcapsules. Scale bar = 10 μm . Arrows indicate presence of intact capsules. Reproduced with permission from [176].

Ma et al. reported a different stimulus for charge-shifting of a polymer within a multilayer [181]. The authors demonstrated that multilayers constructed from polycationic and polyanionic poly(ferrocenyl silane)s responded to oxidation by $FeCl_3$ with swelling, enhanced permeability and ultimately disassembly. These effects were caused

by the excessive positive charges induced on the ferrocene during oxidation. Interestingly, by applying capping layers of (PSS#PAH) they were able to retain the enhanced permeability, while preventing destabilization of the multilayer, thus allowing for control over multilayer permeability. Several other authors reported on redox responsive multilayers responding to electric potentials [182, 183].

An important aspect of the degradation behavior is the time frame in which this process takes place. Liang et al. have reported in a recent publication the assembly of multilayer capsules based on the pH-responsive polymer poly(2-diisopropylaminoethyl methacrylate) (PDPA) [184]. Through copolymerization with lauryl methacrylate they obtained a polymer that allowed for single component multilayer capsules based on the hydrophobic interactions between C_{12} chains. This resulted in capsules that swell rapidly in response to endosomal pH (i.e. pH 6) due to protonation of PDPA. The authors demonstrated this process to be reversible and showed controlled release of different model drugs [184].

Yet another trigger for changes in the charge ratio of polymers has been reported to be carbohydrates [185]. This effect was achieved by synthesizing a copolymer of the polycation poly(2-(dimethylamino)ethyl methacrylate) (PDMAEMA) and phenyl boronic acid (PBA) groups. Phenylboronic acid exists in equilibrium between its neutral trigonal form and its anionic tetrahedral form. PBAs are further known to form a reversible cyclic boronic ester with diols (Figure 2.12). This reaction lowers the pK_a of the boronic acids by 2-4 units, thus shifting the equilibrium towards the negatively charged form. This has triggered extensive research into PBAs as carbohydrate sensors [186-190]. De Geest et al. demonstrated that multilayers composed of the PDMAEMA-PBA copolymer and PSS were responsive to glucose close to physiologically relevant concentrations (5-10 mM), though regrettably not at physiological pH [185]. Further optimization of the initial pK_a of the boronic acid group [191] employed might lead to systems sensitive at physiological pH.

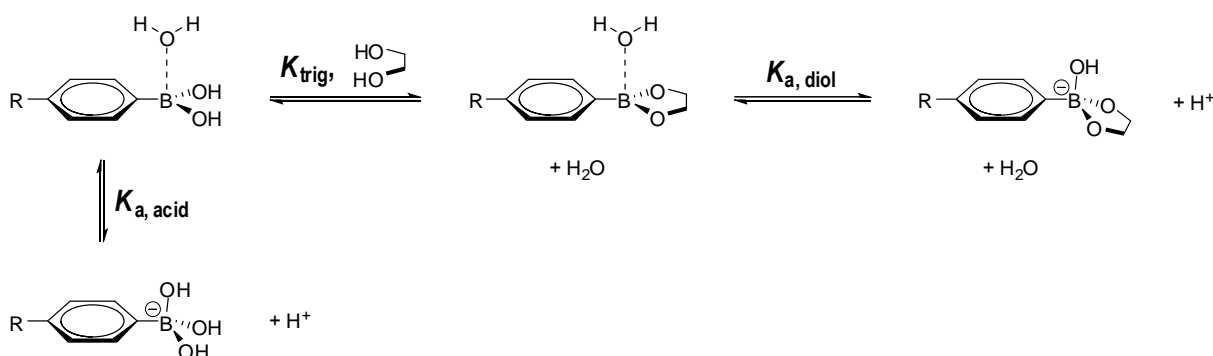


Figure 2.12 Thermodynamic cycle of boronic ester formation and boron / boronate ion transition.

2.4.2 MULTILAYERS COMPOSED OF INHERENTLY ACTIVE, RESPONSIVE, OR DEGRADABLE POLYMERS

Multilayers owe their stability to the multiplicity of interactions between consecutive layers. Therefore, upon degradation of one of the multilayer components and resulting decreases in polymer molar mass, multilayer disassembly is observed. Several research groups have investigated polymers with (bio)degradable links in their backbone. A well-studied example are poly(β -amino ester)s, which degrade through hydrolysis [192]. By monitoring the release of complementary PSS it was observed that release periods could be controlled by varying the hydrophobicity of the polymer. Further control was achieved by combining different polymers into a single multilayered construct [192]. Applicability of this system in gene therapy was investigated by replacing the polyanion PSS with plasmid DNA (pDNA). The authors observed release of transcriptionally active pDNA over a range of three days [193]. The authors further investigated the application of the multilayers for transcutaneous delivery of pDNA into the skin of mice *in vivo*, showing potential applicability for vaccine delivery (Figure 2.13)

[21]. Similarly, Blacklock et al. investigated the assembly and dissolution of multilayers of pDNA and an artificial peptide with reducible disulfide linkages in the backbone [194]. Multilayers disassembled selectively in the presence of a reducing agent, releasing the co-assembled pDNA. The same research group further demonstrated through the use of reducible hyperbranched poly(amido amine) (RHB) that higher and longer lasting transfection could be achieved as compared to (DNA#PEI) multilayers [195]. The authors speculate that highly localized release in the reducing microenvironment of the cellular membrane could lead to enhanced gene delivery efficiency.

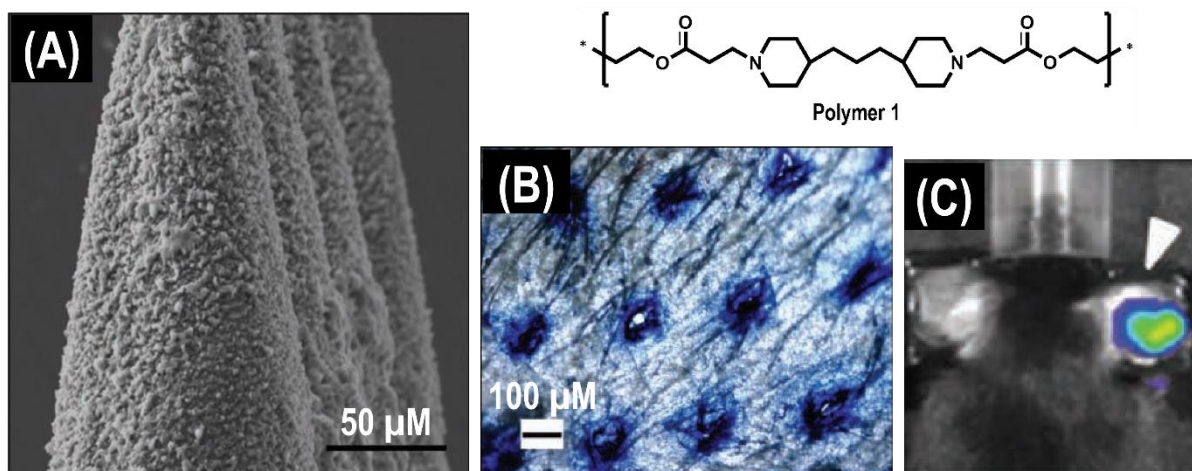


Figure 2.13 (A) Scanning electron microscope image of (polymer 1#pDNA)-coated PLGA microneedle arrays. (B) Optical micrograph of mouse ear following penetration of multilayer-coated PLGA microneedle arrays and staining with trypan blue. (C) Representative bioluminescence signal of treated mouse ear with efficacy that depends on the layer number and treatment duration. Reproduced with permission from [21].

Polymers are an essential part of biological systems and as such enzymes exist to modify and process these natural polymers. Natural polymers (i.e. polypeptides, nucleic acids, polysaccharides) have been demonstrated to retain their availability to these enzymes within multilayers. Following addition of an enzyme that is able to degrade at least one of the layer components, film disassembly was achieved. Reported enzymes consist of proteases [176, 196-200], nucleases [201], lysozyme [202], chitosanase [203], and hyaluronidase [204].

Similarly, enzymes can be incorporated into multilayers as active components themselves. This allows for the construction of biocatalytic thin films, a concept well-established in the literature [205]. A large number of enzymes have been incorporated into multilayers and shown to retain enzymatic activity [206, 207]. A recent example highlights the potential in the biomedical field, Andreasen et al. thoroughly studied the incorporation of β -galactosidase into multilayers [208]. These multilayers have potential in drug delivery through surface-mediated enzyme prodrug therapy, where a systemically administered prodrug is locally activated by β -galactosidase, thus allowing for external control in dosing as well as highly localized delivery [208].

Alternative active components have been incorporated into multilayers as well [209-211]. For example Addison and Biggs et al. reported the incorporation of pH-responsive block copolymer micelles (BCM) into multilayers. These can be used as drug reservoirs within the multilayer that retain their pH responsiveness and thus allow for a controlled release from the multilayer. Both planar multilayers as well as capsules were obtained from positively charged BCMs of poly(2-(dimethylamino)ethyl methacrylate)-block-poly(2-(diethylamino)ethyl methacrylate) (PDMAEMA-*b*-PDEAEMA) and PSS. It was further demonstrated that PSS could be exchanged for anionic BCMs to obtain alternating layers of micelles [212-214]. Similarly, films stabilized by hydrogen bonding were reported between PNIPAm-*b*-PDEA micelles and tannic acid [215]. These films remained stable at slightly acidic pH, but released hydrophobic cargo from the BCM core. Both thermoresponsive polymers and BCMs have been used to construct multilayers and endow them with responsiveness [216, 217]. Liposomes have been incorporated into

multilayers as well, either as responsive reservoirs [218] or for the encapsulation of active components (i.e. enzymes) to protect them from environmental influences, while maintaining their activity [219].

A quickly growing application of nucleic acid technology is aptamers [220, 221]. Aptamers are short sequences of single stranded DNA or RNA that are able to bind a large variety of analytes with very high selectivity. The specific sequence for a specific analyte is usually selected from a large pool of random sequences in an iterative process. The binding ability of aptamers originates from their three dimensional structure, which folds around the analyte of interest [220, 221]. Sultan et al. co-assembled aptamers into (PAH#PSS) multilayer capsules [222]. Interestingly, the authors found that binding of the analyte to the incorporated aptamers resulted in an enhanced permeability of the multilayer. It is speculated that the analyte triggers conformational changes of the aptamers inside the film, thus disturbing the multilayer enough to increase its permeability. The same group later demonstrated multilayer capsules with aptamers as structural components in the capsule core. These capsules ruptured on addition of the analyte [223]. Both modes (i.e. enhanced permeability, capsule rupture) have applications in drug delivery and sensor designs by incorporating aptamers specific for therapeutically relevant targets. The potential of this system was recently demonstrated by another group that employed an aptamer-containing multilayer as a switchable barrier between an etchant and a plasmonic nanoparticle sensor [224]. Upon binding of the analyte the enhanced permeability of the film allowed access of the etchant to the surface-immobilized nanoparticles, resulting in a visible color change. The authors argue that this general approach may be extrapolated to a wide range of aptamers to construct facile dip-and-read sensors [224].

Dam et al. recently explored a novel approach by threading cyclodextrins onto PEG and locking them in place with a disulfide-stabilized cap (Figure 2.14) [225]. Post-modification of cyclodextrins with charged moieties allowed for LbL assembly of these rod-shaped stiff supramolecular structures. Physiological concentrations of glutathione, a reducing agent present in the cytoplasm of cells, resulted in release of the capping group through disulfide cleavage and rapid film disassembly. Biocompatibility of both PEG and cyclodextrins is a major advantage, while the latter may also have potential as drug carriers, making these systems interesting candidates for drug delivery [225].

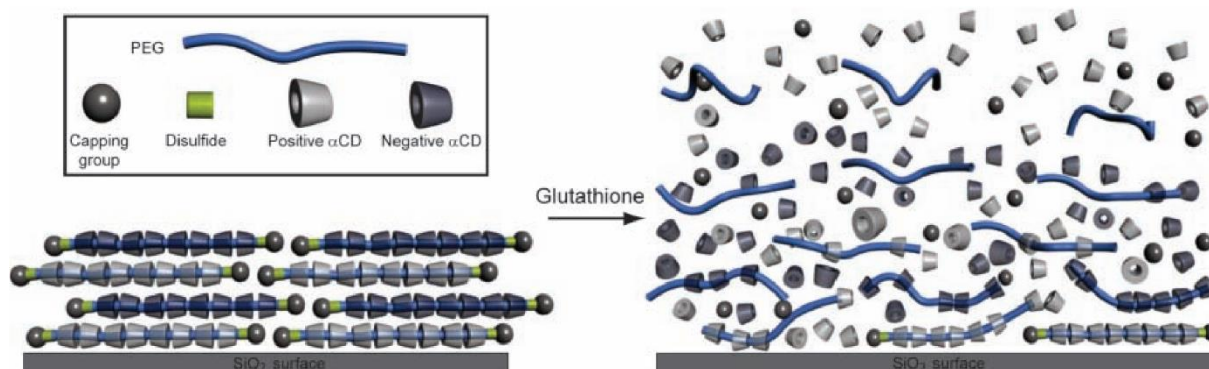


Figure 2.14 Schematic illustration of multilayers from dimethylethylenediamine- (positively charged) and glycine- (negatively charged) functionalized PEG-threaded cyclodextrins with disulfide capping. Presence of reducing agent such as glutathione results in multilayer disassembly. Reproduced with permission from [225].

2.4.3 RESPONSIVE MULTILAYERS THROUGH SPECIFIC DISRUPTION OF INTER-LAYER BONDS

An alternative approach to building up layers of interacting components is by forming bonds that are susceptible to the presence of external chemical moieties. As discussed in the previous sections in the case of crosslinks introduced subsequent to assembly, these linkages can be engineered to be susceptible to commonly employed degradation pathways (i.e. hydrolytic, enzymatic, reducing). An advantage of introducing these inter-layer crosslinks as part of the assembly process is the reduced number of total assembly steps, as well as avoiding potentially toxic and difficult to remove crosslinking agents [226]. Build-up of multilayers through host-guest

interactions between subsequent layers is another effective approach. These interactions can later be disrupted by introducing moieties that competitively bind to these bonds, replacing the inter-layer interactions and thus disrupting the multilayer [227-229]. Interesting in this approach is the fact that these systems have potential to be reversible, as removal of the stimuli allows reformation of the interlayer bonds and thus re-stabilization of the multilayer.

Sato et al. capitalized on the well-studied interactions between lectins and carbohydrates [227, 228], as well as between streptavidin and biotin [230]. In the case of multilayers composed of lectins (concanavalin A) and glycopolymers, addition of carbohydrates with higher affinity to the lectin resulted in film destabilization. Similarly, multilayers of respectively streptavidin- and biotin-labeled polymers were destabilized by the presence of biotin [227, 228, 230]. A glucose-triggered release of insulin was proposed from multilayer capsules constructed from lectins and glycopolymers. However, this system needs to be further improved in its glucose sensitivity to become practical for *in vivo* applications.

As discussed earlier phenyl boronic acids are able to bind polyols in a dynamic manner through the formation of cyclic boronic esters. As such, formation of multilayers between phenylboronic acid (PBA)-functionalized polymers and polyols has received considerable attention. Addition of sugars with high binding constants for PBA effects disruption of these multilayers. Films of PBA-functionalized PAAc and mannan responded to glucose only at high pH [229]. Whereas multilayers of PVA and PBA-functionalized poly(acrylamide) responded at near physiological pH [231]. As is the case with boronic acids in general, including the examples presented throughout this chapter, these multilayers demonstrate much higher sensitivity towards other sugars or carbohydrates besides mere glucose. For example, sensitivity to fructose has been reported to be one order of magnitude higher than for glucose [229]. Regrettably, side-by-side comparisons of sensitivity to different sugars are often missing. As such the challenge lies in developing systems sensitive selectively to glucose at a physiologically relevant concentration range (5-10 mM), while being able to function at physiological pH.

Multilayers that disassemble in the presence of chelating agents were reported by Krass et al. by the construction of multilayers from a pyridine functionalized polymer and transition metal ions [232]. Addition of chelating agents disrupts the metal ion coordination bonds and thus leads to film disruption. Similarly, multilayer fabricated from alternating layers of cyclodextrin- and adamantane-grafted chitosan were shown to disassemble upon addition of molecules that compete with this host-guest interaction [233].

Multilayers assembled through click-chemistry between azide- and alkyne-functionalized dextran were reported [226]. Conjugation of azide and alkyne groups was achieved through a carbonate linkage. Hydrolytic degradation of this linkage resulted in multilayer disassembly under physiological conditions.

Nucleic acids hold a special place within natural polymers as they allow for extremely specific inter- and intra-polymer interactions due to base pair hybridization. The potential of this is well illustrated by the impressive array of 2D and 3D structures that have been assembled in this field in what has been coined DNA origami [234-236]. Johnston et al. have made use of specific base pair hybridization to assemble multilayers composed purely of DNA [237]. By introducing a binding sequence specific to a certain restriction enzyme they were able to demonstrate specific degradation of the multilayers (Figure 2.15). A system reported later using a peptide analogue of DNA showed similar results, but allowed for greater stability in biological media [238]. DNA multilayers can be programmed to degrade in the presence of complementary DNA sequences that specifically target the sequences responsible for film stabilization [239].

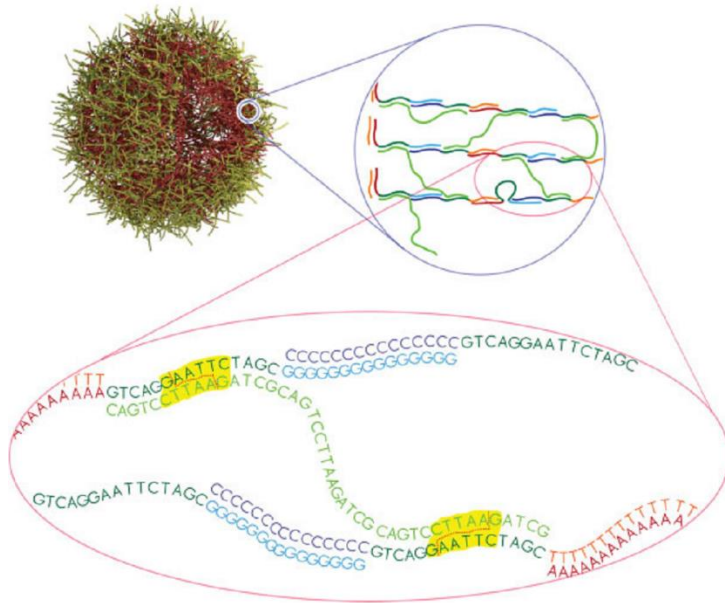


Figure 2.15 Schematic illustration of DNA-hybridization driven multilayer of (A₁₅-X₁₅-G₁₅#T₁₅-X₁₅-C₁₅). The unhybridized X strands (dark green) in the multilayers were treated with triblock complementary X strand (light green) to introduce interlayer crosslinking for improved stability. Yellow highlights indicate the specific sequence to be cleaved by the *Eco*RI restriction enzyme to induce multilayer dissolution. Reproduced with permission from [237].

2.5 CONCLUSION AND PROSPECTS

Layer-by-layer assembly offers a very versatile and particularly economical method, not only for the functionalization of practically any existing surface, but also as a complete delivery system by itself. The ability to tune the thin film both in thickness and amount of incorporated materials, in combination with the more intricate details of multilayer architectures is a major advantage of the LbL assembly technique. Among others, multilayers can be tuned to load specific active compounds to achieve very high loadings within the multilayer, and hence on the surface of the coated materials. The multilayered architecture and the interplay of various materials with different properties as multilayer components offer a direct approach to achieve sequential release of cooperative active agents, in addition to providing a simple means to tune release or degradation profiles.

Drawn by these promises, a lot of research has been invested in the fundamental molecular understanding of the LbL assembly process and the resulting multilayer products, as well as in the translation of existing and novel biomaterials and functional polymers to be exploited for LbL assembly. The extensive research in the development of new smart biomaterials is anticipated to continue which may give rise to novel multilayer systems. Deeper understanding into specific multilayer systems will not only help in their development towards a perceived goal, but also provide additional information on the physicochemical aspects of LbL assemblies in general. This in turn may further help establish new opportunities for applications.

Despite substantial research in the LbL assembly field, several major challenges remain to be addressed. These include the need to increase the mechanical stability [160] of these thin film systems to lengthen shelf life, and the need to find faster and more reproducible methods for large-scale production. The report by Shiratori and co-workers on roll-to-roll process for fabrication of large-area thin multilayers dated to 2004 is one such examples [10]. Although many new LbL fabrication techniques have been reported over the past years, a lot of them still require long processing times, or complex devices, especially in the case of fabricating smaller multilayer capsules. Attempts to decrease the size of multilayer constructs from micro- to nanocapsules have so far received only limited attention, though precisely these nanostructures may have tremendous application potential in nanomedicine. For therapeutic applications, detailed *in vivo* studies need to be carried out to assess the true potential of these multilayers. The work of Hammond and co-workers referred to in this Chapter provides the first report on *in situ* DNA delivery from multilayer-coated microneedles *in vivo* [21], while Lynn and co-workers quite recently reported the *in vivo* study on the same multilayer coatings on stents [13]. Other authors have also reported on *in vivo* studies of multilayer capsules [240, 241]. With a lot of opportunities yet to be discovered, the development of novel multilayers that provides orchestrated responses to various biological and chemical stimuli is expected to continue well in the future.

2.6 REFERENCES

- [1] J.B. Schlenoff, S.T. Dubas, T. Farhat, Sprayed Polyelectrolyte Multilayers, *Langmuir*, 16 (2000) 9968-9969.
- [2] K.L. Cho, H. Lomas, A.J. Hill, F. Caruso, S.E. Kentish, Spray Assembled, Cross-Linked Polyelectrolyte Multilayer Membranes for Salt Removal, *Langmuir*, 30 (2014) 8784-8790.
- [3] C.H. Porcel, A. Izquierdo, V. Ball, G. Decher, J.C. Voegel, P. Schaaf, Ultrathin coatings and (poly(glutamic acid)/polyallylamine) films deposited by continuous and simultaneous spraying, *Langmuir*, 21 (2005) 800-802.
- [4] S.S. Lee, J.D. Hong, C.H. Kim, K. Kim, J.P. Koo, K.B. Lee, Layer-by-layer deposited multilayer assemblies of ionene-type polyelectrolytes based on the spin-coating method, *Macromolecules*, 34 (2001) 5358-5360.
- [5] H.E. Karahan, L. Eyuboglu, D. Kiyilar, A.L. Demirel, pH-stability and pH-annealing of H-bonded multilayer films prepared by layer-by-layer spin-assembly, *Eur. Polym. J.*, 56 (2014) 159-167.
- [6] Y. Fu, S.-J. Li, J. Xu, M. Yang, J.-D. Zhang, Y.-H. Jiao, J.-C. Zhang, K. Zhang, Y.-G. Jia, Facile and Efficient Approach to Speed up Layer-by-Layer Assembly: Dipping in Agitated Solutions, *Langmuir*, 27 (2010) 672-677.
- [7] B.S. Shim, P. Podsiadlo, D.G. Lilly, A. Agarwal, J. Leet, Z. Tang, S. Ho, P. Ingle, D. Paterson, W. Lu, N.A. Kotov, Nanostructured thin films made by diwetting method of layer-by-layer assembly, *Nano Lett.*, 7 (2007) 3266-3273.
- [8] M. Toda, Y. Chen, S.K. Nett, A.N. Itakura, J. Gutmann, R. Berger, Thin Polyelectrolyte Multilayers Made by Inkjet Printing and Their Characterization by Nanomechanical Cantilever Sensors, *J. Phys. Chem. C*, 118 (2014) 8071-8078.
- [9] C. Priest, A. Quinn, A. Postma, A.N. Zelikin, J. Ralston, F. Caruso, Microfluidic polymer multilayer adsorption on liquid crystal droplets for microcapsule synthesis, *Lab on a Chip*, 8 (2008) 2182-2187.
- [10] K. Fujimoto, S. Fujita, B. Ding, S. Shiratori, Fabrication of Layer-by-Layer Self-Assembly Films Using Roll-to-Roll Process, *Japanese Journal of Applied Physics*, 44 (2005) L126.
- [11] K. Ren, L. Fourel, C.G. Rouvière, C. Albiges-Rizo, C. Picart, Manipulation of the adhesive behaviour of skeletal muscle cells on soft and stiff polyelectrolyte multilayers, *Acta Biomater.* 6 (2010) 4238-4248.
- [12] E. Lojou, P. Bianco, Buildup of polyelectrolyte-protein multilayer assemblies on gold electrodes. Role of the hydrophobic effect, *Langmuir : the ACS journal of surfaces and colloids*, 20 (2004) 748-755.
- [13] E.M. Saurer, C.M. Jewell, D.A. Roenneburg, S.L. Bechler, J.R. Torrealba, T.A. Hacker, D.M. Lynn, Polyelectrolyte Multilayers Promote Stent-Mediated Delivery of DNA to Vascular Tissue, *Biomacromolecules*, 14 (2013) 1696-1704.
- [14] L.C. Bradley, M. Gupta, Formation of Heterogeneous Polymer Films via Simultaneous or Sequential Depositions of Soluble and Insoluble Monomers onto Ionic Liquids, *Langmuir*, 29 (2013) 10448-10454.
- [15] J. de Groot, M. Dong, W.M. de Vos, K. Nijmeijer, Building Polyzwitterion-Based Multilayers for Responsive Membranes, *Langmuir*, 30 (2014) 5152-5161.
- [16] J. Seo, J.L. Lutkenhaus, J. Kim, P.T. Hammond, K. Char, Effect of the layer-by-layer (LbL) deposition method on the surface morphology and wetting behavior of hydrophobically modified PEO and PAA LbL films, *Langmuir*, 24 (2008) 7995-8000.
- [17] A.L. Larkin, R.M. Davis, P. Rajagopalan, Biocompatible, Detachable, and Free-Standing Polyelectrolyte Multilayer Films, *Biomacromolecules*, 11 (2010) 2788-2796.
- [18] C. Holmes, J. Daoud, P.O. Bagnaninchi, M. Tabrizian, Polyelectrolyte Multilayer Coating of 3D Scaffolds Enhances Tissue Growth and Gene Delivery: Non-Invasive and Label-Free Assessment, *Adv. Healthc. Mater.*, 3 (2014) 572-580.
- [19] P.C. DeMuth, A.V. Li, P. Abbink, J. Liu, H. Li, K.A. Stanley, K.M. Smith, C.L. Lavine, M.S. Seaman, J.A. Kramer, A.D. Miller, W. Abraham, H. Suh, J. Elkhader, P.T. Hammond, D.H. Barouch, D.J. Irvine, Vaccine delivery with microneedle skin patches in nonhuman primates, *Nat Biotechnol*, 31 (2013) 1082-1085.
- [20] E.M. Saurer, R.M. Flessner, S.P. Sullivan, M.R. Prausnitz, D.M. Lynn, Layer-by-Layer Assembly of DNA- and Protein-Containing Films on Microneedles for Drug Delivery to the Skin, *Biomacromolecules*, 11 (2010) 3136-3143.
- [21] P.C. DeMuth, X. Su, R.E. Samuel, P.T. Hammond, D.J. Irvine, Nano-Layered Microneedles for Transcutaneous Delivery of Polymer Nanoparticles and Plasmid DNA, *Adv. Mater.*, 22 (2010) 4851-4856.
- [22] Y. Kim, A.L. Larkin, R.M. Davis, P. Rajagopalan, The Design of In Vitro Liver Sinusoid Mimics Using Chitosan-Hyaluronic Acid Polyelectrolyte Multilayers, *Tissue Engineering Part A*, 16 (2010) 2731-2741.
- [23] B. Wang, CHAPTER 2 Functional Multilayered Polyelectrolyte Assemblies on Biological Cells, in: *Cell Surface Engineering: Fabrication of Functional Nanoshells*, The Royal Society of Chemistry, 2014, pp. 4-27.
- [24] R. Georgieva, S. Moya, E. Donath, H. Baumler, Permeability and conductivity of red blood cell templated polyelectrolyte capsules coated with supplementary layers, *Langmuir*, 20 (2004) 1895-1900.
- [25] H. Ai, Layer-by-layer capsules for magnetic resonance imaging and drug delivery, *Adv Drug Deliver Rev*, 63 (2011) 772-788.
- [26] F. Ridi, M. Bonini, P. Baglioni, Magneto-responsive nanocomposites: Preparation and integration of magnetic nanoparticles into films, capsules, and gels, *Adv. Colloid Interface Sci.*, 207 (2014) 3-13.
- [27] R.L. Muhlbauer, T.L. Pruyn, W.T. Puckett, R.A. Gerhardt, Effect of graphitic filler size and shape on the microstructure, electrical percolation behavior and thermal properties of nanostructured multilayered carbon films deposited onto paper substrates, *J. Mater. Res.*, 29 (2014) 472-484.
- [28] C.Q. Peng, Y.S. Thio, R.A. Gerhardt, Conductive paper fabricated by layer-by-layer assembly of polyelectrolytes and ITO nanoparticles, *Nanotechnology*, 19 (2008).

- [29] P. Yang, N. Murase, Preparation and photoluminescence of SiO₂-CdTe multilayer film by layer-by-layer self-assembly, *Journal of Physics: Conference Series*, 152 (2009) 012009.
- [30] R.C. Smith, M. Riollano, A. Leung, P.T. Hammond, Layer-by-Layer Platform Technology for Small-Molecule Delivery, *Angewandte Chemie-International Edition*, 48 (2009) 8974-8977.
- [31] G.K. Such, A.P.R. Johnston, F. Caruso, Engineered hydrogen-bonded polymer multilayers: from assembly to biomedical applications, *Chem. Soc. Rev.*, 40 (2011) 19-29.
- [32] E. Kharlampieva, V. Kozlovskaya, S.A. Sukhishvili, Layer-by-Layer Hydrogen-Bonded Polymer Films: From Fundamentals to Applications, *Adv. Mater.*, 21 (2009) 3053-3065.
- [33] M. Matsusaki, H. Ajiro, T. Kida, T. Serizawa, M. Akashi, Layer-by-Layer Assembly Through Weak Interactions and Their Biomedical Applications, *Adv. Mater.*, 24 (2012) 454-474.
- [34] J. Zhao, F.S. Pan, P. Li, C.H. Zhao, Z.Y. Jiang, P. Zhang, X.Z. Cao, Fabrication of Ultrathin Membrane via Layer-by-Layer Self-assembly Driven by Hydrophobic Interaction Towards High Separation Performance, *ACS Appl. Mater. Interfaces*, 5 (2013) 13275-13283.
- [35] T. Serizawa, S. Hashiguchi, M. Akashi, Stepwise Assembly of Ultrathin Poly(vinyl alcohol) Films on a Gold Substrate by Repetitive Adsorption/Drying Processes, *Langmuir*, 15 (1999) 5363-5368.
- [36] T. Akagi, T. Fujiwara, M. Akashi, Inkjet Printing of Layer-by-Layer Assembled Poly(lactide) Stereocomplex with Encapsulated Proteins, *Langmuir*, 30 (2014) 1669-1676.
- [37] T. Serizawa, K. Hamada, M. Akashi, Polymerization within a molecular-scale stereoregular template, *Nature*, 429 (2004) 52-55.
- [38] D. Kamei, H. Ajiro, C. Hongo, M. Akashi, Solvent Effects on Isotactic Poly(methyl methacrylate) Crystallization and Syndiotactic Poly(methacrylic acid) Incorporation in Porous Thin Films Prepared by Stepwise Stereocomplex Assembly, *Langmuir*, 25 (2008) 280-285.
- [39] Y. Shimazaki, S. Ito, N. Tsutsumi, Adsorption-Induced Second Harmonic Generation from the Layer-by-Layer Deposited Ultrathin Film Based on the Charge-Transfer Interaction, *Langmuir*, 16 (2000) 9478-9482.
- [40] Z. Liu, Y. Yi, J. Gauczinski, H. Xu, M. Schönhoff, X. Zhang, Surface Molecular Imprinted Layer-by-Layer Film Attached to a Porous Membrane for Selective Filtration, *Langmuir*, 27 (2011) 11806-11812.
- [41] O. Crespo-Biel, B. Dordi, D.N. Reinhoudt, J. Huskens, Supramolecular layer-by-layer assembly: Alternating adsorptions of guest- and host-functionalized molecules and particles using multivalent supramolecular interactions, *J. Am. Chem. Soc.*, 127 (2005) 7594-7600.
- [42] C. Li, G.-F. Luo, H.-Y. Wang, J. Zhang, Y.-H. Gong, S.-X. Cheng, R.-X. Zhuo, X.-Z. Zhang, Host-Guest Assembly of pH-Responsive Degradable Microcapsules with Controlled Drug Release Behavior, *The Journal of Physical Chemistry C*, 115 (2011) 17651-17659.
- [43] A. Van der Heyden, M. Wilczewski, P. Labbe, R. Auzely, Multilayer films based on host-guest interactions between biocompatible polymers, *Chem. Commun.*, (2006) 3220-3222.
- [44] S. Takahashi, K. Sato, J.-i. Anzai, Layer-by-layer construction of protein architectures through avidin-biotin and lectin-sugar interactions for biosensor applications, *Anal Bioanal Chem*, 402 (2012) 1749-1758.
- [45] T. Crouzier, C.H. Beckwith, K. Ribbeck, Mucin Multilayers Assembled through Sugar-Lectin Interactions, *Biomacromolecules*, 13 (2012) 3401-3408.
- [46] K. Müller, J.F. Quinn, A.P.R. Johnston, M. Becker, A. Greiner, F. Caruso, Polyelectrolyte Functionalization of Electrospun Fibers, *Chem Mater*, 18 (2006) 2397-2403.
- [47] A.P.R. Johnston, E.S. Read, F. Caruso, DNA Multilayer Films on Planar and Colloidal Supports: Sequential Assembly of Like-Charged Polyelectrolytes, *Nano Lett.*, 5 (2005) 953-956.
- [48] D.E. Bergbreiter, K.-S. Liao, Covalent layer-by-layer assembly-an effective, forgiving way to construct functional robust ultrathin films and nanocomposites, *Soft Matter*, 5 (2009) 23-28.
- [49] C.R. Kinnane, K. Wark, G.K. Such, A.P.R. Johnston, F. Caruso, Peptide-Functionalized, Low-Biofouling Click Multilayers for Promoting Cell Adhesion and Growth, *Small*, 5 (2009) 444-448.
- [50] Y.-h. Li, D. Wang, J.M. Buriak, Molecular Layer Deposition of Thiol-Ene Multilayers on Semiconductor Surfaces, *Langmuir*, 26 (2010) 1232-1238.
- [51] Z.Q. Tou, C.C. Chan, S. Leong, A fiber-optic pH sensor based on polyelectrolyte multilayers embedded with gold nanoparticles, *Measurement Science & Technology*, 25 (2014) 7.
- [52] D. Sarauli, C.G. Xu, B. Dietzel, B. Schulz, F. Lisdat, A multilayered sulfonated polyaniline network with entrapped pyrroloquinoline quinone-dependent glucose dehydrogenase: tunable direct bioelectrocatalysis, *Journal of Materials Chemistry B*, 2 (2014) 3196-3203.
- [53] J. Luo, Y.Z. Chen, Q. Ma, R. Liu, X.Y. Liu, Layer-by-layer assembled ionic-liquid functionalized graphene-polyaniline nanocomposite with enhanced electrochemical sensing properties, *J. Mater. Chem. C*, 2 (2014) 4818-4827.
- [54] G.A. Evtugyn, V.B. Stepanova, A.V. Porfireva, A.I. Zamaleeva, R.R. Fakhrullin, Electrochemical DNA Sensors Based on Nanostructured Organic Dyes/DNA/Polyelectrolyte Complexes, *J. Nanosci. Nanotechnol.*, 14 (2014) 6738-6747.
- [55] W.X. Xu, X.F. Li, J.Y. Cao, H.Z. Zhang, H.M. Zhang, Membranes with well-defined ions transport channels fabricated via solvent-responsive layer-by-layer assembly method for vanadium flow battery, *Sci Rep*, 4 (2014) 9.
- [56] N. Joseph, P. Ahmadiannamini, R. Hoogenboom, I.F.J. Vankelecom, Layer-by-layer preparation of polyelectrolyte multilayer membranes for separation, *Polymer Chemistry*, 5 (2014) 1817-1831.

- [57] X. Wang, N. Xia, L. Liu, Boronic Acid-Based Approach for Separation and Immobilization of Glycoproteins and Its Application in Sensing, *International Journal of Molecular Sciences*, 14 (2013) 20890-20912.
- [58] J.H. Park, B.S. Kim, Y.C. Yoo, M.S. Khil, H.Y. Kim, Enhanced mechanical properties of multilayer nano-coated electrospun nylon 6 fibers via a layer-by-layer self-assembly, *J. Appl. Polym. Sci.*, 107 (2008) 2211-2216.
- [59] L. Zhai, F.Ç. Cebeci, R.E. Cohen, M.F. Rubner, Stable Superhydrophobic Coatings from Polyelectrolyte Multilayers, *Nano Lett.*, 4 (2004) 1349-1353.
- [60] U. Manna, M.J. Kratochvil, D.M. Lynn, Superhydrophobic Polymer Multilayers that Promote the Extended, Long-Term Release of Embedded Water-Soluble Agents, *Adv. Mater.*, 25 (2013) 6405-6409.
- [61] X. Wang, Y. Wang, S. Bi, Y.G. Wang, X.G. Chen, L.Y. Qiu, J.Q. Sun, Optically Transparent Antibacterial Films Capable of Healing Multiple Scratches, *Adv. Funct. Mater.*, 24 (2014) 403-411.
- [62] J. Hiller, J.D. Mendelsohn, M.F. Rubner, Reversibly erasable nanoporous anti-reflection coatings from polyelectrolyte multilayers, *Nat Mater*, 1 (2002) 59-63.
- [63] D.V. Andreeva, E.V. Skorb, D.G. Shchukin, Layer-by-Layer Polyelectrolyte/Inhibitor Nanostructures for Metal Corrosion Protection, *ACS Appl. Mater. Interfaces*, 2 (2010) 1954-1962.
- [64] X. Zhu, D. Janczewski, S.S.C. Lee, S.L.-M. Teo, G.J. Vancso, Cross-Linked Polyelectrolyte Multi layers for Marine Antifouling Applications, *ACS Appl. Mater. Interfaces*, 5 (2013) 5961-5968.
- [65] Z.F. Dai, H. Mohwald, B. Tiersch, L. Dahne, Nanoengineering of polymeric capsules with a shell-in-shell structure, *Langmuir*, 18 (2002) 9533-9538.
- [66] A.M. Yu, I. Gentle, G.Q. Lu, F. Caruso, Nanoassembly of biocompatible microcapsules for urease encapsulation and their use as biomimetic reactors, *Chem. Commun.*, (2006) 2150-2152.
- [67] P.T. Hammond, Building biomedical materials layer-by-layer, *Mater Today*, 15 (2012) 196-206.
- [68] A. Shukla, B. Almeida, Advances in cellular and tissue engineering using layer-by-layer assembly, *Wiley interdisciplinary reviews. Nanomedicine and nanobiotechnology*, 6 (2014) 411-421.
- [69] L.L. del Mercato, M.M. Ferraro, F. Baldassarre, S. Mancarella, V. Greco, R. Rinaldi, S. Leporatti, Biological applications of LbL multilayer capsules: From drug delivery to sensing, *Adv. Colloid Interface Sci.*, 207 (2014) 139-154.
- [70] B.M. Wohl, J.F.J. Engbersen, Responsive layer-by-layer materials for drug delivery, *J Control Release*, 158 (2012) 2-14.
- [71] G. Decher, J.D. Hong, J. Schmitt, BUILDUP OF ULTRATHIN MULTILAYER FILMS BY A SELF-ASSEMBLY PROCESS .3. CONSECUTIVELY ALTERNATING ADSORPTION OF ANIONIC AND CATIONIC POLYELECTROLYTES ON CHARGED SURFACES, *Thin Solid Films*, 210 (1992) 831-835.
- [72] S.S. Ono, G. Decher, Preparation of Ultrathin Self-Standing Polyelectrolyte Multilayer Membranes at Physiological Conditions Using pH-Responsive Film Segments as Sacrificial Layers, *Nano Letters*, 6 (2006) 592-598.
- [73] J. Jeon, V. Panchagnula, J. Pan, A.V. Dobrynin, Molecular Dynamics Simulations of Multilayer Films of Polyelectrolytes and Nanoparticles, *Langmuir*, 22 (2006) 4629-4637.
- [74] C. Peng, Y.S. Thio, R.A. Gerhardt, Effect of Precursor-Layer Surface Charge on the Layer-by-Layer Assembly of Polyelectrolyte/Nanoparticle Multilayers, *Langmuir*, 28 (2011) 84-91.
- [75] Y. Li, X. Wang, J. Sun, Layer-by-layer assembly for rapid fabrication of thick polymeric films, *Chem. Soc. Rev.*, 41 (2012) 5998-6009.
- [76] J. Schmitt, T. Grunewald, G. Decher, P.S. Pershan, K. Kjaer, M. Losche, INTERNAL STRUCTURE OF LAYER-BY-LAYER ADSORBED POLYELECTROLYTE FILMS - A NEUTRON AND X-RAY REFLECTIVITY STUDY, *Macromolecules*, 26 (1993) 7058-7063.
- [77] B.F. Abu-Sharkh, Structure and mechanism of formation of polyelectrolyte multilayers, *Polymer*, 47 (2006) 3674-3680.
- [78] M. Castelnovo, J.F. Joanny, Formation of polyelectrolyte multilayers, *Langmuir*, 16 (2000) 7524-7532.
- [79] G. Ladam, P. Schaad, J.C. Voegel, P. Schaaf, G. Decher, F. Cuisinier, In Situ Determination of the Structural Properties of Initially Deposited Polyelectrolyte Multilayers, *Langmuir*, 16 (1999) 1249-1255.
- [80] G. Decher, Fuzzy nanoassemblies: Toward layered polymeric multicomposites, *Science*, 277 (1997) 1232-1237.
- [81] D.L. Elbert, C.B. Herbert, J.A. Hubbell, Thin Polymer Layers Formed by Polyelectrolyte Multilayer Techniques on Biological Surfaces, *Langmuir*, 15 (1999) 5355-5362.
- [82] N. Laugel, C. Betscha, M. Winterhalter, J.-C. Voegel, P. Schaaf, V. Ball, Relationship between the Growth Regime of Polyelectrolyte Multilayers and the Polyanion/Polycation Complexation Enthalpy, *The Journal of Physical Chemistry B*, 110 (2006) 19443-19449.
- [83] R.A. McAloney, M. Sinyor, V. Dudnik, M.C. Goh, Atomic Force Microscopy Studies of Salt Effects on Polyelectrolyte Multilayer Film Morphology, *Langmuir*, 17 (2001) 6655-6663.
- [84] B. Schoeler, E. Poptoshev, F. Caruso, Growth of Multilayer Films of Fixed and Variable Charge Density Polyelectrolytes: Effect of Mutual Charge and Secondary Interactions, *Macromolecules*, 36 (2003) 5258-5264.
- [85] D.M. DeLongchamp, M. Kastantin, P.T. Hammond, High-contrast electrochromism from layer-by-layer polymer films, *Chem Mater*, 15 (2003) 1575-1586.
- [86] C. Jiang, X. Liu, C. Luo, Y. Zhang, L. Shao, F. Shi, Controlled exponential growth in layer-by-layer multilayers using high gravity fields, *Journal of Materials Chemistry A*, 2 (2014) 14048-14053.
- [87] P. Lavalle, C. Picart, J. Mutterer, C. Gergely, H. Reiss, J.C. Voegel, B. Senger, P. Schaaf, Modeling the buildup of polyelectrolyte multilayer films having exponential growth, *J. Phys. Chem. B*, 108 (2004) 635-648.

- [88] C. Picart, J. Mutterer, L. Richert, Y. Luo, G.D. Prestwich, P. Schaaf, J.C. Voegel, P. Lavalle, Molecular basis for the explanation of the exponential growth of polyelectrolyte multilayers, *Proceedings of the National Academy of Sciences of the United States of America*, 99 (2002) 12531-12535.
- [89] H.W. Jomaa, J.B. Schlenoff, Accelerated exchange in polyelectrolyte multilayers by "catalytic" polyvalent ion pairing, *Langmuir*, 21 (2005) 8081-8084.
- [90] P. Lavalle, C. Gergely, F.J.G. Cuisinier, G. Decher, P. Schaaf, J.C. Voegel, C. Picart, Comparison of the Structure of Polyelectrolyte Multilayer Films Exhibiting a Linear and an Exponential Growth Regime: An in Situ Atomic Force Microscopy Study, *Macromolecules*, 35 (2002) 4458-4465.
- [91] N.S. Zacharia, D.M. DeLongchamp, M. Modestino, P.T. Hammond, Controlling Diffusion and Exchange in Layer-by-Layer Assemblies, *Macromolecules*, 40 (2007) 1598-1603.
- [92] L. Richert, P. Lavalle, E. Payan, X.Z. Shu, G.D. Prestwich, J.-F. Stoltz, P. Schaaf, J.-C. Voegel, C. Picart, Layer by Layer Buildup of Polysaccharide Films: Physical Chemistry and Cellular Adhesion Aspects, *Langmuir*, 20 (2003) 448-458.
- [93] B. Sun, C.M. Jewell, N.J. Fredin, D.M. Lynn, Assembly of Multilayered Films Using Well-Defined, End-Labeled Poly(acrylic acid): Influence of Molecular Weight on Exponential Growth in a Synthetic Weak Polyelectrolyte System, *Langmuir*, 23 (2007) 8452-8459.
- [94] E.J. Calvo, A. Wolosiuk, Donnan Permselectivity in Layer-by-Layer Self-Assembled Redox Polyelectrolyte Thin Films, *J. Am. Chem. Soc.*, 124 (2002) 8490-8497.
- [95] N. Laugel, F. Boulmedais, A.E. El Haitami, P. Rabu, G. Rogez, J.-C. Voegel, P. Schaaf, V. Ball, Tunable Synthesis of Prussian Blue in Exponentially Growing Polyelectrolyte Multilayer Films†, *Langmuir*, 25 (2009) 14030-14036.
- [96] J.B. Schlenoff, H. Ly, M. Li, Charge and Mass Balance in Polyelectrolyte Multilayers, *Journal of the American Chemical Society*, 120 (1998) 7626-7634.
- [97] T.R. Farhat, J.B. Schlenoff, Doping-Controlled Ion Diffusion in Polyelectrolyte Multilayers: Mass Transport in Reluctant Exchangers, *J. Am. Chem. Soc.*, 125 (2003) 4627-4636.
- [98] M.A. Pechenkin, H. Mohwald, D.V. Volodkin, pH- and salt-mediated response of layer-by-layer assembled PSS/PAH microcapsules: fusion and polymer exchange, *Soft Matter*, 8 (2012) 8659-8665.
- [99] R. Zhang, K. Koehler, O. Kreft, A. Skirtach, H. Moehwald, G. Sukhorukov, Salt-induced fusion of microcapsules of polyelectrolytes, *Soft Matter*, 6 (2010) 4742-4747.
- [100] R.v. Klitzing, J.E. Wong, W. Jaeger, R. Steitz, Short range interactions in polyelectrolyte multilayers, *Current Opinion in Colloid & Interface Science*, 9 (2004) 158-162.
- [101] E. Tjipto, J.F. Quinn, F. Caruso, Assembly of Multilayer Films from Polyelectrolytes Containing Weak and Strong Acid Moieties, *Langmuir*, 21 (2005) 8785-8792.
- [102] M. Salomäki, P. Tervasmäki, S. Areva, J. Kankare, The Hofmeister Anion Effect and the Growth of Polyelectrolyte Multilayers, *Langmuir*, 20 (2004) 3679-3683.
- [103] V. Ball, J.-C. Voegel, P. Schaaf, Effect of Thiocyanate Counterion Condensation on Poly(allylamine hydrochloride) Chains on the Buildup and Permeability of Polystyrenesulfonate/Polyallylamine Polyelectrolyte Multilayers, *Langmuir*, 21 (2005) 4129-4137.
- [104] C.S. Hajicharalambous, J. Lichter, W.T. Hix, M. Swierczewska, M.F. Rubner, P. Rajagopalan, Nano- and sub-micron porous polyelectrolyte multilayer assemblies: Biomimetic surfaces for human corneal epithelial cells, *Biomaterials*, 30 (2009) 4029-4036.
- [105] M. Salomäki, T. Laiho, J. Kankare, Counteranion-Controlled Properties of Polyelectrolyte Multilayers, *Macromolecules*, 37 (2004) 9585-9590.
- [106] M. Salomäki, J. Kankare, Specific Anion Effect in Swelling of Polyelectrolyte Multilayers, *Macromolecules*, 41 (2008) 4423-4428.
- [107] M.M. Stevens, J.H. George, Exploring and engineering the cell surface interface, *Science*, 310 (2005) 1135-1138.
- [108] D.E. Discher, P. Janmey, Y.L. Wang, Tissue cells feel and respond to the stiffness of their substrate, *Science*, 310 (2005) 1139-1143.
- [109] X. Gong, C. Gao, Influence of salt on assembly and compression of PDADMAC/PSSMA polyelectrolyte multilayers, *PCCP*, 11 (2009) 11577-11586.
- [110] W.W. Hu, S.L. Tsou, The effect of alginate on DNA delivery from layer-by-layer assembled films, *Carbohydr. Polym.*, 101 (2014) 240-248.
- [111] S.S. Shiratori, M.F. Rubner, pH-Dependent Thickness Behavior of Sequentially Adsorbed Layers of Weak Polyelectrolytes, *Macromolecules*, 33 (2000) 4213-4219.
- [112] S.A. Sukhishvili, S. Granick, Layered, Erasable Polymer Multilayers Formed by Hydrogen-Bonded Sequential Self-Assembly, *Macromolecules*, 35 (2001) 301-310.
- [113] O. Mermut, C.J. Barrett, Effects of Charge Density and Counterions on the Assembly of Polyelectrolyte Multilayers, *The Journal of Physical Chemistry B*, 107 (2003) 2525-2530.
- [114] S.A. Sukhishvili, S. Granick, Layered, erasable, ultrathin polymer films, *J. Am. Chem. Soc.*, 122 (2000) 9550-9551.
- [115] I. Erel-Unal, S.A. Sukhishvili, Hydrogen-Bonded Hybrid Multilayers: Film Architecture Controls Release of Macromolecules, *Macromolecules*, 41 (2008) 8737-8744.
- [116] I. Erel-Unal, S.A. Sukhishvili, Hydrogen-bonded multilayers of a neutral polymer and a polyphenol, *Macromolecules*, 41 (2008) 3962-3970.

- [117] S. Mehrotra, D. Lynam, R. Maloney, K.M. Pawelec, M.H. Tuszynski, I. Lee, C. Chan, J. Sakamoto, Time Controlled Protein Release from Layer-by-Layer Assembled Multilayer Functionalized Agarose Hydrogels, *Adv. Funct. Mater.*, 20 (2010) 247-258.
- [118] C.C. Buron, C. Filiâtre, F. Membrey, C. Bainier, D. Charrat, A. Foissy, Early steps in layer-by-layer construction of polyelectrolyte films: The transition from surface/polymer to polymer/polymer determining interactions, *J. Colloid Interface Sci.*, 314 (2007) 358-366.
- [119] R. Advincula, E. Aust, W. Meyer, W. Knoll, In Situ Investigations of Polymer Self-Assembly Solution Adsorption by Surface Plasmon Spectroscopy, *Langmuir*, 12 (1996) 3536-3540.
- [120] C. Peng, Y.S. Thio, R.A. Gerhardt, Effect of Precursor-Layer Surface Charge on the Layer-by-Layer Assembly of Polyelectrolyte/Nanoparticle Multilayers, *Langmuir*, 28 (2012) 84-91.
- [121] J.T. Zhang, L.S. Chua, D.M. Lynn, Multilayered thin films that sustain the release of functional DNA under physiological conditions, *Langmuir*, 20 (2004) 8015-8021.
- [122] C. Brunot, B. Grosogeat, C. Picart, C. Lagneau, N. Jaffrezic-Renault, L. Ponsonnet, Response of fibroblast activity and polyelectrolyte multilayer films coating titanium, *Dent. Mater.*, 24 (2008) 1025-1035.
- [123] M. Onda, Y. Lvov, K. Ariga, T. Kunitake, Sequential reaction and product separation on molecular films of glucoamylase and glucose oxidase assembled on an ultrafilter, *J. Ferment. Bioeng.*, 82 (1996) 502-506.
- [124] C. Brunot, L. Ponsonnet, C. Lagneau, P. Farge, C. Picart, B. Grosogeat, Cytotoxicity of polyethyleneimine (PEI), precursor base layer of polyelectrolyte multilayer films, *Biomaterials*, 28 (2007) 632-640.
- [125] D.V. Volodkin, A.I. Petrov, M. Prevot, G.B. Sukhorukov, Matrix Polyelectrolyte Microcapsules: New System for Macromolecule Encapsulation, *Langmuir*, 20 (2004) 3398-3406.
- [126] D.V. Volodkin, N.I. Larionova, G.B. Sukhorukov, Protein Encapsulation via Porous CaCO₃ Microparticles Templating, *Biomacromolecules*, 5 (2004) 1962-1972.
- [127] N.G. Balabushevich, O.P. Tiourina, D.V. Volodkin, N.I. Larionova, G.B. Sukhorukov, Loading the Multilayer Dextran Sulfate/Protamine Microsized Capsules with Peroxidase, *Biomacromolecules*, 4 (2003) 1191-1197.
- [128] O. Shchepelina, M.O. Lisunova, I. Drachuk, V.V. Tsukruk, Morphology and Properties of Microcapsules with Different Core Releases, *Chem Mater*, 24 (2012) 1245-1254.
- [129] X. Qiu, S. Leporatti, E. Donath, H. Möhwald, Studies on the Drug Release Properties of Polysaccharide Multilayers Encapsulated Ibuprofen Microparticles, *Langmuir*, 17 (2001) 5375-5380.
- [130] H. Ai, S.A. Jones, M.M. de Villiers, Y.M. Lvov, Nano-encapsulation of furosemide microcrystals for controlled drug release, *J Control Release*, 86 (2003) 59-68.
- [131] J. Almodóvar, L.W. Place, J. Gogolski, K. Erickson, M.J. Kipper, Layer-by-Layer Assembly of Polysaccharide-Based Polyelectrolyte Multilayers: A Spectroscopic Study of Hydrophilicity, Composition, and Ion Pairing, *Biomacromolecules*, 12 (2011) 2755-2765.
- [132] C.R. Wittmer, J.A. Phelps, W.M. Saltzman, P.R. Van Tassel, Fibronectin terminated multilayer films: Protein adsorption and cell attachment studies, *Biomaterials*, 28 (2007) 851-860.
- [133] C. Picart, R. Elkaim, L. Richert, T. Audoin, Y. Arntz, M.D. Cardoso, P. Schaaf, J.C. Voegel, B. Frisch, Primary cell adhesion on RGD-functionalized and covalently crosslinked thin polyelectrolyte multilayer films, *Adv. Funct. Mater.*, 15 (2005) 83-94.
- [134] P.-H. Chua, K.-G. Neoh, E.-T. Kang, W. Wang, Surface functionalization of titanium with hyaluronic acid/chitosan polyelectrolyte multilayers and RGD for promoting osteoblast functions and inhibiting bacterial adhesion, *Biomaterials*, 29 (2008) 1412-1421.
- [135] L.L. Han, Z.W. Mao, J.D. Wu, Y.Y. Zhang, C.Y. Gao, Influences of surface chemistry and swelling of salt-treated polyelectrolyte multilayers on migration of smooth muscle cells, *Journal of the Royal Society Interface*, 9 (2012) 3455-3468.
- [136] J.M. Garza, P. Schaaf, S. Muller, V. Ball, J.-F. Stoltz, J.-C. Voegel, P. Lavalle, Multicompartment Films Made of Alternate Polyelectrolyte Multilayers of Exponential and Linear Growth, *Langmuir*, 20 (2004) 7298-7302.
- [137] Y. Guan, S. Yang, Y. Zhang, J. Xu, C.C. Han, N.A. Kotov, Fabry-Perot Fringes and Their Application To Study the Film Growth, Chain Rearrangement, and Erosion of Hydrogen-Bonded PVPON/PAA Films, *The Journal of Physical Chemistry B*, 110 (2006) 13484-13490.
- [138] S.T. Dubas, J.B. Schlenoff, Swelling and Smoothing of Polyelectrolyte Multilayers by Salt, *Langmuir*, 17 (2001) 7725-7727.
- [139] R.A. McAloney, V. Dudnik, M.C. Goh, Kinetics of Salt-Induced Annealing of a Polyelectrolyte Multilayer Film Morphology, *Langmuir*, 19 (2003) 3947-3952.
- [140] X. Wang, F. Liu, X. Zheng, J. Sun, Water-Enabled Self-Healing of Polyelectrolyte Multilayer Coatings, *Angew. Chem. Int. Ed.*, 50 (2011) 11378-11381.
- [141] H. Mjahed, G. Cado, F. Boulmedais, B. Senger, P. Schaaf, V. Ball, J.-C. Voegel, Restructuring of exponentially growing polyelectrolyte multilayer films induced by salt concentration variations after film deposition, *J. Mater. Chem.*, 21 (2011) 8416-8421.
- [142] C.Y. Gao, S. Moya, H. Lichtenfeld, A. Casoli, H. Fiedler, E. Donath, H. Mohwald, The decomposition process of melamine formaldehyde cores: The key step in the fabrication of ultrathin polyelectrolyte multilayer capsules, *Macromolecular Materials and Engineering*, 286 (2001) 355-361.

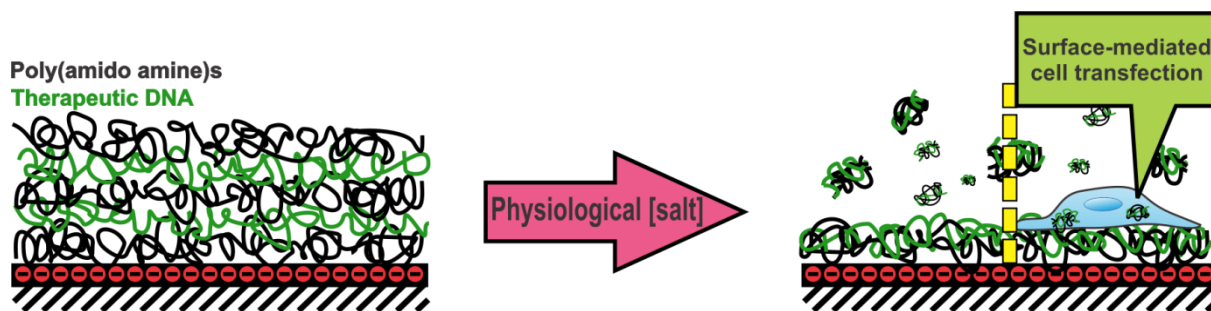
- [143] C. Déjugnat, G.B. Sukhorukov, pH-Responsive Properties of Hollow Polyelectrolyte Microcapsules Templated on Various Cores, *Langmuir*, 20 (2004) 7265-7269.
- [144] A.A. Antipov, G.B. Sukhorukov, Polyelectrolyte multilayer capsules as vehicles with tunable permeability, *Adv. Colloid Interface Sci.*, 111 (2004) 49-61.
- [145] Z. Gui, J. Qian, B. Du, M. Yin, Q. An, Fabrication of free-standing polyelectrolyte multilayer films: A method using polysulfobetaine-containing films as sacrificial layers, *J. Colloid Interface Sci.*, 340 (2009) 35-41.
- [146] R. Polak, T. Crouzier, R.M. Lim, K. Ribbeck, M.M. Beppu, R.N.M. Pitombo, R.E. Cohen, M.F. Rubner, Sugar-Mediated Disassembly of Mucin/Lectin Multilayers and Their Use as pH-Tolerant, On-Demand Sacrificial Layers, *Biomacromolecules*, 15 (2014) 3093-3098.
- [147] J.F. Quinn, F. Caruso, Multivalent-Ion-Mediated Stabilization of Hydrogen-Bonded Multilayers, *Adv. Funct. Mater.*, 16 (2006) 1179-1186.
- [148] K.C. Wood, H.F. Chuang, R.D. Batten, D.M. Lynn, P.T. Hammond, Controlling interlayer diffusion to achieve sustained, multiagent delivery from layer-by-layer thin films, *Proceedings of the National Academy of Sciences*, 103 (2006) 10207-10212.
- [149] W. Tong, C. Gao, Stable microcapsules assembled stepwise from weak polyelectrolytes followed by thermal crosslinking, *Polym. Adv. Technol.*, 16 (2005) 827-833.
- [150] M.C. Kittredge, T.S. Durst, K.W. Kittredge, Heat-induced cross-linking of nylon-like weak polyelectrolyte multilayer films: UV-visible studies of methylene blue loading and rates of release, *Thin Solid Films*, 518 (2010) 3949-3953.
- [151] M.L. Bruening, D.M. Sullivan, Enhancing the Ion-Transport Selectivity of Multilayer Polyelectrolyte Membranes, *Chemistry – A European Journal*, 8 (2002) 3832-3837.
- [152] L. Richert, A.J. Engler, D.E. Discher, C. Picart, Elasticity of native and cross-linked polyelectrolyte multilayer films, *Biomacromolecules*, 5 (2004) 1908-1916.
- [153] S.Y. Yang, D. Lee, R.E. Cohen, M.F. Rubner, Bioinert solution-cross-linked hydrogen-bonded multilayers on colloidal particles, *Langmuir*, 20 (2004) 5978-5981.
- [154] F. Gilde, O. Maniti, R. Guillot, J.F. Mano, D. Logeart-Avramoglou, F. Sailhan, C. Picart, Secondary Structure of rhBMP-2 in a Protective Biopolymeric Carrier Material, *Biomacromolecules*, 13 (2012) 3620-3626.
- [155] G.K. Such, J.F. Quinn, A. Quinn, E. Tjijto, F. Caruso, Assembly of Ultrathin Polymer Multilayer Films by Click Chemistry, *J. Am. Chem. Soc.*, 128 (2006) 9318-9319.
- [156] B.G. De Geest, W. Van Camp, F.E. Du Prez, S.C. De Smedt, J. Demeester, W.E. Hennink, Degradable Multilayer Films and Hollow Capsules via a 'Click' Strategy, *Macromol Rapid Comm*, 29 (2008) 1111-1118.
- [157] S.-F. Chong, R. Chandrawati, B. Städler, J. Park, J. Cho, Y. Wang, Z. Jia, V. Bulmus, T.P. Davis, A.N. Zelikin, F. Caruso, Stabilization of Polymer-Hydrogel Capsules via Thiol-Disulfide Exchange, *Small*, 5 (2009) 2601-2610.
- [158] S. Shu, X. Zhang, Z. Wu, Z. Wang, C. Li, Gradient cross-linked biodegradable polyelectrolyte nanocapsules for intracellular protein drug delivery, *Biomaterials*, 31 (2010) 6039-6049.
- [159] W. Tong, C. Gao, H. Möhwald, Manipulating the Properties of Polyelectrolyte Microcapsules by Glutaraldehyde Cross-Linking, *Chem Mater*, 17 (2005) 4610-4616.
- [160] P. Liu, Stabilization of layer-by-layer engineered multilayered hollow microspheres, *Advances in Colloid and Interface Science*, 207 (2014) 178-188.
- [161] K.F. Ren, T. Crouzier, C. Roy, C. Picart, Polyelectrolyte multilayer films of controlled stiffness modulate myoblast cell differentiation, *Adv. Funct. Mater.*, 18 (2008) 1378-1389.
- [162] S.E. Burke, C.J. Barrett, pH-Dependent Loading and Release Behavior of Small Hydrophilic Molecules in Weak Polyelectrolyte Multilayer Films, *Macromolecules*, 37 (2004) 5375-5384.
- [163] G.B. Sukhorukov, A.A. Antipov, A. Voigt, E. Donath, H. Möhwald, pH-Controlled Macromolecule Encapsulation in and Release from Polyelectrolyte Multilayer Nanocapsules, *Macromol Rapid Comm*, 22 (2001) 44-46.
- [164] J.A. Hiller, M.F. Rubner, Reversible Molecular Memory and pH-Switchable Swelling Transitions in Polyelectrolyte Multilayers, *Macromolecules*, 36 (2003) 4078-4083.
- [165] S. Srivastava, V. Ball, P. Podsiadlo, J. Lee, P. Ho, N.A. Kotov, Reversible Loading and Unloading of Nanoparticles in "Exponentially" Growing Polyelectrolyte LBL Films, *Journal of the American Chemical Society*, 130 (2008) 3748-3749.
- [166] K. Ren, T. Crouzier, C. Roy, C. Picart, Polyelectrolyte multilayer films of controlled stiffness modulate myoblast cell differentiation, *Adv. Funct. Mater.*, 18 (2008) 1378-1389.
- [167] A. Schneider, G. Francius, R. Obeid, P. Schwinté, J. Hemmerlé, B. Frisch, P. Schaaf, J.-C. Voegel, B. Senger, C. Picart, Polyelectrolyte Multilayers with a Tunable Young's Modulus: Influence of Film Stiffness on Cell Adhesion, *Langmuir*, 22 (2005) 1193-1200.
- [168] L. Richert, P. Lavalle, D. Vautier, B. Senger, J.F. Stoltz, P. Schaaf, J.C. Voegel, C. Picart, Cell interactions with polyelectrolyte multilayer films, *Biomacromolecules*, 3 (2002) 1170-1178.
- [169] P. Tryoen-Toth, D. Vautier, Y. Haikel, J.C. Voegel, P. Schaaf, J. Chluba, J. Ogier, Viability, adhesion, and bone phenotype of osteoblast-like cells on polyelectrolyte multilayer films, *Journal of Biomedical Materials Research*, 60 (2002) 657-667.
- [170] J.M. Garza, N. Jessel, G. Ladam, V. Dupray, S. Muller, J.-F. Stoltz, P. Schaaf, J.-C. Voegel, P. Lavalle, Polyelectrolyte Multilayers and Degradable Polymer Layers as Multicompartment Films, *Langmuir*, 21 (2005) 12372-12377.

- [171] A.A. Antipov, G.B. Sukhorukov, S. Leporatti, I.L. Radtchenko, E. Donath, H. Möhwald, Polyelectrolyte multilayer capsule permeability control, *Colloids and Surfaces A: Physicochemical and Engineering Aspects*, 198-200 (2002) 535-541.
- [172] A.I. Petrov, A.A. Antipov, G.B. Sukhorukov, Base-acid equilibria in polyelectrolyte systems: From weak polyelectrolytes to interpolyelectrolyte complexes and multilayered polyelectrolyte shells, *Macromolecules*, 36 (2003) 10079-10086.
- [173] A.A. Antipov, G.B. Sukhorukov, Polyelectrolyte multilayer capsules as vehicles with tunable permeability, *Advances in Colloid and Interface Science*, 111 (2004) 49-61.
- [174] S.A. Sukhishvili, S. Granick, Layered, erasable polymer multilayers formed by hydrogen-bonded sequential self-assembly, *Macromolecules*, 35 (2002) 301-310.
- [175] K. Sato, K. Yoshida, S. Takahashi, J.-i. Anzai, pH- and sugar-sensitive layer-by-layer films and microcapsules for drug delivery, *Advanced Drug Delivery Reviews*, In Press, Corrected Proof (2011).
- [176] B.G. De Geest, R.E. Vandenbroucke, A.M. Guenther, G.B. Sukhorukov, W.E. Hennink, N.N. Sanders, J. Demeester, S.C. De Smedt, Intracellularly degradable polyelectrolyte microcapsules, *Advanced Materials*, 18 (2006) 1005-1009.
- [177] J. Zhang, D.M. Lynn, Ultrathin multilayered films assembled from "charge-shifting" cationic polymers: Extended, long-term release of plasmid DNA from surfaces, *Advanced Materials*, 19 (2007) 4218-4223.
- [178] X. Liu, J. Zhang, D.M. Lynn, Ultrathin multilayered films that promote the release of two DNA constructs with separate and distinct release profiles, *Advanced Materials*, 20 (2008) 4148-4153.
- [179] X. Liu, J. Zhang, D.M. Lynn, Polyelectrolyte Multilayers Fabricated from 'Charge-Shifting' Anionic Polymers: A New Approach to Controlled Film Disruption and the Release of Cationic Agents from Surfaces, *Soft Matter*, 4 (2008) 1688-1695.
- [180] B. Sun, D.M. Lynn, Release of DNA from polyelectrolyte multilayers fabricated using 'charge-shifting' cationic polymers: Tunable temporal control and sequential, multi-agent release, *Journal of Controlled Release*, 148 (2010) 91-100.
- [181] Y. Ma, W.F. Dong, M.A. Hempenius, H. Möhwald, G. Julius Vancso, Redox-controlled molecular permeability of composite-wall microcapsules, *Nature Materials*, 5 (2006) 724-729.
- [182] Y. Ma, W.-F. Dong, M.A. Hempenius, H. Mohwald, G.J. Vancso, Redox-controlled molecular permeability of composite-wall microcapsules, *Nat Mater*, 5 (2006) 724-729.
- [183] K.C. Wood, N.S. Zacharia, D.J. Schmidt, S.N. Wrightman, B.J. Andaya, P.T. Hammond, Electroactive controlled release thin films, *Proceedings of the National Academy of Sciences of the United States of America*, 105 (2008) 2280-2285.
- [184] K. Liang, G.K. Such, A.P.R. Johnston, Z. Zhu, H. Ejima, J.J. Richardson, J. Cui, F. Caruso, Endocytic pH-triggered degradation of nanoengineered multilayer capsules, *Advanced Materials*, 26 (2014) 1901-1905.
- [185] B.G. De Geest, A.M. Jonas, J. Demeester, S.C. De Smedt, Glucose-responsive polyelectrolyte capsules, *Langmuir*, 22 (2006) 5070-5074.
- [186] H. Fang, G. Kaur, B.H. Wang, Progress in boronic acid-based fluorescent glucose sensors, *J. Fluoresc.*, 14 (2004) 481-489.
- [187] H. Shibata, Y.J. Heo, T. Okitsu, Y. Matsunaga, T. Kawanishi, S. Takeuchi, Injectable hydrogel microbeads for fluorescence-based in vivo continuous glucose monitoring, *Proceedings of the National Academy of Sciences of the United States of America*, 107 (2010) 17894-17898.
- [188] M. Ikeda, K. Fukuda, T. Tanida, T. Yoshii, I. Hamachi, A supramolecular hydrogel containing boronic acid-appended receptor for fluorocolorimetric sensing of polyols with a paper platform, *Chem. Commun.*, 48 (2012) 2716-2718.
- [189] M.B. Lerner, N. Kybert, R. Mendoza, R. Villechenon, M.A.B. Lopez, A.T.C. Johnson, Scalable, non-invasive glucose sensor based on boronic acid functionalized carbon nanotube transistors, *Appl. Phys. Lett.*, 102 (2013).
- [190] C. Zhang, M.D. Losego, P.V. Braun, Hydrogel-Based Glucose Sensors: Effects of Phenylboronic Acid Chemical Structure on Response, *Chem Mater*, 25 (2013) 3239-3250.
- [191] D.G. Hall, *Boronic Acids - Preparation and applications in organic synthesis and medicine*, John Wiley & Sons, 2005.
- [192] J. Zhang, N.J. Fredin, J.F. Janz, B. Sun, D.M. Lynn, Structure/property relationships in erodible multilayered films: Influence of polycation structure on erosion profiles and the release of anionic polyelectrolytes, *Langmuir*, 22 (2006) 239-245.
- [193] E.M. Saurer, C.M. Jewell, J.M. Kuchenreuther, D.M. Lynn, Assembly of erodible, DNA-containing thin films on the surfaces of polymer microparticles: Toward a layer-by-layer approach to the delivery of DNA to antigen-presenting cells, *Acta Biomaterialia*, 5 (2009) 913-924.
- [194] J. Blacklock, H. Handa, D. Soundara Manickam, G. Mao, A. Mukhopadhyay, D. Oupicky, Disassembly of layer-by-layer films of plasmid DNA and reducible TAT polypeptide, *Biomaterials*, 28 (2007) 117-124.
- [195] J. Blacklock, Y.Z. You, Q.H. Zhou, G. Mao, D. Oupicky, Gene delivery in vitro and in vivo from bioreducible multilayered polyelectrolyte films of plasmid DNA, *Biomaterials*, 30 (2009) 939-950.
- [196] K. Ren, J. Ji, J. Shen, Tunable DNA release from cross-linked ultrathin DNA/PLL multilayered films, *Bioconjugate Chemistry*, 17 (2006) 77-83.
- [197] C.J. Ochs, G.K. Such, B. Städler, F. Caruso, Low-fouling, biofunctionalized, and biodegradable click capsules, *Biomacromolecules*, 9 (2008) 3389-3396.
- [198] C.J. Ochs, G.K. Such, Y. Yan, M.P. Van Koeveden, F. Caruso, Biodegradable click capsules with engineered drug-loaded multilayers, *ACS Nano*, 4 (2010) 1653-1663.
- [199] C.J. Ochs, G.K. Such, F. Caruso, Modular assembly of layer-by-layer capsules with tailored degradation profiles, *Langmuir*, 27 (2011) 1275-1280.
- [200] T. Borodina, E. Markvicheva, S. Kunizhev, H. Möhwald, G.B. Sukhorukov, O. Kreft, Controlled release of DNA from self-degrading microcapsules, *Macromolecular Rapid Communications*, 28 (2007) 1894-1899.

- [201] T. Serizawa, M. Yamaguchi, M. Akashi, Time-controlled desorption of ultrathin polymer films triggered by enzymatic degradation, *Angewandte Chemie - International Edition*, 42 (2003) 1115-1118.
- [202] C. Picart, A. Schneider, O. Etienne, J. Mutterer, P. Schaaf, C. Egles, N. Jessel, J.C. Voegel, Controlled degradability of polysaccharide multilayer films in vitro and in vivo, *Adv. Funct. Mater.*, 15 (2005) 1771-1780.
- [203] Y. Itoh, M. Matsusaki, T. Kida, M. Akashi, Enzyme-responsive release of encapsulated proteins from biodegradable hollow capsules, *Biomacromolecules*, 7 (2006) 2715-2718.
- [204] A. Szarapak, D. Cui, F. Dubreuil, B.G. De Geest, L.J. De Cock, C. Picart, R. Auzély-Velty, Designing hyaluronic acid-based layer-by-layer capsules as a carrier for intracellular drug delivery, *Biomacromolecules*, 11 (2010) 713-720.
- [205] K. Ariga, Q. Ji, T. Mori, M. Naito, Y. Yamauchi, H. Abe, J.P. Hill, Enzyme nanoarchitectonics: organization and device application, *Chem. Soc. Rev.*, 42 (2013) 6322-6345.
- [206] G. Decher, M. Ecker, J. Schmitt, B. Struth, Layer-by-layer assembled multicomposite films, *Current Opinion in Colloid and Interface Science*, 3 (1998) 32-39.
- [207] J.F. Rusling, E.G. Hvastkovs, D.O. Hull, J.B. Schenkman, Biochemical applications of ultrathin films of enzymes, polyions and DNA, *Chemical Communications*, (2008) 141-154.
- [208] S.O. Andreasen, B. Fejerskov, A.N. Zelikin, Biocatalytic polymer thin films: optimization of the multilayered architecture towards in situ synthesis of anti-proliferative drugs, *Nanoscale*, 6 (2014) 4131-4140.
- [209] L. Hosta-Rigau, P. Schattling, B.M. Teo, M.E. Lyngø, B. Städler, Recent progress of liposomes in nanomedicine, *J. Mat. Chem. B*, (2014).
- [210] B.M. Teo, L. Hosta-Rigau, M.E. Lyngø, B. Städler, Liposome-containing polymer films and colloidal assemblies towards biomedical applications, *Nanoscale*, 6 (2014) 6426-6433.
- [211] Z. Zhu, S.A. Sukhishvili, Layer-by-layer films of stimuli-responsive block copolymer micelles, *Journal of Materials Chemistry*, 22 (2012) 7667-7671.
- [212] S. Biggs, K. Sakai, T. Addison, A. Schmid, S.P. Armes, M. Vamvakaki, V. Bütün, G. Webber, Layer-by-layer formation of smart particle coatings using oppositely charged block copolymer micelles, *Advanced Materials*, 19 (2007) 247-250.
- [213] T. Addison, O.J. Cayre, S. Biggs, S.P. Armes, D. York, Incorporation of block copolymer micelles into multilayer films for use as nanodelivery systems, *Langmuir*, 24 (2008) 13328-13333.
- [214] T. Addison, O.J. Cayre, S. Biggs, S.P. Armes, D. York, Polymeric microcapsules assembled from a cationic/zwitterionic pair of responsive block copolymer micelles, *Langmuir*, 26 (2010) 6281-6286.
- [215] I. Erel, Z. Zhu, A. Zhuk, S.A. Sukhishvili, Hydrogen-bonded layer-by-layer films of block copolymer micelles with pH-responsive cores, *Journal of Colloid and Interface Science*, 355 (2011) 61-69.
- [216] J. Zhou, M.V. Pishko, J.L. Lutkenhaus, Thermoresponsive Layer-by-Layer Assemblies for Nanoparticle-Based Drug Delivery, *Langmuir*, 30 (2014) 5903-5910.
- [217] T. Liao, M.D. Moussallem, J. Kim, J.B. Schlenoff, T. Ma, N-isopropylacrylamide-based thermoresponsive polyelectrolyte multilayer films for human mesenchymal stem cell expansion, *Biotechnol. Progr.*, 26 (2010) 1705-1713.
- [218] M. Ciobanu, B. Heurtaut, P. Schultz, C. Ruhlmann, C.D. Muller, B. Frisch, Layersome: Development and optimization of stable liposomes as drug delivery system, *Int. J. Pharm.*, 344 (2007) 154-157.
- [219] M. Michel, Y. Arntz, G. Fleith, J. Toquant, Y. Haikel, J.-C. Voegel, P. Schaaf, V. Ball, Layer-by-Layer Self-Assembled Polyelectrolyte Multilayers with Embedded Liposomes: Immobilized Submicronic Reactors for Mineralization, *Langmuir*, 22 (2006) 2358-2364.
- [220] A.D. Keefe, S. Pai, A. Ellington, Aptamers as therapeutics, *Nat Rev Drug Discov*, 9 (2010) 537-550.
- [221] K.-M. Song, S. Lee, C. Ban, Aptamers and Their Biological Applications, *Sensors*, 12 (2012) 612-631.
- [222] Y. Sultan, M.C. Derosa, Target binding influences permeability in aptamer-polyelectrolyte microcapsules, *Small*, 7 (2011) 1219-1226.
- [223] X. Zhang, D. Chabot, Y. Sultan, C. Monreal, M.C. Derosa, Target-molecule-triggered rupture of aptamer-encapsulated polyelectrolyte microcapsules, *ACS Applied Materials and Interfaces*, 5 (2013) 5500-5507.
- [224] B. Malile, J.I.L. Chen, Morphology-based plasmonic nanoparticle sensors: Controlling etching kinetics with target-responsive permeability gate, *Journal of the American Chemical Society*, 135 (2013) 16042-16045.
- [225] H.H. Dam, F. Caruso, Construction and Degradation of Polyrotaxane Multilayers, *Adv. Mater.*, 23 (2011) 3026-3029.
- [226] B.G. De Geest, W. Van Camp, F.E. Du Prez, S.C. De Smedt, J. Demeester, W.E. Hennink, Degradable multilayer films and hollow capsules via a 'click' strategy, *Macromolecular Rapid Communications*, 29 (2008) 1111-1118.
- [227] K. Sato, Y. Imoto, J. Sugama, S. Seki, H. Inoue, T. Odagiri, T. Hoshi, J.I. Anzai, Sugar-induced disintegration of layer-by-layer assemblies composed of concanavalin A and glycogen, *Langmuir*, 21 (2005) 797-799.
- [228] K. Sato, D. Kodama, J.I. Anzai, Sugar-sensitive thin films composed of concanavalin A and sugar-bearing polymers, *Analytical Sciences*, 21 (2005) 1375-1378.
- [229] T. Levy, C. Déjugnat, G.B. Sukhorukov, Polymer microcapsules with carbohydrate-sensitive properties, *Adv. Funct. Mater.*, 18 (2008) 1586-1594.
- [230] H. Inoue, K. Sato, J.I. Anzai, Disintegration of layer-by-layer assemblies composed of 2-iminobiotin-labeled poly(ethyleneimine) and avidin, *Biomacromolecules*, 6 (2005) 27-29.
- [231] Z. Ding, Y. Guan, Y. Zhang, X.X. Zhu, Layer-by-layer multilayer films linked with reversible boronate ester bonds with glucose-sensitivity under physiological conditions, *Soft Matter*, 5 (2009) 2302-2309.

- [232] H. Krass, G. Papastavrou, D.G. Kurth, Layer-by-layer self-assembly of a polyelectrolyte bearing metal ion coordination and electrostatic functionality, *Chemistry of Materials*, 15 (2003) 196-203.
- [233] A. Van Der Heyden, M. Wilczewski, P. Labbé, R. Auzély, Multilayer films based on host-guest interactions between biocompatible polymers, *Chemical Communications*, (2006) 3220-3222.
- [234] T. Torring, N.V. Voigt, J. Nangreave, H. Yan, K.V. Gothelf, DNA origami: a quantum leap for self-assembly of complex structures, *Chem. Soc. Rev.*, 40 (2011) 5636-5646.
- [235] I. Saaem, T.H. LaBean, Overview of DNA origami for molecular self-assembly, *Wiley Interdisciplinary Reviews: Nanomedicine and Nanobiotechnology*, 5 (2013) 150-162.
- [236] B. Sacca, C.M. Niemeyer, DNA Origami: The Art of Folding DNA, *Angewandte Chemie-International Edition*, 51 (2012) 58-66.
- [237] A.P.R. Johnston, L. Lee, Y. Wang, F. Caruso, Controlled degradation of dna capsules with engineered restriction-enzyme cut sites, *Small*, 5 (2009) 1418-1421.
- [238] A.L. Becker, A.P.R. Johnston, F. Caruso, Peptide nucleic acid films and capsules: assembly and enzymatic degradation, *Macromolecular Bioscience*, 10 (2010) 488-495.
- [239] L. Lee, A.P.R. Johnston, F. Caruso, Programmed degradation of DNA multilayer films, *Small*, 10 (2014) 2902-2909.
- [240] Q. Zhao, B. Han, Z. Wang, C. Gao, C. Peng, J. Shen, Hollow chitosan-alginate multilayer microcapsules as drug delivery vehicle: doxorubicin loading and in vitro and in vivo studies, *Nanomedicine: Nanotechnology, Biology and Medicine*, 3 (2007) 63-74.
- [241] L. Yu, Y. Gao, X. Yue, S. Liu, Z. Dai, Novel Hollow Microcapsules Based on Iron-Heparin Complex Multilayers, *Langmuir*, 24 (2008) 13723-13729.

ABSTRACT



Dip-coated multilayered thin films of poly(amido amine)s (PAAs) and DNA have been developed to provide surfaces with cell-transfecting capabilities. Three types of PAAs, differing in side chain functional groups, were synthesized and characterized for their properties in forming multilayered structures with ultrasonicated calf thymus DNA (CTDNA) as model DNA. All three polymers display multilayer build-up in linear profiles as demonstrated by UV spectroscopy. More highly charged side chains were found to provide the lowest deposition of DNA. The surface profiles of the obtained films were investigated by atomic force microscopy (AFM) and static water contact angle measurements to reveal complete surface coverage after at least four layer pair depositions, where alternating patterns of surface profiles were observed depending on whether the cationic polymer or the anionic DNA layer was on top. The stability of the formed surfaces was investigated *in vitro* under physiological and reductive conditions. Owing to the presence of disulfide bonds in the PAA main chain, the films were readily degraded in the presence of 1.0 mM of DTT *in vitro*. Under non-reductive physiological conditions, two of the thicker films underwent thermodynamic rearrangement, which resulted in release of approximately half of the incorporated material within one hour, which was caused by the physiological salt concentration. Further, this unpacking phenomenon proved useful in transfecting COS-7 cells seeded on top of these multilayers containing functional plasmid DNA encoding for green fluorescence protein (GFP). Two out of the three different multilayers facilitated good COS-7 cell attachment, proliferation, and transfection *in vitro* within two days of culture. Fluorescence staining further revealed the presence of DNA-containing released film material among cultured cells. The present work demonstrates the possibility of coating surfaces with thin films that are conveniently adjustable in thickness and amount of active agent to provide cell-transfecting functionality. In this manner transfection can be achieved by simply culturing cells on multilayer-coated surface in their optimal culture condition (in the presence of serum) and without the need of removing transfection agent to avoid cytotoxicity.

[†] Sry D. Hujaya, Jos M.J. Paulusse, Johan F.J. Engbersen, submitted for publication.

3.1 INTRODUCTION

Multilayered thin films containing functional DNA have been of great interest during the past two decades in parallel to the ever-growing interest in the layer-by-layer (LbL) assembly technique in various fields [1]. The possibility to fabricate intricate multilayered structures within nanometer range precision, combined with the versatility of the fabrication technique, have made LbL assembly in the biomedical field an interesting option to easily modify the surface of biomedical devices [2], not only to enhance their performance but also to add additional functionality for therapeutic effect.

Due to the inherent properties of DNA as a natural biological compound, multilayers containing DNA have been investigated for their possibility of providing relatively low-immunogenic coatings [3] and surface-mediated cell transfection on various substrates [4-7]. Multilayers containing a top DNA layer have shown significant increase in primary rat dermal fibroblasts proliferation as compared to non-coated glass surfaces *in vitro*, while *in vivo* tissue response studies also showed that the DNA-coatings are histocompatible without showing signs of inflammation or adverse reactions [3].

Another key parameter in multilayered systems containing DNA is the polyelectrolyte counterpart. Natural polyelectrolytes such as chitosan [8] as well as synthetic polymers such as poly(ethylene imine) (PEI) [9] and poly(allylamine hydrochloride) (PAH) [10] have been successfully incorporated into multilayered systems complementing also their widely studied potency in forming polyplexes with DNA. Multilayers composed of DNA with more than a single type of polyelectrolyte have also been developed where highly-studied polyelectrolytes such as PEI, PAH, and polystyrene sulfonate (PSS) are used mostly for their well-known ability to form stable precursor layers [11, 12] or to provide further distinction in the multilayer architecture and/or enhanced stability [13]. In addition to directly depositing DNA from a DNA solution, optimized cellular uptake of functional DNA has also been achieved by packing DNA in a liposome system [14, 15] or precomplexing DNA with known polyelectrolytes such as PEI and chitosan to form a polyplex prior to the deposition step [16, 17].

Poly(amido amine)s (PAA) denote a class of biodegradable polymers, which has been shown to be able to complex biotherapeutics such as proteins [18], plasmid DNA (pDNA) [19-21], and small interfering RNA (siRNA) [22] with relatively lower toxicity as compared to the standard PEI. The inherent peptidomimetic structure provides these polymers with biocompatibility and degradability while the presence of amines provides the necessary positive charges for the interaction with DNA. Furthermore, the versatility of the synthesis and possibilities to incorporate a wide variety of functionalities make this class of polyelectrolyte an interesting choice to be used in LbL assembly with DNA.

A special property of bioreducible PAAs in relation to the intended applications as bioactive surfaces, relies on the finding that cell membranes have reductive properties owing to the presence of reducing enzymes and thiol groups in proteins present in the cell membrane [23, 24]. This has triggered the attempts of achieving localized controlled release of active agents from bioreducible multilayered thin films. Delivery of DNA in this respect is particularly interesting as there have been many attempts at surface-mediated cell transfection even without incorporation of a multilayer structure [25-27] as pioneered by the group of Oupický [28, 29].

On another note, multilayered coatings may also be viewed as a delivery system that releases therapeutic agents, in the sense similar to a hydrogel, for example. Therapeutic agents to be released are incorporated during multilayer assembly and are subsequently released either via simple diffusion [30], biodegradation of the polyelectrolyte building block [31], or induced by internal [32] or external [33] triggers. In view of cell transfecting surfaces, Lynn and Bechler reported that the two multilayer components (i.e. hydrolysable poly(β -amino ester) and DNA) were found to co-localize within transfected cells cultured in the vicinity of the surface, indicating that either polymer-DNA complex is released, or the separate components are released and later form complex in cell culture medium before being internalized by cells [34].

Here we present the syntheses of three PAAs and the characterization for their properties in forming multilayered thin films with ultrasonicated calf thymus DNA (CTDNA) as model DNA. The effect of structural differences among the three polymers have been evaluated for their properties to form multilayers that could act as bioactive surfaces. Release profiles were studied based on the relative DNA content within the constructs under physiological conditions and in reducing environment. Finally the ensembles containing reporter plasmid pCMV-GFP (i.e. pDNA encoding green fluorescence protein (GFP)) were assessed for their efficacy in surface-mediated cell transfection of COS-7 cells.

3.2 MATERIALS AND METHODS

N,N'-Cystamine bisacrylamide (CBA, 99.9%) was purchased from Polysciences (Eppelheim, Germany). 4-amino-1-butanol (ABOL, 98.0%), *N*-Boc-1,4-diaminobutane (NBDAB, $\geq 97.0\%$), histamine dihydrochloride (HIS.2HCl, $\geq 99.0\%$), calcium chloride (CaCl_2 , $\geq 93.0\%$), triethylamine (TEA, $\geq 99.0\%$), *tert*-butylamine (*t*BA, $\geq 99.5\%$), trifluoroacetic acid (TFA, $\geq 99.0\%$), sodium chloride (NaCl, $\geq 99.5\%$), calf thymus DNA sodium salt (CTDNA, type 1, fibers, 16.7 A260 unit/mg solid, 6.0% sodium), dithiothreitol (DTT, $\geq 99.0\%$), sulfuric acid (H_2SO_4 , 95-98%), and hydrogen peroxide (H_2O_2 , 30 wt% in H_2O) were purchased from Sigma-Aldrich (Zwijndrecht, The Netherlands). Sodium dihydrogen phosphate monohydrate ($\text{NaH}_2\text{PO}_4 \cdot \text{H}_2\text{O}$, 99.0-102.0%) and disodium hydrogen phosphate dihydrate ($\text{Na}_2\text{HPO}_4 \cdot 2\text{H}_2\text{O}$, 99.5%) were purchased from Merck (Darmstadt, Germany). All reagents and solvents were purchased at the highest purity available and used as received. Milli-Q water (18.2 M Ω -cm at 25 °C) was obtained from a Synergy® water purification system (Millipore).

PBS buffer was prepared by dissolving 1.54 g of $\text{Na}_2\text{HPO}_4 \cdot 2\text{H}_2\text{O}$, 0.30 g of $\text{NaH}_2\text{PO}_4 \cdot \text{H}_2\text{O}$, and 8.20 g of NaCl into 1.00 L of Milli-Q water and adjusting the pH to 7.4.

CTDNA solution in water was prepared by dissolving shredded CTDNA into Milli-Q water to the final concentration of 1.0 mg/mL. The solution was placed in an ice bath and then sonicated (Sonoplus HD2070, Bandelin, Berlin, Germany) for 20 min at 10% power, 20 kHz frequency, and 7 cycles (i.e. 0.7 s of active interval followed by 0.3 s of passive interval).

^1H -NMR spectra were recorded on an AVANCE III-400MHz NMR (Bruker, Wormer, The Netherlands) spectrometer. Gel permeation chromatograms were recorded on a Polymer Labs GPC 220 in 0.1 M NaOAc buffer pH 4 with 25% methanol as eluent and 0.7 mL/min flow rate against poly(ethylene glycol) (PEG) standards.

Ultraviolet (UV) characterization of multilayered thin films was performed in the dry state using a UV-2401 PC (Shimadzu, 's-Hertogenbosch, The Netherlands). Each film fabricated on UV-transparent 7.5 x 37 x 1 mm quartz glass (Ted Pella, Redding, USA) was measured in three different arbitrary positions. Absorbance scan was carried out in the 200-400 nm wavelength range. All data points were then corrected for baseline offset by subtracting the absorbance value at 400 nm from each data point. Relative absorbance values were obtained by normalizing each data point with the respective value at time 0.

AFM characterization was performed on a Multimode AFM (Bruker, Wormer, The Netherlands) with Nanoscope IV controller in contact mode using an MSCT cantilever with moderate spring constant of 0.5 N/m. Multilayered thin film samples were fabricated on single side polished silicon wafer (n-type, 525 μm thick, MESA+NanoLab, Enschede, The Netherlands) diced into 7.5 x 32 mm pieces.

Contact angle measurements were performed on a Krüss G10 (KRÜSS, Hamburg, Germany) contact angle measuring instrument.

Poly-D-lysine-coated 96-well plates (PDL-TCPS) for multilayer build-up for cell culture and transfection experiments were purchased from Greiner (Alphen aan den Rijn, The Netherlands).

pCMV-GFP pDNA reporter gene was purchased from PlasmidFactory (Bielefeld, Germany) at 1.0 mg/mL concentration in water for injection (WFI).

COS-7 cells (European Collection of Animal Cell Cultures (ECACC) Catalogue No. 87021302) were grown in DMEM containing 4.5 g/L glucose and GlutaMAX™ (Invitrogen, Breda, The Netherlands) supplemented with 2% (v/v) PennStrep (Lonza, Breda, The Netherlands) and 10% (v/v) fetal bovine serum (Lonza, Breda, The Netherlands).

Cell imaging was performed at 4X, 10X, 20X, and/or 40X objectives using EVOS digital inverted microscope (EMS, Wageningen, The Netherlands) equipped with GFP, RFP and DAPI light cubes for expressed GFP, EthD-1, and Hoechst 33258 fluorescence imaging, respectively. EthD-1 and Hoechst 33258 was purchased from Invitrogen (Breda, The Netherlands) and Sigma-Aldrich, respectively.

Fluorescence intensity measurement was carried out in an Infinite M200 PRO plate reader (Tecan, Giessen, The Netherlands). AlamarBlue for cell viability measurements was purchased from Invitrogen (Breda, The Netherlands).

3.2.1 SYNTHESIS OF P(CBA-DAB)

N,N'-Cystamine bisacrylamide (1.01 g; 3.89 mmol) and *N*-Boc-1,4-diaminobutane (0.73 g; 3.84 mmol) were mixed in a brown polymerization flask using 2 mL of methanol/water 3/1 as solvent and containing 200 mM CaCl₂ as catalyst based on a recent report by Zintchenko et al. [35]. Polymerization was carried out under N₂ atmosphere for three days at 70 °C during which a gradual viscosity increase was observed. The polymerization was terminated by adding excess *tert*-butylamine (1.3 mL; 12.3 mmol) into the mixture and stirring at 70 °C for two more days. After bringing the flask to room temperature, the solution was diluted and acidified to pH ~5 by addition of 4 M HCl and purified by ultrafiltration using a 1,000 Da MWCO membrane. The purified polymer solution was then freeze-dried leaving white foam-like solid as the final product in its HCl-salt form (1.06 g; 60% recovery). ¹H-NMR spectroscopy confirmed complete termination.

Deprotection of the BOC-amino side groups in the polymer was carried out by dissolving the polymer in a mixture of methanol/TFA over the course of one day. The solution was then brought to pH ~5 by addition of 1 M NaOH, filtered through a filter paper and dialyzed using a 1,000 Da MWCO. The purified polymer solution was finally freeze-dried to yield a white transparent solid as the final product in its HCl-salt form (0.24 g; 23% recovery). ¹H-NMR spectroscopy confirmed complete deprotection and allowed determination of the number-average MW based on the *tert*-butylamine end-group. ¹H-NMR (D₂O) δ (ppm) = 1.36 (s, 9H, (CH₃)₃R); 1.75 (m, 2H, CH₂CH₂NH₂); 1.86 (m, 2H, CH₂CH₂NR); 2.81 (t, 4H, CH₂CONHRNHCOCH₂); 2.86 (t, 4H, CH₂SSCH₂); 3.05 (t, 2H, CH₂NH₂); 3.29 (t, 2H, NH₂(CH₂)₃CH₂NR); 3.47 (t, 4H, NCOCH₂CH₂NRCH₂); 3.53 (t, 4H, CH₂CH₂SSCH₂CH₂).

3.2.2 SYNTHESIS OF P(CBA-ABOL)

N,N'-Cystamine bisacrylamide (0.53 g; 2.04 mmol) and 4-amino-1-butanol (0.19 g; 2.06 mmol) were mixed in a brown polymerization flask using 1 mL of methanol/water 3/1 as solvent and containing 200 mM CaCl₂ as catalyst [35]. Polymerization was carried out under N₂ atmosphere for two days at 70 °C during which a gradual viscosity increase was observed. The polymerization was terminated by adding excess *tert*-butylamine (0.7 mL; 6.63 mmol) into the mixture and stirring at 70 °C for three more days. After bringing the flask to room temperature, the solution was diluted and acidified to pH ~5 by addition of 4 M HCl and purified by ultrafiltration using a 1,000 Da MWCO membrane. The purified polymer solution was then freeze-dried leaving white transparent solid as the final product in its HCl-salt form (0.39 g; 50% recovery). ¹H-NMR spectroscopy confirmed complete termination and allowed determination of the number-average MW based on the *tert*-butylamine end-group. ¹H-NMR (D₂O) δ (ppm) = 1.35 (s, 9H, (CH₃)₃R); 1.60 (m, 2H, CH₂CH₂NR); 1.77 (m, 2H, CH₂CH₂OH); 2.74 (t, 4H, CH₂CONHRNHCOCH₂); 2.85 (t, 4H, CH₂SSCH₂); 3.22 (t, 2H, HO(CH₂)₃CH₂NR); 3.44 (t, 4H, NCOCH₂CH₂NRCH₂); 3.53 (t, 4H, CH₂CH₂SSCH₂CH₂); 3.62 (t, 2H, CH₂OH).

3.2.3 SYNTHESIS OF P(CBA-HIS)

N,N'-Cystamine bisacrylamide (1.24 g; 4.74 mmol) and histamine dihydrochloride (0.88 g; 4.75 mmol) were mixed in a brown polymerization flask using 2.3 mL of methanol/water 3/1 as solvent and containing 200 mM CaCl₂ as catalyst [35]. Triethylamine (3.3 mL, 23.0 mmol) was added to free the primary amine of histamine

dihydrochloride. Polymerization was carried out under N_2 atmosphere for two days at 70 °C during which a gradual viscosity increase was observed. The polymerization was terminated by adding excess *tert*-butylamine (1.5 mL; 14 mmol) into the mixture and stirring at 70 °C for two more days. After bringing the flask to room temperature, the solution was diluted and acidified to pH ~5 by addition of 4 M HCl and purified by ultrafiltration using a 1,000 Da MWCO membrane. The purified polymer solution was then freeze-dried leaving white transparent solid as the final product in its HCl-salt form (1.14 g; 54% recovery). 1H -NMR spectroscopy confirmed complete termination and allowed determination of the number-average MW based on the *tert*-butylamine end-group. 1H -NMR (D_2O) δ (ppm) = 1.39 (s, 9H, $(CH_3)_3R$); 2.78 – 2.95 (m, 8H, $CH_2CONHRNHCOCH_2$ & CH_2SSCH_2); 3.23 (t, 2H, CCH_2); 3.48 – 3.80 (m, 10H, $(CH_2)_3N$ & $CH_2CH_2SSCH_2CH_2$); 7.45 (s, 1H, $NC=CH$); 8.71 (s, 1H, $N=CH$).

3.2.4 MULTILAYERED THIN FILMS CONSTRUCTION AND BUILD-UP PROFILES

Fresh PAA solutions were prepared short before the start of multilayer build-up from the solid materials which had been re-lyophilized overnight to avoid weighing errors due to their hygroscopic properties. All PAA solutions (2.0 mg/mL) were prepared in PBS buffer at pH 7.4 to avoid possible variations in pH. All CTDNA solutions (1.0 mg/mL) in Milli-Q water were prepared from a single batch.

Prior to the assembly, quartz or silicon wafer substrates (7.5 x 32 mm) were etched for 30 minutes in piranha acid solution to activate the surface, rinsed with copious amounts of Milli-Q water, and dried under N_2 stream. These substrates were then dipped into PAA solution (2.0 mg/mL in PBS buffer pH 7.4) for 10 min, transferred into washing solution containing PBS buffer for 1 min, dipped briefly in a large amount of Milli-Q water, transferred into CTDNA (1.0 mg/mL in Milli-Q water) solution for 10 min, dipped into the second washing solution containing Milli-Q water for 1 min, and finally followed by another brief dipping in Milli-Q. This cycle was repeated to reach the desired number of bilayers. Drying under N_2 stream was performed after every PAA-layer deposition, excluding the very first layer. The resulting ensemble is denoted by PAA-(CTDNA#PAA)_n, where PAA represents the identity of the poly(amido amine) used and n represents the number of bilayer. The first PAA layer is regarded as a precursor layer and therefore excluded from the bilayer number count. Typically, the ensemble consists of 10 bilayer with the poly(amido amine) polymer as the last layer. For every multilayered system, three samples were fabricated in parallel to give estimation for standard deviation. To study the build-up profiles, UV spectra were recorded after each drying step following PAA layer formation. Afterwards, the multilayers were dipped into CTDNA solution to continue multilayer build-up.

Multilayers for cell culture were fabricated directly in the wells of poly-D-lysine-coated 96-well plates (PDL-TCPS, Greiner) by alternatingly dispensing deposition (70 μ L) and washing (2x 100 μ L) solutions under sterile conditions inside the laminar flow hood (LFH). Deposition started with pCMV-GFP (1.0 mg/mL, 30 min for the first layer, 10 min next) as the first layer to a total of 10 bilayers ending with the PAA layer. No intermediate drying steps were applied. At the end of the fabrication the plates were left inside the LFH briefly to dry the films. Coated plates were kept at 4 °C and used as soon as possible (typically overnight). These multilayered samples are designated as PDL-(pCMV-GFP#PAA)₁₀ to indicate the presence of a PDL layer as a precursor layer. Compared to multilayers built on quartz and silicon wafer substrates, these systems substitute the first PAA layer with PDL layer inherent to the well plate surface.

3.2.5 CONTACT ANGLE MEASUREMENTS

Static contact angles (θ) were measured with Milli-Q water (18.2 M Ω -cm) on a Krüss G10 Contact Angle Measuring Instrument. Five drops of Milli-Q water (approximately 1.5 μ L) were measured on five different spots across the surface and averaged to obtain θ . Images were recorded and measured for θ approximately 15 s from the initial contact of the liquid and the surface.

3.2.6 ATOMIC FORCE MICROSCOPY

Multilayers built on silicon wafer substrates were used for AFM microscopy. Imaging was carried out in the middle part of the films (to avoid edge effects/defects) at three different 20 x 20 μm scan areas at 512 x 512 pixels. Images were taken and analyzed using Nanoscope software version 7.30. Height data was flattened using first or second order fitting and root mean square roughness (RMS) was calculated over the scan area. Thickness data was obtained by first scratching the surface using a syringe needle and then scanning over the scratched area to measure the difference in height between the base substrate (i.e. the bottom of the scratch) and the surface of the film. Thicknesses were then measured as the average of one 'depth' measurement and three 'section' measurements across the scratch.

3.2.7 DNA RELEASE PROFILES UNDER PHYSIOLOGICAL CONDITIONS

DNA release profiles of the three multilayered systems in PBS buffer pH 7.4 at 37 °C was investigated by dipping the thin films formed on quartz slides in 2 mL of PBS buffer pH 7.4 solution and incubating them in a water bath with temperature set to 37 °C. From time to time, the samples were removed, briefly dipped in a large amount of Milli-Q water, dried under N_2 stream and measured by UV-Vis spectrophotometer.

3.2.8 DNA RELEASE PROFILES UNDER REDUCING CONDITIONS

Degradability of the three multilayered systems was investigated in a similar fashion as for their DNA release profiles under physiological conditions (Section 3.2.7), though in the presence of 1.0 mM of DTT in the incubation medium. The solution of 1.0 mM DTT in PBS buffer pH 7.4 was prepared fresh directly prior to the start of experiment. Due to instability of DTT in PBS buffer pH 7.4, no solution of over three hours old was used.

3.2.9 CELL VIABILITY AND TRANSFECTION ON MULTILAYERED FILMS

For cell viability and transfection experiments, multilayers were fabricated as described in Section 3.2.4. Directly on the multilayer-coated PDL-TCPS wells, COS-7 cells were seeded at a seeding density of 4500 cells/sample in complete medium with serum and left to proliferate at 37 °C in humidified atmosphere with 5% CO_2 .

Cell morphology and transfection efficiency were recorded after 6, 24 and 48 hours of culture. At the end of the 2 d culture period, cells were stained with EthD-1 and Hoechst 33258 followed by subsequent fluorescence imaging. As (negative for transfection and positive for metabolic activity) controls, cells were also seeded on non-tissue culture (TC)-treated, polystyrene well plates. Experiments were done in triplicates.

For quantitative metabolic activity comparison between the three different polymer systems, after 48 h of culture, AlamarBlue (AB) was added at 10 v/v% of total medium volume in every well and incubated for another 4h after which fluorescence intensity of resorufin (i.e. metabolically-reduced resazurin) was recorded using a plate reader. As positive controls, cells were also seeded on non-TC-treated polystyrene well plates. All fluorescence intensities were corrected by subtracting the values with those of their respective no-cell control wells. All experiments were carried out in triplicates.

To study the effect of burst release of thicker multilayers on transfection efficiency, cells were seeded on pCHIS films which had and had not been previously washed by incubating in PBS buffer pH 7.4 inside the incubator for 1 h. The extent of transfection efficiency was assessed qualitatively using fluorescence imaging.

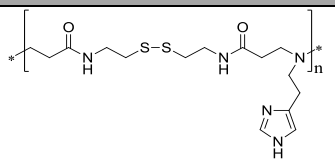
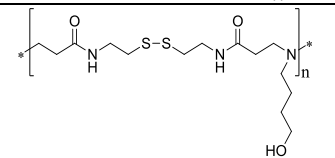
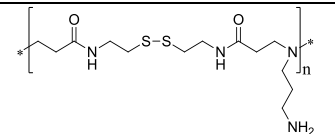
3.3 RESULTS AND DISCUSSION

3.3.1 SYNTHESSES OF PCDAB, PCABOL, AND PCHIS

To study the effect of structural differences of the polymers on multilayer build-up, PAAs with different side chain functional groups were synthesized via CaCl_2 -catalyzed Michael-type addition polymerization (Table 3.1). To obtain the highest degrees of polymerization, the polymerization was performed using an equimolar mixture of free amine and bisacrylamides. Moreover, solvent was kept to a minimum amount to increase the rate of the polymerization. N_2 gas as a protective atmosphere, in combination with a brown reaction flask, were used to prevent radical formation. CaCl_2 was employed as a Lewis acid, which is known to catalyze the addition of nucleophilic amines to α,β -unsaturated carbonyl compounds [35]. All polymerizations were run for two to three days at 70°C to maximize the degree of polymerization, but no longer in order to avoid retro-Michael reaction and possible amide hydrolysis. Polymerizations were terminated by adding excess *tert*-butylamine (*t*BA), resulting statistically in one *t*BA end group per polymer chain, provided the ideal stoichiometry was achieved. Neutralization and dialysis were then carried out to obtain the PAA product in aqueous solution. Water was removed via lyophilization to obtain the pure polymer in its salt form. For p(CBA-DAB), an extra BOC-deprotection step was necessary, which was carried out by dissolving the dry product in a methanol/TFA mixture, which was stirred overnight at RT.

From the $^1\text{H-NMR}$ spectra, the observed singlet corresponding to the *t*BA end group was used to make an estimation of the number-average molecular weight (M_n) for each polymer. Polydispersity index (PDI) values were obtained from GPC, together with the weight (M_w) and number (M_n) average molecular weight, relative to PEG standards. These data are shown in detail in Table 3.1.

Table 3.1 Summary of $^1\text{H-NMR}$ and GPC characterizations on the molecular weights in kg/mol and PDI of PAA products.

PAA name	PAA structure	$^1\text{H-NMR}$ end group analysis		GPC (PEG standard)		
		n	M_n	M_w	M_n	PDI
p(CBA-HIS) (pCHIS)		15	5.5	4.6	3.6	1.26
p(CBA-ABOL) (pCABOL)		26	9	3.8	3.2	1.18
p(CBA-DAB) (pCDAB)		19	6.6	7.3	5.5	1.34

The (physico-)chemical difference between the three different PAAs is mainly based on the different properties of the side chains. Under the physiological conditions applied for the build-up and application of the resulting multilayers, the primary amine in the pCDAB side chains provide additional positive charges ($\text{pK}_a \sim 9$) for stronger electrostatic interactions with the negatively-charged DNA. As compared to the neutral primary alcohol of pCABOL, the histamine side group in pCHIS has a pK_a of 5.8 which provides an intermediate pH-sensitive amount of extra positive charge as compared to pCDAB's primary amine.

As the build-up of multilayers studied here depends largely on the electrostatic interactions between the polymers and the DNA, a structure-property relationship could be derived by studying the effect of PAA identity on its build-up profiles with DNA. Additionally, these structural differences are also expected to play a role in cell attachment

and cytotoxicity as it is known that materials with higher positive charges are more prone to display cytotoxicity [36]. For an optimal surface-mediated transfection, a PAA should be non-toxic, facilitate multilayer build-up, and achieve maximal transfection efficiency.

3.3.2 MULTILAYERED THIN FILMS CONSTRUCTION

Build-up profiles of each multilayer were obtained by observing the increase in absorbance of CTDNA at 260 nm after deposition of each bilayer. The topmost layer was always the PAA layer to protect the DNA and promote future cell adhesion. As shown in Figure 3.1, the build-up profiles of the three multilayered systems designated as pCDAB-(CTDNA#pCDAB)₁₀, pCABOL-(CTDNA#pCABOL)₁₀, and pCHIS-(CTDNA#pCHIS)₁₀ are relatively linear. For each type of film, three parallel build-up experiments were carried out to give an indication of the reproducibility of the assembly. The polymer pCDAB gave highly reproducible multilayer formation with DNA and exhibits very low standard deviation. This trend is generally preserved even when the build-up was continued up to 30 bilayers (data not shown). On the other hand, for pCHIS and pCABOL-based multilayers, the standard deviations are generally higher, especially at higher bilayer numbers. The general trend in increase of DNA adsorption during build-up of the multilayer indicates comparable amounts of incorporated DNA. However, the two types of films possess different physical appearances. pCHIS-(CTDNA#pCHIS) multilayers often appear turbid, causing in some cases high (UV) baseline shifts, while pCABOL-(CTDNA#pCABOL) multilayers are generally more homogeneously transparent.

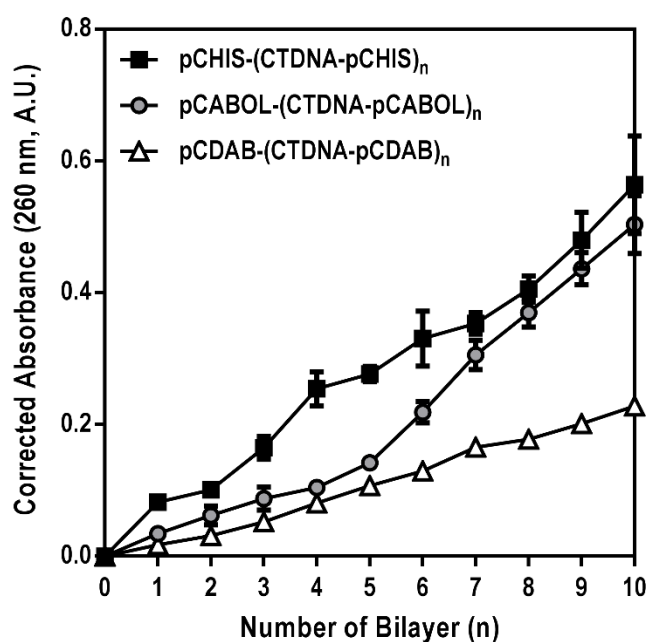


Figure 3.1 Build-up profiles of three multilayers prepared using PAA-polymers with different side groups.

In relating the structural differences in the three PAAs with their layer build-up properties with DNA, it is interesting to note that the PAA with the highest cationic charge density (i.e. the pCDAB polymer) incorporates the lowest amount of DNA in each deposition cycle, while pCHIS and pCABOL result in deposition of at least twice the amount of DNA per cycle. Considering that the main interactions during multilayer build-up are electrostatic interactions, one would intuitively expect that the PAA that can interact most strongly with DNA would facilitate deposition of more DNA. Therefore, the observed phenomenon indicates that factors other than the strength of electrostatic interaction also determine multilayer build-up properties.

The much observed effects of salt concentration and pH of the deposition solution on multilayer build-up profiles have been described in the literature [37, 38]. In general, the incremental thickness of adsorbed layers is found to decrease with increasing polyelectrolyte charge density. Therefore, strong polyelectrolytes are found to have higher incremental thickness only in the presence of higher salt concentration which would mask (i.e. decrease) their apparent charge density. In contrast, the incremental thickness of weak polyelectrolytes highly depends on the pH of the deposition solution which determines the extent of the polyelectrolyte's charge density. The fact that in the same deposition pH, PAA-polymers with higher charge density lead to the lowest deposition of DNA is in agreement with this trend. It is thermodynamically [39] more favorable for pCDAB, having the highest charge density, to assume a flatter conformation on the surface and therefore lower amounts of DNA are needed to compensate for surface charge reversal. On the other hand, pCABOL with less charge density would assume a conformation that is more similar to its conformation in free solution and appear more as loops on the surface (i.e. with less contact points with the surface per chain), increasing the relative surface area to facilitate more DNA deposition. This argument is also supported by the fact that the surface roughness values of pCDAB-films at various bilayer numbers (see Figure 3.2) are always significantly lower than those of pCABOL-films, especially when the pCDAB is the topmost layer.

As previously indicated, compared to pCABOL, pCHIS polymer possesses higher charge density at the deposition pH of 7.4 due to the presence of the imidazole ring with a pKa of 5.8. However, this translates to only ~10% of the polymer side chain to be positively-charged. Therefore, it is not surprising that the pCHIS multilayer build-up profile is much closer to that of pCABOL than pCDAB. However, as will be explained further below, the imidazole ring induces an additional effect on multilayer build-up not yet apparent in Figure 3.1.

AFM characterization was also carried out to study the build-up profiles of the different multilayers. Thickness for the single-bilayered film of pCHIS system was measured ~10 nm. For the other two polymers, the single-bilayered films were too thin to locate the scratch. The build-up profiles in terms of layer thickness were plotted in Figure 3.2 and the obtained data correlates well with the UV-data shown in Figure 3.1. Both thickness and absorbance values increase relatively linearly with the number of deposition cycles. The same trend is also observed for the surface roughness (RMS). It is interesting to note that RMS values for the pCHIS system were generally lower than for the other two systems, especially considering the relatively higher thickness of the pCHIS system. This can most likely be attributed to the different interaction mechanism on which the multilayer build-up of the pCHIS system is based (see Section 3.3.3).

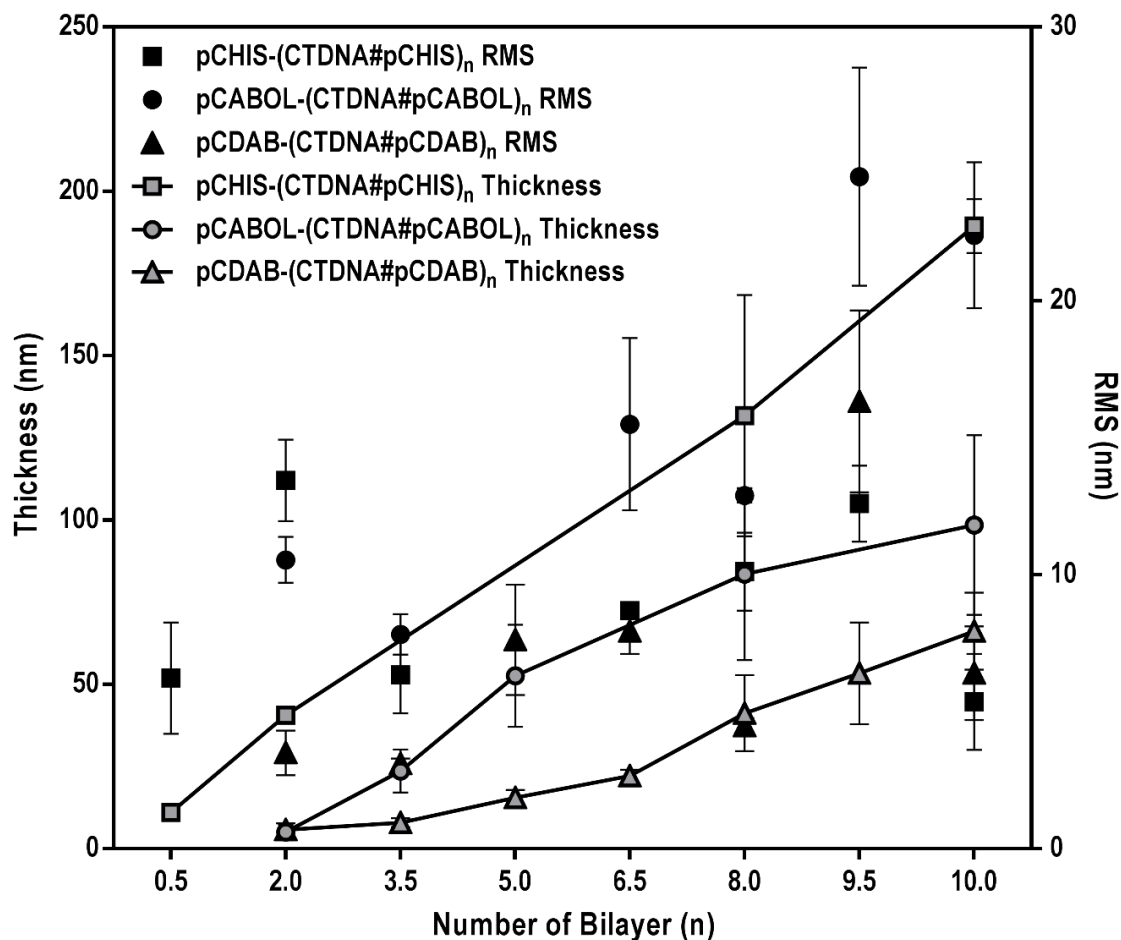


Figure 3.2 Build-up profiles of the three multilayered systems based on AFM. Surface roughness (RMS, nm) and thickness (nm) at different bilayer numbers are shown at the two ordinate axes. Every data point is an average of at least three measurements made on arbitrary positions of the same multilayer sample.

In comparing the thickness data obtained from UV absorbance with the data of AFM, it is important to note that the latter gives insight in the total film thickness attributed to the two constituents of the films (i.e. the PAA polymer and the DNA) while the former can be attributed primarily to the DNA alone. The fact that the thickness of the 10-bilayered pCHIS system is approximately twice the thickness of that of pCABOL system, while the UV absorbance values for DNA content are much closer in agreement, may indicate that the pCHIS-based film incorporates more polymer than DNA as compared to pCABOL-based films. This also agrees well with the physical appearance of pCHIS-based films, which are notably more opaque than the pCABOL-based films. Lastly, similar to the UV-spectroscopy data, AFM data also displays a considerable standard deviation, particularly for the thicker systems at higher bilayer number.

3.3.3 MULTILAYERED THIN FILMS WETTABILITY

Measurement of water contact angles has often been used to indicate alternation of surface coverage in LbL assemblies [28, 40]. When two (oppositely charged) materials provide different water contact angles when forming a uniform layer on a surface, alternating contact angles can be observed as multilayers of the different materials are built-up. Figure 3.3 shows contact angles of multilayers prepared with different bilayer numbers. Bilayer numbers that are integers (2, 5, 8, and 10) represent multilayers with a PAA layer as the outermost layer, while non-integer bilayer numbers (0.5, 3.5, 6.5, and 9.5) represent multilayers with a DNA layer as the outermost layer.

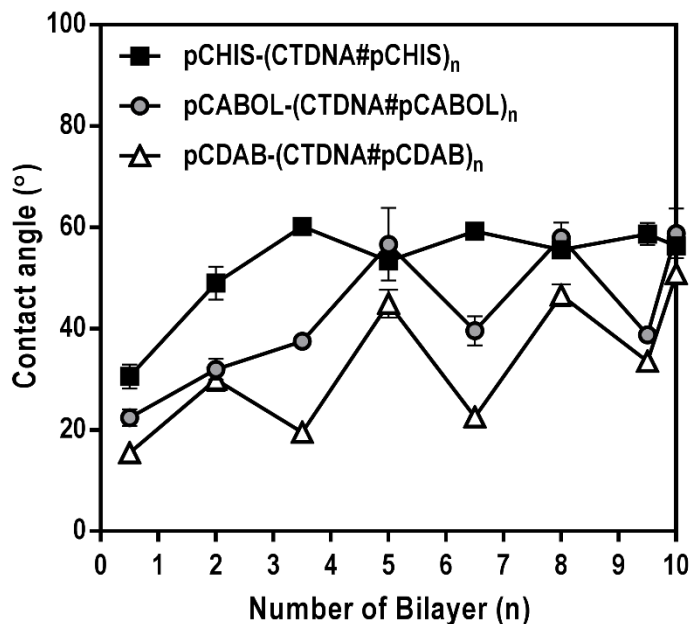


Figure 3.3 Static water contact angles of multilayers with different numbers of bilayers.

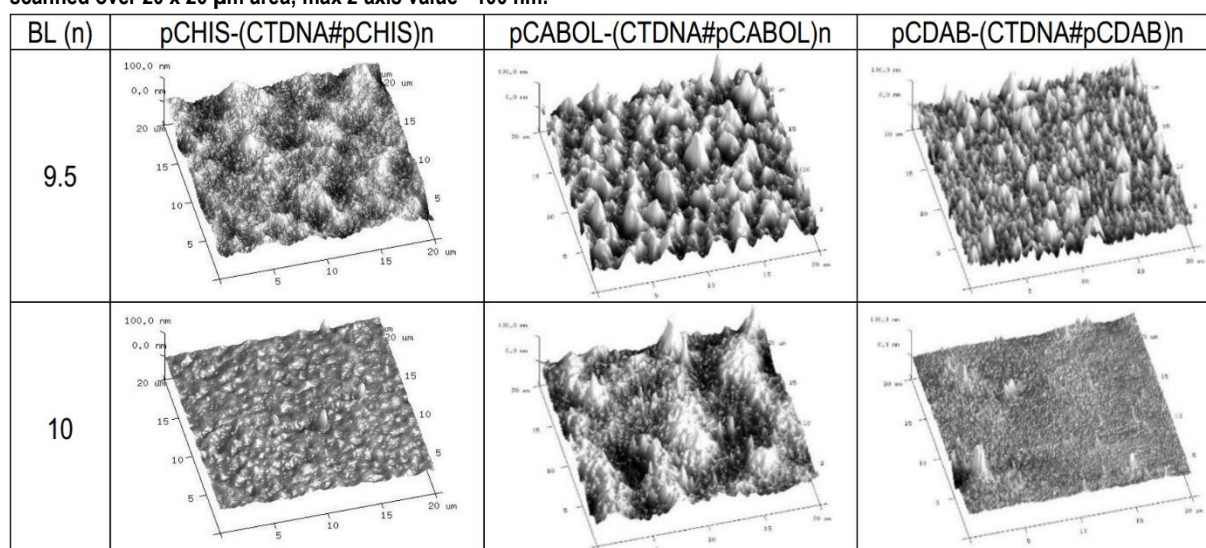
Figure 3.3 indicates that the early deposition steps do not provide completely uniform layers, except for the pCDAB-(CTDNA#pCDAB) system. Complete surface coverage can be achieved after at least 4 bilayer formation, where the water contact angles now alternate between the more hydrophilic surface of CTDNA and the more hydrophobic surface of PAA. However, this phenomenon is much less pronounced for the pCHIS-(CTDNA#pCHIS) system, displaying similar water contact angles for both surfaces after the fourth bilayer. The presence of the histamine group in pCHIS leads to the formation of a more hydrophobic surface, even after DNA coverage.

As a natural amino acid, histamine has been shown to interact with DNA via both hydrogen bonding and intercalation [41]. This interaction is most likely further enhanced with the histamine moieties being the pendant group of a polymeric backbone. The topmost pCHIS layer dynamically integrates with incoming DNA resulting in a relatively hydrophobic surface. In the context of multilayer formation, this phenomenon may also indicate extensive mixing of layers resulting in a less stratified multilayer structure [42].

3.3.4 MULTILAYERED THIN FILM SURFACE PROFILES

In addition to determining surface roughness, AFM was used to study the surface profiles of the various multilayered systems. Table 3.2 shows the surface profiles of the three different multilayers at 9.5 and 10 bilayer numbers to represent DNA and PAA topmost layers, respectively. All images are shown using the same height scale range (max z-axis 100 nm). The characteristics of the surface profiles tend to be preserved with respect to the identity of the outermost layer of the films also from the earlier bilayer numbers (data not shown). DNA topmost layers generally display sharp height differences. PAA topmost layers, on the other hand, tend to be more homogeneous with shorter and more equally-spaced elevations. This trend in alternating surface roughness is also observed from the RMS data shown in Figure 3.2.

Table 3.2 Surface profiles of the three multilayered systems at 9.5 (DNA topmost) and 10 (PAA topmost) bilayer numbers scanned over 20 x 20 μm area; max z-axis value= 100 nm.



3.3.5 DNA RELEASE PROFILES UNDER PHYSIOLOGICAL CONDITIONS

Incubation of the prepared multilayers in PBS buffer pH 7.4 at 37 °C may give insight into how the films behave in physiological environment, specifically, the effect of physiological pH, salt concentration and temperature. To be able to act as cell-transfecting surfaces, the films need to deliver transfection agents into the cells. In that respect, this study may also serve to indicate a release profile of incorporated therapeutic DNA. To approach the ideal sink conditions, after every incubation time point, the films were briefly dipped in a large amount of Milli-Q water to remove loosely attached material before being dried. The dipping solution was also refreshed after every intermitting measurement.

Figure 3.4 shows the DNA release profile based on absorbance values at 260 nm normalized to 100% at time zero. The profile depicts a trend where films from PAA with higher positive charge (pCDAB-based film) seem to be more stable and retain incorporated DNA while films from PAA with less charge (pCHIS- and pCABOL-based film) tend to more rapidly release their DNA content within a few hours of incubation under physiological conditions. Despite the apparent difference, it needs to be noted that when taking into account the initial DNA content, the two multilayers with higher initial DNA content (i.e. pCHIS- and pCABOL-based films) are the ones to rapidly release their DNA content to finally reach a relatively similar DNA content level as that of the most stable multilayer (i.e. pCDAB-based film).

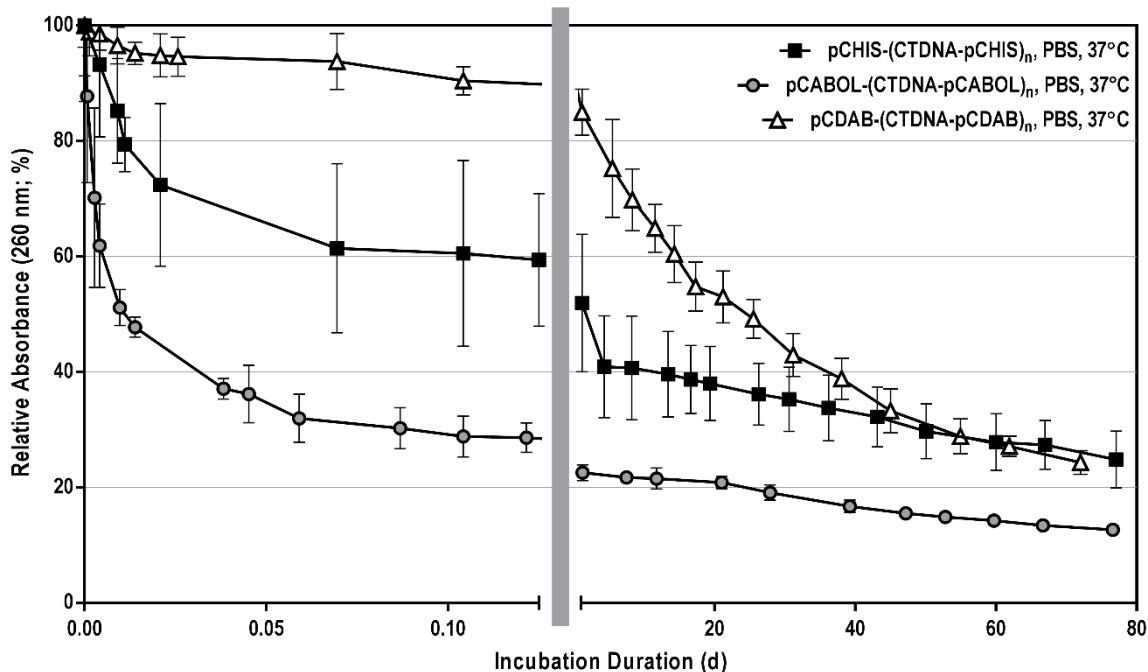


Figure 3.4 DNA release profiles of multilayers under physiological conditions (PBS buffer pH 7.4 at 37 °C) *in vitro*. The left part of the abscissa shows the trend of fast decrease (burst release) within 0.125 d (3 h) in the initial phase of the incubation while the right part shows the much slower decrease throughout the rest of the long incubation duration. Relative absorbance values are shown by normalizing the absorbance values at every time point to that of time 0.

Since the most likely chemical degradation under the established physiological conditions is slow amide hydrolysis, the fast decrease in multilayer's 260 nm absorption can only be caused by rearrangement or disassembly of the multilayered ensembles. The possibility of disassembling multilayered systems was considered based on the fact that the burst release is observed only for the thicker films and that higher thickness may induce instability as minor defects in each layer are progressively transferred in further build-up of the layers. To verify this, 5 bilayered-pCHIS-(CTDNA#pCHIS) multilayers were built-up and incubated under the same conditions. The observed stability trend was identical to that observed for the 10-bl system (data not shown). This indicates that the burst release phenomenon is less likely caused by disassembly, but more likely thermodynamic rearrangement within the multilayered film to reach a more stable state which in turn leads to release of excess material.

The thermodynamic rearrangement is considered especially because this burst release phenomenon takes place only in the presence of physiological salt concentration. When salt was excluded in the incubation medium, all multilayers retain their DNA content in a profile similar to that of pCDAB-based film (data not shown). This leads to the argument that this phenomenon is most likely induced by two factors: deficiency of positive charges in pCABOL and pCHIS at pH 7.4 in combination with low molecular weight of the polymers. Low molecular weight leads to less multivalent interactions, promoting entropically-driven detachment from DNA on the surface, while the deficiency of positive charges makes it easier for salt ions to intervene the electrostatic interactions between the PAA and DNA. In later stages, the release of material is slowed down after the system reaches a more stable state. The presence of the charged substrate helps keep the remaining layers together, while amide hydrolysis slowly proceeds to degrade the remaining films. Similar salt-induced deconstruction has been reported previously by Ren et al. and Schöler and Caruso for DNA-containing multilayers [43, 44] and others [45-47], although mostly at higher salt concentrations than 0.15 M utilized in this study.

Surface profiles of the three different films at 10 bilayers, after being incubated in PBS buffer pH 7.4 at 37 °C for 1 h, are shown in Figure 3.5. The surfaces were in general rougher as compared to the respective surfaces

before rearrangement (roughness increases were ~40% and ~20% for pCHIS- and pCDAB-systems, respectively). Notably, the pCABOL-based system (the roughest of the three prior to incubation in PBS) showed the presence of high features most likely indicating the still-attached released complexes/aggregates of pCABOL and DNA, causing high increase in surface roughness of up to 170%. AFM scratch tests on these films revealed the expected decreases in thickness; i.e. from the original thicknesses of 190, 99, and 66 nm for pCHIS, pCABOL, and pCDAB system respectively, the thicknesses decreased to 135, 55, and 54 nm respectively after incubation under physiological conditions.

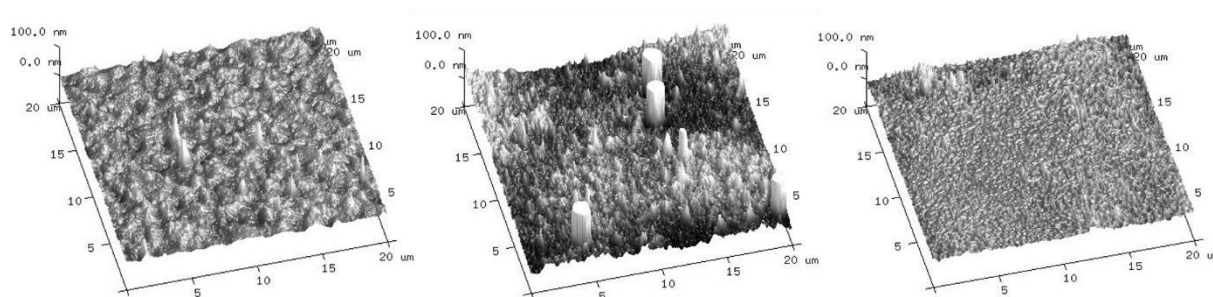


Figure 3.5 Surface profiles of (from left to right) pCHIS-(CTDNA#pCHIS)₁₀, pCABOL-(CTDNA#pCABOL)₁₀, and pCDAB-(CTDNA#pCDAB)₁₀ multilayers after being incubated in PBS buffer pH 7.4 at 37 °C shown using the same height scaling as that used in Table 3.2 (max z-axis value= 100 nm).

Although Figure 3.4 only shows the release based on the percentage of released DNA content, the rearrangement in these multilayered constructs may actually result in the burst release of *not* the naked DNA, but a **complex** composed of DNA and polymer. Following a 1 h incubation of a pCHIS-(CTDNA#pCHIS)₁₀ multilayers in PBS medium pH 7.4, dynamic light scattering measurements revealed the presence of polydisperse (PDI ~1) particles in the size range of ~700 nm. Polyplexes are usually formed and measured at a specific polymer/DNA weight ratio in medium without salt. However, despite the initial homogenous particle sizes, polyplexes are also known to become unstable upon mixing with serum-containing cell culture medium in which transfections are carried out [48]. Similarly, the thicker multilayers fabricated in this study undergo rearrangement in the presence of cell culture medium, releasing materials that are likely thermodynamically stable complexes of DNA and polymer. It is therefore expected that these films are able to induce transfection at least through the released polymer-DNA complexes.

3.3.6 *IN VITRO* REDUCTIVE DEGRADATION OF MULTILAYERED THIN FILMS

Owing to the presence of disulfide bonds in the main chain of the three PAAs used to build multilayers, the resulting multilayers have reducible properties. However, due to the structural differences between the three PAAs the respective films may show different stability profiles under the same reducing conditions. Furthermore, a similar PAA lacking disulfide linkages may also be used to serve as a negative control to verify that the observed degradation is indeed due to the presence of disulfide bonds in the main chain of the PAAs. In this study, pMDAB (synthesized with *N,N*-methylene bisacrylamide (MBA) instead of the disulfide-containing CBA) was used as the non-reducible counterpart of pCDAB.

To investigate the degradability of the multilayers, films were incubated in a solution of 1.0 mM DTT in PBS buffer at pH 7.4. The degradation profiles for pCHIS-(CTDNA#pCHIS)₁₀ and pCDAB-(CTDNA#pCDAB)₁₀ are shown in Figure 3.6. Profiles of pCHIS-(CTDNA#pCHIS)₁₀ and pCDAB-(CTDNA#pCDAB)₁₀ in PBS buffer at pH 7.4 without DTT are shown for comparison. The pCABOL-(CTDNA#pCABOL)₁₀ films degrade substantially faster than the other multilayers and practically no film was left already after the first minute of incubation under reducing conditions (data not shown). The control pMDAB system exposed to the same reducing conditions displayed a

similar stability profile as the pCDAB system treated without DTT, confirming that the degradation was indeed caused by the reduction of disulfide bonds.

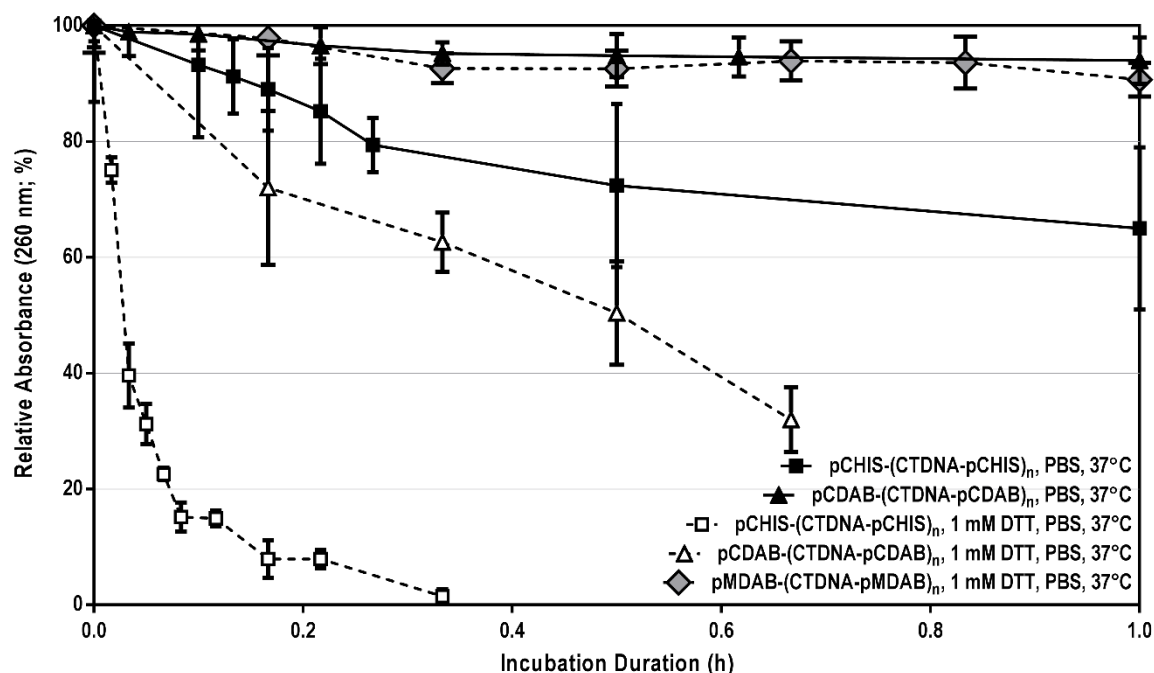


Figure 3.6 Degradation profiles of pCHIS-(CTDNA#pCHIS)₁₀ and pCDAB-(CTDNA#pCDAB)₁₀ multilayers with and without the presence of 1.0 mM DTT in PBS buffer pH 7.4 at 37 °C. Relative absorbance values are shown by normalizing the corrected absorbance values at every time points to that of time 0.

Figure 3.6 shows that the investigated multilayers undergo rapid degradation in the presence of 1.0 mM of DTT under physiological conditions. From the observed degradation trend pCABOL > pCHIS > pCDAB, it can be proposed that degradation is enhanced by the higher porosity (looser structure) induced by the thermodynamic rearrangement of the thicker films. The higher porosity promotes diffusion of negatively-charged DTT into the lower parts of the multilayered systems causing more rapid reduction and break down of the films.

3.3.7 CELL VIABILITY AND TRANSFECTION ON MULTILAYERED THIN FILMS

To investigate whether cells are able to attach and proliferate, and are susceptible to transfection, when grown on multilayers, functional plasmid DNA (pCMV-GFP) encoding for GFP was used to substitute for the inexpensive CTDNA that had been used to study the characteristics of multilayer build-up, DNA release, degradation, wettability, and surface profiles. Poly-D-lysine-coated 96-well plates (PDL-TCPS) were used as the substrate for multilayer build-up to facilitate handling and cell distribution. Albeit no characterization was conducted on multilayers built in these wells, multilayer formation could be easily confirmed by light microscopy readily available in cell culture laboratories.

COS-7 cells were seeded on multilayer-coated PDL-TCPS wells at a seeding density of 4,500 cells/well for 96-well plates (i.e. ~13,000 cells/cm²). Initial cell attachment and morphology were monitored 6 h after seeding by light microscopy. Microscopy images of COS-7 cells seeded on different surfaces are shown in Figure 3.7.

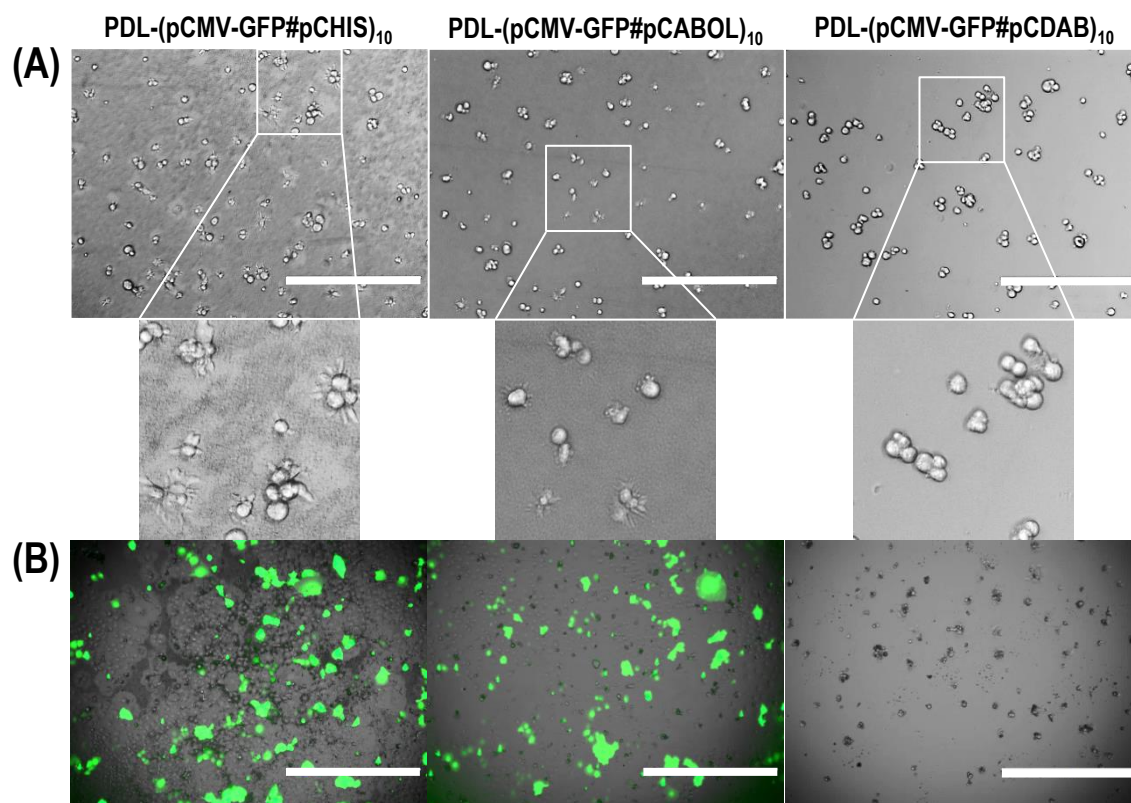


Figure 3.7 (A) Light microscopy images of COS-7 cells 6 h after seeding on the three different multilayers at 10X magnification (bars = 400 μm); (B) Overlay of GFP fluorescence and light microscope images of COS-7 cells seeded on the same multilayers after 48 h of culture at 4X magnification (bars = 400 μm).

Figure 3.7a shows that the pCHIS-based system provides best cell attachment followed by pCABOL-based multilayer. pCDAB-based films on the other hand, impede COS-7 cell attachment as observed by the rounded morphology of the cells. On this latter system, cells tend to aggregate rather than attaching to the surface regardless of the high positive charge on the surface. Figure 3.7a also shows a rough surface profile for the pCHIS system, owing to the thickness of the multilayer. After 48 h, the cells were further imaged for GFP expression. Figure 3.7b shows representative overlay images of the cells cultured on the three different films after 2 d of culture.

From Figure 3.7b, it can be seen that the PDL-(pCMV-GFP#pCABOL)₁₀ and PDL-(pCMV-GFP#pCHIS)₁₀ multilayers are able to transfect cells, whereas the PDL-(pCMV-GFP#pCDAB)₁₀ did not display transfection. The extent of cell transfection is optimal after 2 d of culture. Qualitative observation at day three did not show significant increases in transfection (data not shown). Upon closer investigation of the cell morphology at these later time points, it becomes apparent that the PDL-(pCMV-GFP#pCDAB)₁₀ system suppresses cell attachment and proliferation. This was further confirmed by performing the AlamarBlue assay to quantitatively assess metabolic activity of cells cultured on the different surfaces after two days. The fluorescence intensity of metabolically-reduced resazurin is shown in Figure 3.8 as %metabolic activity relative to cells cultured on polystyrene (PS) control. This figure indicates that COS-7 cells were able to proliferate to similar extents on pCABOL-based and pCHIS-based multilayers as well as on non-tissue culture treated PS surfaces. On the other hand, pCDAB-based multilayer displayed significantly poorer COS-7 cell proliferation, confirming higher cytotoxicity, most likely due to the higher amount of cationic charges on this polymer as further corroborated by the cell morphology shown in Figure 3.7a.

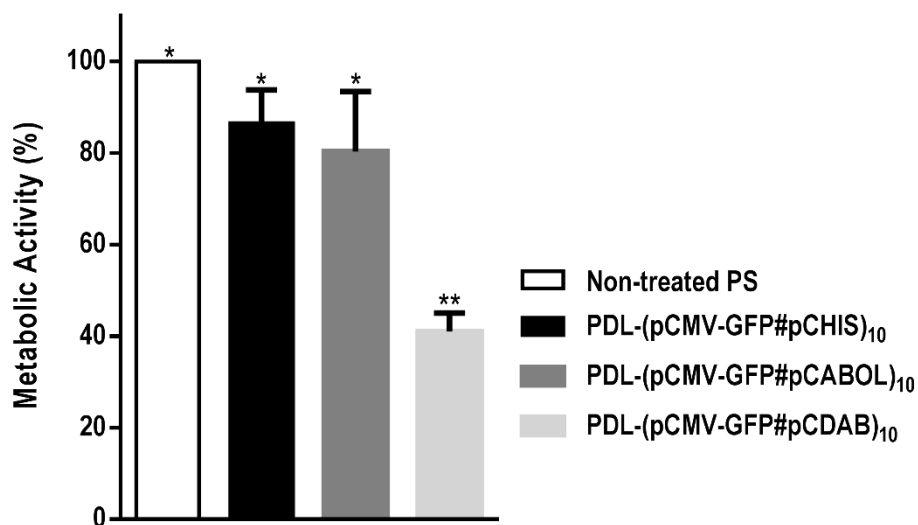


Figure 3.8 Metabolic activity of COS-7 cells cultured on various multilayered surfaces relative to PS control. *) Not significantly different from one another ($p > 0.05$), **) significantly different from the rest of the data ($p < 0.05$).

The metabolic activity of transfected cells as shown in Figure 3.8 was further assessed qualitatively by staining the cells with Hoechst 33258 (blue) and EthD-1 (red) for both live and dead cells, respectively. Representative overlay images of transfected cells on pCABOL and pCHIS-based systems are shown in Figure 3.9. In both systems, the detected transfected cells stained negative for EthD-1, indicating good viability with well-defined nuclei. Further, the rough features that have been persistently observed for pCHIS samples (see Figure 3.7) can now be seen to stain positive for both Hoechst 33258 and EthD-1, staining for DNA. These features are most likely visible fragments of released polymer-DNA complexes (see Section 3.3.5). This observation is most likely possible due to the thick nature of the pCHIS films compared to the thinner pCABOL films.

In order to further understand the effect of rapid release (discussed in Section 3.3.5) on transfection efficiency, an experiment was carried out in which COS-7 cells were seeded with the same seeding density on regular “unwashed” pCHIS films and “washed” pCHIS films. The extent of GFP expression on both systems after 2 days of culture is represented in Figure 3.10. In general, transfection efficiency was much lower for the “washed” system than for the “unwashed” system which indicates that the fast initial release results in the release of transfection agent. Further, to assess whether the released transfection agent is still active for transfection, cell culture medium that has been used to incubate multilayers without cells under physiological conditions for 1 h was added to cells cultured on non-multilayer-coated surface and the extent of transfection was observed after 2 d of culture. Interestingly, no transfection was observed (data not shown). It is possible that the released transfection agent became deactivated/degraded upon contact with cell culture medium albeit only for 1 h. This result signifies the necessity of direct contact between the multilayers and the cells to be treated. This direct contact possibly encourages rapid intracellular uptake of active transfection agents through a restriction of space.

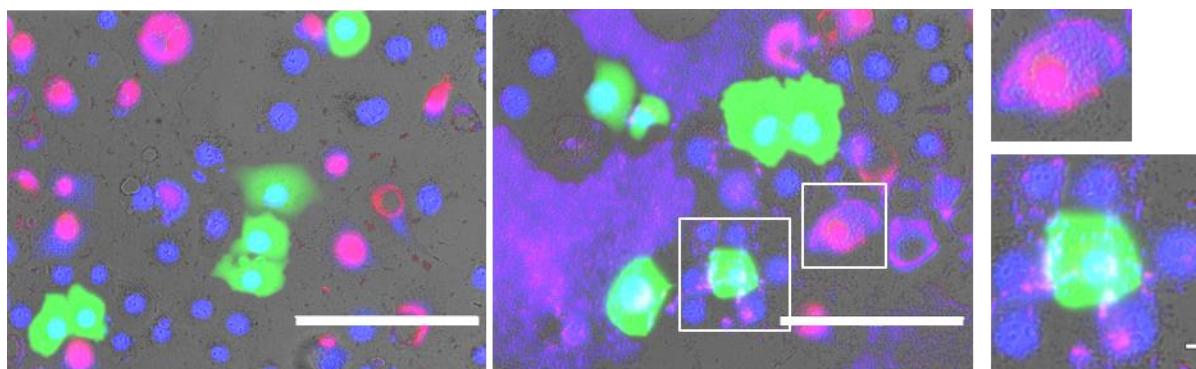


Figure 3.9 Representative overlay images of COS-7 cells stained with Hoechst 33258 (blue, live) and EthD-1 (red, dead) after 2 days of culture on top of PDL-(pCMV-GFP#pCABOL)₁₀ (left) and PDL-(pCMV-GFP#pCHIS)₁₀ (right) at 20X magnification. Bars = 200 μm.

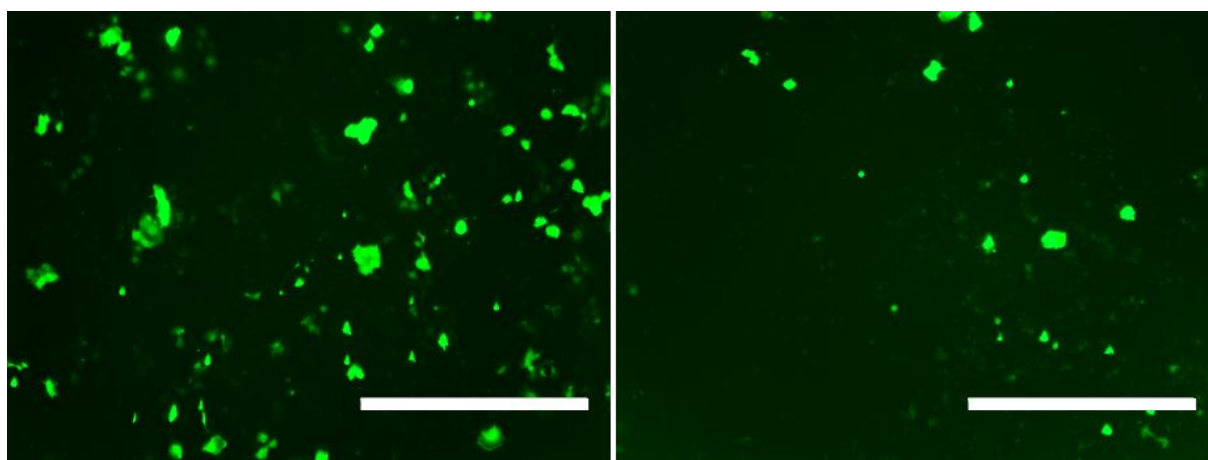


Figure 3.10 Representative GFP fluorescence images of COS-7 cells seeded on top of "unwashed" (left) and "washed" (right) PDL-(pCMV-GFP#pCHIS)₁₀ multilayer after 48 h of culture. Images were at 4X magnification (scale bar = 1,000 μm).

With respect to transfection efficiency, the current transfection efficiency (~11%, qualitatively) can likely be further optimized. Therefore, more extensive optimization of transfection efficiency in relation to cell seeding density, bilayer number, and identity of topmost layer are reported in Chapter 8.

3.4 CONCLUSIONS

Poly(amido amine)s, being peptidomimetic polymers with inherent positive charge under physiological conditions, show good interaction with DNA and readily form multilayered thin films. Three bio-reducible poly(amido amine)s with different side chains show different layer build-up profiles and film properties. For all three systems, uniform coverage was obtained after at least 4 deposition cycles and throughout the deposition cycles the build-up of 10 bilayers progressed in a linear manner. Thicker multilayers with higher material deposition were obtained from pCHIS (containing imidazole moieties in the polymer side chains) and pCABOL (containing primary alcohols in the polymer side chains) polymers, while pCDAB (containing primary amines in the polymer side chains) having the highest cationic charge density was found to lead to the thinnest films with the lowest material deposition. The polymers pCABOL and pCHIS with less, yet still sufficient, positive charges gave rise to a rougher structure, providing more surface area for the counter polyelectrolyte (in this case DNA) to deposit onto, while more positively-charged polymer (pCDAB) tends to deposit a more compact layer, providing less area for the incoming counter polyelectrolyte. Ultraviolet spectroscopy data of the layers were in good agreement with thickness measurement via atomic force microscopy. At 10 bilayers, both pCHIS and pCABOL-based multilayers incorporated relatively similar amount of DNA. However, pCHIS-based films were much thicker, possibly indicating higher polymer to DNA ratio than pCABOL-based films.

In the presence of physiological salt concentration, the thicker pCABOL- and pCHIS- based films were found to rapidly release film components (i.e. approximately half of initial DNA content within 1 h), most likely in the form of polymer-DNA complexes. *In vitro* cell experiments with COS-7 cells demonstrate that pCABOL- and pCHIS-based multilayered systems can facilitate cell attachment and proliferation. However, the pCDAB-based multilayer, which is very stable under physiological conditions, displayed only limited cell attachment and higher cytotoxicity, most likely due to the higher cationic charge density of this polymer. Out of the three different polymers, pCABOL- and pCHIS-based multilayered systems were able to transfect COS-7 cells cultured on top of the multilayers containing plasmids encoding for GFP after 2 days of incubation. In this study transfection efficiencies of up to 11% of the total COS-7 cells cultured on pCABOL- and pCHIS-based multilayers were observed qualitatively.

In conclusion multilayers from poly(amido amine)s and DNA offer the possibility to endow surfaces with cell-transfecting capabilities. To this purpose, a release mechanism is necessary to release DNA in a transfection-active formulation. We have observed from this study that a burst release mechanism as observed for pCABOL- and pCHIS-based films may help transfection to a rapid early start. We believe that the multilayered systems presented in this study hold great potential to be used as cell-transfecting coatings for various biomaterials for biomedical applications.

3.5 REFERENCES

- [1] K. Ariga, Q.M. Ji, J.P. Hill, Y. Bando, M. Aono, Forming nanomaterials as layered functional structures toward materials nanoarchitectonics, *Npg Asia Mater*, 4 (2012) 1884-4049.
- [2] P.T. Hammond, Building biomedical materials layer-by-layer, *Mater Today*, 15 (2012) 196-206.
- [3] J.J. van den Beucken, X.F. Walboomers, M.R. Vos, N.A. Sommerdijk, R.J. Nolte, J.A. Jansen, Biological responses to multilayered DNA-coatings, *Journal of biomedical materials research. Part B, Applied biomaterials*, 81 (2007) 231-238.
- [4] S. De Koker, L.J. De Cock, P. Rivera-Gil, W.J. Parak, R. Auzely Velty, C. Vervaet, J.P. Remon, J. Grooten, B.G. De Geest, Polymeric multilayer capsules delivering biotherapeutics, *Adv Drug Deliv Rev*, 63 (2011) 748-761.
- [5] C.M. Jewell, J. Zhang, N.J. Fredin, M.R. Wolff, T.A. Hacker, D.M. Lynn, Release of plasmid DNA from intravascular stents coated with ultrathin multilayered polyelectrolyte films, *Biomacromolecules*, 7 (2006) 2483-2491.
- [6] E.M. Saurer, R.M. Flessner, S.P. Sullivan, M.R. Prausnitz, D.M. Lynn, Layer-by-Layer Assembly of DNA- and Protein-Containing Films on Microneedles for Drug Delivery to the Skin, *Biomacromolecules*, 11 (2010) 3136-3143.
- [7] E.M. Saurer, C.M. Jewell, J.M. Kuchenreuther, D.M. Lynn, Assembly of erodible, DNA-containing thin films on the surfaces of polymer microparticles: toward a layer-by-layer approach to the delivery of DNA to antigen-presenting cells, *Acta Biomater*, 5 (2009) 913-924.
- [8] Y. Hu, K. Cai, Z. Luo, R. Zhang, L. Yang, L. Deng, K.D. Jandt, Surface mediated in situ differentiation of mesenchymal stem cells on gene-functionalized titanium films fabricated by layer-by-layer technique, *Biomaterials*, 30 (2009) 3626-3635.
- [9] F. Yamauchi, K. Kato, H. Iwata, Layer-by-layer assembly of poly(ethyleneimine) and plasmid DNA onto transparent indium-tin oxide electrodes for temporally and spatially specific gene transfer, *Langmuir*, 21 (2005) 8360-8367.
- [10] Y. Lvov, G. Decher, G. Sukhorukov, Assembly of Thin-Films by Means of Successive Deposition of Alternate Layers of DNA and Poly(Allylamine), *Macromolecules*, 26 (1993) 5396-5399.
- [11] D. Richard, I. Nguyen, C. Affolter, F. Meyer, P. Schaaf, J.C. Voegel, D. Bagnard, J. Ogier, Polyelectrolyte multilayer-mediated gene delivery for semaphorin signaling pathway control, *Small*, 6 (2010) 2405-2411.
- [12] J.T. Zhang, L.S. Chua, D.M. Lynn, Multilayered thin films that sustain the release of functional DNA under physiological conditions, *Langmuir*, 20 (2004) 8015-8021.
- [13] K. Ray, R. Badugu, J.R. Lakowicz, Polyelectrolyte layer-by-layer assembly to control the distance between fluorophores and plasmonic nanostructures, *Chem Mater*, 19 (2007) 5902-5909.
- [14] P.C. DeMuth, J.J. Moon, H. Suh, P.T. Hammond, D.J. Irvine, Releasable layer-by-layer assembly of stabilized lipid nanocapsules on microneedles for enhanced transcutaneous vaccine delivery, *ACS Nano*, 6 (2012) 8041-8051.
- [15] Q.H. Jiang, L. Liu, J.W. Shen, S. Peel, G.L. Yang, S.F. Zhao, F.M. He, Influence of multilayer rhBMP-2 DNA coating on the proliferation and differentiation of MC3T3-E1 cells seeded on roughed titanium surface, *J Biomed Mater Res A*, 100 (2012) 2766-2774.
- [16] Q.K. Lin, K.F. Ren, J. Ji, Hyaluronic acid and chitosan-DNA complex multilayered thin film as surface-mediated nonviral gene delivery system, *Colloid Surface B*, 74 (2009) 298-303.
- [17] F. Meyer, V. Ball, P. Schaaf, J.C. Voegel, J. Ogier, Polyplex-embedding in polyelectrolyte multilayers for gene delivery, *Biochim. Biophys. Acta*, 1758 (2006) 419-422.
- [18] G. Coue, C. Freese, R.E. Unger, C.J. Kirkpatrick, J.F. Engbersen, Bioresponsive poly(amidoamine)s designed for intracellular protein delivery, *Acta Biomater*, 9 (2013) 6062-6074.
- [19] C. Lin, C.J. Blaauboer, M.M. Timoneda, M.C. Lok, M. van Steenbergen, W.E. Hennink, Z. Zhong, J. Feijen, J.F. Engbersen, Bioreducible poly(amido amine)s with oligoamine side chains: synthesis, characterization, and structural effects on gene delivery, *J Control Release*, 126 (2008) 166-174.
- [20] C. Lin, J.F. Engbersen, Effect of chemical functionalities in poly(amido amine)s for non-viral gene transfection, *J Control Release*, 132 (2008) 267-272.
- [21] M. Piest, C. Lin, M.A. Mateos-Timoneda, M.C. Lok, W.E. Hennink, J. Feijen, J.F.J. Engbersen, Novel poly(amido amine)s with bioreducible disulfide linkages in their diamino-units: Structure effects and in vitro gene transfer properties, *J Control Release*, 132 (2008) E12-E13.
- [22] L.J. van der Aa, P. Vader, G. Storm, R.M. Schiffelers, J.F.J. Engbersen, Optimization of poly(amido amine)s as vectors for siRNA delivery, *J. Control. Release*, 150 (2011) 177-186.
- [23] N. Donoghue, P.T. Yam, X.M. Jiang, P.J. Hogg, Presence of closely spaced protein thiols on the surface of mammalian cells, *Protein Sci*, 9 (2000) 2436-2445.
- [24] B. Sahaf, K. Heydari, L.A. Herzenberg, L.A. Herzenberg, The extracellular microenvironment plays a key role in regulating the redox status of cell surface proteins in HIV-infected subjects, *Arch Biochem Biophys*, 434 (2005) 26-32.
- [25] D. Luo, W.M. Saltzman, Enhancement of transfection by physical concentration of DNA at the cell surface, *Nat Biotechnol*, 18 (2000) 893-895.
- [26] T. Segura, M.J. Volk, L.D. Shea, Substrate-mediated DNA delivery: role of the cationic polymer structure and extent of modification, *J Control Release*, 93 (2003) 69-84.
- [27] H. Shen, J. Tan, W.M. Saltzman, Surface-mediated gene transfer from nanocomposites of controlled texture, *Nat Mater*, 3 (2004) 569-574.
- [28] J. Blacklock, H. Handa, D. Soundara Manickam, G. Mao, A. Mukhopadhyay, D. Oupicky, Disassembly of layer-by-layer films of plasmid DNA and reducible TAT polypeptide, *Biomaterials*, 28 (2007) 117-124.



- [29] J. Blacklock, Y.Z. You, Q.H. Zhou, G. Mao, D. Oupicky, Gene delivery in vitro and in vivo from bioreducible multilayered polyelectrolyte films of plasmid DNA, *Biomaterials*, 30 (2009) 939-950.
- [30] E. Redolfi Riva, A. Desii, S. Sartini, C. La Motta, B. Mazzolai, V. Mattoli, PMMA/Polysaccharides Nanofilm Loaded with Adenosine Deaminase Inhibitor for Targeted Anti-inflammatory Drug Delivery, *Langmuir*, 29 (2013) 13190-13197.
- [31] K.C. Wood, H.F. Chuang, R.D. Batten, D.M. Lynn, P.T. Hammond, Controlling interlayer diffusion to achieve sustained, multiagent delivery from layer-by-layer thin films, *Proceedings of the National Academy of Sciences*, 103 (2006) 10207-10212.
- [32] B.-S. Kim, H.-i. Lee, Y. Min, Z. Poon, P.T. Hammond, Hydrogen-bonded multilayer of pH-responsive polymeric micelles with tannic acid for surface drug delivery, *Chem. Commun.*, (2009) 4194-4196.
- [33] D.J. Schmidt, J.S. Moskowitz, P.T. Hammond, Electrically Triggered Release of a Small Molecule Drug from a Polyelectrolyte Multilayer Coating, *Chem Mater*, 22 (2010) 6416-6425.
- [34] S.L. Bechler, D.M. Lynn, Characterization of Degradable Polyelectrolyte Multilayers Fabricated Using DNA and a Fluorescently-Labeled Poly(β -amino ester): Shedding Light on the Role of the Cationic Polymer in Promoting Surface-Mediated Gene Delivery, *Biomacromolecules*, 13 (2012) 542-552.
- [35] A. Zintchenko, L.J. van der Aa, J.F. Engbersen, Improved synthesis strategy of poly(amidoamine)s for biomedical applications: catalysis by "green" biocompatible earth alkaline metal salts, *Macromol. Rapid Commun.*, 32 (2011) 321-325.
- [36] S.T. Kim, K. Saha, C. Kim, V.M. Rotello, The role of surface functionality in determining nanoparticle cytotoxicity, *Acc. Chem. Res.*, 46 (2013) 681-691.
- [37] G. Decher, J. Schmitt, Fine-Tuning of the film thickness of ultrathin multilayer films composed of consecutively alternating layers of anionic and cationic polyelectrolytes, in: C. Helm, M. Lösche, H. Möhwald (Eds.) *Trends in Colloid and Interface Science VI*, Steinkopff, 1992, pp. 160-164.
- [38] S.S. Shiratori, M.F. Rubner, pH-dependent thickness behavior of sequentially adsorbed layers of weak polyelectrolytes, *Macromolecules*, 33 (2000) 4213-4219.
- [39] S.Y. Park, M.F. Rubner, A.M. Mayes, Free energy model for layer-by-layer processing of polyelectrolyte multilayer films, *Langmuir*, 18 (2002) 9600-9604.
- [40] K. Cai, Y. Hu, Y. Wang, L. Yang, Build up of multilayered thin films with chitosan/DNA pairs on poly(D,L-lactic acid) films: physical chemistry and sustained release behavior, *J Biomed Mater Res A*, 84 (2008) 516-522.
- [41] A.J. Ruiz-Chica, A. Soriano, I. Tunon, F.M. Sanchez-Jimenez, E. Silla, F.J. Ramirez, FT-Raman and QM/MM study of the interaction between histamine and DNA, *Chem Phys*, 324 (2006) 579-590.
- [42] G. Ladam, P. Schaad, J.C. Voegel, P. Schaaf, G. Decher, F. Cuisinier, In situ determination of the structural properties of initially deposited polyelectrolyte multilayers, *Langmuir*, 16 (2000) 1249-1255.
- [43] K.F. Ren, Y.X. Wang, J. Ji, Q.K. Lin, J.C. Shen, Construction and deconstruction of PLL/DNA multilayered films for DNA delivery: Effect of ionic strength, *Colloid Surface B*, 46 (2005) 63-69.
- [44] C. Schüler, F. Caruso, Decomposable Hollow Biopolymer-Based Capsules, *Biomacromolecules*, 2 (2001) 921-926.
- [45] A.J. Nolte, N. Takane, E. Hindman, W. Gaynor, M.F. Rubner, R.E. Cohen, Thin Film Thickness Gradients and Spatial Patterning via Salt Etching of Polyelectrolyte Multilayers, *Macromolecules*, 40 (2007) 5479-5486.
- [46] H. Mjehed, J.-C. Voegel, B. Senger, A. Chassepot, A. Rameau, V. Ball, P. Schaaf, F. Boulmedais, Hole formation induced by ionic strength increase in exponentially growing multilayer films, *Soft Matter*, 5 (2009) 2269-2276.
- [47] Y. Tokuda, T. Miyagishima, K. Tomida, B. Wang, S. Takahashi, K. Sato, J.-i. Anzai, Dual pH-sensitive layer-by-layer films containing amphoteric poly(diallylamine-co-maleic acid), *J. Colloid Interface Sci.*, 399 (2013) 26-32.
- [48] P.R. Dash, M.L. Read, L.B. Barrett, M.A. Wolfert, L.W. Seymour, Factors affecting blood clearance and in vivo distribution of polyelectrolyte complexes for gene delivery, *Gene Ther*, 6 (1999) 643-650.

ABSTRACT

Multilayered thin films from weak polyelectrolytes often suffer from stability issues both physically and chemically. For bioactive delivery applications, instability of such systems may result in the burst release of valuable payloads which could also lead to toxicity. Herein, the study of stability improvement of multilayered thin films based on poly(amido amine)s (i.e. weak positively-charged polyelectrolytes) and DNA is reported, typically in relation to stability under physiological conditions. Two homopolymers (p(CBA-ABOL), containing primary alcohol side chain and p(CBA-DAB) containing primary amine side chain) and their random copolymers, p(CBA-ABOL_{90%}/DAB_{10%}) and p(CBA-ABOL_{65%}/DAB_{35%}) were synthesized and studied for the effect of charge density on multilayer build-up and stability with DNA. It was found that increasing ABOL content resulted in higher incremental increase of the amount of incorporated DNA per deposition cycle, but also in decreasing stability, resulting in up to more than half payloads released within only 1 h for ABOL-homopolymer multilayers. To maintain higher incremental increase while improving stability, in an approach directed at chemical crosslinking, the 90%ABOL films were treated after assembly with glutaraldehyde (GA). The stability profile was drastically improved both under physiological conditions and in the presence of reductive agent which degrades the disulfide bonds in the polymer main chain. AFM surface profiles and contact angles were recorded for these copolymer-based films after every other layer deposition, and after GA crosslinking. During multilayer build-up no alternating patterns in surface profile and contact angle of topmost layer were observed, which is in contrast to those of 100%DAB and 100%ABOL homopolymer systems. GA crosslinking was also found to cause no significant difference in the surface profiles. In an *in vitro* cell culture study of COS-7 cells on top of GA-crosslinked 90%ABOL films with GFP-encoded pDNA as the DNA component, cell attachment was poorer on the GA-crosslinked films than on a 100%ABOL system, but better than on a 100%DAB system. Transfection efficiency in the crosslinked multilayers was reduced compared to the non-crosslinked analog, most likely due to insufficient release of pDNA from the GA-crosslinked films. The non-crosslinked 90%ABOL multilayers successfully mediated transfection, albeit significantly lower than that of 100%ABOL-homopolymer, most likely also due to reduced release of pDNA. This study illustrates the importance of finding an optimal degree of physical or chemical crosslinking of the multilayer to obtain sufficient stability of the film on one hand and sufficient rate of degradation on the other hand to allow controlled release of bioactive compounds from these thin film systems.

[‡] Sry D. Hujaya, Jos M.J. Paulusse, Johan F.J. Engbersen, submitted for publication.

4.1 INTRODUCTION

Previously we reported a series of bioreducible multilayered thin films prepared from linear poly(amido amine)s (PAAs) [1-3] aimed at surface-mediated cell transfection (Chapter 3). The chosen PAAs were able to promote deposition of DNA in a linear fashion. However, the films were found to undergo rearrangement when exposed to physiological salt concentration, resulting in fast burst release of approximately half of the incorporated polymer and DNA. This rearrangement/release phenomenon was found to be crucial to their performance in surface-mediated cell transfection *in vitro*, causing these films to act as polyplex-releasing surfaces.

In this chapter, to further understand the instability/rearrangement in weak-polyelectrolyte-based multilayers, the development of more stable multilayers and the effects thereof on cell-transfecting properties is described. The ability of cells to locally induce degradation of a multilayered surface on which they grow has been reported previously [4]. More recently, Blacklock et al. reported that transfection of cells cultured on the surface of a stable multilayer from a reducible poly(amido amine) dendrimer and DNA may take place through reduction of the polycation by reducing enzymes present on the cellular membrane [5]. It is therefore speculated that even without a burst release phase, transfection could still be achieved via this cell-induced degradation that would lead to transfection in a more controlled and longer sustained manner.

In the previous study (Chapter 3), PAAs with higher charge density (i.e. p(CBA-DAB), containing protonated primary amine side chains) were found to give more stable films than PAAs lacking these extra cationic groups (p(CBA-ABOL)). However, the p(CBA-DAB) multilayers gave poor performance in mediating cell transfection, whereas the p(CBA-ABOL) multilayers displayed rapid release/rearrangement under physiological salt conditions and good mediation of cell transfection. Based on these findings, it is hypothesized that copolymers with an optimal composition of the two types of side groups could result in a multilayered system with both increased stability and good transfection capability. Two concepts were investigated in this study, (i) the effect of increasing extent of physical crosslinking within the multilayers through variation of the percentage of cationic side chains in the PAA polymers, and in addition to that (ii) the effect of chemical crosslinking to reinforce the obtained films with glutaraldehyde.

Glutaraldehyde (GA) is considered as a very economical and fast fixating agent for bioprostheses and cells, and for crosslinking and/or immobilizing various proteins/polysaccharides on surfaces [6]. It has also been used to crosslink gelatin and alginate-based drug carriers to decrease their dissolution rate under physiological conditions [7]. In the preparation of multilayered thin films, GA has been used to induce a chemical interlayer crosslink in multilayers [8, 9] aimed to increase stability [10] and/or immobilize proteins [11]. By controlling the percentage of the reacting primary amine side chains in the PAA copolymers, the extent of GA crosslinking may be controlled and thus optimized to avoid cytotoxicity [12]. Adami et al. reported that depending on the GA molar equivalency used, GA-crosslinked protein-DNA polyplexes can provide up to two times higher levels of transfection in a steady manner over longer periods as compared to the non-crosslinked polyplexes [13].

The reaction mechanism of GA crosslinking itself has been of much debate [7]. Although it is still widely accepted that the GA reaction with amines results in Schiff base formation, it is often argued that the chemical robustness of GA crosslinks cannot be attributed simply through the formation of unstable imine. The possibility of cyclization and auto-polymerization further complicate the mechanism to the point where the reactive GA species is difficult to determine. In this study, a general GA crosslinking procedure is applied where dilute GA solution is used to favor the presence of monomeric GA for reaction with primary amines of the PAA copolymer. The general multilayer crosslinking scheme through Schiff base formation is shown in Figure 4.1.

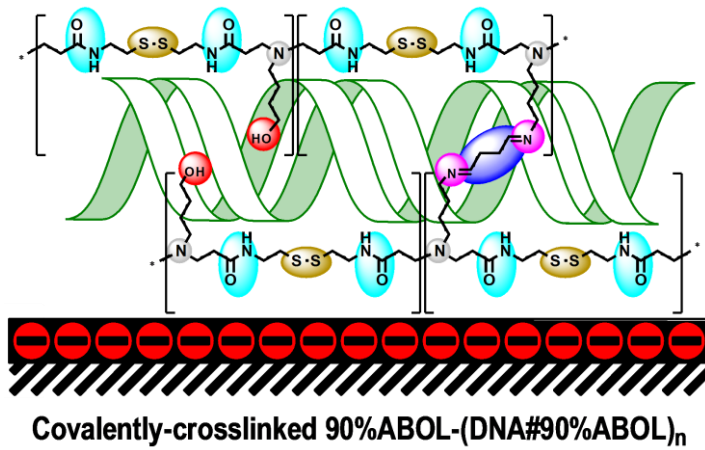
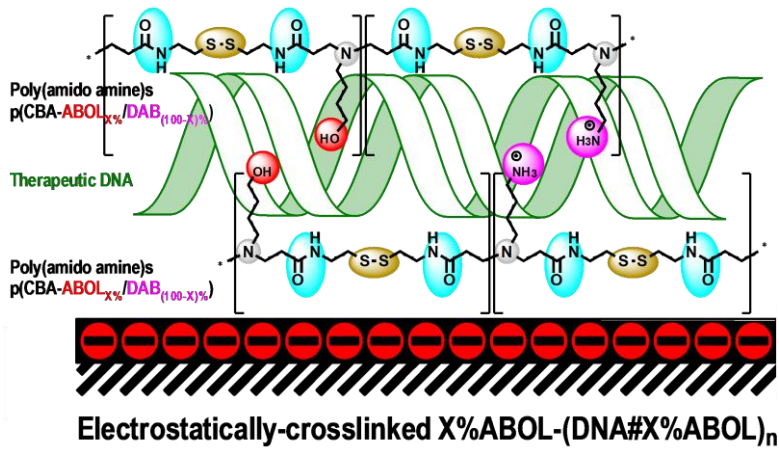


Figure 4.1 (Co)polymer structures and schematic representations of electrostatically-crosslinked, copolymer-based multilayers (top) and inter-layer GA crosslinking through Schiff base formation (bottom). DNA double helix structure is intentionally exaggerated to represent a single DNA layer.

4.2 MATERIALS AND METHODS

N,N'-Cystamine bisacrylamide (CBA, 99.9%) was purchased from Polysciences (Eppelheim, Germany). 4-amino-1-butanol (ABOL, 98.0%), *N*-Boc-1,4-diaminobutane (NBDAB, ≥97.0%), calcium chloride (CaCl₂, ≥93.0%), triethylamine (TEA, ≥99.0%), *tert*-butylamine (*t*BA, ≥99.5%), trifluoroacetic acid (TFA, ≥99.0%), sodium chloride (NaCl, ≥99.5%), calf thymus DNA sodium salt (CTDNA, type 1, fibers, 16.7 A260 unit/mg solid, 6.0% sodium), and glutathione (≥98.0%) were purchased from Sigma-Aldrich (Zwijndrecht, The Netherlands). Sodium dihydrogen phosphate monohydrate (NaH₂PO₄·H₂O, 99.0-102.0%) and disodium hydrogen phosphate dihydrate (Na₂HPO₄·2H₂O, 99.5%) were purchased from Merck (Darmstadt, Germany). Solvents were of reagent grade and used without further purification unless otherwise noted. Milli-Q water (18.2 MΩ·cm at 25 °C) was obtained from a Synergy® water purification system (Millipore).

PBS buffer was prepared by dissolving 1.54 g of Na₂HPO₄·2H₂O, 0.30 g of NaH₂PO₄·H₂O, and 8.20 g of NaCl into 1.00 L of Milli-Q water and adjusting the pH to 7.4.

CTDNA solution in water was prepared by dissolving shredded CTDNA into Milli-Q water to the final concentration of 1.0 mg/mL. The solution was placed in an ice bath and then sonicated (Sonoplus HD2070, Bandelin, Berlin, Germany) for 20 min at 10% power, 20 kHz frequency, and 7 cycles (i.e. 0.7 s of active interval followed by 0.3 s of passive interval).

¹H-NMR spectra were recorded on an AVANCE III-400MHz NMR (Bruker, Wormer, The Netherlands) spectrometer. Gel permeation chromatograms were recorded on a Polymer Labs GPC 220 in 0.1 M NaOAc buffer pH 4 with 25% methanol as eluent and 0.7 mL/min flow rate against poly(ethylene glycol) (PEG) standards.

Ultraviolet (UV) characterization of multilayered thin films was performed in the dry state using a UV-2401 PC (Shimadzu, 's-Hertogenbosch, The Netherlands) UV spectrophotometer. Each film fabricated on UV-transparent 7.5 x 37 x 1 mm quartz glass (Ted Pella, Redding, USA) was measured in three different arbitrary positions. Absorbance scan was carried out in the 200-400 nm wavelength range. All data points were then corrected for baseline offset by subtracting the absorbance value at 400 nm from each data point. Relative absorbance values were obtained by normalizing each data point with the respective value at time 0.

AFM characterization was performed on a Multimode AFM (Bruker, Wormer, The Netherlands) with Nanoscope IV controller in contact mode using an MSCT cantilever with moderate spring constant of 0.5 N/m. Multilayered thin film samples were fabricated on single side polished silicon wafer (n-type, 525 μm thick, MESA+NanoLab, Enschede, The Netherlands) diced into 7.5 x 32 mm pieces.

Contact angle measurements were performed on a Krüss G10 (KRÜSS, Hamburg, Germany) contact angle measuring instrument.

pCMV-GFP plasmid DNA (pDNA) reporter gene was purchased from PlasmidFactory (Bielefeld, Germany) at 1.0 mg/mL concentration in water for injection (WFI).

COS-7 cells (European Collection of Animal Cell Cultures (ECACC) Catalogue No. 87021302) were grown in DMEM containing 4.5 g/L glucose and GlutaMAX™ (Invitrogen, Breda, The Netherlands) supplemented with 2% (v/v) PennStrepp (Lonza, Breda, The Netherlands) and 10% (v/v) fetal bovine serum (Lonza, Breda, The Netherlands).

Cell imaging was performed at 4X, 10X, 20X, and/or 40X objectives using EVOS digital inverted microscope (EMS, Wageningen, The Netherlands) equipped with GFP light cube for expressed GFP fluorescence imaging.

4.2.1 SYNTHESIS OF P(CBA-ABOL) (100%ABOL) AND P(CBA-DAB) (100%DAB)

Syntheses of both p(CBA-ABOL) and p(CBA-DAB) were carried out according to the procedure explained in Chapter 3.

4.2.2 SYNTHESIS OF P(CBA-ABOL_{90%}/DAB_{10%}) (90%ABOL)

N,N'-Cystamine bisacrylamide (1.13 g; 4.34 mmol), *N*-Boc-1,4-diaminobutane (0.09 g; 4.81 mmol), and 4-amino-1-butanol (0.35 g; 3.89 mmol) were mixed in a brown polymerization flask using 2.2 mL of methanol/water 3/1 as solvent and containing 200 mM CaCl₂ as catalyst based on a recent report by Zintchenko et al. [14]. Polymerization was carried out under N₂ atmosphere for three days at 70 °C during which a gradual viscosity increase was observed. The polymerization was terminated by adding excess *tert*-butylamine (1.5 mL; 14.2 mmol) into the mixture and stirring at 70 °C for two more days. After bringing the flask to room temperature, the solution was diluted and acidified to pH ~5 by addition of 4 M HCl and purified by ultrafiltration using a 1,000 Da MWCO membrane. The purified polymer solution was then freeze-dried leaving white foam-like solid as the final product in its HCl-salt form (0.9 g; 57% recovery). ¹H-NMR spectroscopy confirmed complete termination.

Deprotection was carried out by dissolving the polymer in a mixture of methanol/TFA over the course of one day. The solution was then brought to pH ~5 by addition of 1 M NaOH, filtered through a filter paper and dialyzed using a 1,000 Da MWCO membrane. The purified polymer solution was finally freeze-dried to yield white transparent solid as the final product in its HCl-salt form (0.77 g; 86% recovery). ¹H-NMR characterization confirmed complete deprotection and allowed determination of the number-average MW based on the *tert*-butylamine end-group. ¹H-NMR (D₂O) δ (ppm) = 1.39 (s, 9H, (CH₃)₃R); 1.63 (q, 2H, HOCH₂CH₂CH₂); 1.75 (m, 2H, NH₂CH₂CH₂); 1.84 (m, 2H, HOCH₂CH₂ and NH₂CH₂CH₂CH₂); 2.81 (t, 4H, CH₂CONHRNHCOCH₂); 2.88 (t, 4H, CH₂SSCH₂); 3.09 (t, 2H, CH₂NH₃); 3.27 (t, 2H, NHCOCH₂CH₂NHR); 3.49 (t, 4H, NCOCH₂CH₂NRCH₂); 3.56 (t, 4H, CH₂CH₂SSCH₂CH₂); 3.65 (t, 2H, CH₂OH).

4.2.3 SYNTHESIS OF P(CBA-ABOL_{65%}/DAB_{35%}) (65%ABOL)

For the synthesis, the same procedure was followed as described above, using *N,N'*-cystamine bisacrylamide (1.02 g; 3.9 mmol), *N*-Boc-1,4-diaminobutane (0.31 g; 1.59 mmol), and 4-amino-1-butanol (0.21 g; 2.3 mmol). Yield was 0.87 g (57% recovery) and 0.41 g (48% recovery), before and after BOC-deprotection. ¹H-NMR (D₂O) δ (ppm) = 1.36 (s, 9H, (CH₃)₃R); 1.61 (q, 2H, HOCH₂CH₂CH₂); 1.74 (m, 2H, NH₂CH₂CH₂); 1.83 (m, 2H, HOCH₂CH₂ and NH₂CH₂CH₂CH₂); 2.79 (t, 4H, CH₂CONHRNHCOCH₂); 2.85 (t, 4H, CH₂SSCH₂); 3.06 (t, 2H, CH₂NH₃); 3.25 (t, 2H, NHCOCH₂CH₂NHR); 3.46 (t, 4H, NCOCH₂CH₂NRCH₂); 3.53 (t, 4H, CH₂CH₂SSCH₂CH₂); 3.62 (t, 2H, CH₂OH).

4.2.4 MULTILAYERED THIN FILMS CONSTRUCTION AND BUILD-UP PROFILES

Fresh PAA solutions were prepared short before the start of multilayer build-up from the solid materials, which had been re-lyophilized overnight to avoid weighing errors due to their hygroscopic properties. All PAA solutions (2.0 mg/mL) were prepared in PBS buffer at pH 7.4 to avoid possible variations in pH. All CTDNA solutions (1.0 mg/mL) in Milli-Q water were prepared from a single batch.

Prior to assembly, quartz or silicon wafer substrates (7.5 x 32 mm) were etched for 30 minutes in piranha acid solution, rinsed with copious amounts of Milli-Q water, and dried under N₂ stream. These substrates were then dipped into PAA solution (2.0 mg/mL in PBS buffer pH 7.4) for 10 min, transferred into washing solution containing PBS buffer for 1 min, dipped briefly in a large amount of Milli-Q water, transferred into CTDNA (1.0 mg/mL in Milli-Q water) solution for 10 min, dipped into the second washing solution containing Milli-Q water for 1 min, and finally followed by another brief dipping in Milli-Q. This cycle was repeated to reach the desired number of bilayers. Drying under N₂ stream was performed after every PAA-layer deposition, excluding the very first layer.

The resulting ensemble is denoted by PAA-(CTDNA#PAA)_n, where PAA represents the identity of the poly(amido amine) used and *n* represents the number of bilayer. The first PAA layer is regarded as a precursor layer and therefore excluded from the bilayer number count. Typically, the ensemble consists of 10 bilayer with the poly(amido amine) polymer as the last layer. For every multilayered system, three samples were fabricated in parallel to give estimation for standard deviation. To study the build-up profiles, UV spectra were recorded after each drying step following PAA layer formation. Afterwards, the multilayers were dipped into CTDNA solution to continue multilayer build-up.

To study the build-up profiles of every multilayer, UV spectra were recorded after each drying step; i.e. after every PAA-layer deposition, excluding the very first layer. Afterwards, the multilayers were dipped into CTDNA solution to continue multilayer build-up.

4.2.5 CHEMICAL CROSSLINKING WITH GLUTARALDEHYDE

Crosslinking of the multilayers using glutaraldehyde was carried out by dipping 90%ABOL-(CTDNA#90%ABOL)₁₀ multilayers in a 2.5 wt% GA solution in water at RT for 3 hours. After the incubation, all films were incubated in a large amount of Milli-Q water at RT overnight to ensure that all unreacted GA were removed from the films. The films were then dried under N₂ stream.

As controls, similar multilayers were also subjected to this treatment, though in absence of GA.

4.2.6 CONTACT ANGLE MEASUREMENTS

Static contact angles (θ) were measured with Milli-Q water (18.2 M Ω -cm) on a Krüss G10 Contact Angle Measuring Instrument. Five drops of Milli-Q water (approximately 1.5 μ L) were measured on five different spots across the surface and averaged to obtain θ . Images were recorded and measured for θ approximately 15 s from the initial contact of the liquid and the surface.

4.2.7 ATOMIC FORCE MICROSCOPY

Multilayers built on silicon wafer substrates were used for AFM microscopy. Imaging was carried out in the middle part of the films (to avoid edge effects/defects) at three different 20 x 20 μ m scan areas at 512 x 512 pixels. Images were taken and analyzed using Nanoscope software version 7.30. Height data was flattened using first or second order fitting and root mean square roughness (RMS) was calculated over the scan area. To estimate film thickness, a scratch was made using a small syringe needle and imaged as described. Thicknesses were measured as the average of one 'depth' measurement and three 'section' measurements across the scratch.

4.2.8 FILM STABILITY UNDER PHYSIOLOGICAL CONDITIONS

Stability profiles of the three multilayers in PBS buffer pH 7.4 at 37 °C was investigated by dipping the multilayers formed on quartz slides in 2 mL of PBS buffer pH 7.4 solution and incubating them in a water bath with temperature set to 37 °C. From time to time, the multilayers were removed, briefly dipped in a large amount of Milli-Q water, dried under N₂ stream and measured by UV-Vis spectrophotometer.

4.2.9 DEGRADATION PROFILES UNDER REDUCING CONDITIONS

Degradability of the multilayered thin films was investigated in a similar fashion as for their stability profiles under physiological conditions (Section 4.2.8), though in the presence of 5.0 mM of glutathione in the incubation medium. The solution of 5.0 mM glutathione in PBS buffer pH 7.4 was prepared fresh directly prior to the start of experiment. Due to instability of glutathione in PBS buffer pH 7.4, no solution of over three hours old was used.

4.2.10 CELL CULTURE AND TRANSFECTION

Multilayered thin films were fabricated as described in Section 4.2.4 on 0.7 x 1.8 cm microscope glass slides as substrates. These multilayered systems were placed in tissue culture (TC)-treated 12-well plates after being sterilized in 70% ethanol for at least 20 min followed by three consecutive washing steps with sterile water and air drying inside the laminar flow hood (no change in spectral properties was found based on UV spectroscopy). On top of these films COS-7 cells were seeded at seeding densities of 20,000 cells/sample and left to attach for at least 15 h, after which images were recorded and 1.5 mL of fresh medium was added to every well. Cells were then left to proliferate further at 37 °C in humidified atmosphere with 5% CO₂. After 2 days of culture, signs of transfection were imaged using an EVOS digital inverted microscope. Experiments were performed in triplicate for each sample. As positive controls, cells were seeded directly on TC-treated well plates on approximately the same surface area as for cells seeded on sample constructs.

To further quench any free glutaraldehyde left in the multilayered systems, some GA-crosslinked films were also treated with ethanolamine by incubation in 1 M ethanolamine solution in Milli-Q with pH adjusted to 9 for 30 min before being washed further overnight in Milli-Q water.

4.3 RESULTS AND DISCUSSION

4.3.1 SYNTHESIS OF THE PAA COPOLYMERS P(CBA-ABOL_{90%}/DAB_{10%}) AND P(CBA-ABOL_{65%}/DAB_{35%})

Two random PAA copolymers with different percentage of hydroxybutyl (ABOL) and aminobutyl (DAB) side chains were synthesized via CaCl₂-catalyzed Michael addition polymerization. To obtain the highest degrees of polymerization, Michael-addition polymerization was performed using an equimolar mixture of free amine and bisacrylamides. Moreover, solvent was kept to a minimum amount to increase the rate of the polymerization. N₂ gas as protective atmosphere, in combination with a brown reaction flask, were used to prevent radical formation. CaCl₂ was employed as a Lewis acid, which is known to catalyze the addition of nucleophilic amines to α,β -unsaturated carbonyl compounds [15]. All polymerizations were run for two to three days at 70 °C to maximize the degree of polymerization, though not longer in order to avoid retro-Michael reaction and possible amide hydrolysis. Polymerizations were terminated by adding excess *tert*-butylamine (*t*BA), resulting in statistically one *t*BA end group per polymer chain, provided the ideal stoichiometry was achieved. Neutralization and dialysis were then carried out to obtain the PAA product in aqueous solution. Water was removed via lyophilization to obtain the pure polymer in its salt form. For polymers and copolymers containing DAB side chains, an extra BOC-deprotection step was necessary, which was carried out by dissolving the dry product in a methanol/TFA mixture, and stirring overnight at RT. The chemical structure of the obtained copolymers is given in Chart 4.1.

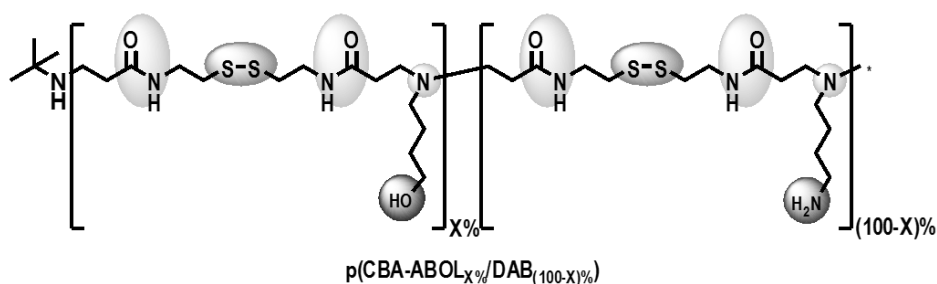


Chart 4.1 Chemical structure of the p(CBA-ABOL_{x%}/DAB_{(100-x)%}) copolymers.

From the ¹H-NMR spectra, the observed singlet corresponding to the *t*BA end group was used to make an estimation of the number-average molecular weight (MW) for each polymer. Polydispersity index (PDI) values were obtained from GPC, together with the weight (M_w) and number (M_n) average molecular weight, relative to PEG standards. These data are shown in detail in Table 4.1. The percentage of ABOL and DAB functionalization is estimated by comparing the integration values of the two most-upfield signals (not the *t*Bu singlet signal). The quintet at 1.63 ppm corresponds solely to the ABOL-side chain, but the multiplets at 1.75 and 1.84 ppm correspond to both ABOL and DAB side chain. The difference between the two multiplets' integration values and that of the quintet gives the integration value of 4 protons exclusively belonging to the DAB side chain.

Table 4.1 ¹H-NMR and GPC characterizations on the molecular weights in kg/mol and PDI of PAA products.

PAA name	Abbreviation	¹ H-NMR end group analysis		GPC (PEG standard)		
		n	M_n	M_w (kDa)	M_n (kDa)	PDI
p(CBA-ABOL)	100%ABOL	26	9.0	3.8	3.2	1.18
p(CBA-ABOL _{90%} /DAB _{10%})	90%ABOL	38	11.2	n/a		
p(CBA-ABOL _{65%} /DAB _{35%})	65%ABOL	20	7.9	4.6	3.5	1.32
p(CBA-DAB)	100%DAB	19	6.6	7.3	5.5	1.34

The DAB content in the copolymers was kept minimal to reduce possible cytotoxicity, while maintaining maximal DNA deposition. As with other step-growth polymerization reactions, control of molecular weight is limited by the equimolarity and reactivity of the reactants. It is therefore difficult to synthesize polymer or copolymer with similar

molecular weight. However, we have observed that moderate differences in molecular weight between batches of a PAA do not significantly influence the polymer's properties in multilayer formation with DNA (data not shown). Therefore it is assumed that the effect of the molecular weight differences obtained in the copolymers are not of influence on their properties as multilayer component.

4.3.2 MULTILAYERED THIN FILMS CONSTRUCTION

Build-up profiles of each multilayer were obtained by observing the increase in absorbance of CTDNA at 260 nm after deposition of each bilayer. The topmost layer was always the PAA layer to protect the DNA and promote future cell adhesion. Figure 4.2 shows the build-up profiles of the CTDNA multilayers formed with p(CBA-ABOL), designated as 100%ABOL-(CTDNA#100%ABOL)₁₀, with p(CBA-DAB), designated as 100%DAB-(CTDNA#100%DAB)₁₀, and with the two copolymer p(CBA-ABOL_{90%}/DAB_{10%}), designated as 90%ABOL-(CTDNA#90%ABOL)₁₀, and p(CBA-ABOL_{65%}/DAB_{35%}), designated as 65%ABOL-(CTDNA#65%ABOL)₁₀.

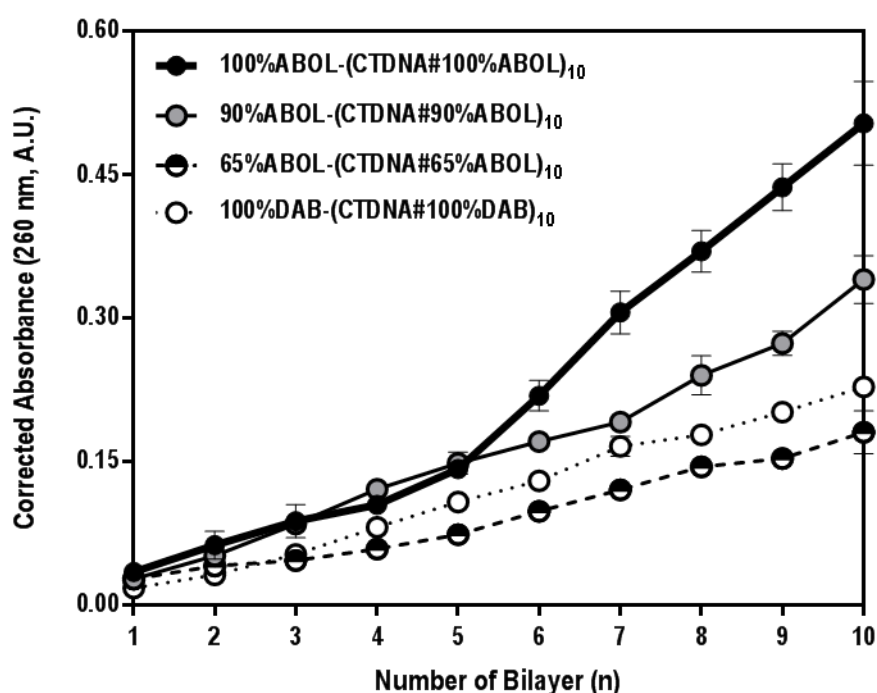


Figure 4.2 Build-up profiles of multilayers prepared using various PAA (co)polymers and CTDNA.

Figure 4.2 demonstrates a tendency of increasing DNA incorporation with increasing ABOL content of the PAAs, which is in agreement with our previous result comparing three homopolymers with side chains of different charge density. Deposition of PAA polymer with lower DAB content (i.e. lower charge density) most likely leads to less compact polymer conformation, due to necessary folding of the polymer backbone to expose cationic charges from the protonated tertiary amino group to the negatively charged DNA surface. This increased surface area of densely packed PAA can also accommodate more incoming polyelectrolyte (DNA in this case) to deposit and subsequently reverse the surface charge from positive to negative again [16, 17]. The almost 40% decrease in DNA incorporation at 10 bl of the 90%ABOL copolymer is in accordance with this idea. However, Figure 4.2 also shows that the DNA incorporation proceeds not proportional to the percentage of ABOL in the copolymer since the DNA build-up of the 65%ABOL is even slightly less than that of the 100%DAB system. This trend suggests that the copolymers may behave differently than the two homopolymers in their interaction with DNA during the multilayer build-up. The presence of both primary amines and primary alcohol side groups in the copolymers may give rise to additional intramolecular interactions not present in the homopolymer systems, causing changes in structural orientation in solution and during deposition on a surface (see Section 4.3.4 and 4.3.5). It has been

reported that structural orientation of polyelectrolytes in solution plays a role in their multilayer deposition and build-up behavior. This is often manifested as dependence on pH and ionic strength of the deposition solution, and the effect is especially prominent with weak and lower molecular weight polyelectrolytes [16-18].

4.3.3 STABILITY PROFILES OF ELECTROSTATICALLY-CROSSLINKED MULTILAYERS

To investigate whether improvements in multilayered film stability could be achieved by using PAA copolymers with different percentages of ABOL and DAB, the stability profiles of films built up from PAA copolymers with 90%ABOL/10%DAB and 65%ABOL/35%DAB in PBS pH 7.4 at 37 °C were investigated and compared with the relevant homopolymers p(CBA-ABOL) and p(CBA-DAB), designated as 100%ABOL and 100%DAB, respectively, as previously investigated in Chapter 3. The stability profiles, as measured by UV (Figure 4.3) shows the expected trend of increasing film stability with increasing DAB content, indicating that charge density is indeed a crucial factor in the multilayer stability of weak polyelectrolytes. With a pKa of ~9, the DAB side group is mostly protonated at pH 7.4, contributing strongly to the electrostatic interaction with DNA, while the primary alcohol can only provide weak hydrogen bond interactions with DNA, which makes multilayers with this polymer more susceptible to interfering electrostatic interactions by ions (Na^+ , Cl^- , H_2PO_4^- , and HPO_4^{2-}) present in the PBS buffer.

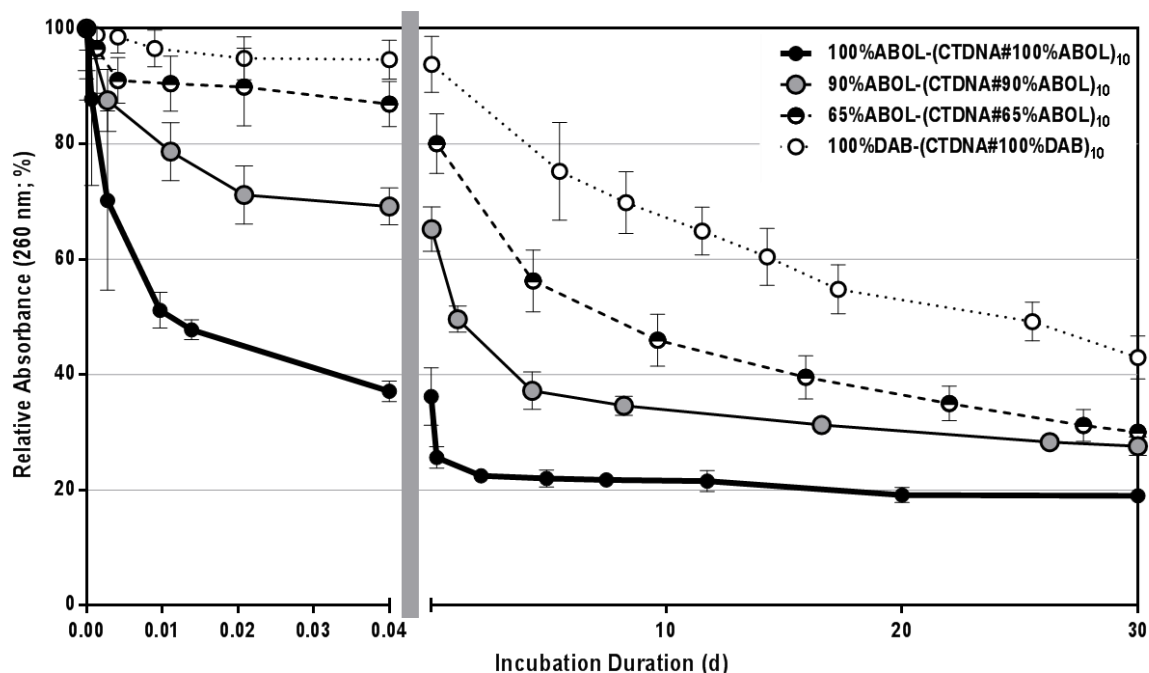


Figure 4.3 Stability profiles of copolymer systems as compared to the homopolymers under physiological conditions (PBS buffer pH 7.4 at 37 °C) *in vitro*. The left part of the abscissa shows the trend of fast decrease (burst release) within 0.04 d (1 h) in the initial phase of the incubation while the right part shows the much slower decrease throughout the rest of the long incubation duration.

4.3.4 GLUTARALDEHYDE CROSSLINKING: UV-VIS CHARACTERIZATIONS

In the previous sections it is shown that increasing charge density in PAAs by the presence of the protonated primary amino groups in the side chains of DAB leads to higher stability of multilayers (Section 4.3.3), but also results in lower incremental increase of DNA incorporation (Section 4.3.2). The latter effect is a drawback, since to reach higher DNA content, more cycles of deposition are needed which would significantly increase processing time. The 90%ABOL copolymer, for example, may still maintain ~70% of its initial DNA content upon incubation under physiological conditions, but when considering the initial 40% lower DNA content at 10 bl compared to the

100%ABOL system, the copolymer system is left with the same amount of DNA at the end of 1 h incubation as with the 100%ABOL. Therefore, with the goal to maintain higher incremental increase in DNA incorporation while increasing stability, the 90%ABOL films were crosslinked with glutaraldehyde (GA).

The multilayered system 90%ABOL-(CTDNA#90%ABOL)₁₀ was subjected to 3 h crosslinking by immersion in 2.5% GA solution in water. The films were then dried and UV spectra were recorded, before being incubated in Milli-Q water overnight, after which another UV characterization step was performed. The overnight incubation in Milli-Q water was carried out to ensure complete crosslinking reaction and removal of traces of GA in the construct. The effects of the crosslinking step on DNA content and UV spectral properties of the films with the relevant controls (with Milli-Q instead of GA in Milli-Q) are displayed in Figure 4.4.

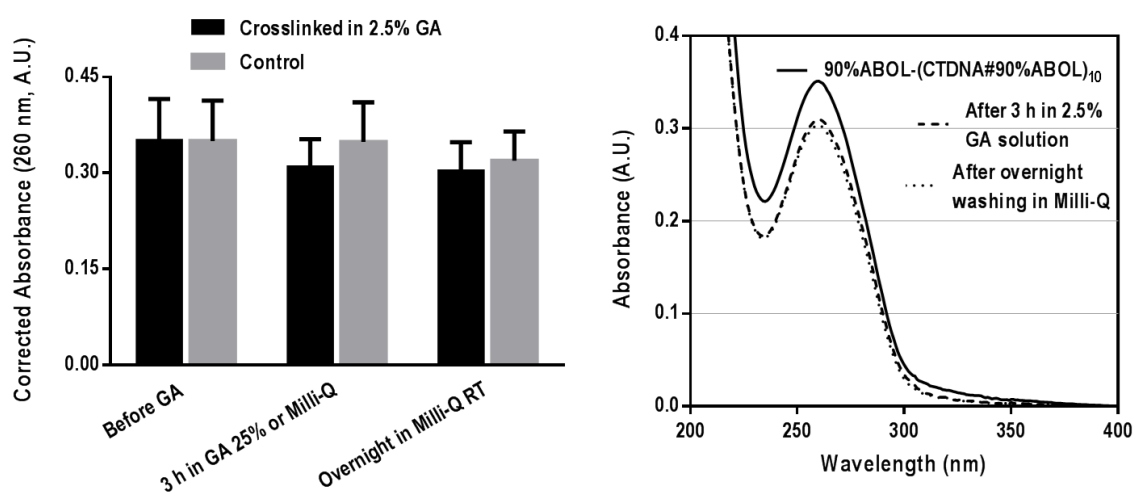


Figure 4.4 Effect of GA crosslinking and subsequent washings on absorbance values at 260 nm (left) and the respective UV spectra (right).

Figure 4.4 shows that upon incubation in pure water or GA solution for 3 h at RT, followed by overnight incubation in Milli-Q, the change in the absorbance values at 260 nm for all samples was not significant. The control films (i.e. non-GA-crosslinked) stayed stable during the overnight incubation in water (without GA), further confirming that instability/burst release is only observed in the presence of salt in the incubation medium.

It is known that aldehyde and imine show UV absorption at 280-300 nm due to their $n-\pi^*$ transition. More specifically, GA in water displays a specific absorption peak at around 280 nm [19]. However, Figure 4.4 does not show detectable differences in terms of spectral shapes of the films before and after crosslinking. This is most likely due to the very low extinction coefficient of the typical $n-\pi^*$ transition, in combination with low degree of GA crosslinking within the films. This further indicates that no excessive unreacted aldehyde groups of GA were present in the films.

4.3.5 CONTACT ANGLE MEASUREMENTS

Changes in contact angles have been used to characterize the alternation in the top-surface during build-up of multilayered systems [20, 21] and also to indicate that a chemical modification has successfully taken place [22]. Figure 4.5 shows the contact angles of the 90%ABOL-(CTDNA#90%ABOL)₁₀ multilayered system at various bilayer numbers. As with the homopolymer systems, complete surface coverage was achieved only after about 4 deposition cycles. Typically, 0.5 and 2-bl systems show lower contact angles indicating incomplete layer coverage on silicon wafer substrate, which is generally more hydrophilic after being piranha-activated. However, unlike the homopolymer systems, bilayer numbers higher than 4 do not show alternating contact angle values between the polymer and DNA topmost layer, the values remain relatively constant. Particularly, DNA topmost

layers of the copolymer system have contact angles at least ten degrees higher than DNA topmost layers of the homopolymer systems while the copolymer topmost layers have contact angles that fall in between the two homopolymer systems. It is interesting to note that these contact angle values of copolymer topmost layers are closer to those of 100%ABOL homopolymer system, agreeing to the higher ABOL content of the copolymer.

The higher contact angle values of DNA topmost layers in the copolymer system, compared to those in homopolymer systems may be due to a different conformation assumed by DNA upon interaction with the copolymer layer. This is also indicated by the DNA-topmost AFM surface profiles (Figure 4.6). It is known that different copolymer systems provide different complexation efficiencies in polyplex systems [3]. This may likewise also translate to differences in conformation behavior upon layer deposition and the subsequent surface profiles.

Figure 4.5 also shows that no significant differences are observed in the water contact angle of the crosslinked system and the non-crosslinked system. This is consistent with the absence of significant differences found for these systems in the UV-Vis characterization. GA crosslinking generally results in significant increase in water contact angle [22], attributed to the increase in hydrophobic content (alkyl chain of GA) on the surface. However, Figure 4.5 shows a minor decrease of $\sim 8.5^\circ$ after GA crosslinking, which may indicate that only moderate crosslinking has taken place, as intended through the presence of only 10% primary amine group in the PAA that can react with GA.

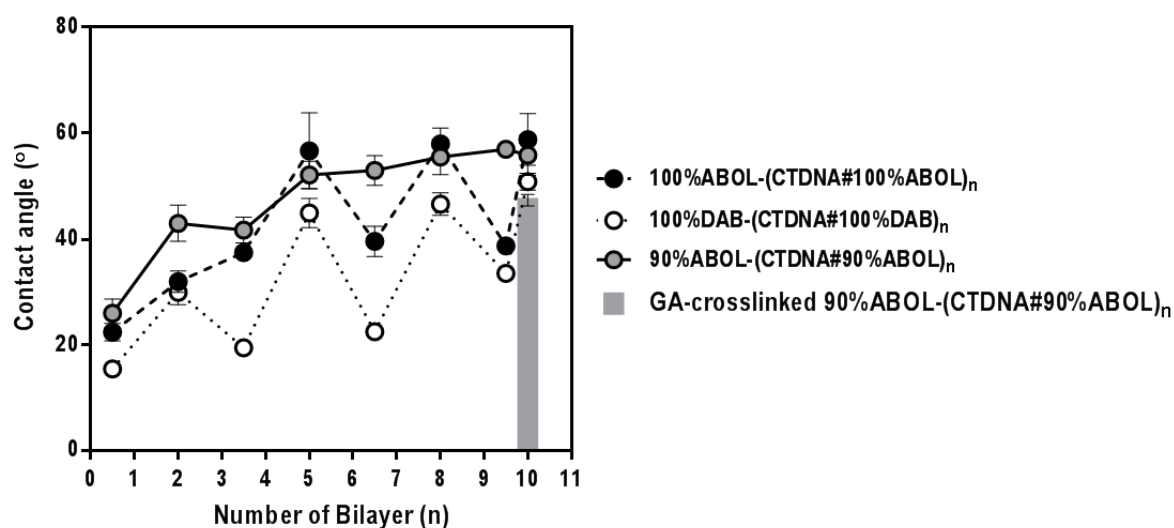


Figure 4.5 Static water contact angles of 90%ABOL-(CTDNA#90%ABOL) multilayer at various bilayer numbers (n) and the effect of GA crosslinking post-assembly. Contact angle data of the relevant homopolymer systems are also given for reference.

4.3.6 ATOMIC FORCE MICROSCOPY

To further confirm the observations from contact angle measurements, surface profiles of the 90%ABOL-based films were characterized by AFM. Figure 4.6 shows the different surface profiles of the multilayers, while maintaining equal height scale range. In comparison to the AFM results shown in Chapter 3, the surface profiles observed here are more similar to polymer-topmost layers, but with relatively higher surface roughness (Figure 4.7). These AFM results agree with the conclusion obtained from the contact angle data by showing that no alternating pattern of surface profiles can be distinguished for this multilayered system. Also in agreement with the contact angle data, the last step of GA crosslinking did not cause major differences in surface profiles.

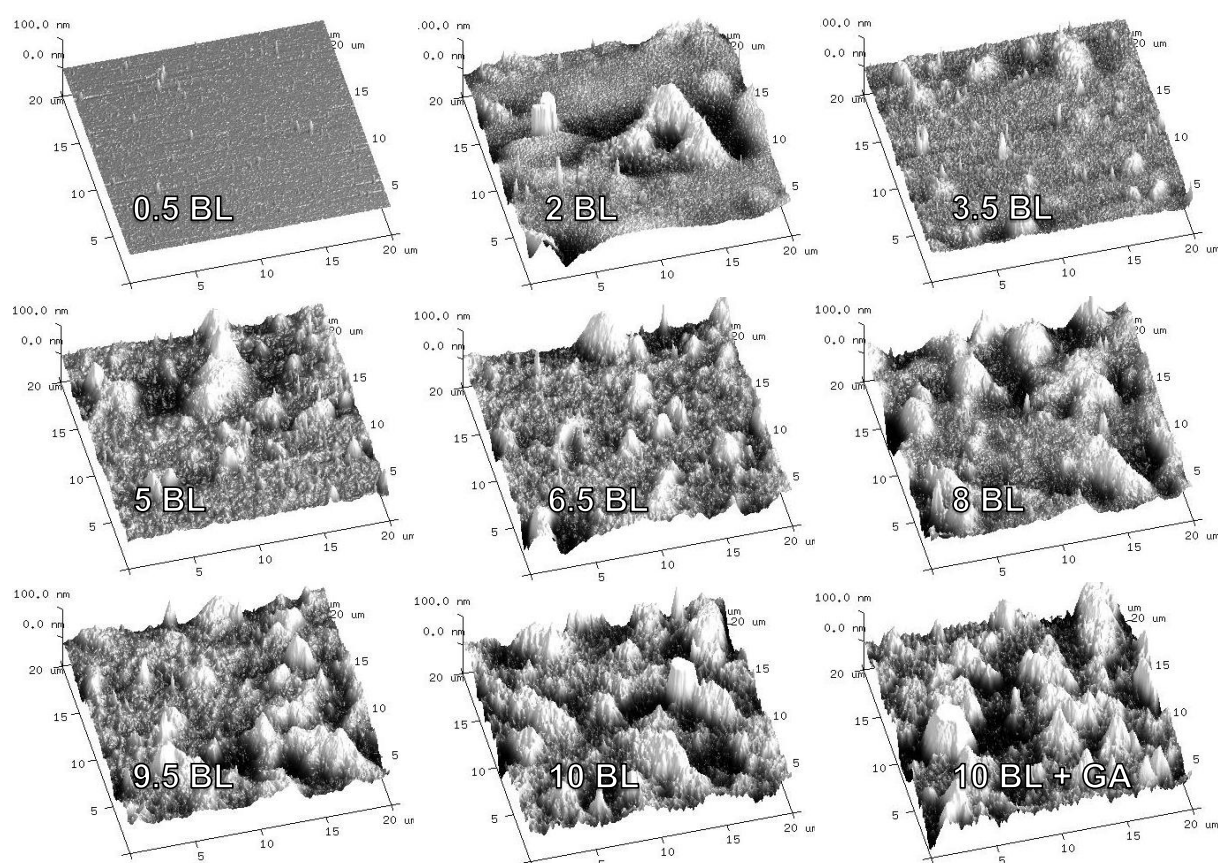


Figure 4.6 AFM surface profiles of 90%ABOL-(CTDNA#90%ABOL) at various bilayer numbers.

Further, the thicknesses of multilayered thin films at various stages of the build-up were also investigated through the AFM scratch test (Figure 4.7). This experiment revealed that a 10-bilayered 90%ABOL-(CTDNA#90%ABOL) film had an average thickness of 138 ± 39 nm, slightly thicker (taking into account the high standard deviation) than a 10-bilayered 100%ABOL homopolymer system (98 ± 27 nm). These thickness data and the significantly lower UV absorbance values of the copolymer system as compared to that of the 100%ABOL homopolymer system may indicate that the former system contain a higher polymer/DNA ratio. Agreeing to the UV-spectroscopy data (Figure 4.4), GA crosslinking caused a slight decrease in thickness (i.e. from 138 ± 39 nm to 129 ± 36 nm) and no significant difference in the surface roughness before and after the crosslinking treatment.

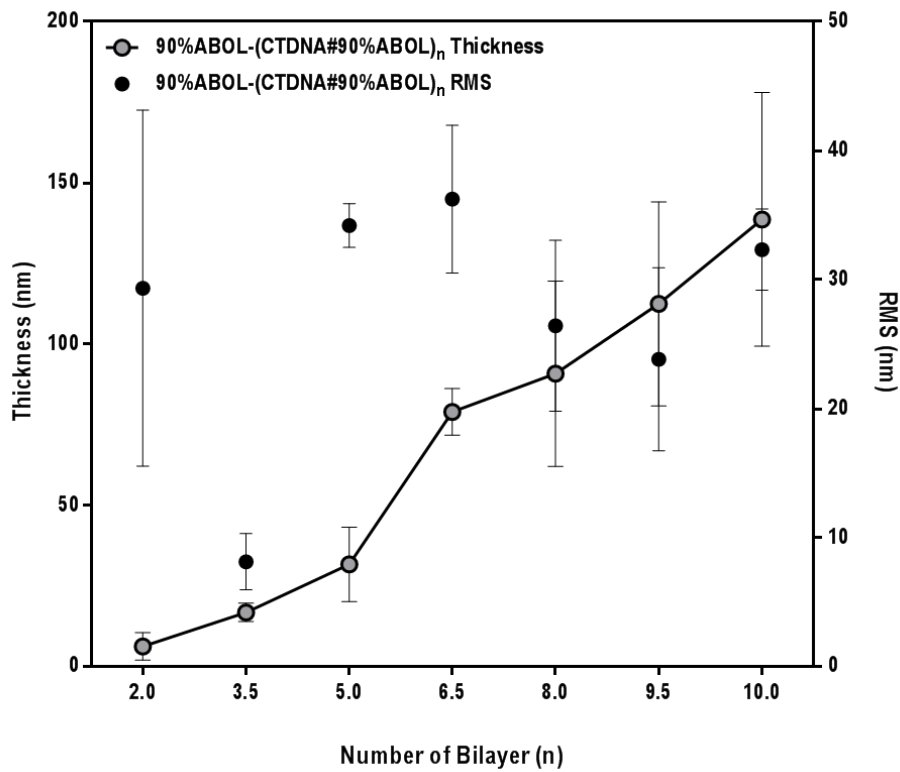


Figure 4.7 AFM surface roughness (RMS) and thickness of 90%ABOL-(CTDNA#90%ABOL) multilayer at various bilayer numbers.

4.3.7 PHYSIOLOGICAL STABILITY PROFILES OF GA-CROSSLINKED MULTILAYERS

To evaluate the effect of GA crosslinking on film stability, the 90%ABOL-(CTDNA#90%ABOL)₁₀ multilayers, both GA-crosslinked and non-crosslinked, were subjected to incubation in PBS buffer pH 7.4 at 37 °C for different time periods. The resulting stability profiles, as measured by UV spectroscopy, are shown in Figure 4.8. While the non-GA-crosslinked copolymer system rearranges rapidly under physiological conditions (losing ~30% of the DNA content in the first hour), the GA-crosslinked system still retained ~65% of its DNA after more than 30 days. This multilayered system further retained even more DNA than the 100%DAB homopolymer system after 10 days of incubation. This tremendous increase in stability indicates that covalent GA crosslinks were successfully formed within the multilayers and contribute strongly to the slower release of DNA from the multilayered system.

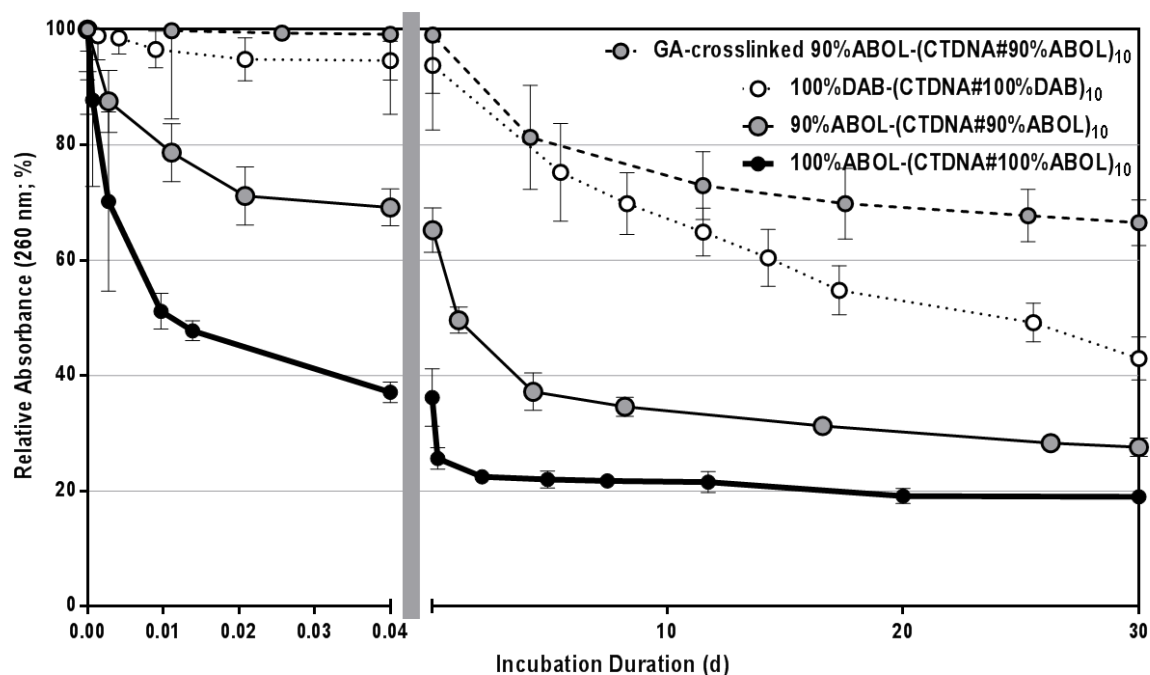


Figure 4.8 Stability profiles of GA-crosslinked copolymer systems as compared with the homopolymers and non-crosslinked system under physiological conditions (PBS buffer pH 7.4 at 37 °C) *in vitro*. The left part of the abscissa shows the trend of fast decrease (burst release) within 0.04 d (1 h) in the initial phase of the incubation while the right part shows the much slower decrease throughout the rest of the long incubation duration.

Taking into account the different initial DNA contents of respective systems, the relative stability improvements obtained through increasing charge density and GA crosslinking are summarized in Table 4.2. From this table, it can be concluded that GA crosslinking provides the highest improvement in physiological stability while maintaining the possibility to load high amounts of DNA per deposition cycle.

Table 4.2 Summary of physiological stability improvements of multilayers from (co)polymers of PAA, and after GA crosslinking.

Multilayer	Initial DNA content*	DNA content after 1 h*
100%ABOL	0.50 ± 0.04	0.19 ± 0.01
90%ABOL/10%DAB	0.34 ± 0.02	0.24 ± 0.01
90%ABOL/10%DAB + GA crosslinking	0.30 ± 0.04 **	0.30 ± 0.04
65%ABOL/35%DAB	0.18 ± 0.02	0.16 ± 0.01
100%DAB	0.23 ± 0.01	0.22 ± 0.01

*) DNA contents were indicated by UV absorbance values at 260 nm. **) Slight decrease from non-crosslinked 90%ABOL as indicated in Figure 4.4.

4.3.8 REDUCTIVE DEGRADATION PROFILES OF GA-CROSSLINKED MULTILAYERS

As described previously, all of the PAAs used in this study possess disulfide linkages in the polymer main chain. As a result, the obtained multilayers readily degrade under reducing conditions. To study the different degradation profiles of films with and without GA crosslinking, glutathione (a natural reducing tripeptide) is employed at 5.0 mM concentration to mimic the natural concentration in animal cells [23]. Figure 4.9 shows that while the non-GA-crosslinked films degrade completely within ~12 h of incubation under the reducing condition, only ~30% of the GA-crosslinked films is degraded within the same time period. For this latter system, reduction progressed much more slowly, reaching ~60% after 30 days of incubation. The result clearly indicates that GA crosslinking also increases the film stability against reduction by glutathione. Since glutathione reduces only disulfide bonds in the polymer main chain, the covalent GA crosslinks (interlayer crosslinks in particular) remain intact and hold the structure together. As a result, the crosslinked system would degrade more slowly than the non-crosslinked system under biological conditions, especially since the latter may also rearrange/release readily without glutathione.

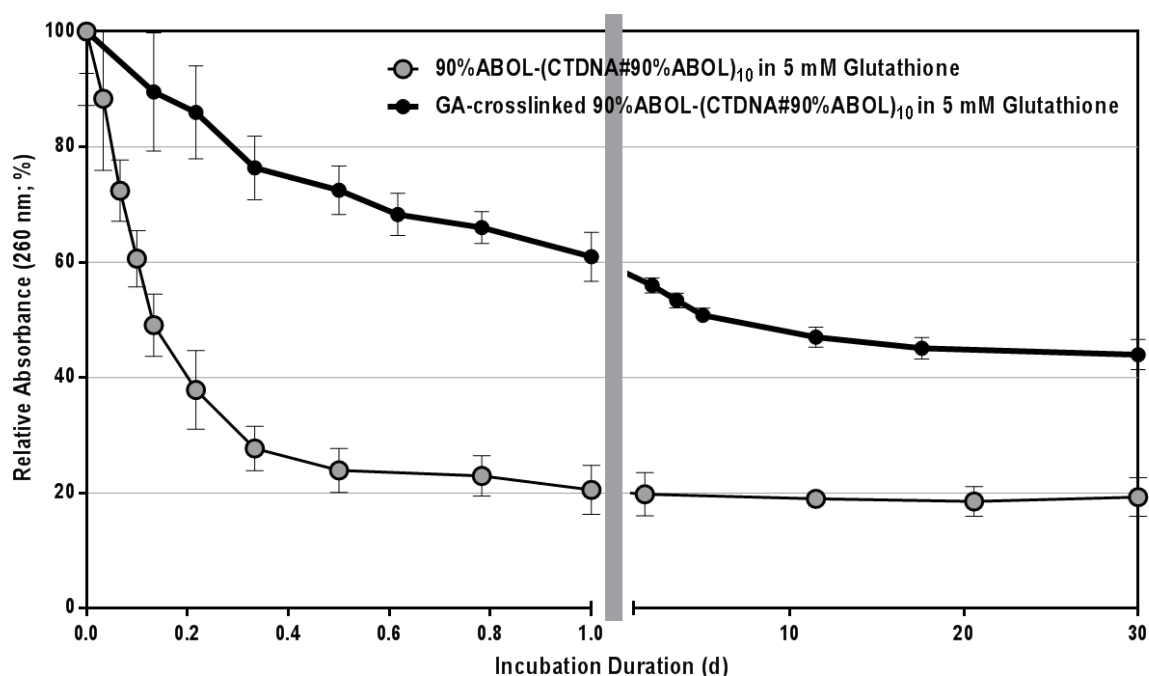


Figure 4.9 Degradation profiles of GA-crosslinked copolymer systems as compared to non-crosslinked system in the presence of 5.0 mM of glutathione under physiological conditions (PBS buffer pH 7.4 at 37 °C) *in vitro*. The left part of the abscissa shows the trend of fast decrease (burst release) within 1 d in the initial phase of the incubation while the right part shows the much slower decrease throughout the rest of the long incubation duration.

4.3.9 CELL CULTURE AND TRANSFECTION

The cell proliferation and transfecting capabilities of 90%ABOL-(DNA#90%ABOL)₁₀ multilayers were studied with GFP-encoding pCMV-GFP plasmid DNA (pDNA) as the DNA layer. The GFP produced by transfected cells can be readily detected and act as a reporter for the transfection efficiency. Multilayers with and without GA crosslinking were investigated and compared with the results obtained with the two homopolymers. Cell viability was qualitatively assessed by following the morphology of cells seeded on the different surfaces of multilayer-coated glass substrates. At approximately 15 h post-seeding, bright-field images of cells were recorded as shown in Figure 4.10.

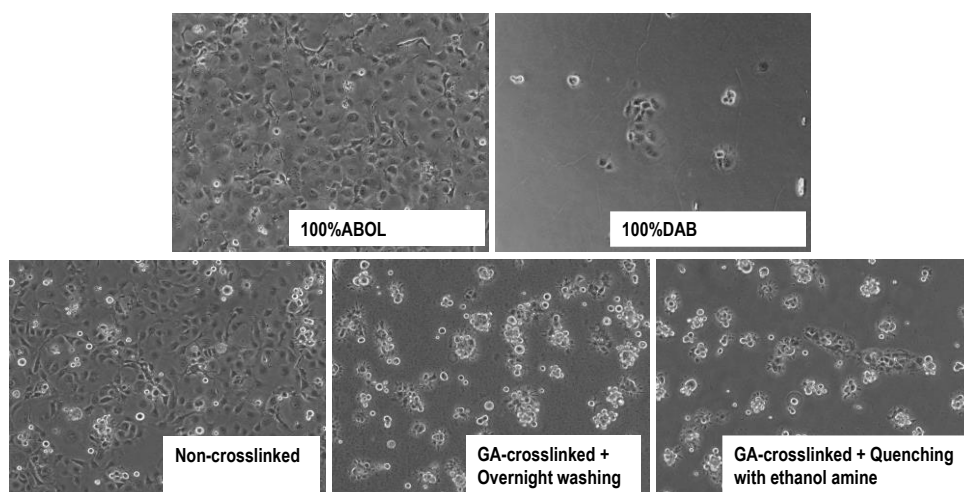


Figure 4.10 COS-7 cell morphology cultured on different surfaces 15 h post-seeding at 10X magnification.

Figure 4.10 shows that as was previously observed for the homopolymer multilayers (Chapter 3), 100%ABOL multilayers were biocompatible, facilitating cellular attachment to the same extent as on polystyrene culture plates (data not shown). On the other hand, 100%DAB multilayers were cytotoxic to cells and facilitated only minor cell attachment. The non-crosslinked multilayer provided good cell attachment, but ever so slightly inferior to 100%ABOL multilayers due to the presence of 10% DAB side chains. The presence of only 10% primary amines did not seem to significantly increase the overall toxicity of the surface, which is very much in contrast to the 100%DAB homopolymer system showing very poor cell attachment. Cells cultured on the GA-crosslinked multilayers had poorer morphology (regardless of the additional ethanol amine quenching steps) when compared to those cultured on non-crosslinked copolymer systems, but slightly better when compared to the 100%DAB system.

After two days of culture, indications of transfection were observed through fluorescence microscopy of the fluorescent GFP expressed by transfected cells (Figure 4.11). In agreement with the trend observed for cell attachment and viability, COS-7 cell transfection was more successful on non-crosslinked films than on GA-crosslinked films. No transfection was observed for the GA-crosslinked and 100%DAB films, while small amounts of transfection were observed for the non-crosslinked films (especially at the edges of cell monolayer) as shown in Figure 4.11.

The fact that the non-crosslinked system performed better than the GA-crosslinked film may be attributed to two significant factors. Firstly, as shown in Figure 4.10, GA crosslinking causes increase in cytotoxicity of the surface which results in cells not being in their optimal condition to be transfected. Secondly, as the stability of the GA-crosslinked films increases, there is much less release of transfection agent to be taken up by the cells.

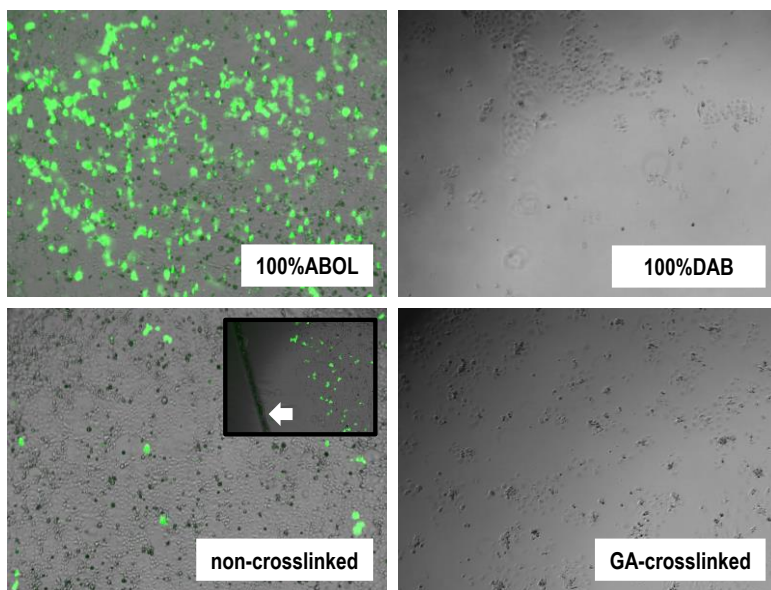


Figure 4.11 Overlaid brightfield and GFP images of COS-7 cells cultured on top of various multilayers after 2 d at 4X magnification. Inset in the non-crosslinked image shows a representative edge of cell monolayer where higher transfection efficiency was observed; arrow indicates the corner of the glass substrate.

Upon comparing the 90%ABOL and 100%ABOL-based multilayers, much lower transfection efficiency is observed for the former which may be attributed to one major factor. The 90%ABOL system contains **and** releases less DNA than the 100%ABOL at the same 10 bilayers used.

All of the discussions presented here indicate that there is an intricate interplay between the stability of multilayered systems and the DNA-release kinetics in relation to transfection efficiency of these weak polyelectrolyte-based multilayered constructs. As the therapeutic agent of interest (i.e. DNA) is a polyelectrolyte which is an integral part of the multilayer, release is inevitably accompanied by dissolution/decomposition of the multilayered structure. In this respect, increase in stability should not completely cease DNA release. It is therefore important to take into account the release kinetics, in relation to the treatment duration within which an effect is desired.

In the present study, aside from the cytotoxicity effects, GA crosslinking of only 10% primary amine side chains apparently increases the stability of the multilayer to such a high extent that within the 2 days of cell culture, DNA is not released in a sufficient quantity and form (e.g. as polyplex) to give an optimal cell transfection. The type and degree of crosslinking mechanism is, therefore, very important. Other types of crosslinking reactions that cause no cytotoxicity and provide degradable linkages (such as amide or ester linkages) can be considered to obtain multilayers with better controlled release of DNA payload within the desired period of treatment.

Furthermore, although increasing physical crosslinking (DAB content) has not been found to prevent the rapid initial (burst) release and provide more controlled release, there is an improvement in the stability of the films, where only about 30% of initial DNA content is burst released instead of 60% observed for the 100%ABOL system. In this sense, the lower transfection efficiency can be regarded as an effect of a successful attempt at slowing down the burst release phase. As future recommendations, it will be interesting to increase the layer number to load more DNA, lower cell seeding density, and perform cell culture over longer duration to study the possibility of more sustained release and transfection.

4.4 CONCLUSIONS

To study the effect of increasing multilayer stability on surface-mediated cell transfection, two approaches have been investigated in this study; i.e. introduction of two new copolymers of p(CBA-ABOL) containing several percentages of amine side chain functionality known to provide more stable films, in combination with glutaraldehyde-crosslinking of the obtained copolymer-based multilayer. The first approach aims at improving the films physically by introducing groups with higher positive charges to interact more strongly with DNA. The second approach aims at improving the films chemically by covalently linking polymer layers within the films, thus improving the stability even further.

Two p(CBA-ABOL/DAB) copolymers with different ABOL and DAB contents were synthesized and characterized. Increasing ABOL content was found to increase the relative amount of DNA deposition per layer, albeit not proportionally. Increasing DAB content by only 10% caused decrease of up to 40% total DNA content after 10 cycles of deposition while 35% DAB content brought DNA deposition to even slightly lower than 100%DAB system.

In vitro stability tests indicated the expected increase in stability with increasing DAB content. Increasing the DAB content by 10% causes the burst release to be prevented to only half of that observed for 100%ABOL films.

On the basis of maintaining higher incremental DNA deposition per cycle while increasing stability, glutaraldehyde (GA) crosslinking was carried out on the 90%ABOL-(CTDNA#90%ABOL)₁₀ films. UV, AFM, and contact angle measurements did not reveal pronounced differences in surface profiles upon GA crosslinking. However, *in vitro* stability study showed significantly increased stability of the GA-crosslinked system as compared to the non-crosslinked system indicating successful crosslinking. The GA-crosslinked multilayer also showed higher stability against reduction by glutathione.

In vitro COS-7 cell culture experiments and cell transfections demonstrated that 100%ABOL multilayer was significantly more superior than all the other multilayers in facilitating both COS-7 cell attachment and transfection. 100%DAB multilayer was cytotoxic and did not provide transfection. The non-crosslinked 90%ABOL-(pCMV-GFP#90%ABOL)₁₀ films showed good cell attachment and a small extent of transfection, although significantly lower than the transfection efficiency achieved by the 100%ABOL homopolymer system. On the GA-crosslinked multilayer, limited COS-7 cell attachment was observed that was slightly better than that observed on the 100%DAB homopolymer system. The GA-crosslinked system, however, displayed no transfection albeit showing slightly improved cell attachment. These findings were explained as a result of lower release of DNA upon stability increase of the multilayers.

The current study indicates that in the design of DNA-based multilayered thin films for surface-mediated cell transfection, careful tuning of film stability and DNA release kinetics is a crucial factor. As shown by the non-crosslinked 90%ABOL system, less and slower release of active agent leads to lower transfection efficiency as compared to the 100%ABOL system. Furthermore, whenever interlayer crosslinking is intended to prevent burst release or provide more controlled release, careful selection of crosslinking mechanism is important. GA utilized in this study provided less desirable effect not only through the additional cytotoxicity, but also due to the hampered release within the relevant time scale of treatment/culture duration.

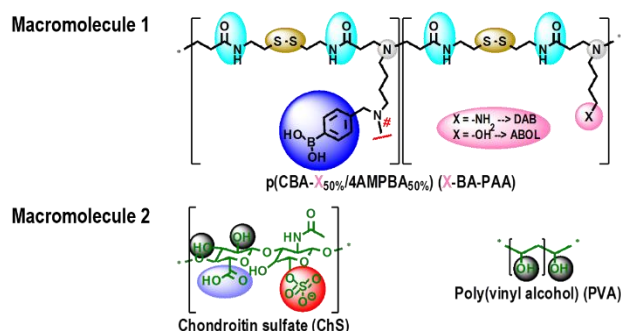
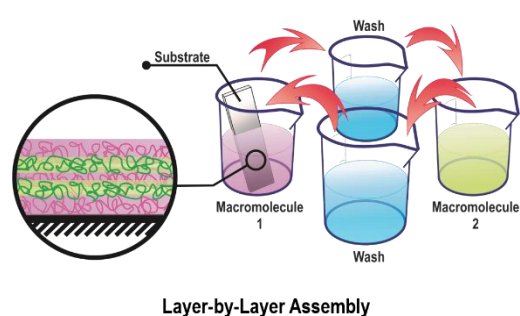
In conclusion, increasing stability of a weak-polyelectrolyte-based multilayer can be achieved through both increase in polyelectrolyte charge density and addition of covalent interlayer crosslinks. The increase in stability, however, may result in slower or insufficient release of active agent, especially if the active agent is an integral part of the multilayer structure. Therefore, the two factors have to be carefully considered when designing a stable multilayer that provides sustained release, especially in relation to the intended duration of treatment/application.

4.5 REFERENCES

- [1] G. Coué, C. Freese, R.E. Unger, C. James Kirkpatrick, J.F.J. Engbersen, Bioresponsive poly(amidoamine)s designed for intracellular protein delivery, *Acta Biomater*, 9 (2013) 6062-6074.
- [2] M. Piest, M. Ankoné, J.F.J. Engbersen, Carbohydrate-interactive pDNA and siRNA gene vectors based on boronic acid functionalized poly(amido amine)s, *J Control Release*, 169 (2013) 266-275.
- [3] L.J. van der Aa, P. Vader, G. Storm, R.M. Schiffelers, J.F.J. Engbersen, Optimization of poly(amido amine)s as vectors for siRNA delivery, *J. Control. Release*, 150 (2011) 177-186.
- [4] J.M. Garza, N. Jessel, G. Ladam, V. Dupray, S. Muller, J.-F. Stoltz, P. Schaaf, J.-C. Voegel, P. Lavalle, Polyelectrolyte Multilayers and Degradable Polymer Layers as Multicompartment Films, *Langmuir*, 21 (2005) 12372-12377.
- [5] J. Blacklock, Y.-Z. You, Q.-H. Zhou, G. Mao, D. Oupický, Gene delivery in vitro and in vivo from bioreducible multilayered polyelectrolyte films of plasmid DNA, *Biomaterials*, 30 (2009) 939-950.
- [6] A. Jayakrishnan, S.R. Jameela, Glutaraldehyde as a fixative in bioprostheses and drug delivery matrices, *Biomaterials*, 17 (1996) 471-484.
- [7] I. Migneault, C. Dartiguenave, M.J. Bertrand, K.C. Waldron, Glutaraldehyde: behavior in aqueous solution, reaction with proteins, and application to enzyme crosslinking, *Biotechniques*, 37 (2004) 790-+.
- [8] W. Tong, C. Gao, H. Möhwald, Single Polyelectrolyte Microcapsules Fabricated By Glutaraldehyde-Mediated Covalent Layer-By-Layer Assembly, *Macromol Rapid Comm*, 27 (2006) 2078-2083.
- [9] U. Manna, J. Dhar, R. Nayak, S. Patil, Multilayer single-component thin films and microcapsules via covalent bonded layer-by-layer self-assembly, *Chem. Commun.*, 46 (2010) 2250-2252.
- [10] A. Xiong, X. Lu, Y. Ma, Y. Qin, P. Zhang, J. Shi, Z.-X. Guo, Cross-linked multilayer composite films and microcapsules embedded carbon nanotubes, *Mater. Lett.*, 105 (2013) 132-135.
- [11] F. Bucatariu, C.-A. Ghiorghita, F. Simon, C. Bellmann, E.S. Dragan, Poly(ethyleneimine) cross-linked multilayers deposited onto solid surfaces and enzyme immobilization as a function of the film properties, *Appl. Surf. Sci.*, 280 (2013) 812-819.
- [12] E. Zeiger, B. Gollapudi, P. Spencer, Genetic toxicity and carcinogenicity studies of glutaraldehyde—a review, *Mutation Research/Reviews in Mutation Research*, 589 (2005) 136-151.
- [13] R.C. Adami, K.G. Rice, Metabolic stability of glutaraldehyde cross-linked peptide DNA condensates, *J. Pharm. Sci.*, 88 (1999) 739-746.
- [14] A. Zintchenko, L.J. van der Aa, J.F. Engbersen, Improved synthesis strategy of poly(amidoamine)s for biomedical applications: catalysis by "green" biocompatible earth alkaline metal salts, *Macromol. Rapid Commun.*, 32 (2011) 321-325.
- [15] C. Lin, C.-J. Blaauboer, M.M. Timoneda, M.C. Lok, M. van Steenberg, W.E. Hennink, Z. Zhong, J. Feijen, J.F.J. Engbersen, Bioreducible poly(amido amine)s with oligoamine side chains: Synthesis, characterization, and structural effects on gene delivery, *J Control Release*, 126 (2008) 166-174.
- [16] S.S. Shiratori, M.F. Rubner, pH-dependent thickness behavior of sequentially adsorbed layers of weak polyelectrolytes, *Macromolecules*, 33 (2000) 4213-4219.
- [17] P. Ott, J. Gensel, S. Roesler, K. Trenkenschuh, D. Andreeva, A. Laschewsky, A. Fery, Cross-Linkable Polyelectrolyte Multilayer Films of Tailored Charge Density, *Chem Mater*, 22 (2010) 3323-3331.
- [18] O. Mermut, C.J. Barrett, Effects of Charge Density and Counterions on the Assembly of Polyelectrolyte Multilayers, *The Journal of Physical Chemistry B*, 107 (2003) 2525-2530.
- [19] J.-i. Kawahara, T. Ohmori, T. Ohkubo, S. Hattori, M. Kawamura, The structure of glutaraldehyde in aqueous solution determined by ultraviolet absorption and light scattering, *Anal. Biochem.*, 201 (1992) 94-98.
- [20] N. Aggarwal, N. Altgarde, S. Svedhem, K. Zhang, S. Fischer, T. Groth, Study on multilayer structures prepared from heparin and semi-synthetic cellulose sulfates as polyanions and their influence on cellular response, *Colloid Surface B*, 116 (2014) 93-103.
- [21] W. Li, D.W. Xu, Y. Hu, K.Y. Cai, Y.C. Lin, Surface modification of titanium substrates with silver nanoparticles embedded sulfhydrylated chitosan/gelatin polyelectrolyte multilayer films for antibacterial application, *J. Mater. Sci.-Mater. Med.*, 25 (2014) 1435-1448.
- [22] S.D. Tuong, H. Lee, H. Kim, Chemical fixation of polyelectrolyte multilayers on polymer substrates, *Macromol. Res.*, 16 (2008) 373-378.
- [23] T.P. Akerboom, H. Sies, Assay of glutathione, glutathione disulfide, and glutathione mixed disulfides in biological samples, *Methods Enzymol.*, 77 (1981) 373-382.

Multilayered Thin Films from Boronic Acid-Functionalized Poly(amido amine)s with Poly(vinyl alcohol) and Chondroitin Sulfate[§]

ABSTRACT

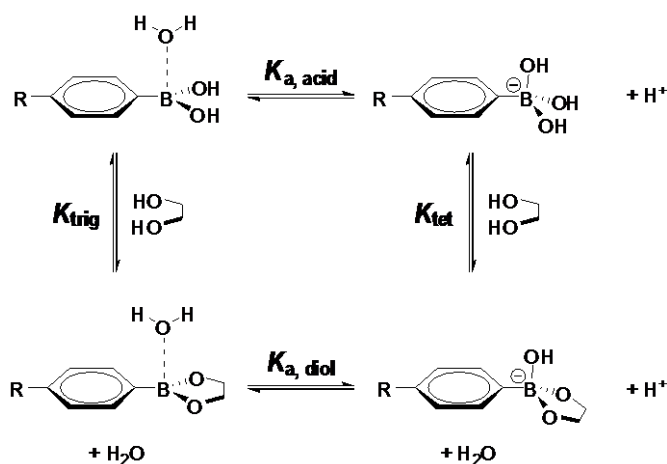


Two branched random copolymers of phenylboronic acid-functionalized poly(amido amine)s (BA-PAA), differing in the content of primary amine (DAB-BA-PAA) or primary alcohol (ABOL-BA-PAA) side groups, have been synthesized and characterized for their properties in forming multilayered thin films with poly(vinyl alcohol) (PVA) and chondroitin sulfate (ChS). The two BA-PAA facilitate multilayer formation with both PVA and ChS. PVA-based multilayers were thin, reaching ~100 nm at 10 bilayers, whereas ChS-based multilayers were thick, reaching ~600 nm at the same number of bilayers. All of the multilayers are stable under physiological conditions *in vitro* and are responsive to various reducing agents, owing to the presence of disulfide bonds in the polymer main chain. Under acidic pH, PVA-based films underwent fast disassembly or dissolution within minutes, with higher observed rates at lower pH. The ChS-based films showed a more complicated behavior, with highest stability at physiological pH, lowest stability at pH 6 and intermediate stability at pH 4. PVA-based films were found to be responsive to glucose at physiological pH at the investigated glucose concentrations of 10, 20, and 100 mM, with higher concentrations causing more pronounced film disassembly. ChS-based films, on the other hand, were only slightly responsive to glucose at 100 mM. It is proposed that the PVA-based multilayer formation relies predominantly on boronic acid-diol interaction, while multilayer formation with ChS relies more on the electrostatic interactions. Furthermore, all of the investigated multilayered films displayed biocompatibility in cell culture experiment, promoting attachment and proliferation of COS-7 cells grown on the films *in vitro*. The investigated multilayers show promise as multi-responsive drug releasing surfaces for various biomedical applications.

[§] Sry D. Hujaya, Jos M.J. Paulusse, Johan F.J. Engbersen, submitted for publication.

5.1 INTRODUCTION

In the development of multi-responsive drug delivery systems, the reversible ester formation of boronic acid (BA) with diols (Scheme 5.1) has been of widespread interest [1, 2]. This interaction is considered quite special not only due to its specific coordinative covalent nature, but also due to the dynamic properties of the interaction [3, 4]. This chemistry is very relevant to the biomedical field as it takes place under physiological conditions, is highly sensitive to pH, and concerns diol-moieties which can be found in many biologically relevant compounds and macromolecules, most notably carbohydrates and sugars. Therefore, this ester formation has been widely exploited for development of blood glucose sensors [5-9], separation agents [10-12], and therapeutic delivery systems (hydrogels [13, 14], micro- and nanoparticles [2, 15, 16]) for insulin [17-20], and other drugs [21-23]. Phenylboronic acid, a more reactive derivative of alkylboronic acid in ester formation with diols, has been found to selectively inhibit tumor cells without much effect on non-tumorigenic cell lines [24].



Scheme 5.1 The equilibria of boronate ester formation and relevant Lewis acidity.

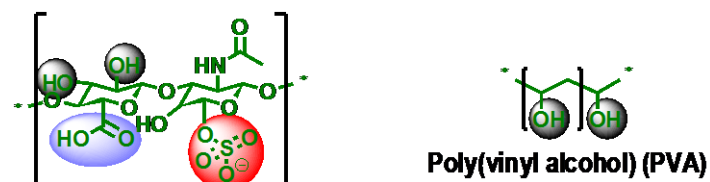
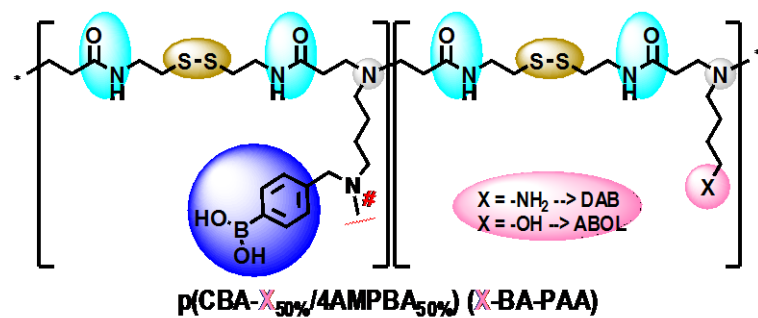
The boronate ester formation has also been exploited to develop multilayered thin films [25-28]. In contrast to most multilayer films formed by LbL technology, these films rely not on simple electrostatic interactions, but on the multi-responsive boronate ester formation, which – combined with the versatility of the layer-by-layer (LbL) dip-coating technique – make them a very promising approach to provide complex 3D structures (e.g. implants, stents, prostheses) with multi-responsive drug releasing properties.

Two phenylboronic acid-functionalized poly(amido amine)s (BA-PAA) differing in the presence of primary amine (DAB-BA-PAA) or primary alcohol (ABOL-BA-PAA) side groups (Chart 5.1) have been synthesized and studied for their properties in forming multilayered thin films with two different diol-containing macromolecules. The presence of disulfide bonds in the polymer main chain renders them responsive to reducing agents. The branched structure of the BA-PAA adds multivalency to strengthen interactions with the diol-containing counterpart and increases overall multilayer stability. However, unlike the poly(amido amine) dendrimers (PAMAM) with high degree of branching, the BA-PAA may still maintain structural flexibility in solution – a feature that has been reported to increase their potency as gene carriers [29, 30]. The linear form of *ortho*-substituted ABOL-BA-PAA itself has been previously reported to self-assemble into nanoparticles capable of intracellular delivery of alizarin red S (a diol-containing small molecule) as model drug with the BA-PAA polymer [16], implying the possibility of achieving nanoparticle-releasing multilayered system.

The other multilayer components, poly(vinyl alcohol) (PVA) and chondroitin sulfate (ChS) are chosen to represent widely-studied diol-containing macromolecules that are in principle suitable for biomedical applications. PVA is a popular US Food and Drug Administration (FDA)-approved biomaterial [31, 32], used in the preparation of adhesives, paper and packaging, textiles, toys, cosmetics, eye drops, embolization agents, and is commercially

available in various molecular weights. ChS is a carbohydrate found in cartilage and bone extracellular matrix. It is a linear biopolymer of repeating *N*-acetyl-D-galactosamine and D-glucuronic acid disaccharide, and is often consumed as supplement for treatment of osteoarthritis [33-35].

In this Chapter, the two BA-PAA s are paired with both PVA and ChS to form multilayers. The build-up profiles and properties of the resulting ensembles are described in relation to the underlying intermolecular interactions. As a control, DAB-Bn-PAA (i.e. DAB-BA-PAA without the BA moiety, but rather a benzyl-moiety) was also synthesized and used to verify the role of BA-diol interactions. Chart 5.1 depicts the chemical structures of the four main multilayer components.



Chondroitin sulfate (ChS)

Chart 5.1 Chemical structures of DAB-BA-PAA, ABOL-BA-PAA, ChS, and PVA utilized as main components for multilayer formation. Control polymer DAB-Bn-PAA is similar to DAB-BA-PAA but with benzyl moiety instead of the phenylboronic acid moiety.

5.2 MATERIALS AND METHODS

N,N'-Cystamine bisacrylamide (CBA, 99.9%) was purchased from Polysciences (Eppelheim, Germany). Sodium sulfate (Na_2SO_4 , 99%) was purchased from Acros (Landsmeer, The Netherlands). 4-Amino-1-butanol (ABOL, 98.0%), *N*-Boc-1,4-diaminobutane (NBDAB, $\geq 97.0\%$), 4-formylphenylboronic acid (4FPBA, $\geq 95.0\%$), sodium borohydride (NaBH_4 , $\geq 98.0\%$), *N*-benzyl-1,4-butanediamine (BnDAB), calcium chloride (CaCl_2 , $\geq 93.0\%$), triethylamine (TEA, $\geq 99.0\%$), *tert*-butylamine (*t*BA, $\geq 99.5\%$), trifluoroacetic acid (TFA, $\geq 99.0\%$), sodium chloride (NaCl , $\geq 99.5\%$), Mowiol® 4-98, 6-98, 56-98 (PVA, ~27 kDa, ~47 kDa, ~195 kDa), Chondroitin 4-sulfate sodium salt from bovine trachea (ChS, $\leq 10\%$ water), glucose ($\geq 99.5\%$), and glutathione ($\geq 98.0\%$) were purchased from Sigma-Aldrich (Zwijndrecht, The Netherlands). Sodium dihydrogen phosphate monohydrate ($\text{NaH}_2\text{PO}_4 \cdot \text{H}_2\text{O}$, 99.0-102.0%), disodium hydrogen phosphate dihydrate ($\text{Na}_2\text{HPO}_4 \cdot 2\text{H}_2\text{O}$, 99.5%), citric acid ($\geq 99\%$), and trisodium citrate dihydrate ($\geq 99\%$) were purchased from Merck (Darmstadt, Germany). Solvents were of reagent grade and used without further purification unless otherwise noted. Milli-Q water ($\text{M}\Omega\text{-cm}$ at 25 °C) was obtained from a Synergy® water purification system (Millipore).

PBS buffer was prepared by dissolving 1.54 g of $\text{Na}_2\text{HPO}_4 \cdot 2\text{H}_2\text{O}$, 0.30 g of $\text{NaH}_2\text{PO}_4 \cdot \text{H}_2\text{O}$, and 8.20 g of NaCl into 1.00 L of Milli-Q water and adjusting the pH to 7.4.

Citrate buffered saline (CBS buffer) pH 4, 5, and 6 were prepared by dissolving citric acid, trisodium citrate dihydrate and NaCl in the appropriate amounts in Milli-Q and adjusting the pH with HCl or NaOH .

$^1\text{H-NMR}$ spectra were recorded on an AVANCE III-400MHz NMR (Bruker, Wormer, The Netherlands) spectrometer.

UV characterization of multilayered thin films was performed in the dry state using a UV-2401 PC (Shimadzu, 's-Hertogenbosch, The Netherlands). Each film fabricated on UV-transparent 7.5 x 37 x 1 mm quartz glass (Ted Pella, Redding, USA) was measured in three different arbitrary positions. Absorbance scan was carried out in the 200-400 nm wavelength range. All data points were then corrected for baseline offset by subtracting the absorbance value at 400 nm from each data point. Relative absorbance values were obtained by normalizing each data point with the respective value at time 0.

AFM characterization was performed on a Multimode AFM (Bruker, Wormer, The Netherlands) with Nanoscope IV controller in contact mode using an MSCT cantilever with moderate spring constant of 0.5 N/m. Multilayered thin film samples were fabricated on single side polished silicon wafer (n-type, 525 μm thick, MESA+NanoLab, Enschede, The Netherlands) diced into 7.5 x 32 mm pieces.

Contact angle measurements were performed on a Krüss G10 (KRÜSS, Hamburg, Germany) contact angle measuring instrument.

Poly-D-lysine-coated 96-well plates (PDL-TCPS) for multilayer build-up for cell culture and transfection experiments were purchased from Greiner (Alphen aan den Rijn, The Netherlands).

COS-7 cells (European Collection of Animal Cell Cultures (ECACC) Catalogue No. 87021302) were grown in DMEM containing 4.5 g/L glucose and GlutaMAX™ (Invitrogen, Breda, The Netherlands) supplemented with 2% (v/v) PennStrepp (Lonza, Breda, The Netherlands) and 10% (v/v) fetal bovine serum (Lonza, Breda, The Netherlands).

Cell imaging was performed at 4X, 10X, 20X, and/or 40X objectives using EVOS digital inverted microscope (EMS, Wageningen, The Netherlands) equipped with RFP and DAPI light cubes for EthD-1 and Hoechst 33258 fluorescence imaging, respectively. EthD-1 and Hoechst 33258 was purchased from Invitrogen (Breda, The Netherlands) and Sigma-Aldrich, respectively.

Fluorescence intensity measurements were carried out in an Infinite M200 PRO plate reader (Tecan, Giessen, The Netherlands). AlamarBlue for cell viability measurements was purchased from Invitrogen (Breda, The Netherlands).

5.2.1 SYNTHESIS OF 4-((4-AMINOBYTYLAMINO)METHYL)PHENYLBORONIC ACID (4AMPBA)

For the synthesis of 4-((4-aminobutylamino)methyl)phenylboronic acid, 4-formylphenylboronic acid (3.12 g, 20.8 mmol) was mixed with *N*-Boc-1,4-diaminobutane (4.03 g, 20.8 mmol) in a round-bottom flask. The reactants were dissolved in 25 mL of methanol and stirred under nitrogen atmosphere at room temperature for at least four hours to let the imine formation proceed to completion. To the brownish solution, sodium borohydride (0.79 g, 21.3 mmol) was then added portion-wise. The imine reduction was observed from the change in color of the solution to yellow, indicating shortening of double bond conjugation. This reaction was let to proceed for two hours after which the remaining methanol was evaporated under reduced pressure, and the rest of the solid product mixture was dissolved in Milli-Q water and extracted with equal volume of chloroform for 6 times followed by one time backwashing. The chloroform phases were collected, and dried with Na₂SO₄. The water-free chloroform solution was then evaporated under reduced pressure, leaving the BOC-protected solid product behind. Molar yield: ~60%. The BOC-protected product was deprotected by first dissolving the product in 15 mL of methanol in a round-bottom flask. HCl gas (prepared by drop-wise addition of H₂SO₄ to NaCl) was then purged into the solution under nitrogen stream. The reaction was left to continue for at least an hour to proceed to completion. The volatile components in the solution were then evaporated to yield the product as a pinkish white powder in its HCl salt form. The product was further dried *in vacuo* and stored in the freezer. Yield: 87%. ¹H-NMR (HCl salt, CD₃OD, 400 MHz) δ (ppm) = 1.66 (q, 2H, NH₂CH₂CH₂); 1.82 (q, 2H, NH₂CH₂CH₂CH₂); 2.97 (t, 2H, NH₂CH₂); 3.09 (t, 2H, ArCH₂NHCH₂); 4.21 (s, 2H, ArCH₂NH); 7.48 (d, 2H, ArH); 7.76 (d, 2H, ArH).

5.2.2 SYNTHESIS OF P(CBA-DAB_{50%}/4AMPBA_{50%}) (DAB-BA-PAA)

N,N'-Cystamine bisacrylamide (2.02 g; 7.76 mmol), *N*-Boc-1,4-diaminobutane (0.74 g; 3.88 mmol), and 4AMPBA (1.14 g; 3.88 mmol) were mixed in a brown polymerization flask using 2 mL of methanol/water 3/1 as solvent and containing 200 mM CaCl₂ as catalyst based on recent report by Zintchenko et al. [36]. Triethylamine (1.3 mL; 9.7 mmol) was also added to free the amines in 4AMPBA for Michael addition reaction. Polymerization was carried out under N₂ atmosphere for seven days at 70 °C during which a gradual viscosity increase was observed. The polymerization was terminated by adding *tert*-butylamine (2.5 mL; 23.47 mmol) into the mixture and stirring at 70 °C for two more days. After bringing the flask to room temperature, the solution was diluted and acidified to pH ~4 by addition of 4 M HCl and purified by ultrafiltration using a 1,000 Da MWCO membrane. The purified polymer solution was then freeze-dried leaving white yellowish solid as the BOC-protected product in its HCl-salt form (2.1 g; 54% recovery). ¹H-NMR characterization was performed to confirm complete conversion of terminal acrylate groups by reaction with *tert*-butylamine.

Deprotection was carried out with HCl gas as mentioned in the synthesis of the 4AMPBA monomer. After evaporation of volatile components, the solid was redissolved in water, brought to slightly acidic pH, filtered and further purified by ultrafiltration using a 1,000 Da MWCO membrane. The purified polymer solution was finally freeze-dried to yield a light yellow solid as the final product in its HCl-salt form (0.92 g; 44% recovery). ¹H-NMR characterization was performed to confirm complete deprotection. ¹H-NMR (D₂O) δ (ppm) = 1.35 (s, 9H, (CH₃)₃R); 1.75 (m, 4H, CH₂CH₂NH₂ & CH₂CH₂CH₂N(BA)); 1.86 (m, 4H, CH₂CH₂CH₂NH₂ & CH₂CH₂CH₂N(BA)); 2.79 – 2.83 (broad, 16H, CH₂CONHRNHCOCH₂ & CH₂SSCH₂); 3.05 (m, 4H, CH₂NH₂ and CH₂NH(BA)); 3.28 (t, 4H, N(CH₂)₃CH₂); 3.47 – 3.49 (broad, 16H, NCOCH₂CH₂NRCH₂ and CH₂CH₂SSCH₂CH₂); 4.25 (2H, s, **branched** ArH-CH₂-N-(CH₂)₂); 4.42 (2H, s, ArH-CH₂-NH); 7.52 (2H, d, ArH), 7.83 (2H, d, ArH). Degree of BA functionalization was estimated at 53%, 19% of which reacted further through the benzylic amine to form branches.

5.2.3 SYNTHESIS OF P(CBA-ABOL_{50%}/4AMPBA_{50%}) (ABOL-BA-PAA)

N,N'-Cystamine bisacrylamide (1.08 g; 4.17 mmol), 4-amino-1-butanol (0.19 g; 2.13 mmol), and 4AMPBA (0.62 g; 2.09 mmol) were mixed in a brown polymerization flask using 2.3 mL of methanol/water 3/1 as solvent and containing 200 mM CaCl₂ as catalyst based on recent report by Zintchenko et al. [36]. Triethylamine (1.5 mL; 10.7 mmol) was also added to deprotonate the amines in 4AMPBA for Michael addition reaction. Polymerization was carried out under N₂ atmosphere for two days at 70 °C during which a gradual viscosity increase was observed. The polymerization was terminated by adding excess of *tert*-butylamine (2.2 mL; 20.9 mmol) into the mixture and stirring at 70 °C for six more days until no trace of acrylates was detected with ¹H-NMR. After bringing the reaction mixture to room temperature, the solution was diluted with water and acidified to pH ~4 by addition of 4 M HCl and purified by ultrafiltration using a 1,000 Da MWCO membrane. The purified polymer solution was then freeze-dried leaving white fluffy solid as the HCl-salt form (0.58 g; 31% recovery). ¹H-NMR characterization was performed to confirm complete conversion of terminal acrylate groups by reaction with *tert*-butylamine and estimation of degree of polymerization. ¹H-NMR (D₂O) δ (ppm) = 1.36 (s, 9H, (CH₃)₃R); 1.60 (m, 4H, CH₂CH₂CH₂N(BA) & CH₂CH₂CH₂OH); 1.78 (m, 4H, CH₂CH₂CH₂N(BA) & CH₂CH₂OH); 2.70 (t, 8H, CH₂CONHRNHCOCH₂); 2.83 (t, 8H, CH₂SSCH₂); 3.09 (t, 2H, CH₂CH₂CH₂N(BA)); 3.20 (t, 2H, CH₂CH₂CH₂CH₂OH); 3.29 (t, 2H, CH₂CH₂CH₂CH₂N(BA)); 3.35 – 3.58 (broad, 16H, CH₂CH₂SSCH₂CH₂ & CH₂CH₂CONHRNHCOCH₂CH₂); 3.61 (t, 2H, HOCH₂); 4.25 (2H, s, **branched** ArH-CH₂-N-(CH₂)₂); 4.31 (broad, 2H, s, ArH-CH₂-NH); 7.50 (2H, d, ArH), 7.83 (2H, d, ArH). Degree of BA functionalization was estimated at 52%, 59% of which reacted further through the benzylic amine to form branches.

5.2.4 SYNTHESIS OF P(CBA-DAB_{50%}/BNDAB_{50%}) (DAB-BN-PAA)

The polymer DAB-Bn-PAA that serves as a negative control for the boronic acid activity of the DAB-BA-PAA and ABOL-BA-PAA polymers was synthesized by mixing *N,N'*-cystamine bisacrylamide (1.32 g; 5.0 mmol), *N*-Boc-1,4-diaminobutane (0.47 g; 2.5 mmol), and BnDAB (0.45 g; 2.5 mmol) in a brown polymerization flask using 2.6 mL of methanol/water 3/1 as solvent and containing 200 mM CaCl₂ as catalyst based on recent report by Zintchenko et al. [36]. Polymerization was carried out under N₂ atmosphere for two days at 70 °C during which a gradual viscosity increase was observed. The polymerization was terminated by adding *tert*-butylamine (1.8 mL; 16.9 mmol) into the mixture and stirring at 70 °C for two more days until no trace of acrylates was detected with ¹H-NMR. After bringing the flask into room temperature, the solution was diluted and acidified to pH ~4 by addition of 4 M HCl and purified by ultrafiltration using a 1,000 Da MWCO membrane. The purified polymer solution was then freeze-dried leaving yellowish solid as the BOC-protected product in its HCl-salt form (1.5 g; 65% recovery). ¹H-NMR characterization was performed to confirm complete conversion of terminal acrylate groups by reaction with *tert*-butylamine

Deprotection was carried out with HCl gas as described in the synthesis of the 4AMPBA monomer. After evaporation of volatile components, the solid was redissolved in slightly acidic water, though part of the solid was insoluble. The soluble portion was filtered and further purified by ultrafiltration using a 1,000 Da MWCO membrane. The purified polymer solution was finally freeze-dried to yield brownish solid as the final product in its HCl-salt form (0.15 g; 10% recovery). ¹H-NMR characterization was performed to confirm complete deprotection. ¹H-NMR (D₂O) δ (ppm) = 1.36 (s, 9H, (CH₃)₃R); 1.76 (m, 4H, CH₂CH₂NH₂ & CH₂CH₂CH₂N(Bn)); 1.86 (m, 4H, CH₂CH₂CH₂NH₂ & CH₂CH₂CH₂N(Bn)); 2.80 (t, 8H, CH₂CONHRNHCOCH₂); 2.84 (t, 8H, CH₂SSCH₂); 3.05 (m, 4H, CH₂NH₂ and CH₂NH(Bn)); 3.28 (broad, 4H, N(CH₂)₃CH₂); 3.38 – 3.8 (broad, 16H, NCOCH₂CH₂NRCH₂ and CH₂CH₂SSCH₂CH₂); 4.25 (2H, s, **branched** ArH-CH₂-N-(CH₂)₂); 4.41 (2H, s, ArH-CH₂-NH); 7.52 (5H, s, ArH). Degree of BA functionalization was estimated at 60%, 21% of which reacted further through the benzylic amine to form branches.

5.2.5 MULTILAYERED THIN FILM CONSTRUCTION AND BUILD-UP PROFILES

Fresh BA-PAA solutions were prepared short before the start of multilayer build-up from the solid materials which had been re-lyophilized overnight to avoid weighing errors due to their hygroscopic properties. All BA-PAA solutions (2.0 mg/mL) were prepared in PBS buffer at pH 7.4 to avoid possible variations in pH.

Prior to the assembly, quartz or silicon wafer substrates (7.5 x 32 mm) were etched for 30 minutes in piranha acid to activate the surface, rinsed with copious amounts of Milli-Q water, and dried under N₂ stream. These substrates were then dipped into BA-PAA solution (2.0 mg/mL in PBS buffer pH 7.4) for 5 min, transferred into washing solution containing PBS buffer for 1 min, dipped briefly in a large amount of Milli-Q water, transferred into ChS or PVA (2.0 mg/mL in Milli-Q water and PBS buffer pH 7.4, respectively) solution for 5 min, dipped into the second washing solution containing Milli-Q water or PBS buffer for 1 min, and finally followed by another brief dipping in Milli-Q. This cycle was repeated to reach the desired number of bilayers. Drying under N₂ stream was performed after every BA-PAA-layer deposition, excluding the very first layer. The resulting ensemble is denoted by BA-PAA-(ChS or PVA#BA-PAA)_n, where BA-PAA represents the identity of the BA-functionalized poly(amido amine) used and *n* represents the number of bilayer. The first BA-PAA layer is regarded as a precursor layer and therefore excluded from the bilayer number count. Typically, the ensemble consists of 10 bilayers with the BA-PAA as the last layer. For every multilayered system, three samples were fabricated in parallel to give estimation for standard deviation. To study the build-up profiles, UV spectra were recorded after each drying step following BA-PAA layer formation. Afterwards, the multilayers were dipped into ChS or PVA solution to continue multilayer build-up.

Multilayers for cell culture were fabricated directly in the wells of poly-D-lysine-coated 96-well plates (PDL-TCPS, Greiner) by alternatingly dispensing deposition (70 μL) and washing (2x 100 μL) solutions under sterile conditions inside the laminar flow hood (LFH). Deposition started with ChS or PVA (2.0 mg/mL, 30 min for the first layer, 5 min next) as the first layer to a total of 10 bilayers ending with the BA-PAA layer. No intermediate drying steps were applied. At the end of the fabrication the plates were left inside the LFH briefly to dry the films. Coated plates were kept at 4 °C and used as soon as possible (typically overnight). These multilayered samples are designated as PDL-(ChS or PVA#BA-PAA)₁₀ to indicate the presence of a PDL layer as a precursor layer. Compared to multilayers built on quartz and silicon wafer substrates, these systems substitute the first BA-PAA layer with PDL layer inherent to the well plate surface.

5.2.6 CONTACT ANGLE MEASUREMENTS

Static contact angles (θ) were measured with Milli-Q water (18.2 MΩ-cm) on a Krüss G10 Contact Angle Measuring Instrument. Five drops of Milli-Q water (approximately 1.5 μL) were measured on five different spots across the surface and averaged to obtain θ . Images were recorded and measured for θ approximately 15 s from the initial contact of the liquid and the surface.

5.2.7 ATOMIC FORCE MICROSCOPY

Multilayers built on silicon wafer substrates were used for AFM microscopy. Imaging was carried out in the middle part of the films (to avoid edge effects/defects) at three different 20 x 20 μm scan areas at 512 x 512 pixels. Images were taken and analyzed using Nanoscope software version 7.30. Height data was flattened using first or second order fitting and root mean square roughness (RMS) was calculated over the scan area. Thickness data was obtained by first scratching the surface using a syringe needle and then scanning over the scratched area to measure the difference in height between the base substrate (i.e. the bottom of the scratch) and the surface of the film. Thicknesses were then measured as the average of one 'depth' measurement and three 'section' measurements across the scratch.

5.2.8 STABILITY PROFILES UNDER PHYSIOLOGICAL CONDITIONS

Stability profiles of the six different multilayers in PBS buffer pH 7.4 at 37 °C was investigated by dipping the thin films formed on quartz slides in 2 mL of PBS buffer pH 7.4 solution and incubating them in a water bath with temperature set to 37 °C. From time to time, the samples were removed, briefly dipped in a large amount of Milli-Q water, dried under N₂ stream and measured by UV-Vis spectrophotometer.

5.2.9 MULTILAYER DEGRADATION UNDER REDUCING CONDITIONS

Degradability of the six different multilayers were investigated in a similar way as for the investigation of their respective stability profiles under physiological conditions (Section 5.2.8), though in the presence of 2.5 mM of DTT, 10 mM glutathione, or 0.4 mM glutathione in the incubation media. The solutions containing DTT or glutathione in PBS buffer pH 7.4 were prepared fresh, directly prior to the start of experiment. Due to instability of DTT and glutathione in PBS buffer pH 7.4, no solution of over three hours old was used.

5.2.10 RESPONSIVENESS TO ACIDIC PH

The responsiveness of the six different multilayers in different acidic pH values was investigated in a similar way as for the investigation into their respective stability profiles under physiological conditions (Section 5.2.8), but with citrate buffered saline (CBS) at pH 4, 5, and 7, instead of PBS at pH 7.4.

5.2.11 RESPONSIVENESS TO VARIOUS GLUCOSE CONCENTRATIONS

The responsiveness of the six different multilayers in the presence of glucose was investigated in a similar way as for the investigation of their respective stability profiles under physiological conditions (Section 5.2.8), but in the presence of 10, 20, or 100 mM of glucose in the incubation media.

5.2.12 COS-7 CELL VIABILITY ON MULTILAYERED FILMS

For cell viability experiments, multilayers were fabricated as described in Section 5.2.5. Directly on the multilayer-coated PDL-TCPS wells, COS-7 cells were seeded at a seeding density of 10,000 cells/sample in complete medium with serum and left to proliferate at 37 °C in humidified atmosphere with 5% CO₂.

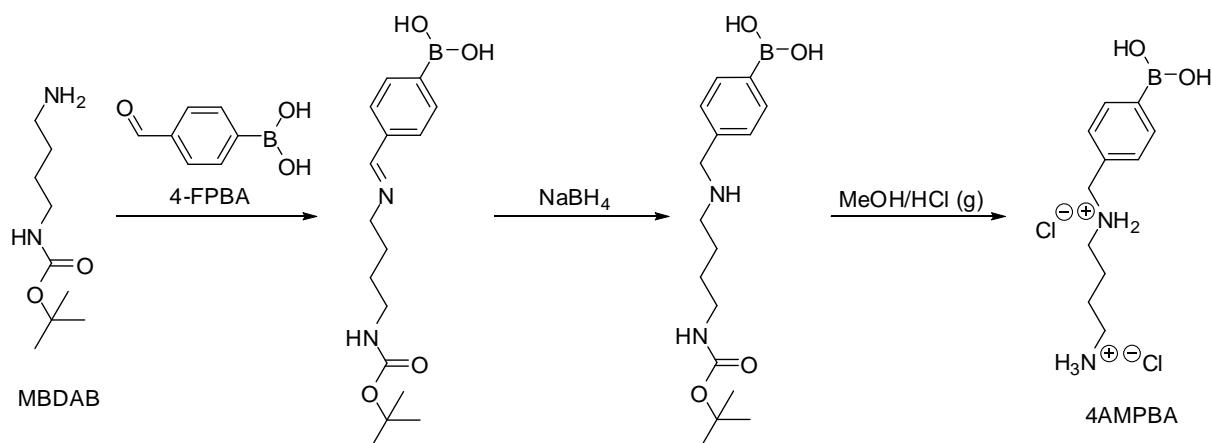
Cell morphology was recorded after 6 and 48 hours of culture. At the end of the 2 day culture period, cells were stained with EthD-1 and Hoechst 33258 followed by subsequent fluorescence imaging. As positive controls, cells were also seeded on non-tissue culture (TC)-treated, polystyrene well plates. Experiments were done in triplicate.

For quantitative metabolic activity comparison between the different multilayers, after 48 h of culture, AlamarBlue (AB) was added at 10 v/v% of total medium volume in every well and cells were incubated for another 4 h after which fluorescence intensity of resorufin (i.e. metabolically-reduced resazurin) was recorded using a plate reader. As positive controls, cells were also seeded on non-TC-treated polystyrene well plates. All fluorescence intensities were corrected by subtracting the values with those of their respective no-cell control wells. All experiments were carried out in triplicates.

5.3 RESULTS AND DISCUSSION

5.3.1 SYNTHESIS OF THE MONOMER 4AMPBA AND THE COPOLYMERS DAB-BA-PAA, ABOL-BA-PAA, AND DAB-BN-PAA

Syntheses of the BA-PAA started with the synthesis of the BA-functional monomer. The monomer 4AMPBA was synthesized as illustrated in Scheme 5.2. The reaction started with the formation of imine between NBDAB and 4FPBA under nitrogen atmosphere. After one day, the light yellow transparent solution turned slightly brown indicating formation of imine which lengthens the double-bond conjugation in the new compound. This newly formed imine bond was reacted with excess of NaBH_4 upon which the color of the solution turned yellowish again. This color change indicates that the conjugation length in the product is decreased, which is in accordance with the reduction of the imine bond. After isolation under reduced pressure, the product was further purified via extraction in DCM/water mixture. The product dissolved more readily in the organic DCM phase while the charged borate salt that was formed as side product dissolved more readily in the aqueous phase. Deprotection by treatment of the product in methanol with HCl gas readily yielded the final product in its HCl salt form. $^1\text{H-NMR}$ showed the disappearance of the 9-proton singlet in 1.4 ppm which indicated complete deprotection. Following exhaustive lyophilization, the purity of the product was confirmed using a known amount of *N,N*-dimethylformamide as internal standard in $^1\text{H-NMR}$ sample characterization to be roughly 90-94%.



Scheme 5.2 Reaction scheme for the synthesis of monomer 4AMPBA.

Syntheses of the three random copolymers DAB-BA-PAA, ABOL-BA-PAA, and DAB-Bn-PAA followed similar procedure as reported in previous chapters. The ratio of amino monomers DAB/4AMPBA and ABOL/4AMPBA was chosen 50/50 in each BA-PAA to provide a balance between the more polar DAB or ABOL side chain and the more apolar 4AMPBA side chain, which is important to ensure solubility of the copolymer in aqueous solutions. To free the primary amine of 4AMPBA, excess amount of TEA was added to the reaction mixture. Compared to the syntheses of linear PAAs reported in the previous chapters, polymerization solutions of these BA-PAA reached higher viscosity much faster due to the branching of the benzylic secondary amine. Thus, a portion of the product came out of solution upon reaching high molecular weight. This portion was not readily soluble in water and were not included for further purification through ultrafiltration and lyophilization. Nevertheless, this did not significantly affect polymerization yield, except for the control polymer DAB-Bn-PAA where the majority of product came out of solution during BOC-deprotection and was lost, likely due to the higher hydrophobicity of the non-boronated polymer.

The $^1\text{H-NMR}$ spectrum and structural elucidation of DAB-BA-PAA are shown in Figure 5.1. The other two copolymers provide comparable spectra and their structural elucidations are carried out similarly. All of the three spectra show no trace of unreacted acrylamide groups which are known to be toxic. The degree of BA or Bn-

functionalization could be estimated from the integration values of the aromatic protons in relation to the protons of cystamine or butylene moiety. Presence of two singlets at 4.42 and 4.25 ppm indicates branching in the secondary amine of the 4AMPBA monomer. Reacted secondary amine of the 4AMPBA monomer would have the methylene protons chemical shift shifted upfield (Figure 5.1, d) from that of the unreacted 4AMPBA secondary amine (Figure 5.1, c). The ratio of integration values of the more upfield singlet (Figure 5.1, d) as compared to the total (Figure 5.1, c+d) integration values of the two singlets indicates that ~19% of the incorporated 4AMPBA reacted further through its secondary amine, translating to a total of ~10% branching.

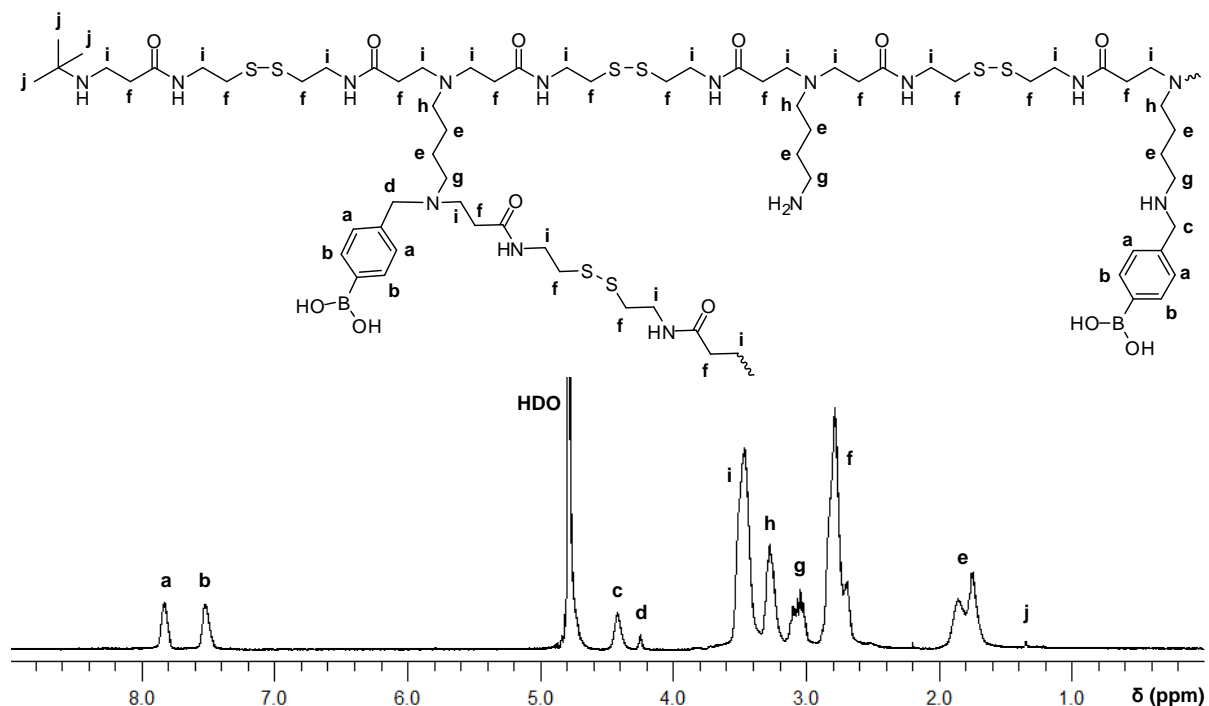
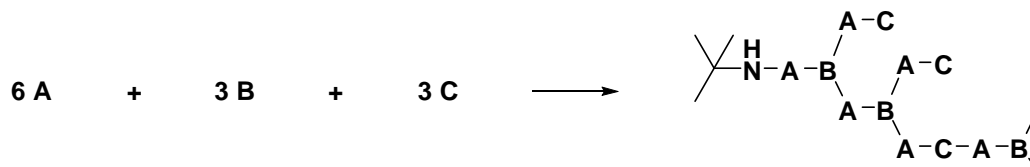


Figure 5.1 $^1\text{H-NMR}$ spectrum and structural elucidation of DAB-BA-PAA.

Number average molecular weight (M_n) can be estimated via the *t*Bu end group (Figure 5.1, j). Considering the 1:1.5 CBA:reactive amine ratio, and assuming only one *t*Bu end group is present per polymer chain to react with a single unreacted acrylamide end in the branched polymer chain (Scheme 5.3), the number of repeating unit is ~27, translating to M_n of 11.5 kg/mol. Table 5.1 summarizes the $^1\text{H-NMR}$ elucidation for the three random branched copolymers synthesized. Attempts to obtain molecular weight (MW) and PDI via GPC did not provide satisfactory result, due to the BA interaction with the polyol-based stationary column.

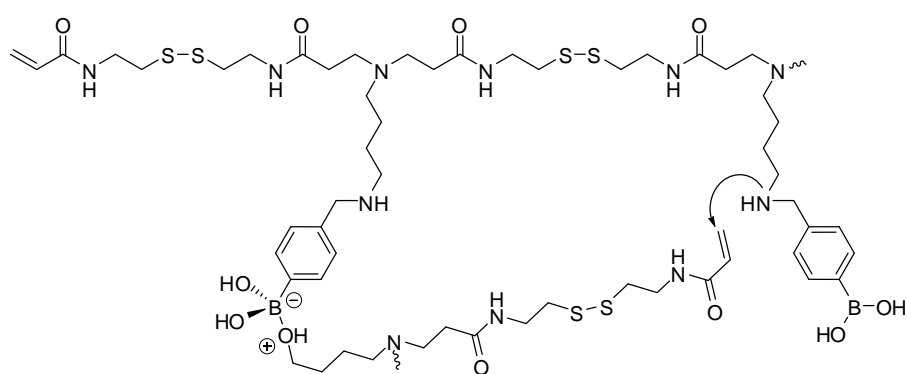


Scheme 5.3 The schematic stoichiometric reaction with A = difunctional CBA, B = difunctional BA or Bn containing amine, and C = monofunctional amine.

Table 5.1 Summary of $^1\text{H-NMR}$ spectra elucidation (%BA or Bn functionalization, degree of branching, number of repeat unit, and M_n) of the branched PAA copolymers.

PAA name	%BA or Bn		% Branching	No. of repeat unit	M_n (kg/mol)
	%repeat unit	%branched			
DAB-BA-PAA	53.5	19.1	10.2	27.2	11.5
ABOL-BA-PAA	52.5	59.3	31.1	31.9	13.4
DAB-Bn-PAA	60.0	21.4	12.8	23.4	9.5

As shown in Table 5.1, both the molecular weight and the degree of branching are relatively low in comparison with some reports on the one-pot-synthesized hyperbranched polymers [37, 38] but are in agreement with a previous report utilizing the same CBA, ABOL and similar reaction procedure [29]. Although this previous report concluded no significant difference in the branched vs linear PAA, we note significant increase in molecular weight of BA-containing PAAs reported in this study in comparison with previously reported linear BA-containing PAA [16]. The previously reported linear BA-PAA was synthesized at 50 °C. The reactivity of the secondary amine in 4AMPBA and BnDAB was most likely enhanced by the increase in reaction temperature to 70 °C. The increase in reactivity is not significant as indicated by the relatively low degree of branching. In addition to the moderate increase in reaction temperature, branching was most likely limited by polymer solubility in the polymerization solvent (a high molecular weight insoluble portion was filtered off), and steric hindrance. It is interesting to note that ABOL-BA-PAA displayed a higher degree of branching as compared to DAB-BA-PAA. The interaction of the alcohol side chains with boronic acid possibly increases affinity between reactants (Scheme 5.4). Moreover, ABOL-BA-PAA may be more soluble than BOC-protected DAB-BA-PAA during polymerization, making it easier for the former to reach higher degree of polymerization.



Scheme 5.4 Schematic illustration of possible interaction between primary alcohol and boronic acid side groups of ABOL-BA-PAA.

In relation to multilayer build-up, it is hypothesized that the presence of branching in this polymer is beneficial in providing more multivalent interactions to stabilize the construct. Since the deposition involves mainly the interaction of the polymer with a surface, the effect of minor differences in MW is expected to be less prominent than the chemical features of the three polymers. Herein the structure-function relationships are described mainly in terms of BA and Bn functionality in the polymers, their interactions with ChS and PVA, and the possible boronate ester formation.

5.3.2 MULTILAYERED THIN FILM BUILD-UP: EFFECTS OF MOLECULAR WEIGHT OF PVA

PVA is commercially available in various molecular weights (MW) and therefore provides an excellent means to study the effect of PVA molecular weight on multilayer build-up. With increasing PVA MW, the relative diol concentration in the deposition solution increases while the BA concentration stays constant. The three different molecular weights of PVA chosen are 27 kDa, 47 kDa, and 195 kDa. Multilayer formation was carried out as mentioned in Section 5.2.5. Build-up profiles of the DAB-BA-PAA polymer with three different PVA molecular weights are shown in Figure 5.2. Absorbance values stated are those at the maximum wavelength of absorption through UV spectroscopy as explained further in Section 5.3.3.

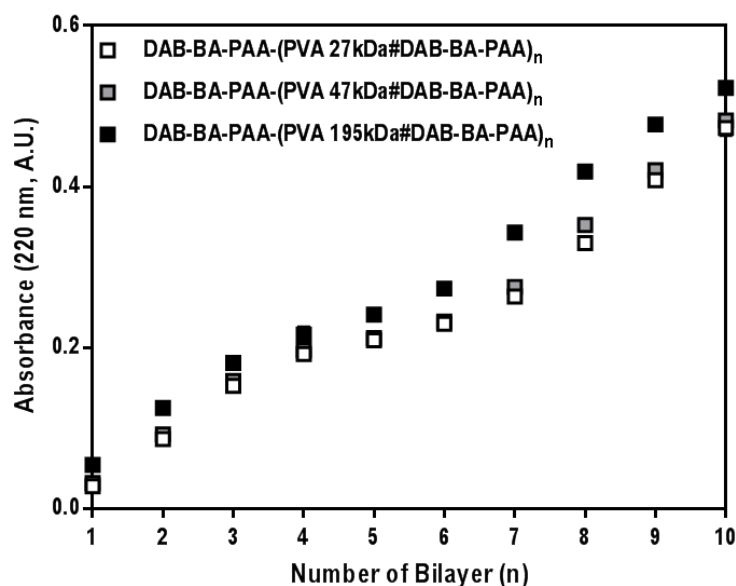


Figure 5.2 Build-up profiles of DAB-BA-PAA polymer with different molecular weight PVA.

Figure 5.2 shows that regardless of the molecular weight of PVA used, the build-up profile remains linear and to similar extents. Increasing diol concentration in the PVA deposition solution does not lead to pronounced increase in BA-PAA deposition. This is very much in contrast to the findings on PVA-based films utilizing weak hydrogen bonding as the only driving force [39] and serves as an indication that the boronic ester formation plays a major role in the build-up of the multilayered system of DAB-BA-PAA and PVA. As the diol concentration is very much in excess to the BA concentration, not much increase in BAPAA deposition is observed upon increasing the molecular weight of the PVA as no additional boronic ester formation is possible. Similarly, multilayer stability under physiological conditions was also found to not be affected by the difference in PVA molecular weight, although there is a notable increase in surface roughness as the PVA MW increases due to folding needed for longer chains to be deposited on the surface (data not shown). The lowest PVA MW (i.e. 27 kDa) is sufficient in facilitating optimal deposition and build-up of the BA-containing polymer and keeping the construct stable under physiological conditions. This PVA MW is selected for the following subsequent studies.

5.3.3 MULTILAYERED THIN FILM BUILD-UP: CHS VERSUS PVA

As indicated in the previous section, the study of build-up profiles and the relative incremental increase in material deposition was carried out through the UV spectra of the multilayers in the dry state which were recorded after every deposition cycle, starting from 1 bl (with BA-PAA layer on top). The UV spectra of the different multilayers were similar with respect to whether DAB-BA-PAA, ABOL-BA-PAA, or DAB-Bn-PAA was employed as the BA- or Bn-functionalized polymer. Therefore, as a representative example, the UV spectra of DAB-BA-PAA-based systems at increasing bilayer numbers are displayed in Figure 5.3. Depending on whether ChS or PVA was incorporated, the UV spectra had maxima at 258 nm and 227 nm, respectively. On the ChS system, the maximum at 227 nm appears as a shoulder with much higher absorption that exceeds the ideal absorption of ≤ 1 A.U. for maintained linearity at higher bilayer numbers. Therefore the more reliable maximum at 258 nm is used for further study on the ChS system.

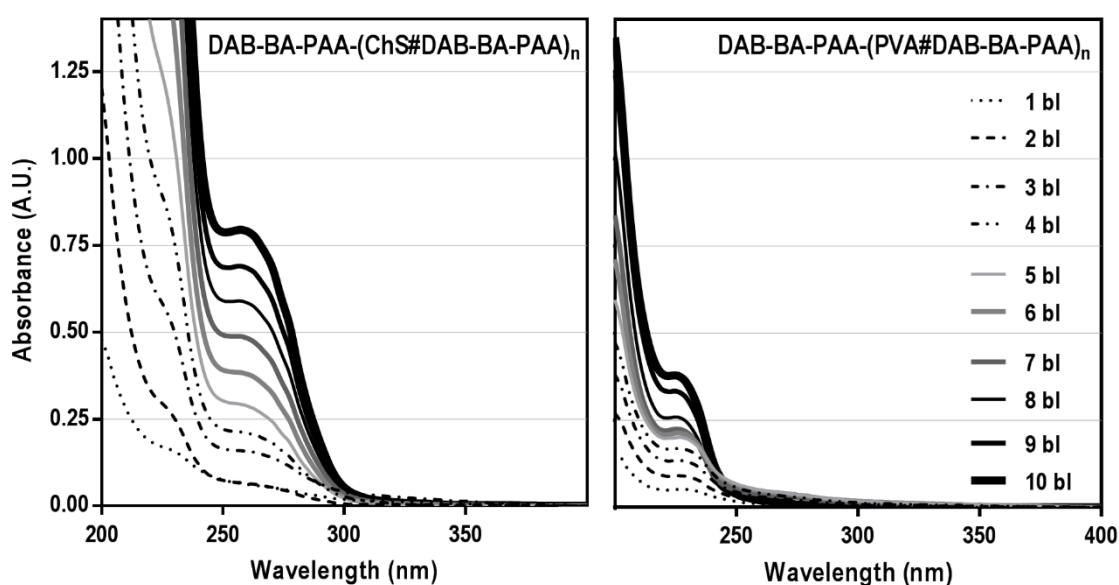


Figure 5.3 UV spectra of DAB-BA-PAA-(ChS#DAB-BA-PAA) and DAB-BA-PAA-(PVA#DAB-BA-PAA) at various bilayer numbers.

To understand the origin of the observed absorption maxima, the UV spectra of the solutions of relevant multilayer components are shown in Figure 5.4. From this figure, the maximum at 227 nm can be attributed to the absorption of the phenyl moiety of DAB-BA-PAA, (ABOL-BA-PAA and DAB-Bn-PAA, data not shown), which is also confirmed by the spectrum of the p(CBA-DAB) homopolymer solution where such a signal is not observed. The maximum at 258 nm is attributed to the ChS which shows a distinct peak with notably relatively higher extinction coefficient than the absorption of other components at the same wavelength and concentration.

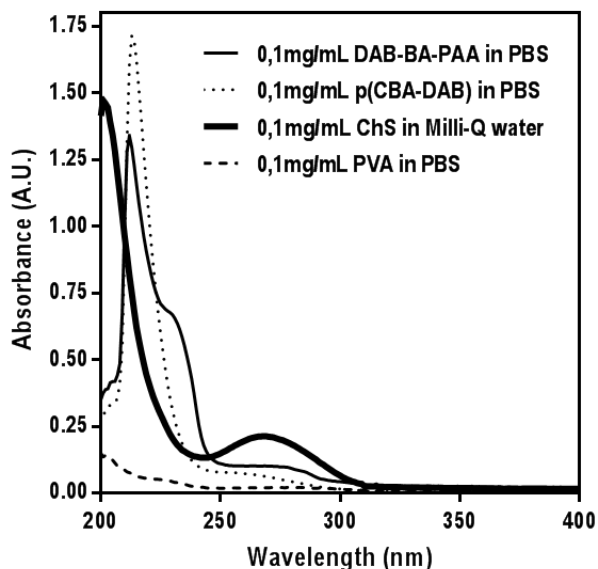


Figure 5.4 Solution state UV spectra of relevant multilayer components.

Based on the respective absorption maxima, build-up profiles can be plotted for the multilayers. All of the BA-based systems exhibit relatively linear build-up profiles as shown in Figure 5.5. The control polymer DAB-Bn-PAA, however, provides a remarkable finding. For this polymer which does not contain a BA moiety, multilayer build-up is positive when paired with ChS, but negative when paired with PVA. This phenomenon indicates that the positive multilayer build-up of PVA-based films in this study depends substantially on the boronate ester formation. This finding also implies that multilayer build-up with ChS may still progress without boronate ester formation.

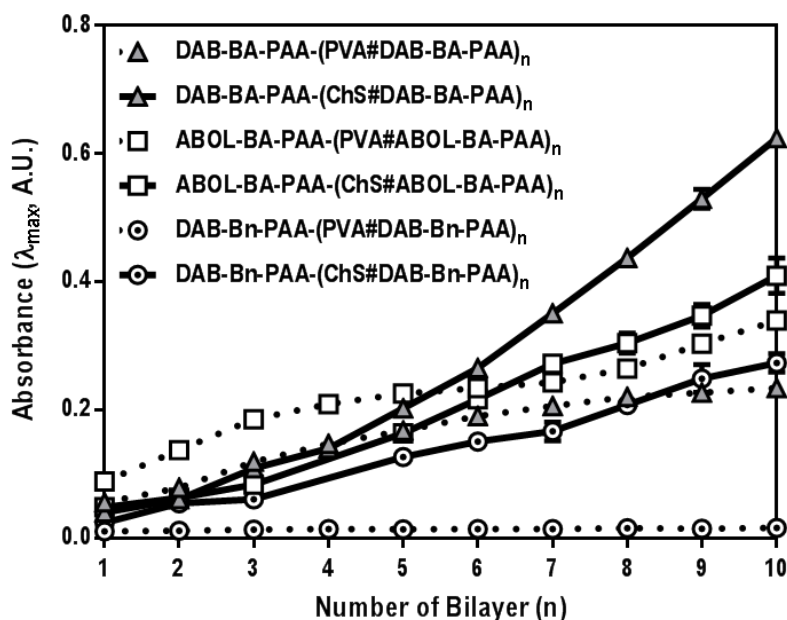


Figure 5.5 Build-up profiles of DAB-BA-PAA-(PVA#DAB-BA-PAA)_n, DAB-BA-PAA-(ChS#DAB-BA-PAA)_n, ABOL-BA-PAA-(PVA#ABOL-BA-PAA)_n, and ABOL-BA-PAA-(ChS#ABOL-BA-PAA)_n multilayers. Absorbance values shown are those at 227 nm for PVA-based films and 258 nm for ChS-based films.

To complement the UV-spectrophotometry data, thickness data was also obtained through AFM scratch tests, i.e. a scratch was made using a small syringe needle across the surface of the film which was further imaged using AFM. Thickness and surface roughness data obtained for the four BA-based multilayers on various bilayer numbers are plotted in Figure 5.6.

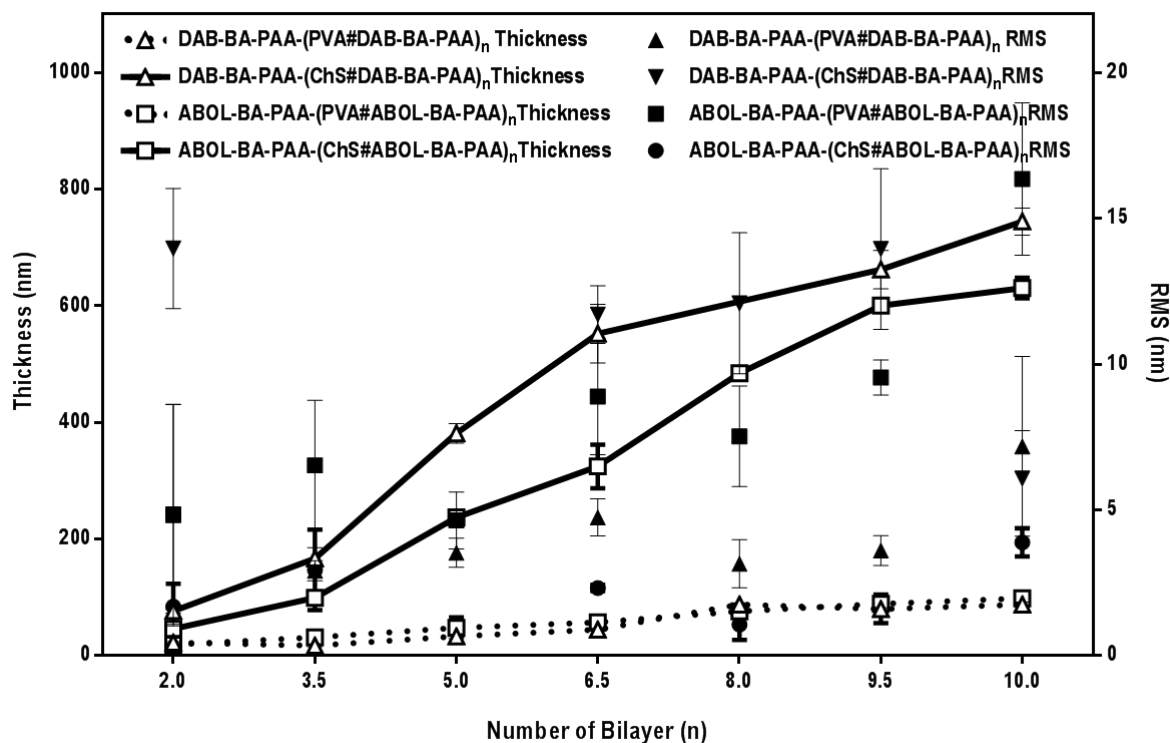


Figure 5.6 Build-up profiles of the multilayered systems based on AFM. Surface roughness (RMS, nm) and thickness (nm) at different bilayer numbers are shown at the two ordinate axes. Every data point is an average of at least three measurements made on arbitrary positions of the same multilayer sample.

Figure 5.6 agrees well with the UV spectrophotometry data displayed in Figure 5.5 in terms of relative build-up profiles of the different systems. However, it is remarkable to note the tremendous difference in thickness between PVA- and ChS-based films, which is not apparent from the UV data due to the difference in λ_{\max} (and subsequently extinction coefficient) used for the different systems. At the same 10 bilayers, ChS-based systems were at least 600 nm thick while PVA-based systems were much thinner at ~100 nm. The thick nature of the ChS-based film was also observed qualitatively by eye through the increased turbidity, especially at higher bilayer numbers. In a computational study, Rodríguez-Carvajal et al. reported that chondroitin 4-sulfate (the ChS variant used in this study) particularly assumes a rigid helical conformation [40], a feature that also contributes to ChS properties as bone extracellular matrix. Moreover, unlike the BA-PAAAs, ChS is a strong polyelectrolyte. Taking into account the findings on the effect of charge density on multilayer build-up [41, 42], it is even less likely that ChS would take up more globular conformation due to charge repulsion. Therefore, the very thick nature of the (ChS#BAPAAAs) multilayers can only be attributed to the increased amount of deposited ChS. As a strong polyelectrolyte, ChS readily binds counter-ions. Especially for chondroitin 4-sulfate, it is reported that small counter-ion binding sites are energetically more favorable [40]. This may facilitate deposition of more ChS chains, effectively increasing the multilayer thickness.

Upon closer examination of the build-up profiles (Figure 5.6 and Figure 5.5), ChS-based films (solid lines) notably display more linear build-up profiles, while for PVA-based films (dotted lines), multilayer growth slows down after approximately 5 bilayers. This change in build-up profile upon 5 bilayer formation (also observed in Figure 5.2) may be explained as an effect of the underlying charged-substrate, which may be particularly prominent in a

system where the driving force for multilayer build-up is not electrostatic interactions [43-45]. The lower thickness of the PVA (in contrast to ChS) system may also contribute to increase the effect.

Another interesting observation can be made from Figure 5.5 on the relation of the extent of material depositions to the two different polymers. For ChS-based films, DAB-BA-PAA promotes higher deposition than ABOL-BA-PAA, while for PVA-based films, the contrary is observed. Since the two polymers possess similar degrees of BA functionalization (Table 5.1), this finding may be explained by the difference in the type of side group (i.e. DAB vs ABOL) of the two polymers, and their effect on overall charge densities of the polymers and interactions with the other multilayer components. DAB-BA-PAA with protonated primary amine side groups has a higher cationic charge density and consequently provide stronger electrostatic interactions with the negatively charged ChS than ABOL-BA-PAA with primary alcohol side groups. Thus, DAB-BA-PAA favors interaction with negatively-charged ChS, while ABOL-BA-PAA favors interaction with PVA, possibly because the hydroxybutyl chains can better accommodate in the PVA layer than the charged DAB chains. These results indicate that possible stronger interactions lead to higher incremental increases of the paired multilayer components. However, this is in contrast to the widely accepted findings that less, but sufficiently-charged polyelectrolytes give rise to increased deposition [42, 46], as well as the results we previously obtained for multilayer build-up of DAB and ABOL linear homopolymers with DNA (Chapter 3). This finding can probably be explained through the presence of more hydrophobic BA moieties in the random branched polymer structure. As previously reported, *ortho*-substituted linear ABOL-BA-PAA spontaneously form nanosized particles in solution, which was attributed to interactions of BA moieties with the primary alcohol side groups in the proximity [16]. The same observation was made for the branched ABOL-BA-PAA in this study. Upon dissolution of the branched ABOL-BA-PAA in glucose-free HEPES buffer pH 7.4 at 0.6 mg/mL, dynamic light scattering (DLS) revealed the presence of particles 94 nm in size with PDI of 0.3. The same phenomenon was observed for the branched DAB-BA-PAA, albeit with much higher PDI of 0.6, indicating a less homogenous particle size distribution. Furthermore, the ABOL-BA-PAA particles have noticeably more positive zeta potential as compared with DAB-BA-PAA (up to +40 and +4 mV, respectively). This indicates a significant difference in the conformation of the two copolymers in solution, which may also play a role in the way they interact with a surface. Most notably, the apparently higher positive charge of ABOL-BA-PAA in solution may lead to stronger interaction with ChS, which further leads to lower incremental increase during layer build-up, as compared with DAB-BA-PAA. On PVA-based films, the higher deposition provided by ABOL-BA-PAA may be due to the ability of primary alcohol groups to facilitate boronate ester formation better than (charged) primary amine groups [39].

5.3.4 CONTACT ANGLE MEASUREMENTS

To examine whether different static water contact angles can provide information on the identity of the topmost layer and the hydrophobicity of the surfaces in general, multilayered systems with different bilayer numbers were measured via the sessile drop method (Figure 5.7). Figure 5.7 shows that at least for the first 2 cycles of deposition of ChS-based multilayers, layer coverage is incomplete and the effect of the bare hydrophilic silicon wafer substrate can still be observed through the lower contact angle values. For the PVA-based multilayers, however, complete surface coverage can be observed as early as the 0.5 bilayer (i.e. film with first precursor polymer layer and the first PVA layer), probably because of the more specific interactions PVA has with the BA-PAA layer.

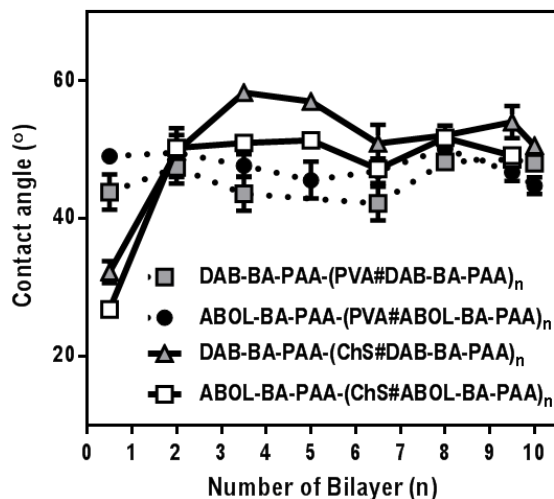


Figure 5.7 Static water contact angles of multilayers at different numbers of bilayers.

At higher bilayer numbers, the contact angle values do not show a marked difference when the top most layer was either the BA-PAA layer, or the ChS or PVA layer. Serizawa et al. reported the average contact angle values of 45° for PVA top-most layers for their LbL-assembled multilayers of PVA with poly(methyl methacrylate) (PMMA) [47], which is relatively similar to the observed value shown in Figure 5.7. Literature reports on contact angles of ChS film mention values between 70° to 80° [48, 49] depending on prior treatment and the nature of the underlying surfaces.

Instead of the static contact angles, advancing and receding contact angles may provide more accurate information on surface profile and hydrophobicity. Moreover, the N₂ drying step employed during film formation may not completely dry the system from trapped water molecules, especially considering the hygroscopic nature of all of the layer components, and therefore may substantially affect the static contact angle values observed. Nevertheless, the obtained data provides information on the onset of complete surface coverage which has to be taken into account for subsequent experiments. The data may also be more relevant for the intended applications where the films are stored at ambient humidity, at room temperature or 4 °C with no notable differences in wettability. In agreement with the contact angle data, the 10-bilayered ChS-based films were always less easily wetted by aqueous solutions (such as cell culture medium) than the respective PVA-based films, regardless of the presence of a BA-PAA topmost layer.

5.3.5 ATOMIC FORCE MICROSCOPY SURFACE PROFILES

In addition to providing thickness information, AFM was also used to gain insights into the possible differences in surface profiles of the different films, and at different bilayer numbers. A digital photograph of the complete set of ABOL-BA-PAA-based samples, both with PVA and ChS at various bilayer numbers is shown in Figure 5.8. DAB-BA-PAA-based films look similar, but with less homogeneous surfaces and increased turbidity. Figure 5.8 shows the typical thin-film interference color pattern observed during build-up on silicon wafers of various multilayers reported in this thesis. Notably, films of ~100 nm thick show deep blue interference color as shown for ABOL-BA-PAA-(PVA#ABOL-BA-PAA)₁₀ in Figure 5.8. In agreement with the thickness data, ABOL-BA-PAA-(ChS#ABOL-BA-PAA) reaches the same thickness much earlier at 3.5 bl and shows the same deep blue color.

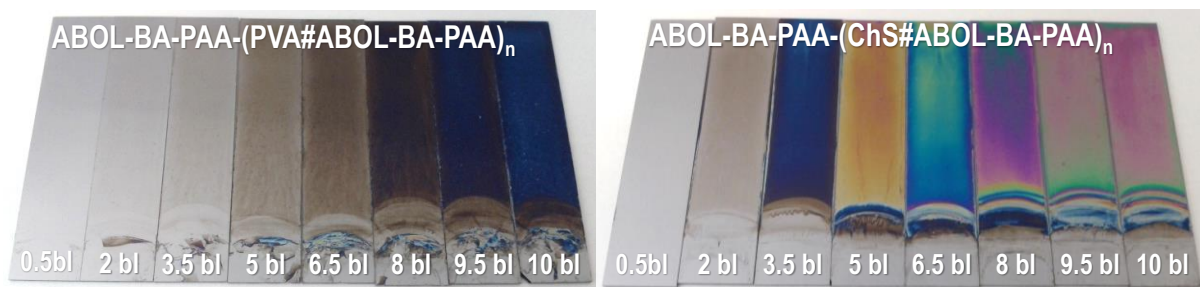
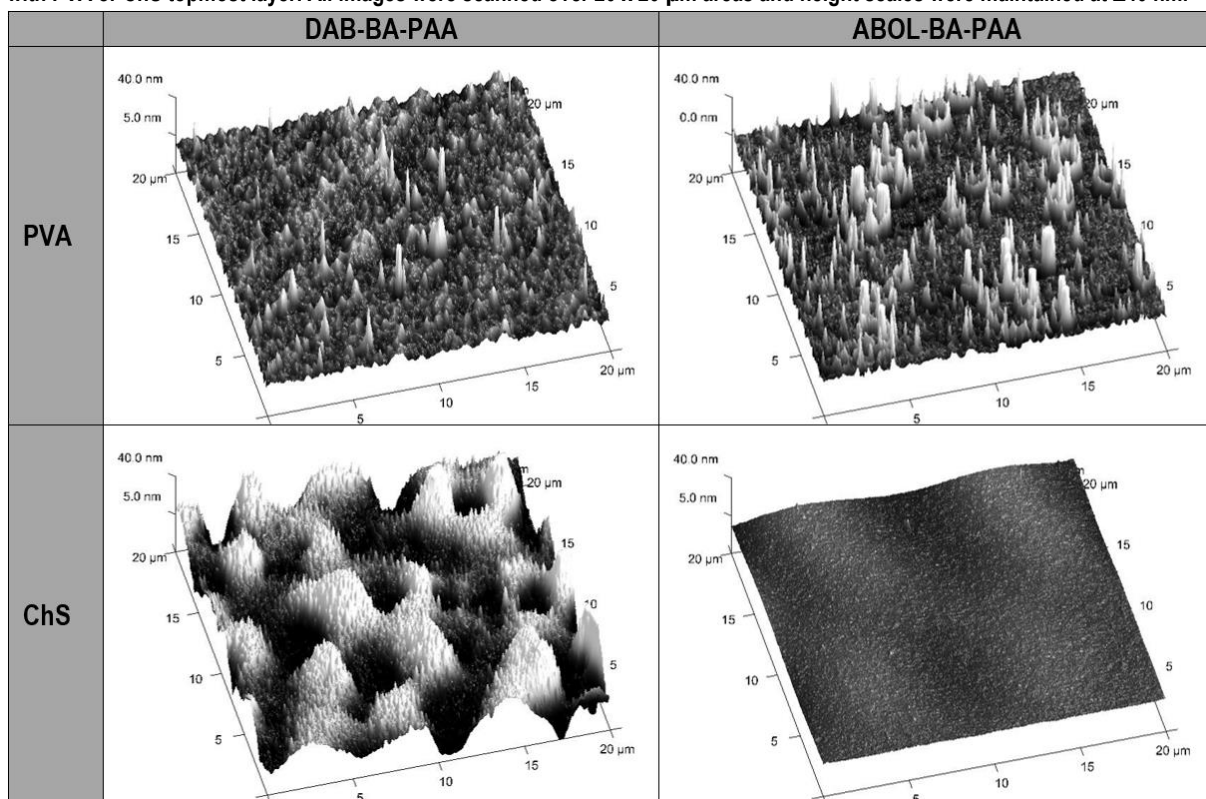


Figure 5.8 Digital photograph of ABOL-BA-PAA-(PVA#ABOL-BA-PAA)_n and ABOL-BA-PAA-(ChS#ABOL-BA-PAA)_n built on silicon wafer at various bilayer numbers.

Similar to the contact angle data, the four multilayered systems do not show alternating surface profiles as observed from AFM. Typical surface profiles of the four different systems shown using the same height scale of ± 40 nm are shown in Table 5.2. All of the PVA-based films show sharp height features indicating high surface roughness. As shown in Figure 5.6, PVA-based films have roughness up to 16 nm at 9.5 and 10 bl. This is typically much higher compared with ChS-based films, especially considering the much thinner nature of the PVA-based films. ChS-based films show very different surface profiles depending on whether it is paired with DAB-BA-PAA or ABOL-BA-PAA. (ChS#DAB-BA-PAA) films are much rougher at all stages of the build-up, with roughness up to 15 nm. Interestingly roughness is enhanced with ChS as the topmost layer. In comparison, (ChS#ABOL-BA-PAA) films are smooth at all stages of the build-up, with the highest roughness obtained at less than 5 nm at the highest bilayer number. This difference in roughness of the two ChS-based films were also observed visually during multilayer build-up.

Table 5.2 Typical surface profiles of the four different multilayers based on AFM. Images were recorded on 9.5-bilayered films, with PVA or ChS topmost layer. All images were scanned over $20 \times 20 \mu\text{m}$ areas and height scales were maintained at ± 40 nm.



5.3.6 STABILITY PROFILES UNDER PHYSIOLOGICAL AND REDUCING CONDITIONS

Investigating multilayered film behavior under physiological conditions may serve to assess their stability in the presence of physiological salt concentration, pH, and temperature. The stability profile may be used to tune the film's behavior, for example, in releasing loaded drugs. Further, both DAB-BA-PAA and ABOL-BA-PAA contain disulfide bonds in the main chain to render them biodegradable under reducing conditions. This could especially be important when the BA-PAAAs are taken up by cells, since it has already been shown that polyplexes of these polymers rapidly degrade in the reducing cytosol due to the presence of a relatively high concentration of glutathione (~5-10 mM) [50]. Moreover, in biological environment, extracellular reductases may contribute to film degradation through the reductive cleavage of the disulfide bonds [51]. To investigate the stability profiles of the four different films under physiological and reducing conditions, the films were incubated in PBS solutions pH 7.4 at 37 °C in the presence or absence of either glutathione (0.4 and 10 mM) or DTT (2.5 mM). From time to time, the films were retrieved, dried under a gentle N₂ stream, and measured for their absorbance values at the respective λ_{\max} .

Figure 5.9 shows the decrease in relative absorbance values in time, i.e. the ratio of absorbance value against the respective value at time zero. Figure 5.9a and b show the results for PVA- and ChS-based systems, respectively. Throughout the incubation time, the four multilayers remain stable under physiological conditions, but are readily degraded in the presence of reducing agents. Higher concentrations of reducing agent degraded the films faster as shown by the use of 0.4 and 10 mM glutathione. It is interesting to note that at 2.5 mM, DTT shows a higher reducing rate than 10 mM glutathione for ChS-based films, but lower for PVA-based films. Glutathione has an extra negative charge due to the presence of glutamic acid in this molecule. It is therefore more negative than DTT and thus may experience more electrostatic repulsion in ChS films. This does not play a role in PVA films. Moreover, from both the UV spectroscopy and thickness characterizations, it is likely that in addition to having much higher thickness, the ChS-based films also contain higher portion of ChS in comparison to the degradable BA-PAAAs and therefore, diffusion of reducing agents into the inner part of the film may be slightly impeded relative to the thinner PVA multilayers. This may further explain the high standard deviation observed for the ChS systems.

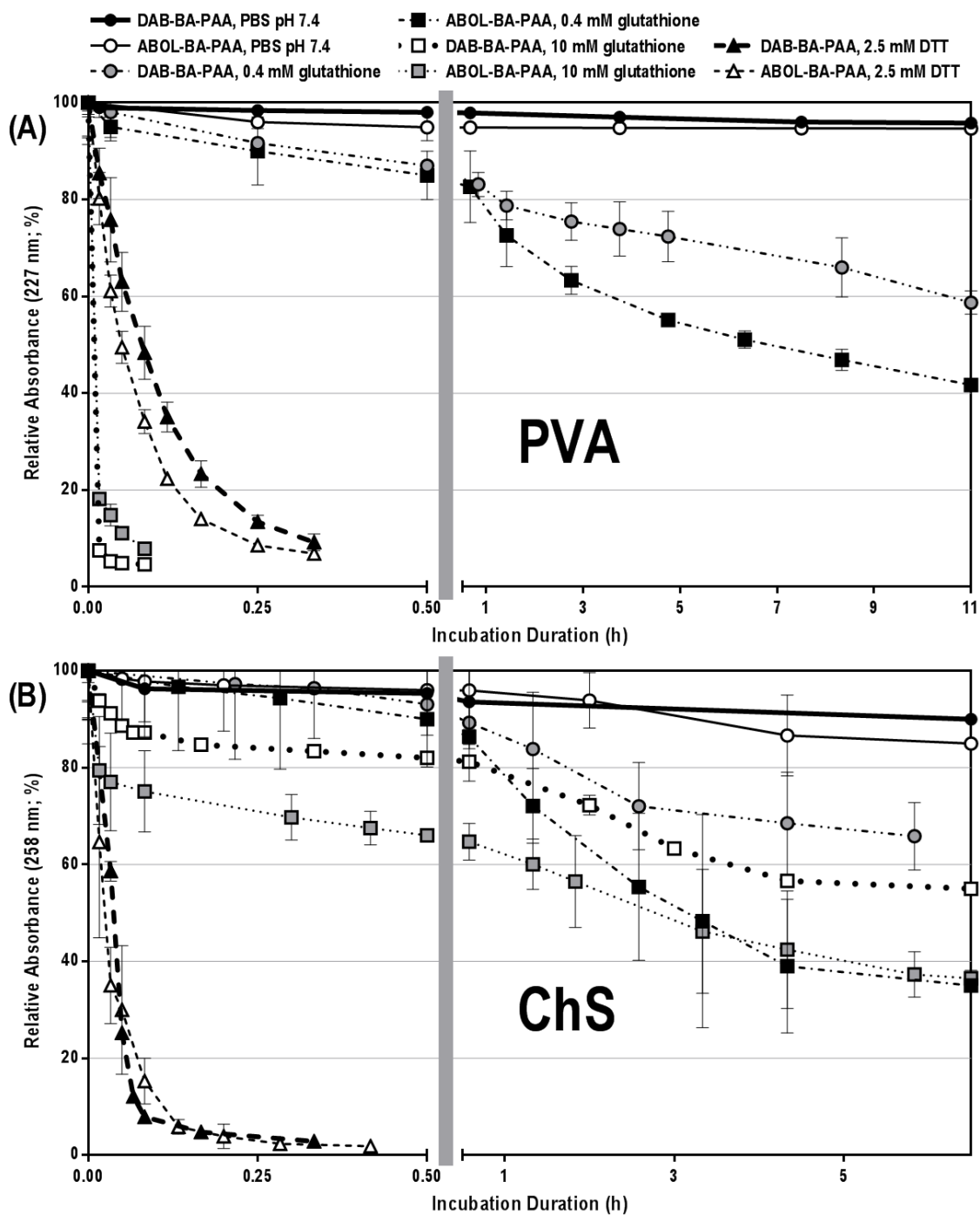


Figure 5.9 Stability profiles of: (A) PVA- and (B) ChS-based multilayers under physiological conditions (PBS pH 7.4 at 37 °C) and in the presence of glutathione (0.4 mM and 10 mM) or DTT (2.5 mM). The left part of the abscissa shows the trend of fast decrease (burst release) within 0.5 h (30 min) in the initial phase of the incubation while the right part shows the much slower decrease throughout the rest of the long incubation duration.

5.3.7 STABILITY PROFILES AT ACIDIC pH

As indicated in Scheme 5.1, the boronate ester formation is sensitive to pH. It is reported that the boronate ester is more stable in tetragonal state (basic conditions) than in the trigonal state [4, 52]. Thus, boronate ester formation is not favored at acidic pH where the trigonal boronic acid dominates. To investigate the responsiveness of the four different multilayers to acidic pH, the different films were incubated in citrate buffered saline (CBS) at pH 4, 5, and 6 at 37 °C. From time to time, the solutions were refreshed, the films were dried, and the relative absorbance is measured as the ratio of the absorbance at a specific time to that at time zero. Figure 5.10a and b show the stability profiles of PVA- and ChS-based films, respectively. The PVA-based films are notably very responsive to acidic conditions, with faster film dissolution at lower acidic pH. Notably, complete dissolution can be achieved after only 3 min of incubation at pH 4. The high responsiveness of the PVA systems may further indicate the strong BA-diol interaction within the multilayered construct. Low pH values diminish possible ester formation that hold the films together. The very rapid kinetics also signify that there is likely only limited significance of other types of interactions present that could be strong enough to prevent the multilayer from dissolution at low pH.

On the other hand, the ChS systems show much slower dissolution with fast initial response only during the first 1 h. Very interestingly, the disassembly rate is faster at elevated pH as opposed to lower pH. For instance, for the (ChS#ABOL-BA-PAA) system, 70% of disassembly is reached after 4 days of incubation at pH 6 while only ~40% is reached under the same conditions at pH 4. The films are, however, relatively stable under physiological pH, with only ~20% disassembly after 2 days of incubation. This trend may further confirm the low tendency of boronate ester formation in ChS-based multilayers. The phenomenon may be explained by the presence of carboxylic acid groups in ChS. In contrast to the sulfate groups, which are negatively charged at all pH values investigated in this study, the carboxylic acid groups having pKa in the range of ~3-5 may undergo drastic change in ionization state in the acidic pH range of 4-6. As such, at pH 4, ChS is much less negatively-charged than at pH 6. On the other hand, more of the amine of the BA-PAA are protonated at pH 4 than at pH 6. The overall effect may be the relative higher stability of the system at pH 4 than at pH 6. Under the physiological pH of 7.4, the amines of BA-PAA are even less positively-charged, but the ChS is fully ionized, leading to a stable system. This stability may be more enhanced by the fact that the films were immersed in the same solvent in which build-up took place, causing less effect of osmotic ion diffusion and destabilization.

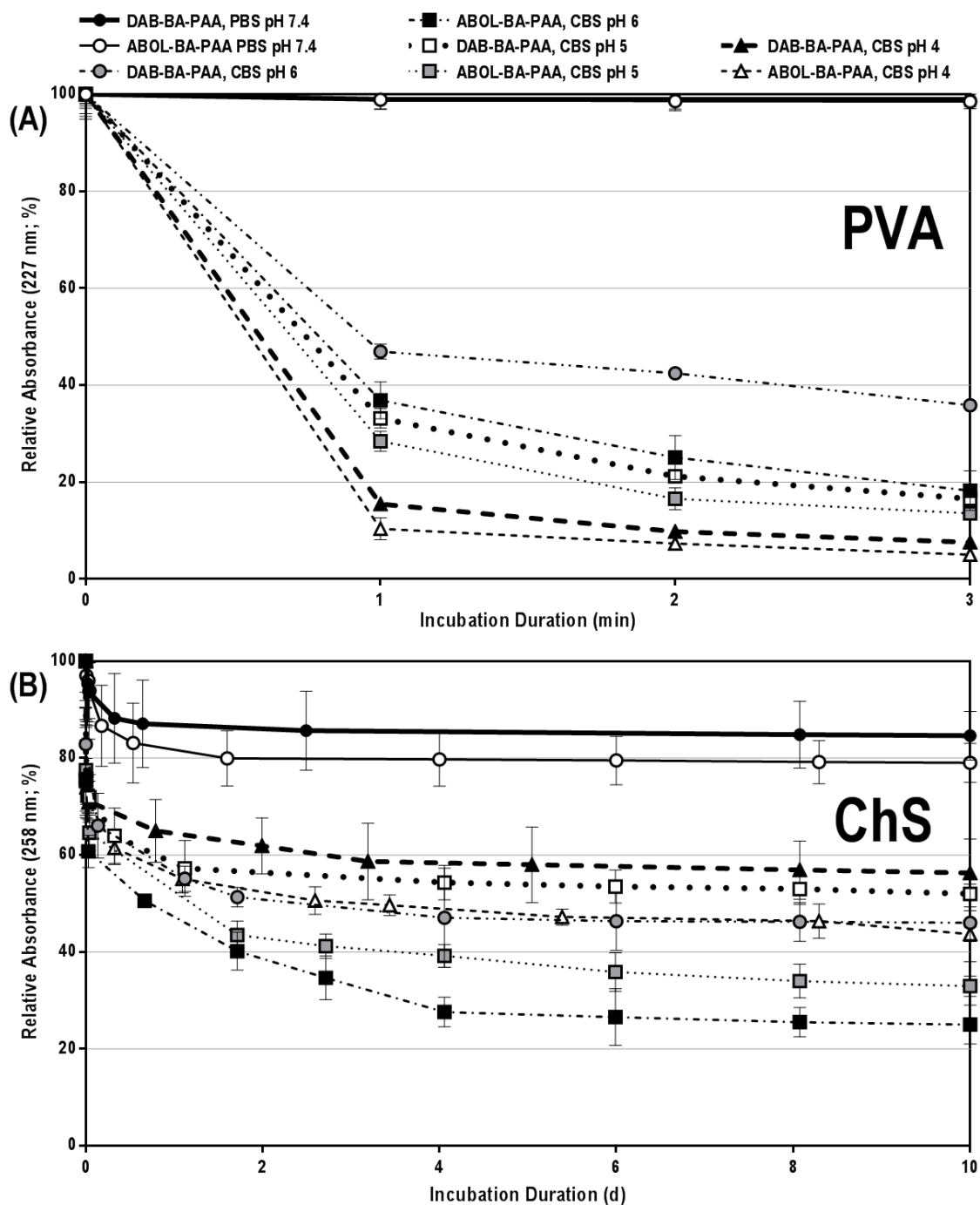


Figure 5.10 Stability profiles of: (A) PVA- and (B) ChS-based multilayers under physiological conditions (PBS pH 7.4 at 37 °C) and in CBS pH 6, 5, and 4.

5.3.8 STABILITY PROFILES IN VARIOUS GLUCOSE CONCENTRATIONS

As indicated in Scheme 5.1, boronate ester formation may be affected by the presence of other diol moieties, such as glucose, through competitive binding. To investigate whether the multilayered systems possess glucose-responsiveness, the multilayers were incubated at various glucose concentrations under physiological conditions. Figure 5.11a and b show the stability profiles of PVA and ChS systems, respectively. From this figure it can be observed that the PVA systems are more responsive to glucose compared to the ChS system, especially apparent at the highest glucose concentration (100 mM). (ChS#DAB-BA-PAA) films show similar profiles with and

without the presence of 100 mM glucose, while (ChS#ABOL-BA-PAA) systems seem to be only slightly responsive to glucose at the same concentration. At lower concentration, the ChS-based films were progressively more stable or identical to their profiles under physiological conditions (data not shown). The low responsiveness of the ChS system to elevated glucose concentrations, despite the long incubation duration, may be due to the more electrostatic nature of the interactions, possibly further enhanced by the thickness of the film limiting diffusion of glucose. As this may indicate that the majority of BA-moieties in the multilayered film are free of ester formation with ChS, this system may be utilized as a depot for drugs which have affinity to the BA-moiety, thereby providing more controlled or triggered release. This possibility is investigated in the following chapter (Chapter 6).

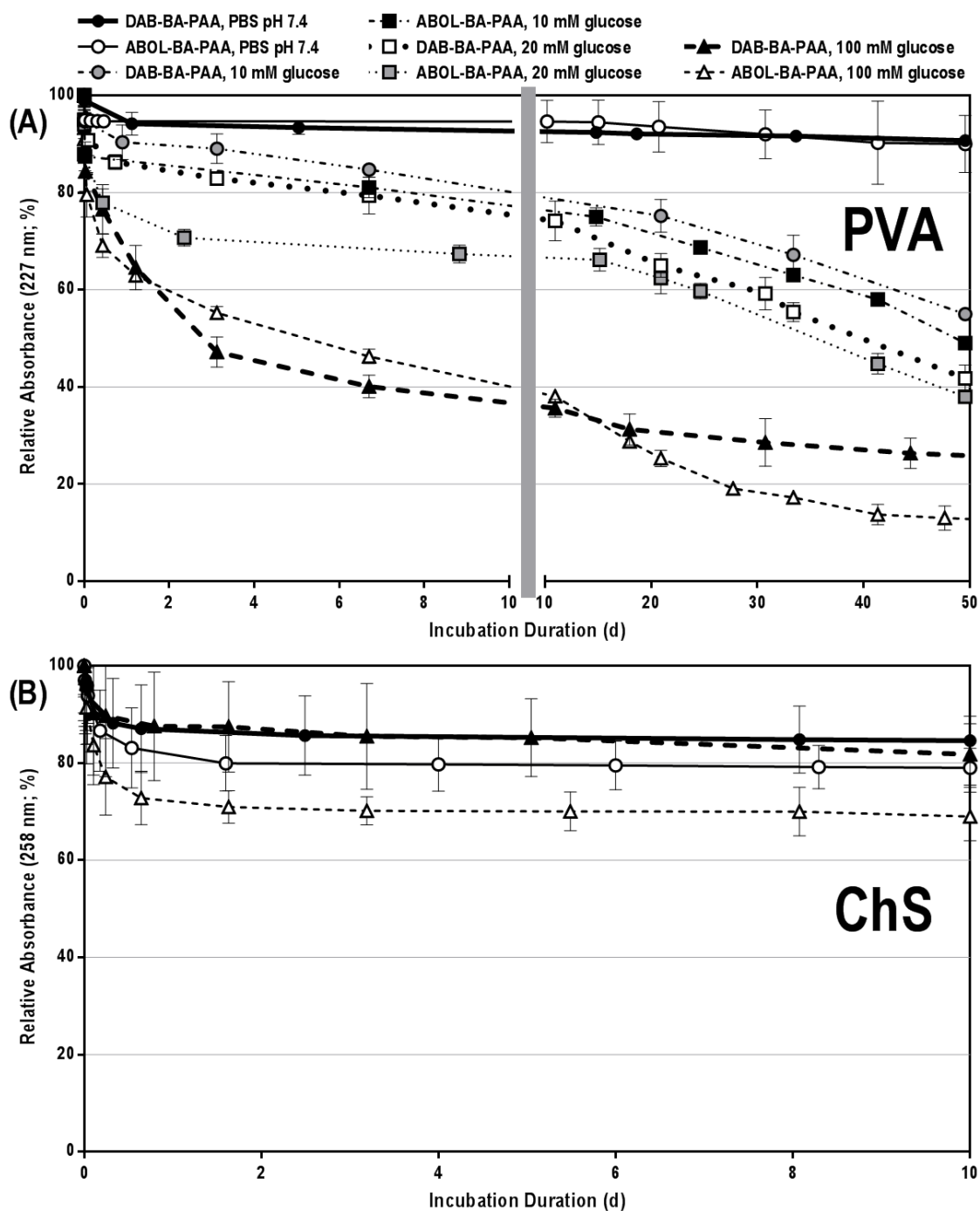


Figure 5.11 Stability profiles of: (A) PVA- and (B) ChS-based multilayers under physiological conditions (PBS pH 7.4 at 37 °C) and in the presence of 10, 20, and 100 mM glucose. For ChS systems, only the 100 mM glucose data is shown for clarity.

The PVA-based films on the other hand, show a clear response to glucose, although with slow kinetics. (PVA#ABOL-BA-PAA) notably reached the same 70% relative absorbance values as (ChS#ABOL-BA-PAA), but at a glucose concentration of only 20 mM, instead of 100 mM for the latter. At 100 mM glucose concentration, (PVA#ABOL-BA-PAA) reaches 40% degree of disassembly following 2 days of incubation. The rate decreases throughout the 50 d incubation time. At both the 10 mM and 20 mM glucose concentrations, the disassembly rate is much slower, but with an apparent trend of glucose responsiveness for the two different polymer systems. The slow and/or low glucose responsiveness (i.e. where higher glucose concentration is needed for significant response) is similar to previous reports on multilayered systems [26, 53] and others [54-58] and is mostly attributed to the weaker binding of phenylboronic acid moieties to glucose than, in this case, to PVA under physiological pH. The current results, however, are relevant for applications where longer sustained release is desired.

From the trends observed in Figure 5.9, Figure 5.10, and Figure 5.11 for both PVA- and ChS-based films, the ABOL-BA-PAA-systems seem to more readily disassemble than DAB-BA-PAA films, or in other words, the latter are more stable. The trend is weak and is usually masked by the more dominant effect of the treatment (i.e. reducing agents, pH, and glucose), but may be attributed to the difference between the primary amine and primary alcohol side chains. The extra positive charges brought in by the primary amines of DAB may help stabilize the layers (both with PVA and ChS), causing less effect against the various treatments, compared to primary alcohol side chains.

5.3.9 COS-7 CELL VIABILITY ON MULTILAYERED SYSTEMS

In order to obtain a functionalized multilayered surface for biomedical applications, it is necessary to study the biocompatibility of the surface. For an *in vitro* experiment, the morphology and metabolic activity of cells cultured on the surface may serve as a preliminary indication. For this experiment, films were built directly on the surfaces of 96-well plates, and COS-7 cells were seeded directly on top of the films to emphasize the effect of the substrates on cell morphology and viability. At the end of the 2 d culture period, metabolic activity was measured. Figure 5.12a shows that at 6 h after cell seeding, all of the cells have attached. All of the COS-7 cells seeded on multilayers seem to have similar morphology to those seeded on regular commercial TCPS (tissue culture-treated polystyrene), i.e. much better than the morphology of the cells seeded on the non-tissue culture treated polystyrene (i.e. untreated PS, normally utilized for suspension culture). However, after 2 d of culture (Figure 5.12b), COS-7 cells on PVA-based films are seen to aggregate, similar to those on untreated PS. The EthD-1 which stains for dead cells (red), however, shows no significant difference in the amount of dead cells. Therefore, to further confirm the results, metabolic activity assay was performed at the end of the 2 d culture experiment.

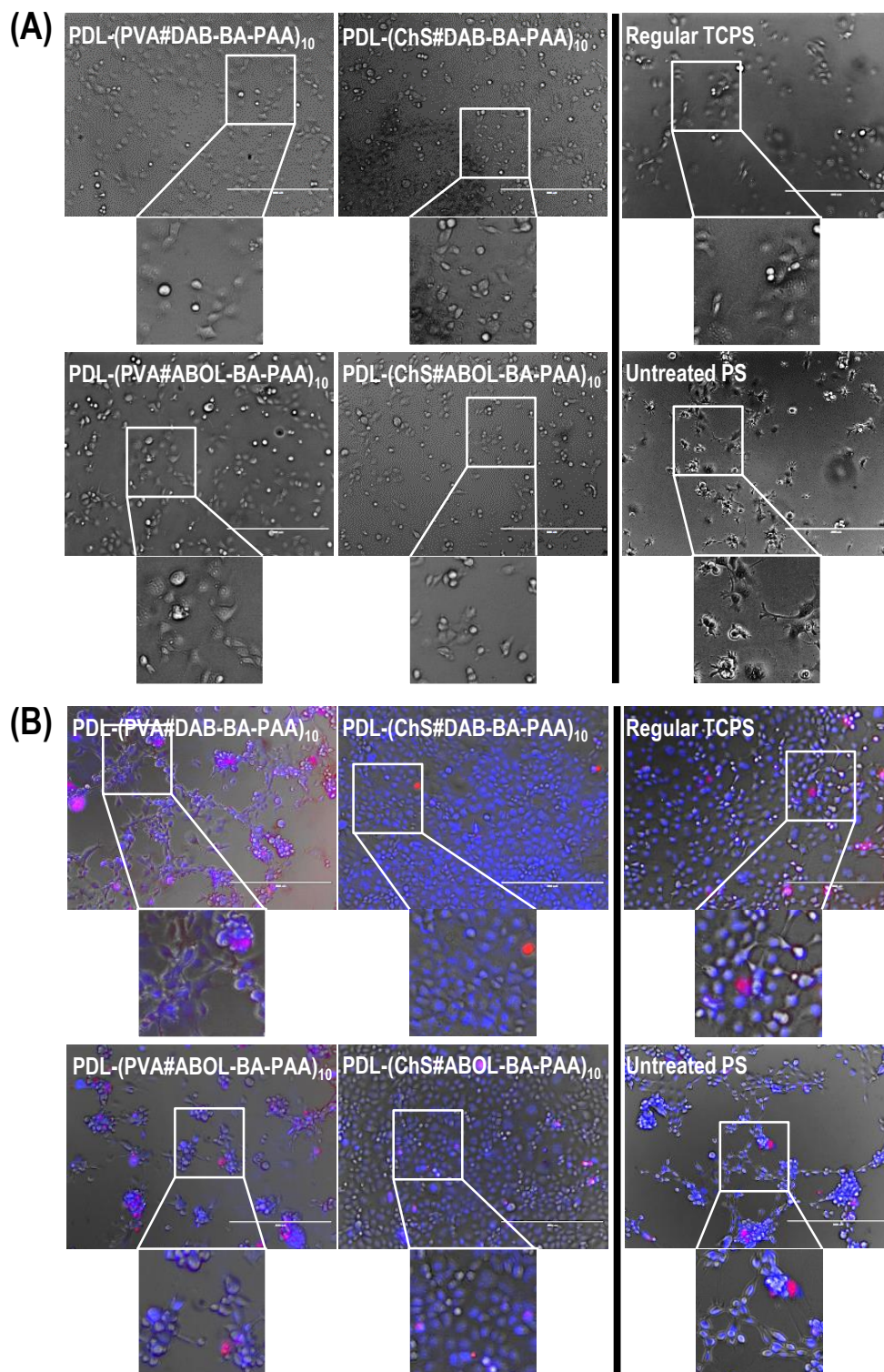


Figure 5.12 COS-7 (A) Light microscopy images of COS-7 cell after 6 h of culture on various surfaces. (B) Overlay fluorescence images following cell staining with Hoechst 33258 (blue, live) and EthD-1 (red, dead) after 2 d of culture on various surfaces. 10X magnification, bars = 400 μ m.

In agreement with the live/dead staining results shown in Figure 5.12b, the alamarblue (AB) assay for metabolic activity (Figure 5.13) indicates that there is no significant difference in the metabolic activity of cells cultured on all of the studied surfaces. As expected, the more charged TCPS provides the best cell proliferation through faster cell attachment, while untreated PS provides slower cell attachment leading to slightly less metabolic activity. On the multilayered systems, ChS-based surfaces facilitate the best cell attachment, morphology and metabolic

activity. Such high biocompatibility is expected given the natural biological origin of ChS. PVA-systems were observed to initially facilitate cell attachment, which means that the surface performs well in adsorbing anchoring proteins to facilitate cell attachment [59, 60]. However, upon longer culture duration the cells start to tend to aggregate, probably indicating slight cytotoxic effect of the surface. Considering the generally accepted biocompatibility of PVA [61], the effect may be induced by interaction of the cells with the BA-PAA. Nevertheless the effect is mild, as the cells still show metabolic activity comparable to all the other surfaces. It can therefore be concluded that all of the multilayered systems investigated in this study are biocompatible.

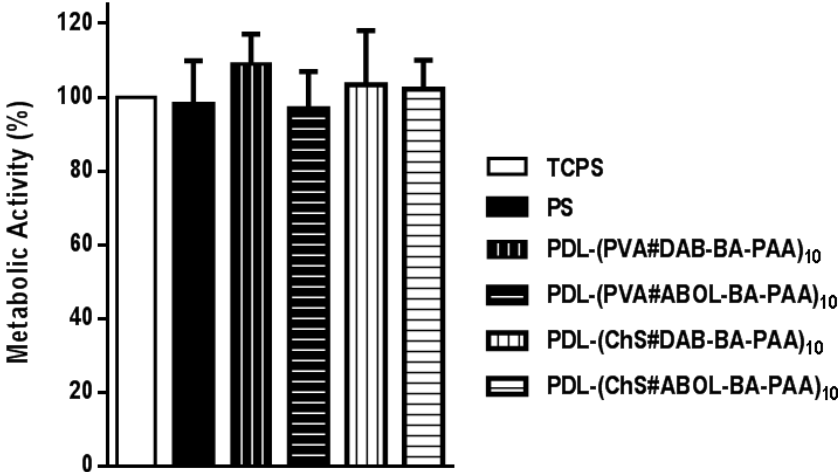


Figure 5.13 Metabolic activity of COS-7 cells cultured on untreated PS and various multilayered surfaces relative to TCPS control. All values are not significantly different from one another ($p > 0.05$).



5.4 CONCLUSIONS

Two branched random copolymers of poly(amido amine)s containing phenylboronic acid functionality (BA-PAA)s have been synthesized and characterized for their possibility in forming multilayered thin films with PVA and ChS. The two BA-PAA)s were ~50% functionalized with the same BA moiety, while the other 50% consisted of either primary amine (DAB) or primary alcohol (ABOL) side chains. The degree of branching was relatively low at ~10-30%, increasing overall molecular weight and possibly multilayer stability, while still facilitating aqueous-solubility at the multilayer assembly pH of 7.4.

Multilayer formation of the two BA-PAA)s with both PVA and ChS were successful, with notable differences between PVA- and ChS-based systems. PVA films were thin, with ~100 nm thickness at 10 bilayer, while ChS films were at least 6 times thicker with possibly higher ChS content. The molecular weight of PVA was found to have no effect on the incremental deposition amount of materials. Furthermore, DAB-Bn-PAA, a control polymer without BA functionality, did not form multilayer with PVA, but with ChS multilayer formation did occur. This indicated that multilayer build-up of BA-PAA)s with PVA was due to boronate ester formation. It was further found that PVA-based BA-PAA) films were responsive to glucose, although with slow kinetics, indicating potential in drug delivery applications where sustained release is desired. In contrast, the positive multilayer formation by the control non-BA polymer (DAB-Bn-PAA) with ChS indicates the dominance of electrostatic interactions in facilitating multilayer formation between BA-PAA)s and ChS. Consequently, these films were only found to be slightly responsive to glucose at the elevated concentration of 100 mM.

All of the films were responsive to various concentrations of glutathione and DTT, owing to the presence of disulfide bonds in the BA-PAA) polymer main chain. Interestingly, for ChS-based films lower concentration of DTT was found to degrade the films much faster than glutathione at four times higher concentration. This trend, which was notably reversed for the PVA-based films, was possibly attributed to the extra negative charge on glutathione which might impede its diffusion in the thicker ChS films.

PVA-based films were found to be highly responsive to changes in pH with faster dissolution of the multilayers at lower pH. Typically, at pH 4 complete dissolution was achieved in 3 min. This high responsiveness was attributed to the boronate ester formation which is known to be sensitive to pH. As the ester formation is not favored at acidic pH, the multilayer cannot maintain integrity and thus disassembles into solution. ChS-based films were also responsive to acidic pH but displaying much slower kinetics, and with a more complicated trend, i.e. the disassembly rate was higher at pH 6 than at pH 4, albeit displaying the highest stability at pH 7.4. This trend was most likely due to the change of ionization state of the protonable amines of BA-PAA)s and the carboxylic acid groups of the ChS in the pH range of 4-6. At pH 4, the higher amount of positive charges of BA-PAA)s superseded the lowering of negative charges of ChS causing overall higher stability at pH 4 than at pH 6 where the less positive charges of BA-PAA)s possibly could not make up for the still reduced amount of negative charges of ChS. The highest stability observed at pH 7.4 was probably promoted by the fact that the films were incubated in the same solution in which multilayer formation was carried out, causing less possibility of osmotic swelling and destabilization.

All of the films were found to be relatively biocompatible, with no significant cytotoxicity effect observed upon culturing COS-7 cells on top of the multilayers. ChS-based films notably provided cell morphology identical to tissue culture-treated PS. On PVA-based films, cells were found to attach well, but were found to slightly aggregate upon longer culture period, although no significant loss of viability was observed through both live/dead staining and metabolic activity assay.

The present study indicates the possibility of using the multilayers for biomedical applications, such as to provide drug releasing surfaces on stents and other implants. For PVA-based films, the presence of the diol-repeating units in PVA can be utilized to incorporate small boronic acid-containing drugs into the films and provide release

that is triggered by reducing agents, glucose, or acidic pH. For ChS-based films, in which part or the majority of the BA moieties of BA-PAA are available for ester formation with guest molecules, the films can be exploited to incorporate diol-containing small molecules such as dopamine and provide its release through the triggers of reducing agents, and acidic pH. These two approaches are presented in the following two chapters.

5.5 REFERENCES

- [1] J.N. Cambre, B.S. Sumerlin, Biomedical applications of boronic acid polymers, *Polymer*, 52 (2011) 4631-4643.
- [2] R. Ma, L. Shi, Phenylboronic acid-based glucose-responsive polymeric nanoparticles: synthesis and applications in drug delivery, *Polymer Chemistry*, 5 (2014) 1503-1518.
- [3] E. Galbraith, A.M. Kelly, J.S. Fossey, G. Kociok-Kohn, M.G. Davidson, S.D. Bull, T.D. James, Dynamic covalent self-assembled macrocycles prepared from 2-formyl-aryl-boronic acids and 1,2-amino alcohols, *New J. Chem.*, 33 (2009) 181-185.
- [4] D.G. Hall, Structure, Properties, and Preparation of Boronic Acid Derivatives. Overview of Their Reactions and Applications, in: *Boronic Acids*, Wiley-VCH Verlag GmbH & Co. KGaA, 2006, pp. 1-99.
- [5] H. Fang, G. Kaur, B.H. Wang, Progress in boronic acid-based fluorescent glucose sensors, *J. Fluoresc.*, 14 (2004) 481-489.
- [6] C. Zhang, M.D. Losego, P.V. Braun, Hydrogel-Based Glucose Sensors: Effects of Phenylboronic Acid Chemical Structure on Response, *Chem Mater*, 25 (2013) 3239-3250.
- [7] M.B. Lerner, N. Kybert, R. Mendoza, R. Villechenon, M.A.B. Lopez, A.T.C. Johnson, Scalable, non-invasive glucose sensor based on boronic acid functionalized carbon nanotube transistors, *Appl. Phys. Lett.*, 102 (2013).
- [8] M. Ikeda, K. Fukuda, T. Tanida, T. Yoshii, I. Hamachi, A supramolecular hydrogel containing boronic acid-appended receptor for fluorocolorimetric sensing of polyols with a paper platform, *Chem. Commun.*, 48 (2012) 2716-2718.
- [9] H. Shibata, Y.J. Heo, T. Okitsu, Y. Matsunaga, T. Kawanishi, S. Takeuchi, Injectable hydrogel microbeads for fluorescence-based in vivo continuous glucose monitoring, *Proceedings of the National Academy of Sciences of the United States of America*, 107 (2010) 17894-17898.
- [10] B. Elmas, M.A. Onur, S. Senel, A. Tuncel, Temperature controlled RNA isolation by N-isopropylacrylamide-vinylphenyl boronic acid copolymer latex, *Colloid. Polym. Sci.*, 280 (2002) 1137-1146.
- [11] X. Wang, N. Xia, L. Liu, Boronic Acid-Based Approach for Separation and Immobilization of Glycoproteins and Its Application in Sensing, *International Journal of Molecular Sciences*, 14 (2013) 20890-20912.
- [12] S. Zhang, X. He, L. Chen, Y. Zhang, Boronic acid functionalized magnetic nanoparticles via thiol-ene click chemistry for selective enrichment of glycoproteins, *New J. Chem.*, (2014).
- [13] M. Piest, X. Zhang, J. Trinidad, J.F.J. Engbersen, pH-responsive, dynamically restructuring hydrogels formed by reversible crosslinking of PVA with phenylboronic acid functionalised PPO-PEO-PPO spacers (Jeffamines[registered sign]), *Soft Matter*, 7 (2011) 11111-11118.
- [14] Y. Guan, Y. Zhang, Boronic acid-containing hydrogels: synthesis and their applications, *Chem. Soc. Rev.*, 42 (2013) 8106-8121.
- [15] Z. Tang, Y. Guan, Y. Zhang, Contraction-type glucose-sensitive microgel functionalized with a 2-substituted phenylboronic acid ligand, *Polymer Chemistry*, 5 (2014) 1782-1790.
- [16] M. Piest, M. Ankoné, J.F.J. Engbersen, Carbohydrate-interactive pDNA and siRNA gene vectors based on boronic acid functionalized poly(amido amine)s, *J Control Release*, 169 (2013) 266-275.
- [17] X. Zhang, S. Lu, C. Gao, C. Chen, X. Zhang, M. Liu, Highly stable and degradable multifunctional microgel for self-regulated insulin delivery under physiological conditions, *Nanoscale*, 5 (2013) 6498-6506.
- [18] Y. Zhao, B.G. Trewyn, I.I. Slowing, V.S.Y. Lin, Mesoporous Silica Nanoparticle-Based Double Drug Delivery System for Glucose-Responsive Controlled Release of Insulin and Cyclic AMP, *J. Am. Chem. Soc.*, 131 (2009) 8398-8400.
- [19] R.N. Jain, X. Huang, S. Das, R. Silva, V. Ivanova, T. Minko, T. Asefa, Functionalized Mesoporous Silica Nanoparticles for Glucose- and pH-Stimulated Release of Insulin, *Z. Anorg. Allg. Chem.*, 640 (2014) 616-623.
- [20] Z. Gu, T.T. Dang, M. Ma, B.C. Tang, H. Cheng, S. Jiang, Y. Dong, Y. Zhang, D.G. Anderson, Glucose-Responsive Microgels Integrated with Enzyme Nanocapsules for Closed-Loop Insulin Delivery, *Acs Nano*, 7 (2013) 6758-6766.
- [21] H. Han, M.E. Davis, Targeted Nanoparticles Assembled via Complexation of Boronic-Acid-Containing Targeting Moieties to Diol-Containing Polymers, *Bioconjugate Chem.*, 24 (2013) 669-677.
- [22] Y. Abo-zeid, W. Irving, B. Thomson, G. Mantovani, M. Garnett, P19: Ribavirin-boronic acid loaded nanoparticles: a possible route to improve hepatitis C treatment, *Journal of Viral Hepatitis*, 20 (2013) 26-27.
- [23] L. Li, Z. Bai, P.A. Levkin, Boronate-dextran: An acid-responsive biodegradable polymer for drug delivery, *Biomaterials*, 34 (2013) 8504-8510.

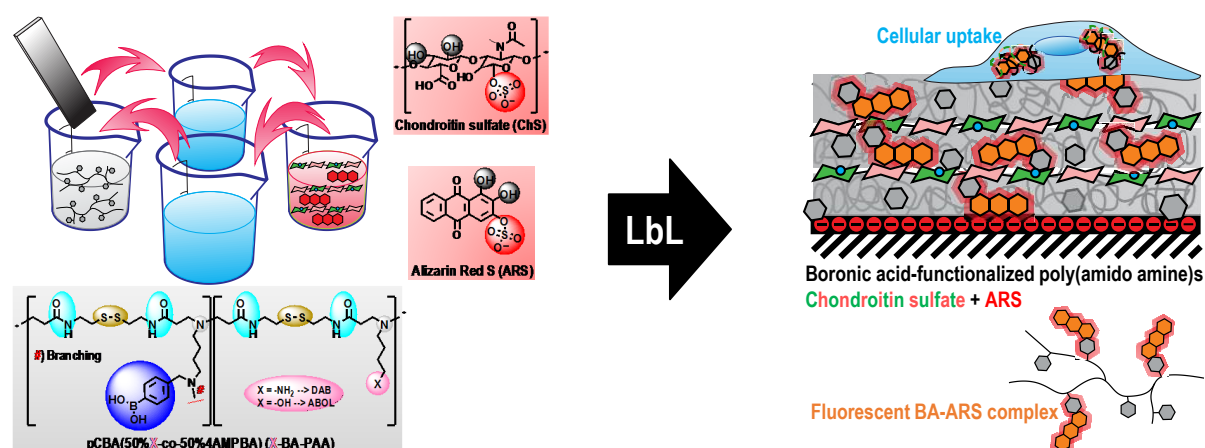
- [24] T.M. Bradke, C. Hall, S.W. Carper, G.E. Plopper, Phenylboronic acid selectively inhibits human prostate and breast cancer cell migration and decreases viability, *Cell Adhesion & Migration*, 2 (2008) 153-160.
- [25] Z. Ding, Y. Guan, Y. Zhang, X.X. Zhu, Synthesis of glucose-sensitive self-assembled films and their application in controlled drug delivery, *Polymer*, 50 (2009) 4205-4211.
- [26] Z. Ding, Y. Guan, Y. Zhang, X.X. Zhu, Layer-by-layer multilayer films linked with reversible boronate ester bonds with glucose-sensitivity under physiological conditions, *Soft Matter*, 5 (2009) 2302-2309.
- [27] R. Watahiki, K. Sato, K. Suwa, S. Niina, Y. Egawa, T. Seki, J.-i. Anzai, Multilayer films composed of phenylboronic acid-modified dendrimers sensitive to glucose under physiological conditions, *Journal of Materials Chemistry B*, (2014).
- [28] Y. Ma, L. Qian, H. Huang, X. Yang, Buildup of gold nanoparticle multilayer thin films based on the covalent-bonding interaction between boronic acids and polyols, *J. Colloid Interface Sci.*, 295 (2006) 583-588.
- [29] F. Martello, M. Piest, J.F.J. Engbersen, P. Ferruti, Effects of branched or linear architecture of bioreducible poly(amido amine)s on their in vitro gene delivery properties, *J Control Release*, 164 (2012) 372-379.
- [30] J. Dennig, Gene transfer in eukaryotic cells using activated dendrimers, *Top. Curr. Chem.*, 228 (2003) 227-236.
- [31] M.H. Alves, B.E.B. Jensen, A.A.A. Smith, A.N. Zelikin, Poly(Vinyl Alcohol) Physical Hydrogels: New Vista on a Long Serving Biomaterial, *Macromol. Biosci.*, 11 (2011) 1293-1313.
- [32] C.M. Hassan, N.A. Peppas, Structure and applications of poly(vinyl alcohol) hydrogels produced by conventional crosslinking or by freezing/thawing methods, in: A. Abe (Ed.) *Biopolymers/Pva Hydrogels/Anionic Polymerisation Nanocomposites*, Springer-Verlag Berlin, Berlin, 2000, pp. 37-65.
- [33] T. Mikami, H. Kitagawa, Biosynthesis and function of chondroitin sulfate, *Biochim. Biophys. Acta-Gen. Subj.*, 1830 (2013) 4719-4733.
- [34] J.M. Erickson, T.M. Messer, Glucosamine and Chondroitin Sulfate Treatment of Hand Osteoarthritis, *J. Hand Surg.-Am. Vol.*, 38A (2013) 1638-1640.
- [35] C. Bottegoni, R.A.A. Muzzarelli, F. Giovannini, A. Busilacchi, A. Gigante, Oral chondroprotection with nutraceuticals made of chondroitin sulphate plus glucosamine sulphate in osteoarthritis, *Carbohydr. Polym.*, 109 (2014) 126-138.
- [36] A. Zintchenko, L.J. van der Aa, J.F. Engbersen, Improved synthesis strategy of poly(amidoamine)s for biomedical applications: catalysis by "green" biocompatible earth alkaline metal salts, *Macromol. Rapid Commun.*, 32 (2011) 321-325.
- [37] K.L. Wooley, C.J. Hawker, R. Lee, J.M.J. Frechet, One-Step Synthesis of Hyperbranched Polyesters. *Molecular Weight Control and Chain End Functionalization*, *Polym. J.*, 26 (1994) 187-197.
- [38] T.T. Jiang, G.H. Jiang, X.H. Wang, Y. Dong, Z. Wei, X. Li, B.L. Tang, Facile one-pot synthesis of fluorescent hyperbranched polymers for optical detection of glucose, *Des. Monomers Polym.*, 17 (2014) 576-581.
- [39] H. Lee, R. Mensire, R.E. Cohen, M.F. Rubner, Strategies for Hydrogen Bonding Based Layer-by-Layer Assembly of Poly(vinyl alcohol) with Weak Polyacids, *Macromolecules*, 45 (2011) 347-355.
- [40] M.A. Rodríguez-Carvajal, A. Imberty, S. Pérez, Conformational behavior of chondroitin and chondroitin sulfate in relation to their physical properties as inferred by molecular modeling, *Biopolymers*, 69 (2003) 15-28.
- [41] J. Choi, M.F. Rubner, Influence of the Degree of Ionization on Weak Polyelectrolyte Multilayer Assembly, *Macromolecules*, 38 (2004) 116-124.
- [42] B. Schoeler, G. Kumaraswamy, F. Caruso, Investigation of the Influence of Polyelectrolyte Charge Density on the Growth of Multilayer Thin Films Prepared by the Layer-by-Layer Technique, *Macromolecules*, 35 (2001) 889-897.
- [43] C. Peng, Y.S. Thio, R.A. Gerhardt, Effect of Precursor-Layer Surface Charge on the Layer-by-Layer Assembly of Polyelectrolyte/Nanoparticle Multilayers, *Langmuir*, 28 (2011) 84-91.
- [44] J. Jeon, V. Panchagnula, J. Pan, A.V. Dobrynin, Molecular Dynamics Simulations of Multilayer Films of Polyelectrolytes and Nanoparticles, *Langmuir*, 22 (2006) 4629-4637.
- [45] S.S. Ono, G. Decher, Preparation of Ultrathin Self-Standing Polyelectrolyte Multilayer Membranes at Physiological Conditions Using pH-Responsive Film Segments as Sacrificial Layers, *Nano Lett.*, 6 (2006) 592-598.
- [46] O. Mermut, C.J. Barrett, Effects of Charge Density and Counterions on the Assembly of Polyelectrolyte Multilayers, *The Journal of Physical Chemistry B*, 107 (2003) 2525-2530.
- [47] T. Serizawa, S. Kamimura, N. Kawanishi, M. Akashi, Layer-by-Layer Assembly of Poly(vinyl alcohol) and Hydrophobic Polymers Based on Their Physical Adsorption on Surfaces, *Langmuir*, 18 (2002) 8381-8385.
- [48] D. Wiegel, J. Kaufmann, K. Arnold, Polar interactions of chondroitinsulfate: Surface free energy and molecular dynamics simulations, *Colloids and Surfaces B: Biointerfaces*, 13 (1999) 143-156.
- [49] R.J. Gonzalez-Paz, G. Lligadas, J.C. Ronda, M. Galia, A.M. Ferreira, F. Boccafocchi, G. Ciardelli, V. Cadiz, Enhancement of Fatty Acid-based Polyurethanes Cytocompatibility by Non-covalent Anchoring of Chondroitin Sulfate, *Macromol. Biosci.*, 12 (2012) 1697-1705.
- [50] G.Y. Wu, Y.Z. Fang, S. Yang, J.R. Lupton, N.D. Turner, Glutathione metabolism and its implications for health, *Journal of Nutrition*, 134 (2004) 489-492.
- [51] C. Lin, J.F.J. Engbersen, The role of the disulfide group in disulfide-based polymeric gene carriers, *Expert Opinion on Drug Delivery*, 6 (2009) 421-439.
- [52] G. Springsteen, B. Wang, A detailed examination of boronic acid-diol complexation, *Tetrahedron*, 58 (2002) 5291-5300.
- [53] B. Wang, Z. Liu, Y. Xu, Y. Li, T. An, Z. Su, B. Peng, Y. Lin, Q. Wang, Construction of glycoprotein multilayers using the layer-by-layer assembly technique, *J. Mater. Chem.*, 22 (2012) 17954-17960.

- [54] T. Yang, R. Ji, X.-X. Deng, F.-S. Du, Z.-C. Li, Glucose-responsive hydrogels based on dynamic covalent chemistry and inclusion complexation, *Soft Matter*, 10 (2014) 2671-2678.
- [55] V. Lapeyre, C. Ancla, B. Catargi, V. Ravaine, Glucose-responsive microgels with a core-shell structure, *J. Colloid Interface Sci.*, 327 (2008) 316-323.
- [56] D. Roy, J.N. Cambre, B.S. Sumerlin, Sugar-responsive block copolymers by direct RAFT polymerization of unprotected boronic acid monomers, *Chem. Commun.*, (2008) 2477-2479.
- [57] B. Wang, R. Ma, G. Liu, Y. Li, X. Liu, Y. An, L. Shi, Glucose-Responsive Micelles from Self-Assembly of Poly(ethylene glycol)-b-Poly(acrylic acid-co-acrylamidophenylboronic acid) and the Controlled Release of Insulin, *Langmuir*, 25 (2009) 12522-12528.
- [58] J.N. Cambre, D. Roy, B.S. Sumerlin, Tuning the sugar-response of boronic acid block copolymers, *J. Polym. Sci., Part A: Polym. Chem.*, 50 (2012) 3373-3382.
- [59] M. Yamaguchi, T. Shinbo, T. Kanamori, P.-c. Wang, M. Niwa, H. Kawakami, S. Nagaoka, K. Hirakawa, M. Kamiya, Surface modification of poly(l-lactic acid) affects initial cell attachment, cell morphology, and cell growth, *J Artif Organs*, 7 (2004) 187-193.
- [60] Z. Ding, J. Chen, S. Gao, J. Chang, J. Zhang, E.T. Kang, Immobilization of chitosan onto poly-l-lactic acid film surface by plasma graft polymerization to control the morphology of fibroblast and liver cells, *Biomaterials*, 25 (2004) 1059-1067.
- [61] C.C. DeMerlis, D.R. Schoneker, Review of the oral toxicity of polyvinyl alcohol (PVA), *Food Chem. Toxicol.*, 41 (2003) 319-326.

CHAPTER 6

Multilayered Thin Films from Boronic Acid-Functionalized Poly(amido amine)s and Chondroitin Sulfate as Drug-Releasing Surfaces**

ABSTRACT



Multilayered surfaces from randomly branched boronic acid-functionalized poly(amido amine)s (BA-PAA)s containing either primary amine (DAB-BA-PAA) or primary alcohol (ABOL-BA-PAA) side groups were prepared through the dip-coating layer-by-layer technique. The BA-PAAs were paired with chondroitin sulfate (ChS) and the catechol compound alizarin red S (ARS), with which BA-moieties reversibly form boronate esters with a specific λ_{\max} (470 nm) and fluorescent characteristics. Build-up of the multilayers and the presence of ARS-boronate esters were followed with UV-Vis spectrophotometry of the films in the dry state. ABOL-BA-PAA multilayers contained higher ARS content than DAB-BA-PAA multilayers at the same number of bilayers. The films were found to be highly responsive to acidic pH, causing faster ARS release at lower pH of 6, 5, and 4, and a shift in λ_{\max} from 470 to 419 nm. At physiological pH, fast initial release of up to ~40% of the ARS content was observed during the first 12 h of incubation, followed by a much slower and gradual release of ARS. Simultaneously, the λ_{\max} of the films shifted to ~510 nm, being the λ_{\max} of free ARS at pH 7.4. The phenomenon is discussed in relation to the dynamic nature of boronate ester formation, and the possible low diffusion coefficient of ARS inside the multilayers. The multilayers were also responsive to glutathione due to presence of disulfide bonds in the BA-PAA main chain and resulted in faster ARS release. The multilayers were only slightly responsive to glucose at 25 and 100 mM, which was attributed to the lower binding affinity of BA towards glucose as compared to ARS. To test the drug delivery capacity of the multilayers, COS-7 cells were cultured on top of multilayer-coated well plates *in vitro*. The cellular uptake of the fluorescent ARS-boronate ester was followed through flow cytometry, where a maximum cellular uptake of up to 30% was observed, after a culture duration of 6 h for both films. Cells cultured on ABOL-BA-PAA multilayers maintained cellular uptake of fluorescent ARS-boronate ester for at least another 6 h before declining, while for DAB-BA-PAA multilayers, the uptake decreased after the first 6 h. The more sustained cellular uptake of ABOL-BA-PAA multilayers was explained as an effect of higher initial ARS content, stronger ARS-boronate ester, and more efficient cellular uptake through the possible release of complexes containing ARS-boronate esters. Finally, confocal microscopy confirmed the presence of ARS-boronate ester-containing particles in the nuclei of cells. The multilayered surfaces presented in this study show promise as a drug-releasing delivery surface for coating stents, prostheses, and other implants.

** Sry D. Hujaya, Karin Roelofs, Jos M.J. Paulusse, Johan F.J. Engbersen, submitted for publication.

6.1 INTRODUCTION

The coating of the surface of materials for biomedical applications with multilayered thin films offers the possibility of providing to these materials a delivery system that is controllable in both the amount of loading and release of bioactive compounds. The amount of incorporated drug can be tuned by the number of layers in the film, which can avoid side effects and wasting of expensive drugs. Release profile and responsiveness can be altered by careful choice of appropriate macromolecules as main multilayer components. Moreover, highly localized delivery of the incorporated drug can be achieved, which may be beneficial for applications such as providing anti-inflammatory or anti-thrombotic properties to the surface of an implant.

Unlike hydrogel systems, where small molecules can be easily incorporated by simply dissolving the compound of interest in the hydrogel-forming solutions, incorporating small molecules via the layer-by-layer (LbL) alternate dipping technique requires that the molecule has strong enough association to at least one of the macromolecules forming the layers to shift the equilibrium away from the entropically more stable dissociated state and to prevent rapid diffusive release from the films. This requirement cannot be easily met, and is particularly difficult to achieve by only electrostatic interactions. Therefore, several techniques are commonly utilized, as reviewed by Pavlukhina and Sukhishvili [1], such as using drug crystals as the substrate for multilayer build-up [2, 3], interlayer crosslinking [4], pre-encapsulation of the drug molecules into micelles or particles [5], linking the drug molecules to one of the macromolecules either covalently (i.e. in a pro-drug approach) [6] or through the use of host-guest interaction [7], and other more specific complexation/interaction mechanisms [8].

An interesting alternative possibility for biologically active molecules possessing a vicinal diol functionality is the utilization of reversible binding of this diol group to boronic acids. The functional boronic acid (BA) moiety has received a lot of attention in the biomedical field, especially in the development of sensor, due to its ability to selectively form dynamic coordinative covalent esters with various diol-containing species such as glucose [9]. In responsive drug delivery applications, the dynamic nature of boronate ester formation has been used to provide glucose responsiveness for treatment of diabetes, obesity, cancer and HIV [10], and to provide binding to the saccharides at the surface of mammalian cells [11, 12]. More interestingly, in hydrogel systems this dynamic covalent interaction provides the hydrogels with the ability to self-heal and adopt the specific shape of containers or cavities, a desirable property for wound-dressing and topical applications [13, 14].

Parallel to the increasing interest in boronate ester formation, ARS has emerged as one of the widely used reporter molecules to analytically determine the binding constants of BA moieties to diols under various relevant conditions [15, 16]. This practice is attributed to the particular fluorescence properties of ARS upon ester formation with a BA moiety under physiologically relevant conditions. Structurally, the anthraquinone derivative ARS contains a catechol moiety responsible for the strong binding with BA. ARS can therefore be seen as a model for catechol-containing drugs such as dopamine, epinephrine/adrenaline, and many others with main pharmacological applications in the nervous system (treatment of Parkinson's, schizophrenia, attention deficit hyperactivity disorder (ADHD)), lung diseases (asthma, chronic obstructive pulmonary disease (COPD)), and heart diseases (cardiac arrest, anaphylaxis, hypertension) [17]. The characteristic fluorescence properties of the ARS-boronate ester may also assist in the characterization of loading, release, responsiveness and/or competitiveness with other diol species, and even for additional imaging purposes [12].

Previously, we reported the preparation and properties of multilayered systems prepared from boronic acid-containing poly(amido amine)s (BA-PAA) and chondroitin sulfate (ChS) (Chapter 5). Multilayer build-up of these films proceeds through electrostatic interactions, mainly through the positively-charged BA-PAA polymer chains and the negatively-charged sulfate-containing ChS. Though possible, boronate ester formation is not observed at a functional level for biomedical applications, i.e. the binding between the BA-moieties in the BA-PAA polymer and the diol groups in ChS is so weak that the BA-moieties are largely present in their boronic acid state. This

Chapter describes a study to utilize the BA-moieties in multilayered BA-PAA films for reversible drug binding and triggered release, using ARS as the model drug molecule.

6.2 MATERIALS AND METHODS

Chondroitin 4-sulfate sodium salt from bovine trachea (ChS, $\leq 10\%$ water), alizarin red S (ARS), glucose ($\geq 99.5\%$), glutathione ($\geq 98.0\%$), sulfuric acid (H_2SO_4 , 95-98%), and hydrogen peroxide (H_2O_2 , 30 wt% in H_2O) were purchased from Sigma-Aldrich (Zwijndrecht, The Netherlands). Sodium dihydrogen phosphate monohydrate ($\text{NaH}_2\text{PO}_4 \cdot \text{H}_2\text{O}$, 99.0-102.0%), disodium hydrogen phosphate dihydrate ($\text{Na}_2\text{HPO}_4 \cdot 2\text{H}_2\text{O}$, 99.5%), citric acid ($\geq 99\%$), and trisodium citrate dihydrate ($\geq 99\%$) were purchased from Merck (Darmstadt, Germany). Solvents were of reagent grade and used without further purification unless otherwise noted. Milli-Q water (18.2 M Ω -cm at 25 °C) was obtained from a Synergy® water purification system (Millipore).

DAB-BA-PAA and ABOL-BA-PAA were synthesized as described previously in Chapter 5.

PBS buffer was prepared by dissolving 1.54 g of $\text{Na}_2\text{HPO}_4 \cdot 2\text{H}_2\text{O}$, 0.3 g of $\text{NaH}_2\text{PO}_4 \cdot \text{H}_2\text{O}$, and 8.2 g of NaCl into 1.0 L of Milli-Q water and adjusting the pH to 7.4.

Citrate buffered saline (CBS buffer) pH 4, 5, and 6 were prepared by dissolving citric acid, trisodium citrate dihydrate and NaCl in the appropriate amounts in Milli-Q and adjusting the pH with HCl or NaOH.

UV characterization of multilayers was performed in the dry state using a UV-2401 PC (Shimadzu, 's-Hertogenbosch, The Netherlands) UV spectrophotometer. Each film fabricated on UV-transparent 7.5 x 37 x 1 mm quartz glass (Ted Pella, Redding, USA) was measured in three different arbitrary positions. Absorbance scan was carried out in the 200-700 nm wavelength range. All data points were then corrected for baseline offset by subtracting the absorbance value at 400 nm from each data point. Relative absorbance values were obtained by normalizing each data point with the respective value at time 0.

Poly-D-lysine-coated 96-well plates (PDL-TCPS) for multilayer build-up for cell culture and transfection experiments were purchased from Greiner (Alphen aan den Rijn, The Netherlands).

COS-7 cells (European Collection of Animal Cell Cultures (ECACC) Catalogue No. 87021302) were grown in DMEM containing 4.5 g/L glucose and GlutaMAX™ (Invitrogen, Breda, The Netherlands) supplemented with 2% (v/v) PennStrepp (Lonza, Breda, The Netherlands) and 10% (v/v) fetal bovine serum (Lonza, Breda, The Netherlands).

Fluorescence microscopy was performed at 4X, 10X, 20X, and/or 40X objectives using EVOS digital inverted microscope (EMS, Wageningen, The Netherlands).

Confocal microscopy was performed on an LSM 510 (Carl Zeiss, Sliedrecht, The Netherlands) using the Zen 2009 software.

Fluorescence-activated cell sorting (FACS) was carried out in a Becton-Dickinson FACSCalibur (Breda, The Netherlands).

6.2.1 MULTILAYERED THIN FILM CONSTRUCTION AND BUILD-UP PROFILES

Fresh BA-PAA solutions were prepared shortly before the start of multilayer build-up from the solid materials, which had been re-lyophilized overnight to avoid weighing errors due to their hygroscopic properties. All BA-PAA solutions (2.0 mg/mL) were prepared in PBS buffer at pH 7.4 to avoid possible variations in pH.

Prior to the assembly, quartz substrates (7.5 x 32 mm) were etched for 30 minutes in piranha acid to activate the surface, rinsed with copious amounts of Milli-Q water, and dried under N_2 stream. These substrates were then dipped into DAB-BA-PAA or ABOL-BA-PAA solution (2.0 mg/mL in PBS buffer pH 7.4) for 5 min, transferred into washing solution containing PBS buffer for 1 min, dipped briefly in a large amount of Milli-Q water, transferred into

ChS+ARS (2.0 mg/mL ChS and 1.0 mM ARS in Milli-Q water) solution for 5 min, dipped into the second washing solution containing Milli-Q water for 1 min, and finally followed by another brief dipping in Milli-Q. This cycle was repeated to reach the desired number of bilayer. Drying under N₂ stream was performed after every BA-PAA layer deposition, excluding the very first layer. The resulting ensemble is denoted by BA-PAA-(ChS+ARS#BA-PAA)_n, where BA-PAA represents either DAB-BA-PAA or ABOL-BA-PAA and n represents the number of bilayer. The first BA-PAA layer is regarded as a precursor layer and therefore excluded from the bilayer number count. Typically, the ensemble consists of 5 or 10 bilayers with the poly(amido amine) polymer as the last layer. For every multilayered system, three samples were fabricated in parallel to give estimation for standard deviation. To study the build-up profiles, UV spectra were recorded after each drying step following BA-PAA layer formation throughout the 200-700 nm range. Every absorbance values were then corrected for baseline shift at 700 nm. Afterwards, the multilayers were dipped into ChS+ARS solution to continue multilayer build-up.

Multilayers for cell culture were fabricated directly in the wells of poly-D-lysine-coated 96-well plates (PDL-TCPS, Greiner) by alternately dispensing deposition (70 μL) and washing (2x 100 μL) solutions under sterile conditions inside the laminar flow hood (LFH). Deposition started with ChS+ARS (2.0 mg/mL ChS and 1.0 mM ARS in Milli-Q water, 30 min for the first layer, 5 min next) as the first layer to a total of 10 bilayers ending with the BA-PAA layer. No intermediate drying steps were applied. At the end of the fabrication process, the plates were left inside the LFH briefly to dry the films. Coated plates were kept at 4 °C and used as soon as possible (typically overnight). These multilayered samples are designated as PDL-(ChS+ARS#BA-PAA)₁₀ to indicate the presence of a PDL layer as a precursor layer. Compared to multilayers built on quartz and silicon wafer substrates, these systems substitute the first BA-PAA layer with PDL layer inherent to the well plate surface.

6.2.2 ARS RELEASE UNDER PHYSIOLOGICAL CONDITIONS AND AT ACIDIC PH

ARS release profiles of the three multilayered systems in PBS buffer pH 7.4 at 37 °C were investigated by dipping the thin films formed on quartz slides in 2 mL of PBS buffer pH 7.4 solution and incubating them in a water bath with temperature set to 37 °C. At regular intervals, the samples were removed, briefly dipped in a large amount of Milli-Q water, dried under N₂ stream and measured by UV-Vis spectrophotometer. The release study at acidic pH (pH 4, 5, and 6) was carried out in a similar fashion, but using citrate buffered saline (CBS) instead of PBS.

6.2.3 ARS RELEASE UNDER VARIOUS REDUCTIVE CONDITIONS

Degradability of the multilayered systems was investigated in a similar way as for the investigation of their respective stability profiles under physiological conditions (Section 6.2.2), but in the presence of 0.4 mM or 10 mM glutathione in the incubation medium. Solutions containing glutathione in PBS buffer at pH 7.4 were prepared fresh directly prior to the start of experiment. Due to instability of glutathione in PBS buffer at pH 7.4, no solution of more than three hours old was used.

6.2.4 ARS RELEASE IN THE PRESENCE OF GLUCOSE

The influence of glucose concentration on ARS release profile was investigated as described in Section 6.2.2 and 6.2.3, but in the presence of 25 mM and 100 mM of glucose. The 25 mM concentration is used to mimic the glucose concentration in cell culture medium. This concentration is roughly 2.5 times the minimal blood glucose level in diabetic patients [18].

6.2.5 PARTICLE UPTAKE BY COS-7 CELLS: FACS

To investigate the possibility of COS-7 cells taking up ARS-boronate ester from the multilayer surface, cells were seeded directly on multilayer-coated wells at 20,000 cells/well in complete medium with serum and left to proliferate at 37 °C under humidified atmosphere with 5% CO₂.

After 0, 3, 6, 12, 24, and 48 h, cells were trypsinized, centrifuged (5 min, 600 g), and analyzed by FACS. Cells were also cultured for 12 h on regular polystyrene (PS) culture plates with and without the addition of free ARS and on multilayered films without ARS as controls to determine live cell population and fluorescence-positive cell population markers. On some multilayered samples treated similarly but without addition of cells, physical force was applied to break down the films into the cell culture medium. The resulting suspension was also analyzed through FACS to locate multilayer remnant population and identify their relative fluorescence intensity.

Excitation of ARS-boronate ester was performed at 488 nm and emission was detected via a 585 nm band-pass filter. At least 20,000 – 30,000 total events were measured to reach 10,000 events for gated living cells. Data analysis was performed using the FACS Cellquest Software. The gate setting was equal for all samples within the same experiment. Dot plots were applied to separate living cells population from dead cells and film residues and particles. From the histogram obtained, markers were drawn to identify cells as live positive cells or live negative cells.

6.2.6 PARTICLE UPTAKE BY COS-7 CELLS: CONFOCAL MICROSCOPY

Samples for confocal microscopy were prepared by culturing cells as described in Section 6.2.4. Following 24 h of culture, cells were trypsinized and recultured inside a cover glass slide imaging chamber (General Electric Healthcare, Eindhoven, The Netherlands) for 6 h to allow the cells to attach. The cells were then washed with PBS, fixed with 3.7% paraformaldehyde for 15 min at RT, washed 3 times with PBS, and stained with Hoechst 33258 (2 μ L/mL in PBS) for 15 min at RT. Samples were then washed 3 times with PBS and mounted on a clean microscope glass slide using aqueous mounting medium (Ibidi, Munich, Germany) and sealed with nail polish.

Confocal microscopy was performed on an LSM 510 (Carl Zeiss, Sliedrecht, The Netherlands) using Zen 2009 software. Both fluorophores (BA-ARS and Hoechst 33258) were excited using a 543 nm argon laser passed through HFT KP 700/S43 and split through an NFT 490. BA-ARS fluorescence was analyzed past a BP 565-615 IR filter and Hoechst 33258 excitation was analyzed past a BP 390-465 IR filter. Z-stack sectioning was performed over 20 slices throughout the 33.75 μ m height range.

6.3 RESULTS AND DISCUSSION

6.3.1 MULTILAYERED THIN FILM BUILD-UP

We have reported previously the syntheses of two randomly branched boronic acid (BA)-functionalized poly(amido amine)s (BA-PAA)s (Chapter 5). The degrees of BA functionalization of the two BA-PAA)s were similar at ~50%, with branching estimated to be ~10 and ~30% for DAB-BA-PAA and ABOL-BA-PAA, respectively, and number average molecular weight of 12 and 14 kg/mol, respectively. Chemical structures of the two polymers, chondroitin sulfate (ChS), and ARS utilized in this study are presented in Chart 6.1.

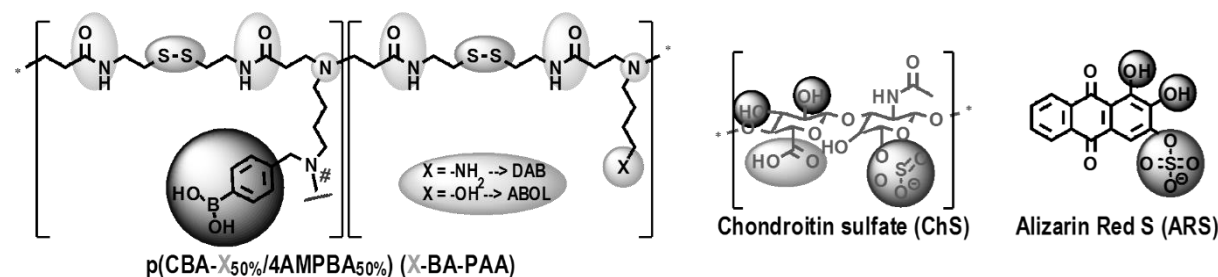


Chart 6.1 Chemical structures of DAB-BA-PAA, ABOL-BA-PAA, ChS, and ARS.

We investigated the incorporation of ARS via post-loading (i.e. building BA-PAA-(ChS#BA-PAA)_n followed by incubation in ARS solution) and parallel loading (i.e. building BA-PAA-(ChS+ARS#BA-PAA)_n directly with ARS in the ChS deposition solution). Upon comparing the two methods, post-loading gave less reproducible results (data not shown), while the parallel loading provides better possibility to achieve a more homogeneous distribution of ARS throughout the entire multilayered constructs. Parallel loading also facilitates incorporation of increased amounts of ARS as compared to the post loading method. In the post-loading method, a total of 1 h incubation of DAB-BA-PAA(ChS#DAB-BA-PAA)₁₀ in 1.0 mM of ARS solution in Milli-Q yielded ~40% less ARS (which did not improve with longer incubation times), than what was achieved via parallel loading, most likely due to the expectedly lower diffusion coefficient of ARS in the inner parts of the multilayered constructs. Due to these reasons, the parallel loading method was chosen to incorporate ARS into the multilayered systems of BA-PAA)s and ChS. ARS was mixed in the ChS deposition solution in water since both ARS and ChS have better solubility in water as opposed to PBS. Dissolution of BA-PAA)s in PBS at pH 7.4, however, facilitates enhanced ARS-boronate ester formation and electrostatic interactions between the ChS and BA-PAA)s, both of which are maximal at neutral pH.

Figure 6.1 shows build-up profiles of DAB-BA-PAA-(ChS+ARS#DAB-BA-PAA)₁₀ and ABOL-BA-PAA-(ChS+ARS#ABOL-BA-PAA)₁₀ based on increases in absorbance at 470 nm. Previously, the build-up of ARS-free multilayers was investigated (Chapter 5). Incorporation of ARS (i.e. a dark red-colored molecule) drastically changes the spectral properties of the films which makes it not possible to relate the UV spectra of these films with previous films without ARS. As the ARS is the model drug of interest for the investigation of both loading and release, and no multilayer build-up was observed in the absence of ChS, it was deemed appropriate to study the film behavior based on the UV-absorption of the ARS content. The opaque nature of the films is very reminiscent of the non-ARS system (Chapter 5), indicating that ChS still makes up the majority of the material in the multilayered system, providing thick films.

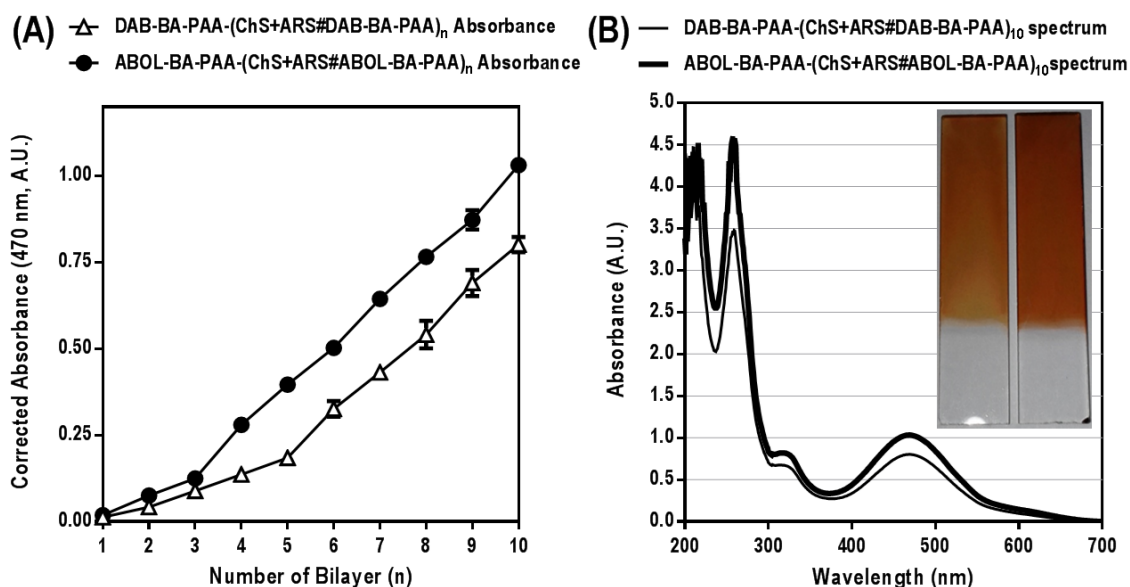


Figure 6.1 (A) UV-Absorption-based build-up profiles and (B) UV spectra of DAB-BA-PAA-(ChS+ARS#DAB-BA-PAA)_n and ABOL-BA-PAA-(ChS+ARS#ABOL-BA-PAA)_n in the dry state of the film. Absorbance values plotted at graph A were those at 470 nm. The inset image in the UV spectra graph B shows the digital photograph of DAB-BA-PAA-(ChS+ARS#DAB-BA-PAA)₁₀ (left) and ABOL-BA-PAA-(ChS+ARS#ABOL-BA-PAA)₁₀ (right).

Figure 6.1 indicates relatively linear build-up profiles for the two BA-PAAs. Both systems display a slow build-up in the early stages of deposition, probably due to incomplete substrate surface coverage, causing repulsion between the substrate and the negatively-charged ARS molecules. The subsequent linear increase of ARS absorbance values indicates that ARS is incorporated systematically as the bilayer number increases. Remarkably, the incorporation of ARS is more efficient in the ABOL-BA-PAA multilayers than in the DAB-BA-PAA multilayers. This is in contrast to expectation, since the previous study (Chapter 5) showed that DAB-BA-PAA facilitated more deposition of ChS and overall thicker films, as compared to ABOL-BA-PAA. However, the previous study was based on the absorbance values at 258 nm specific to ChS and therefore did not provide indication on the amount of incorporated BA-PAAAs. The higher ARS uptake in the ABOL-BA-PAA#ChS multilayers may indicate that the ABOL-BA-PAA multilayer contains higher ABOL-BA-PAA/ChS ratio than the DAB-BA-PAA/ChS ratio in the DAB-BA-PAA multilayer, thereby making it possible to incorporate more ARS into the films through BA-ARS interactions. At 5 and 10 bl, ABOL-BA-PAA-based films contain 2 and 1.3 times more ARS, respectively, than DAB-BA-PAA-based films. The inset in the UV spectra of Figure 6.1 shows the digital photograph of DAB-BA-PAA-(ChS+ARS#DAB-BA-PAA)₁₀ and ABOL-BA-PAA-(ChS+ARS#ABOL-BA-PAA)₁₀. The image reveals that DAB-BA-PAA-(ChS+ARS#DAB-BA-PAA)₁₀ contains less ARS than ABOL-BA-PAA-(ChS+ARS#ABOL-BA-PAA)₁₀.

With DAB-BA-PAA possessing higher positive charge density due to the protonated amine group in the side chain, it may be expected that additional electrostatic interactions with the negatively charged ARS may help to incorporate more ARS in the DAB-BA-PAA#ChS multilayer films in comparison to ABOL-BA-PAA. However, our previous attempts to incorporate various other charged small dyes through parallel loading into multilayers by purely electrostatic interaction were unsuccessful. Often the dyes acted as salts, enhancing deposition of polyelectrolytes without being incorporated (unpublished results). It is therefore expected that ARS-boronate ester formation is the major driving force for the successful incorporation of ARS into the (BA-PAA#ChS) multilayers.

As a pH indicator, ARS with a pK_a of ~4.5 is known to change color from yellow to red in the pH range of 3.5 – 6.5 [19]. Throughout the multilayer build-up, ChS+ARS deposition solution in water was red in color (pH ~7), while

the pH of the BA-PAA deposition solutions was maintained at 7.4 through the use of phosphate buffer. If the color of the ARS in the constructs would be determined solely by the pH of deposition solutions, a red multilayered film with λ_{\max} above 500 nm would be expected. However, the color of the films (Figure 6.1, inset) was orange instead of red, with a λ_{\max} at 470 nm. This multilayer λ_{\max} of 470 nm was maintained throughout the 10 cycles of deposition investigated (data not shown). It is known from the literature that the ARS-phenylboronate ester (BA-ARS) possesses a relatively high association constant (1300 M^{-1} at pH 7.4, 0.10 M phosphate buffer) [9]. In contrast, ChS which contains vicinal diol groups with larger dihedral angles only forms very weak esters with BA, further hampered by electrostatic repulsion from the boronate anion with the sulfate and carboxylic acid groups of ChS. Therefore, the orange color is most likely attributed to ester formation of ARS with phenylboronic acid (BA) moieties in the BA-PAA [15]. This finding of multilayer λ_{\max} at 470 nm is in agreement with a reported λ_{\max} of BA-ARS loaded films previously reported by Ding et al. [20].

As further comparison, DAB-BA-PAA-(PVA+ARS#DAB-BA-PAA)₁₀ – an ARS-loaded multilayer prepared with PVA instead of ChS – was notably red instead of orange (data not shown), indicating significant competition between diols of PVA and ARS for ester formation with BA. Due to the multivalency and high local concentration of vicinal diol groups in PVA, the majority of BA moieties is bound to PVA, leaving the ARS molecules only physically entrapped or loosely bound in this multilayer.

It is important to note that the BA-PAA#ChS multilayer films have an opaque appearance, which especially manifest at higher number of layers. This hampers accurate UV determinations. Therefore, in order to minimize possible errors in UV characterization, the number of bilayers in the subsequent studies on pH-, glucose-responsiveness, and degradation of the layers has been limited to 5 bilayers.

6.3.2 ARS RELEASE PROFILES UNDER PHYSIOLOGICAL CONDITIONS AND AT ACIDIC pH

Due to the pH-sensitive nature of the boronate ester formation [9], ARS is expected to be released at more acidic pH where boronate ester formation is less favorable. To investigate the ARS release profiles from the multilayered systems under physiological conditions and at acidic pH, the films were incubated in PBS pH 7.4, and in CBS at pH 6, 5, or 4 at 37°C. Figure 6.2 indicates that within 12 h of incubation under the physiological conditions (pH 7.4), about 30% and 40% of the incorporated ARS was released for DAB-BA-PAA and ABOL-BA-PAA systems, respectively. ARS release further continued more slowly, reaching a plateau after 10 d of incubation where ~50% of the incorporated ARS was released from the multilayered constructs. The rapid release of ARS under physiological conditions may be facilitated by entropic gain from the liberation of ARS molecules before finally reaching an equilibrium at ~50% ARS content.

ABOL-BA-PAA multilayers, possessing a higher loading of ARS than the DAB-BA-PAA multilayers, released more of its ARS content during the initial rapid release phase. This means that under equal conditions and at the same number of bilayers, much more ARS is released to the incubation medium by the ABOL-BA-PAA system, than in the case of the DAB-BA-PAA system. Also, since the release was only followed by determination of the decrease of the ARS absorbance in the multilayers, it is not deducible from these results whether or not also BA-PAA polymers or ChS were released during the initial release phase. Our previous results with ARS-free multilayers (Chapter 5) showed that up to ~20% of the polymeric components of the multilayers were also released within 2 h of incubation under the same conditions. Therefore, the release observed in Figure 6.2 may represent the release of a mixture of both free and ARS-boronate ester.

At acidic pH, ARS-boronate ester is less stable [9] and leads to more rapid release of ARS. At pH 6 at least two times faster release of ARS is observed, as compared to the release at pH 7.4. At more acidic pH the release proceeds even progressively faster, and complete ARS release was achieved at pH 5 and 4, after 17 h and 5 h, respectively.

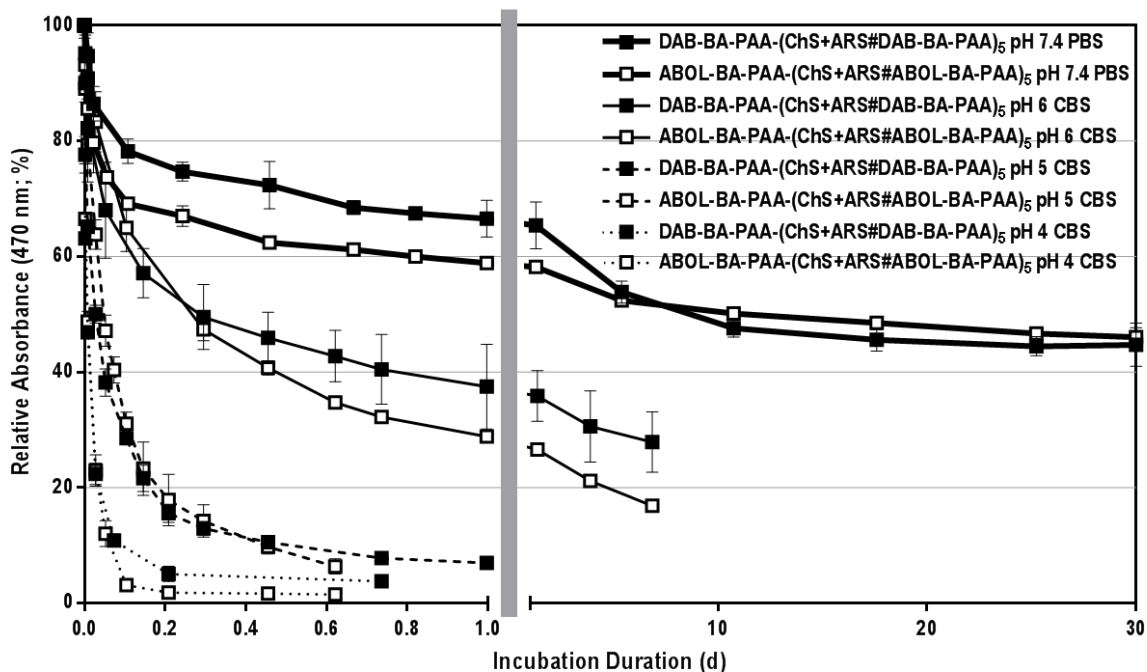
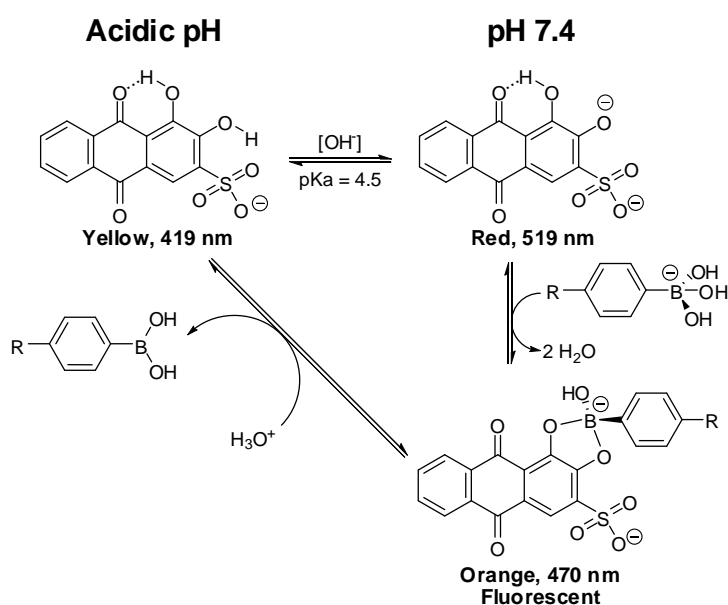


Figure 6.2 ARS release profiles under physiological conditions and acidic pH *in vitro*. The left part of the abscissa shows the trend of fast decrease within 1 d in the initial phase of the incubation while the right part shows the much slower decrease throughout the rest of the long incubation duration.

As discussed previously, ARS is a pH indicator. The equilibria between the ARS species are depicted in Scheme 6.1, including those in the presence of BA moieties. In the presence of BA moieties, the high binding constant between ARS and BA drives the equilibrium towards boronate ester formation with a distinct λ_{\max} . This boronate ester is only stable at neutral to basic pH, where it is predominantly present in the negatively charged tetrahedral form [9]. Therefore, upon decrease of pH, the equilibria are shifted towards the free ARS, which are then shifted further to the yellow species ($\lambda_{\max} = 419$ nm) by the low pH. Figure 6.3 shows the expected decrease in λ_{\max} during the incubation in the different acidic pH values. As shown in Scheme 6.1, this shift in λ_{\max} is accompanied by ARS-boronate ester hydrolysis, leading to ARS release from the films.



Scheme 6.1 Equilibria of various ARS species in acidic and neutral pH values, and in the respective ester formation with BA moiety.

During the first hour of exposure to PBS buffer at pH 7.4, the λ_{max} of the multilayers stays relatively stable at 470 nm, followed by a shift to longer wavelength throughout the rest of the incubation period. The shift in λ_{max} notably reached a maximum value at ~510 nm after about 20 d of incubation. Unlike in the case of acidic pH, this shift in λ_{max} progressed much more slowly, underlining the high binding affinity of the BA to ARS at pH 7.4. The initial 1 h rapid release of ARS (Figure 6.2) was not accompanied by a shift in λ_{max} . This further signifies that indeed most of the incorporated ARS was bound to BA moieties or involved in dynamic ester formation [21] with the BA moieties in the film. In the later stages of incubation, slow gradual boronate ester hydrolysis and diffusion of ARS took place, leaving higher portions of unbound physically-entrapped ARS in the multilayer, resulting in a shift of λ_{max} to that of free ARS at pH 7.4 ($\lambda_{\text{max}} = 519$ nm).

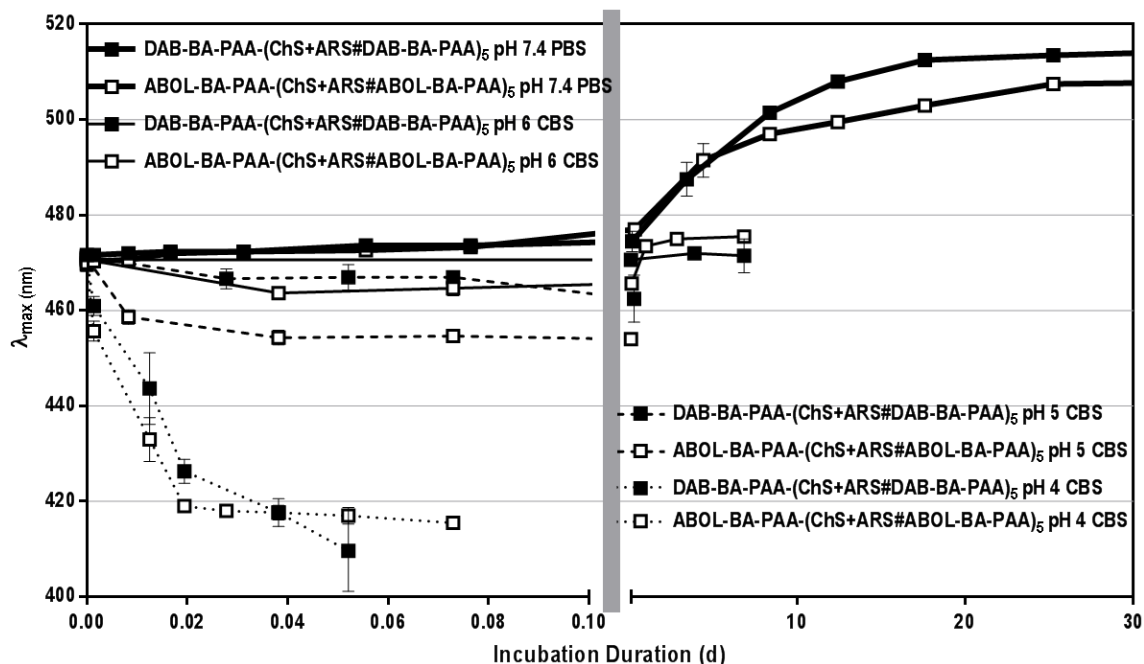


Figure 6.3 Maximum wavelength shift of ARS molecules within DAB-BA-PAA-(ChS+ARS#DAB-BA-PAA)₅ and ABOL-BA-PAA-(ChS+ARS#ABOL-BA-PAA)₅ films at various pH values.

6.3.3 ARS RELEASE PROFILES UNDER VARIOUS REDUCING CONDITIONS

Owing to the presence of disulfide bonds in the main polymer chain of the BA-PAA_s, the resulting multilayered ensembles are responsive to the presence of reducing agents as well. Here, this reducibility is demonstrated by exposing the multilayers to 0.4 mM and 10 mM of glutathione in the incubation solutions of PBS at pH 7.4. Figure 6.4 shows the ARS release profiles under these reducing conditions. In the presence of 0.4 mM glutathione, ARS release was not significantly enhanced as compared to that observed in the absence of glutathione, at least during the first 10 h of incubation. This slow response to 0.4 mM glutathione was also observed for the degradation of the ARS-free multilayers (Chapter 5), and can be attributed to their relatively high structural stability due to the branched structure of the polymers. However, during prolonged incubation, disulfide reduction progressed more extensively (incubation duration > 10 h), ARS release displayed an increased release compared to the release observed in the absence of glutathione. At higher glutathione concentration of 10 mM the accelerated release was more pronounced and complete ARS release and film degradation was achieved after 10 h of incubation.

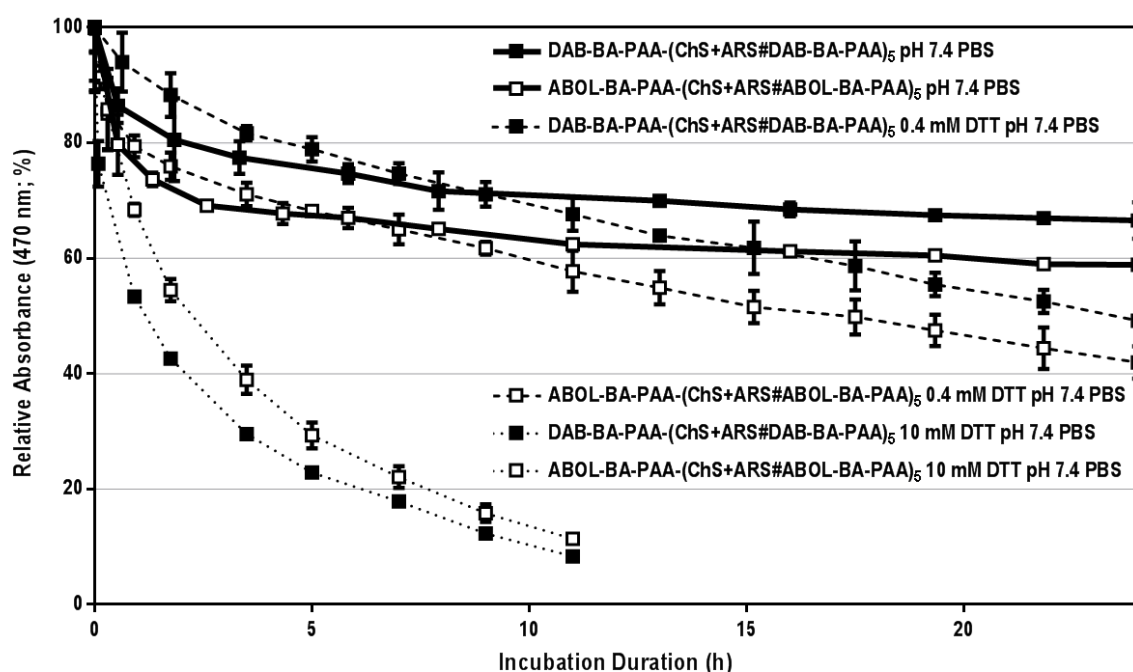


Figure 6.4 Degradation profiles of DAB-BA-PAA-(ChS+ARS#DAB-BA-PAA)₅ and ABOL-BA-PAA-(ChS+ARS#ABOL-BA-PAA)₅ in PBS at pH 7.4 containing 0.4 or 10 mM glutathione at 37°C *in vitro*.

6.3.4 ARS RELEASE PROFILES IN THE PRESENCE OF GLUCOSE

As a diol-containing molecule, glucose may compete with ARS in binding to the BA-moieties in the (BA-PAA#ChS) multilayers, which can result in a glucose-triggered ARS release from the multilayers. However, the results in Figure 6.5 show that ARS release was only slightly increased by the presence of glucose at elevated concentration of 100 mM, and even decreased at 25 mM glucose concentration. At 25 mM glucose concentration, the slightly slower initial ARS release, as compared to the release in the absence of glucose, is probably due to increases in osmotic pressure in the incubation medium, leading to an overall effect of decreased ARS diffusion from the films. In general, the absence of any significant glucose-response is most likely due to the much stronger binding constant of BA with ARS than with glucose (i.e. ~300-fold stronger [9]). Furthermore, pronounced ARS release may have been further hampered by slow diffusion of glucose into and ARS out of the ChS-rich multilayered construct.

Figure 6.5 further shows that albeit minor, ABOL-BA-PAA (white symbols) displayed slightly more increased responsiveness to glucose than DAB-BA-PAA (black symbols). At the same glucose concentration of either 25 or 100 mM, more pronounced ARS release was observed for ABOL-BA-PAA multilayers than for DAB-BA-PAA systems. This may be attributed to the weaker interaction between the neutral primary alcohol side groups of ABOL-BA-PAA with the negatively-charged ChS, as compared to the more positively-charged primary amines of DAB-BA-PAA. In the former case, weaker interaction may lead to pronounced swelling that enhances ARS release, while in the latter case, presence of additional positive charges may restrict release due to electrostatic interaction between ARS and the protonated amines.

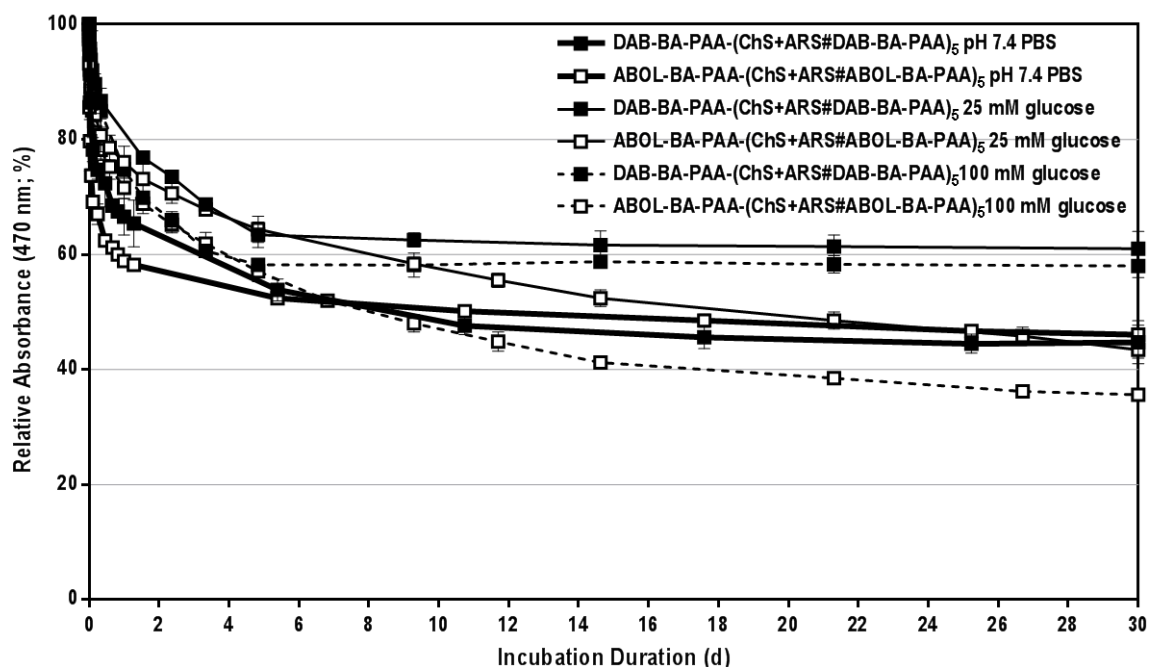
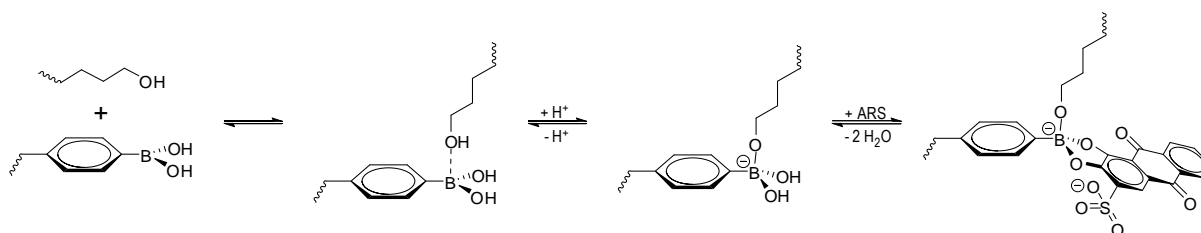


Figure 6.5 ARS release profiles under physiological conditions and in the presence of 25 and 100 mM glucose *in vitro*.

The change in λ_{\max} throughout the incubation in glucose solution (Figure 6.6) shows an apparent trend. The λ_{\max} of DAB-BA-PAA multilayers displays a more rapid red-shift (pointing to free ARS) than ABOL-BA-PAA, with no significant dependence on glucose concentration. Note that a similar trend was observed for films incubated under physiological conditions. DAB-BA-PAA multilayers eventually have higher λ_{\max} than ABOL-BA-PAA multilayers, which could indicate that the ARS-boronate ester in DAB-BA-PAA multilayers is weaker than in the ABOL-BA-PAA system. The pronounced red-shift of λ_{\max} is probably facilitated by the lower diffusion coefficient of negatively-charged ARS from the multilayers, which contains higher amounts of positively-charged primary amine

side groups. Thus, it is likely that in a typical DAB-BA-PAA multilayer, ARS is more readily freed from ester formation with BA, but remains physically entrapped within the multilayers, hence changing λ_{\max} .

Regarding as to why ABOL-BA-PAA may form stronger binding with ARS than DAB-BA-PAA, the reason may be that the primary alcohol side groups of ABOL-BA-PAA in the proximity of BA can provide additional stabilization to the ARS-boronate ester. It is known that boronate esters are more stable in their tetragonal anion form [9]. In a compact layer of BA-PAA, it is likely that a primary alcohol in the vicinity donates its free electron pair, effectively lowering the apparent pKa of the BA (Scheme 6.2). In contrast, as the majority of primary amines in DAB-BA-PAA is protonated, less electron pair donation can be provided by these groups.



Scheme 6.2 Acid-base equilibria between trigonal boronic acid and vicinity primary alcohol side group of ABOL-BA-PAA and the subsequent boronate ester formation with ARS.

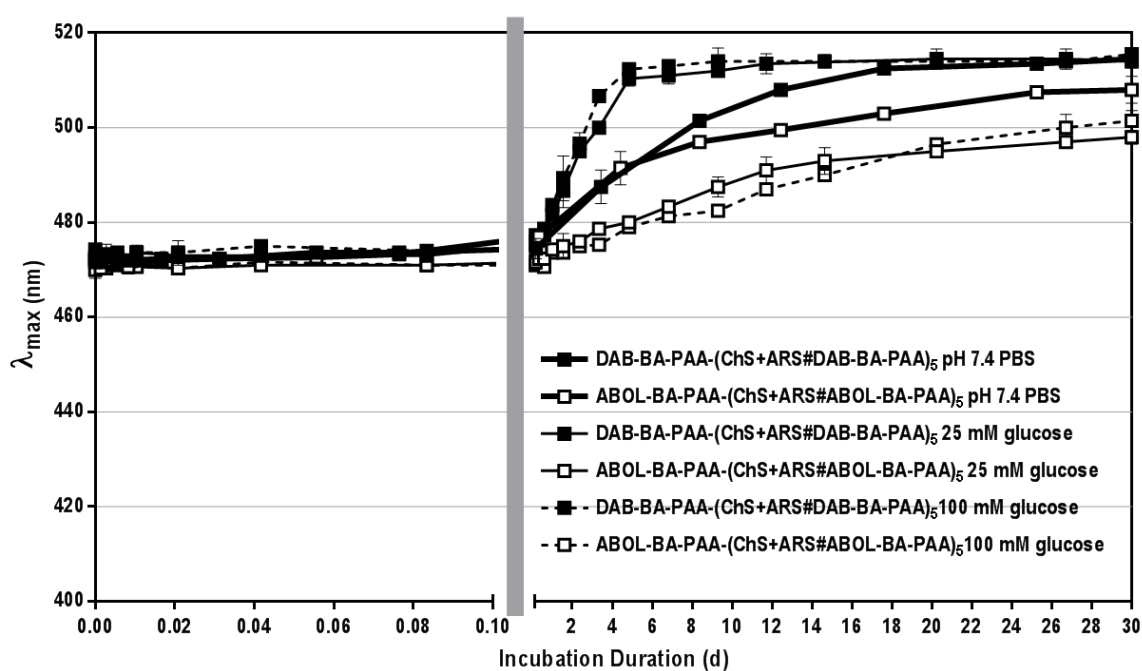


Figure 6.6 Maximum wavelength shift of ARS molecules within DAB-BA-PAA-(ChS+ARS#DAB-BA-PAA)₅ and ABOL-BA-PAA-(ChS+ARS#ABOL-BA-PAA)₅ films in the presence of 25 and 100 mM glucose.

6.3.5 UPTAKE OF ARS BY COS-7 CELLS CULTURED ON TOP OF THE MULTILAYERS

In this study, multilayered thin films of (ChS+ARS#BA-PAA) are investigated as a drug delivery system with the ARS as a model drug. As observed through the previous release study, these multilayers may serve as a drug reservoir to provide sustained release under physiological conditions (Section 6.3.2) or triggered release by change in pH or reductive conditions (Section 6.3.2 and 6.3.3).

The ARS-boronate ester within the multilayered surface is fluorescent and may serve as a fluorescent label for the detection of cellular uptake of ARS-boronate esters. These ARS-boronate esters may be released from the multilayers either in the form of nanoparticles in which ARS is embedded and covalently bound to BA as boronate ester, or as more loosely formed BA-PAA aggregates with weaker ARS binding. Earlier it has been found that ABOL-BA-PAA polymers can self-assemble into nano-sized particles [12]. Dynamic light scattering of 0.6 mg/mL solutions of ABOL-BA-PAA in 50 mM HEPES buffer at pH 7.4 indeed showed homogeneous particles of ~94 nm, with a positive zeta potential (up to +40 mV). The same solution of DAB-BA-PAA showed higher polydispersity and lower zeta potential (+4 mV) (data not shown). This observations may be an indication that multilayers of ABOL-BA-PAA could provide a higher amount of ARS-complexed nanoparticles than the DAB-BA-PAA multilayers. Such an effect could be relevant for cellular uptake of ARS by cells cultured on top of the multilayers since nanoparticles with positive zeta potential are better internalized by cells and contain more stable and longer lasting BA-ARS.

To investigate whether ARS can be delivered by the films to become internalized by cells cultured on the multilayered surfaces, COS-7 cells were cultured on 96-well poly-D-lysine-coated tissue culture-treated polystyrene (PDL-TCPS), coated with (ChS+ARS#BA-PAA)₁₀. The degree of cellular uptake of polymer-bound ARS was determined at 0, 3, 6, 12, 24, and 48 h time points after seeding of the cells on the multilayers. After the designated culture duration, cells were trypsinized, fixed and stored at 4 °C before being measured at the end of the experiment. Trypsinization was found to not cause dissolution of the multilayered surface (data not shown). In addition to the cells cultured on the (ChS+ARS#BA-DAB)₁₀ (entry #1) and (ChS+ARS#BA-ABOL)₁₀ (entry #2) multilayers, several controls were prepared for a more thorough analysis as elaborated in Table 6.1. Multilayered systems without cells (entries #5-8) served as a guideline to separate live cell populations from the population of film debris and/or particles in the FACS analysis. Cells seeded on PS well plates without multilayers (entry #9) served as negative control to help gate for live cells. Cells seeded on multilayers without ARS, (ChS#DAB-BA-PAA)₁₀ (entry #3), and (ChS#ABOL-BA-PAA)₁₀ (entry #4), and on PS with additional ARS in the medium (entry #10) served as a guideline to establish a marker to separate positive cells (i.e. cells that have taken up fluorescent ARS-boronate ester) from negative cells, and to verify that detected fluorescence is only from the ARS-boronate ester. The degree of cellular uptake is presented in two ways; i.e. 1) as percentage of positive cells in the live cell population, and 2) as relative fluorescence intensity of sample suspensions.

Table 6.1 List of samples and controls incorporated during cellular uptake studies and their respective abbreviations.

Entry	Sample Name	Category	Abbreviation
1	(ChS+ARS#DAB-BA-PAA) ₁₀ with cells	ARS	DAB-BA-PAA
2	(ChS+ARS#ABOL-BA-PAA) ₁₀ with cells		ABOL-BA-PAA
3	(ChS#DAB-BA-PAA) ₁₀ with cells	No ARS	DAB-BA-PAA no-ARS
4	(ChS#ABOL-BA-PAA) ₁₀ with cells		ABOL-BA-PAA no-ARS
Controls without cells			
5	(ChS+ARS#DAB-BA-PAA) ₁₀ without cells	No cell	DAB-BA-PAA no-cell
6	(ChS+ARS#ABOL-BA-PAA) ₁₀ without cells		ABOL-BA-PAA no-cell
7	(ChS#DAB-BA-PAA) ₁₀ without cells	No ARS, no cell	DAB-BA-PAA no-ARS-no-cell
8	(ChS#ABOL-BA-PAA) ₁₀ without cells		ABOL-BA-PAA no-ARS-no-cell
Controls without multilayer			
9	PS with cells	PS	PS
10	PS with cells seeded in medium containing ARS	PS+ARS	PS+ARS

Typical dot plots for the different conditions are shown in Figure 6.7a. From the different plots, three distinct regions can be drawn out which represent populations of live cells (R1), particles or multilayer remnants and small particles (R2) or dead cells (R3). Region R2 is determined based on the single population obtained from no-cell controls (entries #5-8) on which shear forces have been applied to disintegrate the multilayered surface. Dot



plot similarity between ARS samples (entry #1-2) and PS (entry #9) and PS+ARS (entry #10) controls indicate that no multilayer components were included in the sample suspensions.

Histograms were plotted to correlate number of events gated on live cells (G1=R1) with the respective fluorescence intensity (Figure 6.7b). Note the distinct difference between cells cultured on PS and PS+ARS where a right shift in cell population is observed for PS+ARS as compared to PS. The shift indicates a slight increase in fluorescence intensity, which is induced by the presence of free unbound ARS. Taking this phenomenon into account, the latter systems were deemed as a more suitable negative control to set the M1 marker to isolate positive (BA-ARS fluorescent) cells from negative populations. Finally, the same marker is applied for the statistical analysis to determine the degree of cellular uptake within positive samples gated for live cells (G1).

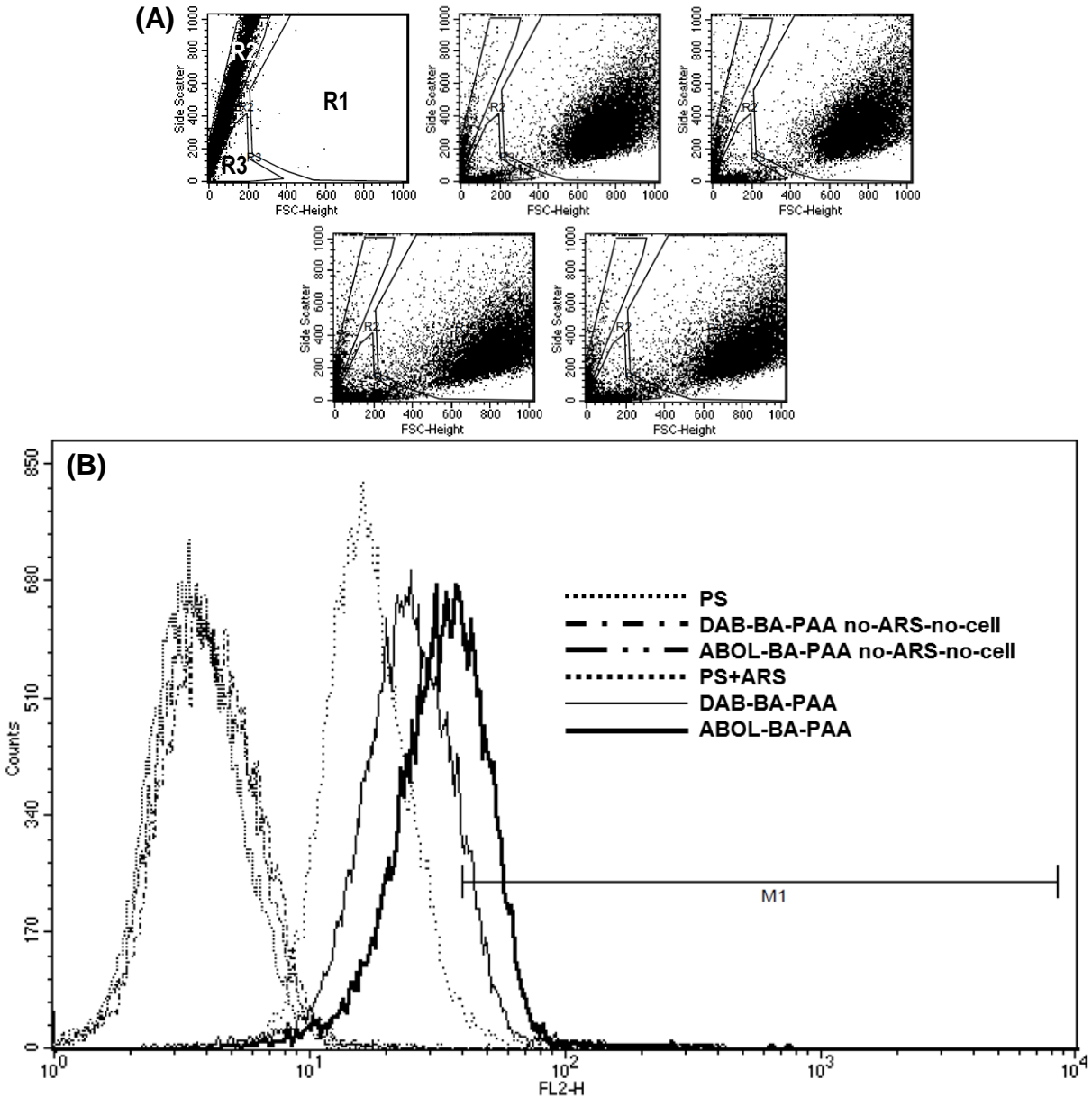


Figure 6.7 (A) Representative dot plots of: (from left to right, top to bottom) multilayer fragments (see text), PS, PS+ARS, DAB-BA-PAA, and ABOL-BA-PAA after 12 h of culture duration. Three regions are also plotted on every dot plot, namely R1 for live cells (biggest region to the right), R3 for dead cells (bottom left corner), and R2 (left part of dot plot) most apparent for multilayer fragment populations shown in the first dot plot. (B) Overlay histogram of various samples gated for live cells (G1=R1).

Figure 6.8a shows the degree of cellular uptake against the different incubation durations. The PS (entry #9), PS+ARS (entry #10), and no-ARS (entry #3-4) controls data were collected after 12 h incubation and showed no visible degree of uptake, despite the long culture duration (Figure 6.8a, first three bars). 0 h incubation data was obtained by collecting the FACS sample directly after cell seeding on multilayered surfaces. As the duration of incubation was simply too short for intracellular uptake, any positive signals of positive cells would indicate physical association of burst-released multilayer components on the cell surface. Figure 6.8a shows that at 0 h, no significant uptake or physical association was detected. Upon longer culture duration, the degree of uptake increased and reached optimal values at 20 and 30% of BA-ARS positive cells for DAB-BA-PAA and ABOL-BA-PAA, respectively, before decreasing to a stable value of 10% after 48 h culture time. Longer culture duration was not attempted as the cells would have grown past confluency, while passaging of the confluent cell monolayer to the same surface did not result in substantial degrees of uptake following another 48 h of culture (data not shown). This observation may indicate that the initial burst release observed in Figure 6.2 is critical in delivering particles to be taken up by the cells. Following the initial 6 h (for DAB-BA-PAA system) and 12 h (for ABOL-BA-PAA system) incubation, cells proliferated and thus decreased the overall degree of cellular uptake.

Another way to follow the extent of BA-ARS uptake by the cells is by determination of the overall fluorescence intensity in the sample suspension, i.e. not only the cells within the M1 marker, but the whole sample suspension, including the positive values from free ARS without BA (see Figure 6.7b). Figure 6.8b shows that at the respective optimal culture duration, the detected fluorescence intensity was approximately two times higher than that of the 0 h value. Further, as opposed to Figure 6.8a where the degree of uptake decreased at least twice past the optimal culture duration, Figure 6.8b shows relatively stable fluorescence intensity possibly indicating that the absolute amount of positive live cells were maintained throughout the 48 h culture duration. Fluorescence intensity detected at 0 h was most likely due to the burst-released free ARS from the films as shown by similar fluorescence intensity detected in the 12 h incubated PS+ARS controls (entry #9, Figure 6.7b). When the fluorescence intensity of every sample is corrected for the fluorescence intensity of the PS+ARS controls, the resulting fluorescence intensity can be regarded to emerge from ARS-boronate ester formation (Scheme 6.1). In that respect, when no-cell controls were subjected to shear forces (entry #5 and 6) in order to measure the relative fluorescence intensity of the multilayer alone, the fluorescence intensity detected was approximately 10 fold the optimal values shown in Figure 6.8b. Typical fluorescence intensity values measured were 380 and 510 A.U. for DAB-BA-PAA (entry #5) and ABOL-BA-PAA (entry #6), respectively. The higher fluorescence intensity of the latter system agrees well with the build-up profile shown in Figure 6.1. The ABOL-BA-PAA system facilitates more deposition of ARS and correspondingly more ester formation with the BA-functionality.

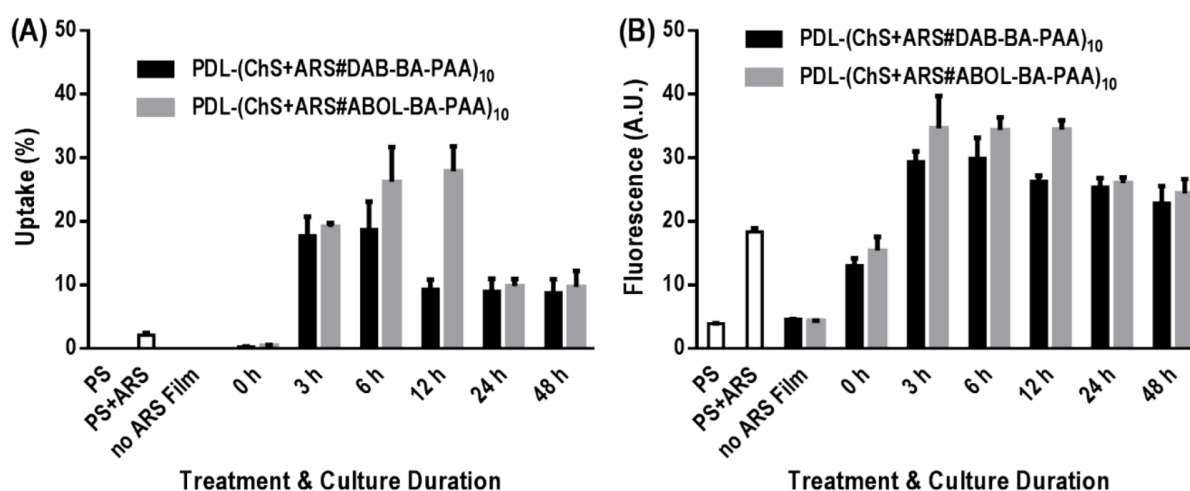


Figure 6.8 (A) Degree of cellular uptake of multilayer components and (B) mean fluorescence intensity/cell against cell culture duration starting from the step of cell seeding on multilayer-coated well plate.

Noticeable differences between the two BA-PAA systems can be observed in Figure 6.8a where the ABOL-BA-PAA system may sustain cellular uptake of proliferating cells up to as long as 12 h, while the DAB-BA-PAA reached the optimal value already after 6 h culture duration. This may be attributed to three factors, i.e. the higher initial incorporation of ARS, better ARS-boronate ester formation, and/or more efficient release of ARS-boronate ester in the former system. As observed in Figure 6.2, ABOL-BA-PAA incorporates and releases more ARS during the initial 12 h rapid release phase. Moreover, as shown in Figure 6.6 and Scheme 6.2, ABOL-BA-PAA potentially also forms stronger ARS-boronate esters through the presence of primary alcohols in the vicinity. Next, it was indicated previously that ABOL-BA-PAA polymer self-assembles into monodispersed nano-sized particles that may be internalized more efficiently by cells [12], whereas DAB-BA-PAA provides more polydispersed particles of lower positive surface charges. As such, albeit showing relatively similar behavior to DAB-BA-PAA throughout the *in vitro* release studies, the ABOL-BA-PAA may eventually provide release of more nanoparticles that are better internalized by cells and contain more stable and longer lasting ARS-boronate ester.

To obtain further insights whether the fluorescent ARS-boronate esters detected by FACS are indeed internalized by cells and not only physically attached onto the outer membrane of the cells, cells which have been cultured for 20 h were trypsinized, reseeded on imaging chambers, and left to attach for roughly 6 h before being stained and fixed for confocal microscopy imaging. Complementing the confocal microscopy, regular fluorescence microscopy was also employed to obtain lower magnification, more global view on the samples. No significant differences were observed between the DAB-BA-PAA and ABOL-BA-PAA systems and therefore images of the latter are shown here as representative results.

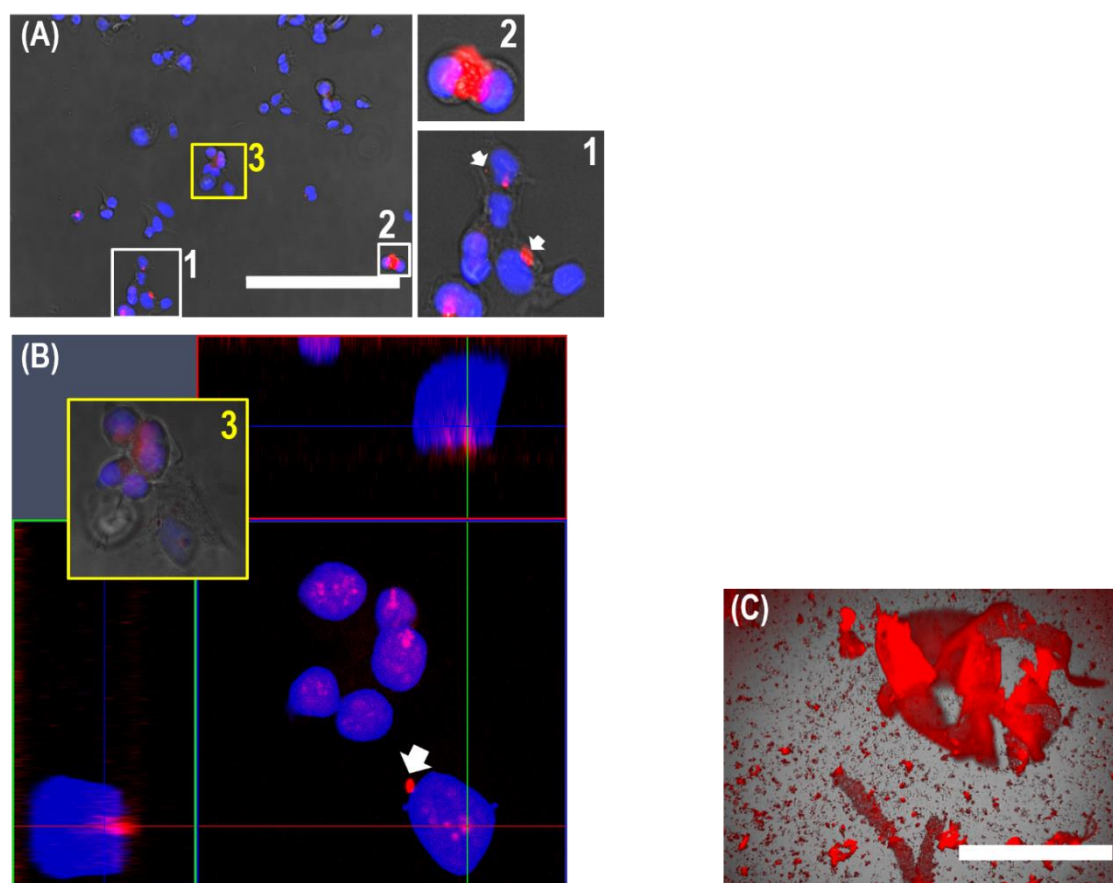


Figure 6.9 (A) Overlaid fluorescence (20X magnification, bar = 200 μm) and (B) confocal (40X magnification) microscopy images of COS-7 cells after 20 h culture duration on a $(\text{ChS}+\text{ARS}\#\text{ABOL-BA-PAA})_{10}$ multilayer sample and reseeded onto clean imaging chambers. Insets show higher magnification of selected clusters of cells (white square) and those specifically imaged through confocal microscopy (yellow square). (C) Overlaid fluorescence image of mechanically destroyed $(\text{ChS}+\text{ARS}\#\text{ABOL-BA-PAA})_{10}$ sample without cells at 4X magnification (bar = 1,000 μm).

Figure 6.9b indicates that most of the observed fluorescent particles are indeed taken up by the cells and are not adhering to the outer cell membranes. Moreover, these particles can be seen to co-localize with the Hoechst-stained nuclei. Larger fluorescent aggregates are also observed, which were physically associated with the cells and/or located at the peri-nuclear region (arrow). As a control, when PDL-(ChS+ARS#ABOL-BA-PAA)₁₀ was mechanically destroyed and observed under the fluorescence microscope (Figure 6.9c), multilayer remnants could be observed, which fluoresced brightly under the same conditions indicating that the observed fluorescent particles indeed came from the multilayered surface onto which cells were cultured. No such fluorescence was observed from cells cultured on PS surfaces (data not shown).

6.4 CONCLUSIONS

Multilayered thin films from boronic acid-functionalized poly(amido amine)s (BA-PAA) and chondroitin sulfate (ChS) have been investigated for their possibility in facilitating cellular uptake of small dye molecule alizarin red S (ARS). The dynamic covalent bonding between the ARS and BA moieties in the polymers facilitates systematic loading during the multilayer build-up and provides easy characterization through the fluorescence properties of the ester. UV spectroscopy shows linear build-up profiles with distinct λ_{\max} indicating successful incorporation of ARS. It is postulated that during build-up, all of the incorporated ARS was present in dynamic equilibrium with BA moieties of the BA-PAA, resulting in a stable maximum wavelength of absorption (λ_{\max}) at 470 nm, corresponding to the λ_{\max} of ARS-boronate ester.

The ARS-boronate ester retains pH responsiveness, and more rapid release is obtained upon lowering pH from neutral (pH 7.4) to pH 6, 5, and 4. Concomitant shifts in λ_{\max} were observed, in agreement with ARS-boronate ester hydrolysis and ARS' properties as a pH indicator. At pH 5 and 4, complete ARS release was achieved in 17 and 5 h, respectively. Under physiological conditions (pH 7.4), it was proposed that initial burst release of up to 40% (12 h) represents the release of excess ARS, which was initially in dynamic equilibrium within the multilayered films. This dynamic equilibrium is maintained for the remaining ARS molecules within the films, thereby maintaining the films' λ_{\max} at the initial 470 nm. After more than 1 h incubation, the λ_{\max} shifted very slowly, reaching a plateau at ~510 nm after 20 d of total incubation, indicating the relatively strong ARS-boronate ester formation at pH 7.4. Parallel to the slow increases in λ_{\max} , ARS was released very slowly, indicating low diffusion coefficients of ARS out of the multilayered structure.

Due to the presence of disulfide bonds in the main chain of the polymers, the films were also responsive to reducing conditions. However, this responsiveness is less prominent in the case of ARS release, especially at lower glutathione concentration, as compared to pH, which directly affects ARS-boronate ester formation. At the high glutathione concentration of 10 mM, complete ARS release was achieved after approximately 10 h.

Due to the possibility of competitive boronate ester formation with other diol-containing molecules such as glucose, ARS release was also investigated in the presence of relatively high glucose concentrations. Notably, no significant response was observed at glucose concentrations of 25 and 100 mM due to the much higher binding constant of BA to ARS than to glucose. The observation of the λ_{\max} change during the glucose incubation experiment indicated that DAB-BA-PAA gave a faster response than ABOL-BA-PAA, i.e. the λ_{\max} red-shifted faster. It was hypothesized that primary alcohol side groups in the vicinity of BA reaction center in ABOL-BA-PAA may help by acting as Lewis bases, consequently lowering the pKa of the BA moiety and form stronger boronate esters with ARS. The faster response of DAB-BA-PAA to glucose, however, did not result in faster apparent ARS release, which was explained as due to low diffusion of ARS out of the multilayered and rigid film, leaving free unbound ARS trapped inside the film to assume its role as pH indicator (i.e. demonstrating higher λ_{\max} at pH 7.4).

For the study of cellular uptake, flow cytometry indicated that compared to the controls, the release of ARS-boronate ester is characterized through the significantly higher fluorescence intensity. Cellular uptake was found to be maximal at 20 and 30% following 6 h of culture for DAB-BA-PAA and ABOL-BA-PAA films, respectively. For the latter system, the degree of cellular uptake was maintained for at least another 6 h, most likely through the higher amount and stronger ARS-boronate ester formed with ABOL-BA-PAA. Confocal microscopy further revealed presence of fluorescent particles that were internalized by cells and often co-localized with the cell nuclei, indicating successful delivery of ARS in its boronate ester form with BA-PAA into the nuclei of the cells cultured on top of the films.

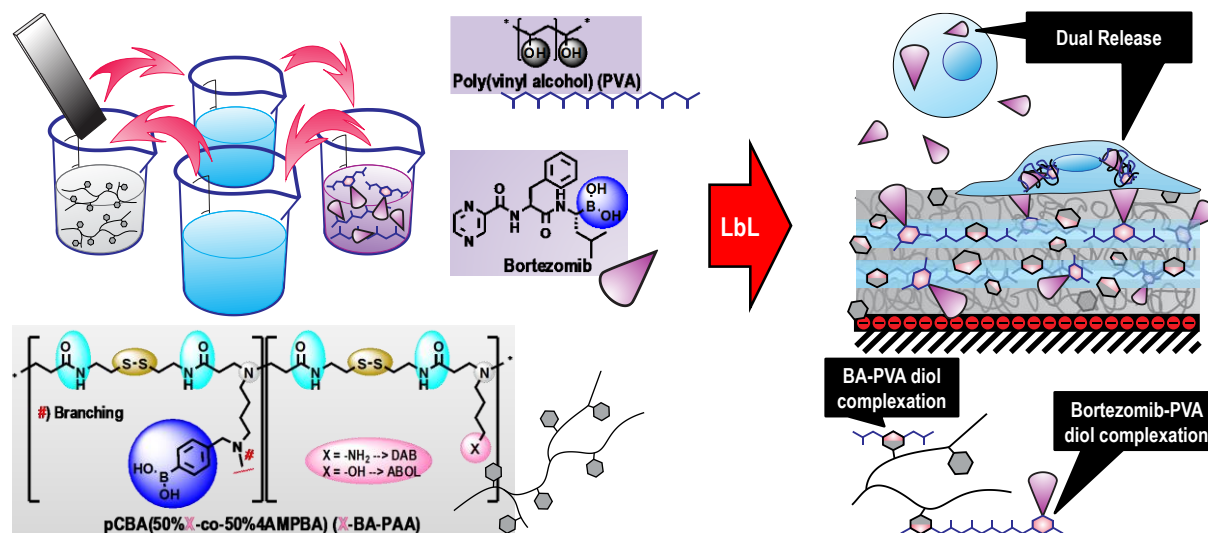
6.5 REFERENCES

- [1] S. Pavlukhina, S. Sukhishvili, Polymer assemblies for controlled delivery of bioactive molecules from surfaces, *Adv Drug Deliver Rev*, 63 (2011) 822-836.
- [2] S. Ye, C. Wang, X. Liu, Z. Tong, Deposition temperature effect on release rate of indomethacin microcrystals from microcapsules of layer-by-layer assembled chitosan and alginate multilayer films, *J Control Release*, 106 (2005) 319-328.
- [3] X. Qiu, S. Loporatti, E. Donath, H. Möhwald, Studies on the Drug Release Properties of Polysaccharide Multilayers Encapsulated Ibuprofen Microparticles, *Langmuir*, 17 (2001) 5375-5380.
- [4] Q.Y. Yi, G.B. Sukhorukov, Photolysis Triggered Sealing of Multilayer Capsules to Entrap Small Molecules, *ACS Appl. Mater. Interfaces*, 5 (2013) 6723-6731.
- [5] N. Ma, H.Y. Zhang, B. Song, Z.Q. Wang, X. Zhang, Polymer micelles as building blocks for layer-by-layer assembly: An approach for incorporation and controlled release of water-insoluble dyes, *Chem Mater*, 17 (2005) 5065-5069.
- [6] B. Thierry, P. Kujawa, C. Tkaczyk, F.M. Winnik, L. Bilodeau, M. Tabrizian, Delivery Platform for Hydrophobic Drugs: Prodrug Approach Combined with Self-Assembled Multilayers, *J. Am. Chem. Soc.*, 127 (2005) 1626-1627.
- [7] R.C. Smith, M. Riollano, A. Leung, P.T. Hammond, Layer-by-Layer Platform Technology for Small-Molecule Delivery, *Angew. Chem. Int. Ed.*, 48 (2009) 8974-8977.
- [8] U. Manna, S. Patil, Borax Mediated Layer-by-Layer Self-Assembly of Neutral Poly(vinyl alcohol) and Chitosan, *The Journal of Physical Chemistry B*, 113 (2009) 9137-9142.
- [9] G. Springsteen, B. Wang, A detailed examination of boronic acid–diol complexation, *Tetrahedron*, 58 (2002) 5291-5300.
- [10] J.N. Cambre, B.S. Sumerlin, Biomedical applications of boronic acid polymers, *Polymer*, 52 (2011) 4631-4643.
- [11] G.A. Ellis, M.J. Palte, R.T. Raines, Boronate-Mediated Biologic Delivery, *J. Am. Chem. Soc.*, 134 (2012) 3631-3634.
- [12] M. Piest, M. Ankoné, J.F.J. Engbersen, Carbohydrate-interactive pDNA and siRNA gene vectors based on boronic acid functionalized poly(amido amine)s, *J Control Release*, 169 (2013) 266-275.
- [13] R.G. Loughlin, M.M. Tunney, R.F. Donnelly, D.J. Murphy, M. Jenkins, P.A. McCarron, Modulation of gel formation and drug-release characteristics of lidocaine-loaded poly(vinyl alcohol)-tetraborate hydrogel systems using scavenger polyol sugars, *European Journal of Pharmaceutics and Biopharmaceutics*, 69 (2008) 1135-1146.
- [14] M. Piest, X. Zhang, J. Trinidad, J.F.J. Engbersen, pH-responsive, dynamically restructuring hydrogels formed by reversible crosslinking of PVA with phenylboronic acid functionalised PPO-PEO-PPO spacers (Jeffamines[registered sign]), *Soft Matter*, 7 (2011) 11111-11118.
- [15] G. Springsteen, B.H. Wang, Alizarin Red S. as a general optical reporter for studying the binding of boronic acids with carbohydrates, *Chem. Commun.*, (2001) 1608-1609.
- [16] H. Fang, G. Kaur, B.H. Wang, Progress in boronic acid-based fluorescent glucose sensors, *J. Fluoresc.*, 14 (2004) 481-489.
- [17] D.P. Yang, H.F. Ji, G.Y. Tang, W. Ren, H.Y. Zhang, How many drugs are catecholics, *Molecules*, 12 (2007) 878-884.
- [18] G.E. Umpierrez, R. Hellman, M.T. Korytkowski, M. Kosiborod, G.A. Maynard, V.M. Montori, J.J. Seley, G. Van den Berghe, Management of Hyperglycemia in Hospitalized Patients in Non-Critical Care Setting: An Endocrine Society Clinical Practice Guideline, *Journal of Clinical Endocrinology & Metabolism*, 97 (2012) 16-38.
- [19] R.W. Sabnis, *Handbook of acid-base indicators*, CRC Press, Taylor and Francis Group, Boca Raton, Florida, United States of America, 2008.
- [20] Z. Ding, Y. Guan, Y. Zhang, X.X. Zhu, Synthesis of glucose-sensitive self-assembled films and their application in controlled drug delivery, *Polymer*, 50 (2009) 4205-4211.
- [21] E. Galbraith, A.M. Kelly, J.S. Fossey, G. Kociok-Kohn, M.G. Davidson, S.D. Bull, T.D. James, Dynamic covalent self-assembled macrocycles prepared from 2-formyl-aryl-boronic acids and 1,2-amino alcohols, *New J. Chem.*, 33 (2009) 181-185.

CHAPTER 7

Multilayered Thin Films from Boronic Acid-Functionalized Poly(amido amine)s and Poly(Vinyl Alcohol) for Surface-Controlled Bortezomib Delivery^{††}

ABSTRACT



Multilayers from branched copolymers of boronic acid-functionalized poly(amido amine)s (BA-PAA)s and poly(vinyl alcohol) (PVA) have been demonstrated as a delivery system for bortezomib, a proteasome inhibitor used to treat multiple myeloma. Ultraviolet-visible (UV) spectrophotometry was used to follow multilayer build-up through the alternate-dipping layer-by-layer technique with bortezomib mixed into the PVA deposition solution. UV spectra of the bortezomib-containing multilayers and their build-up profiles were found to be similar to those of multilayers without bortezomib. No apparent peak of the bortezomib at 270 nm in the film was detected indicating that the concentration of bortezomib in the layers is below 1 μM . Nevertheless, owing to the low effective dose of bortezomib, the incorporated bortezomib was found to be effective in reducing up to 80-90% metabolic activity of COS-7 cells cultured on the surface of the multilayers *in vitro*, relative to cells cultured on multilayers without bortezomib. The cells initially grew normally for the first 20 h after which the metabolic activity abruptly decreased upon longer culture time. By varying the bortezomib concentration in the deposition solution, dose response was observed with increasing efficacy upon increasing bortezomib concentration. The bortezomib efficacy was found to be only slightly affected by the number of bilayers, which can be explained by a highly localized delivery mechanism. It was also observed that when cells were treated with medium which had been used to incubate bortezomib-containing multilayers for one day, dose response was observed in relation to the number of bilayers. Less bilayers exert less efficacy, and vice versa, indicating that the amount of released bortezomib into the incubation medium was proportional to the number of cycles of deposition. The novel multilayered systems offer a new possibility in providing dual therapeutic dosages, i.e. highly localized high-dose treatment of cells directly in contact with the multilayers, and lower-dose treatment of cells further away from the multilayer surface. The former may be tuned specifically through changing the bortezomib concentration in the deposition solution, while the latter may be tuned through both changing the bortezomib concentration and the amount of bilayers.

^{††} Sry D. Hujaya, Jos M.J. Paulusse, Johan F.J. Engbersen, submitted for publication.

7.1 INTRODUCTION

In the development of sophisticated medical devices and biomaterials, layer-by-layer-(LbL) assembled multilayers are among the most inexpensive techniques to easily modify a surface to improve biocompatibility in certain applications, and also provide additional functionalities [1-3]. For example, this versatile technique makes it possible to turn a regular stent into a drug delivery system whose release profile can be easily tuned through the use of appropriate macromolecules. Through the mild, all-aqueous fabrication process, various functional and even native biomacromolecules can be incorporated into the multilayer, turning the surfaces into transfection agents [4-6], differentiation agents [7-11], cell attachment regulators [12-15], drug delivery systems [16-18], and more. The architecture of the multilayers may also be adjusted to easily tune the drug content to provide prolonged therapeutic effects.

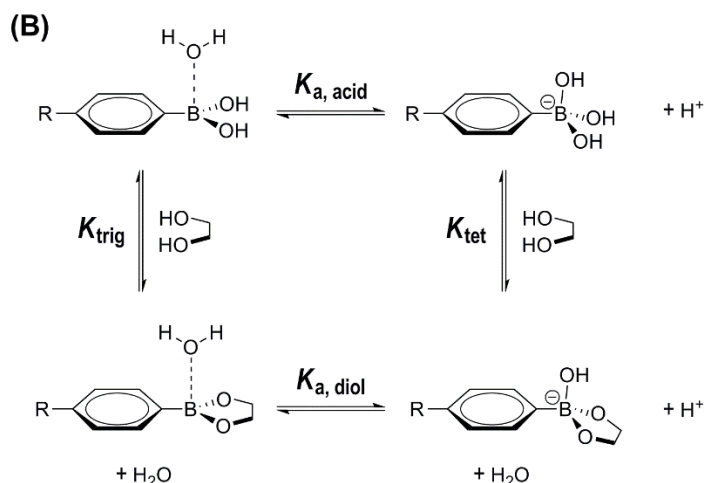
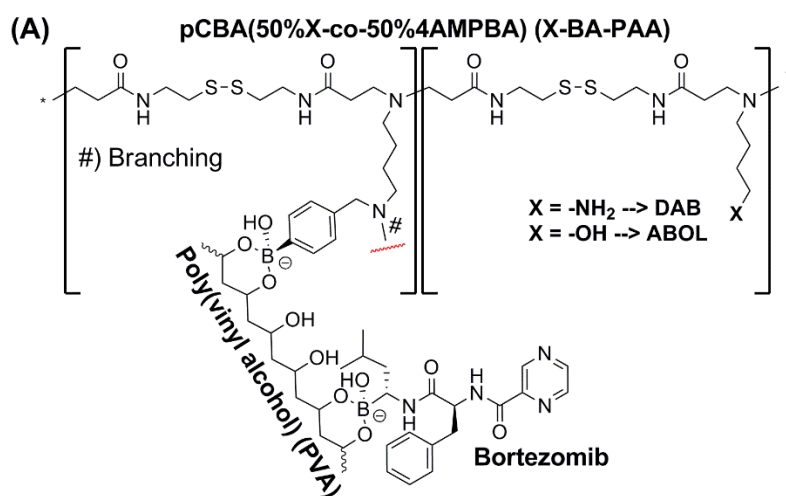
Previously, we have reported the preparation and properties of multilayered systems prepared from randomly branched copolymers of boronic acid-containing poly(amido amine)s (BA-PAA) (Scheme 7.1a) and poly(vinyl alcohol) (PVA) (Chapter 5). Multilayer build-up of these films proceeds through the coordinative covalent ester formation between the BA moieties of the BA-PAA and the diols of PVA (Scheme 7.1b). The chemistry of this boronate ester formation renders the system very responsive to acidic pH, providing complete multilayer disassembly within minutes at pH 6 and below. The multilayers are also responsive to glucose (another diol-containing molecule) but only at higher concentrations and/or longer incubation period due to the much higher binding constant between the BA moieties to diols of PVA than to diols of glucose [19, 20]. Additionally, due to the presence of disulfide bonds in the BA-PAA main chains, the multilayers were also readily degradable in the presence of reducing agents such as glutathione. This may be especially important when the BA-PAA polymers, together with their therapeutic loading are taken up by cells. Multilayers of BA-PAA and PVA were relatively thin, reaching ~100 nm thick at 10 bilayers, and were found to be biocompatible to COS-7 cells *in vitro*. Due to the presence of excess PVA diols in the multilayers with BA-PAA, it is hypothesized that these multilayers can be used to incorporate small BA-containing drugs that can be released sustainably or abruptly through the inherent multilayer responsiveness to pH, reducing agents, and glucose.

As therapeutic agents, boronic acids have found applications in antiviral, antibacterial, and anticancer therapy, mostly due to their properties as Lewis acids, forming coordinative covalent bonds with reactive centers of various enzymes [21, 22]. Among them, bortezomib or Velcade® is a dipeptide proteasome inhibitor that has become one of the most successful drugs for multiple myeloma [23, 24]. Bortezomib works by inhibiting the catalytic centers of proteasomes (i.e. a protease complex present in the cytoplasm) which results in pro-apoptotic effects on especially myeloma cells [25-29]. The BA moiety in bortezomib is one of the most important therapeutic sites, providing covalent linkage to the secondary alcohol of terminal threonine in two of the catalytic centers of proteasomes, thereby stabilizing the hydrogen bonding between the BA and the nucleophilic amine [25].

Incorporation of bortezomib in a BA-PAA and PVA-based multilayered structure may provide triggered, sustained, or prolonged release to improve patient compliance, reduce dosing frequency, and/or open opportunities for new localized routes of administration. For example, despite the effectiveness against multiple myeloma, repeated administration is needed, relapse is still inevitable, and resistance to bortezomib has been reported [30, 31]. The efficacy of bortezomib was also found to be significantly lower on solid tumors as compared to myeloma cells which is attributed to the narrow therapeutic index, leading to side effects such as peripheral neuropathy [32]. Incorporation of bortezomib in a multilayered surface to provide local high-dose for prolonged treatment may improve efficacy and reduce side effects.

The boronic acid moiety in bortezomib has pKa of 8.6 ± 0.1 [33]. Therefore, at physiological pH of 7.4, bortezomib is expected to bind to PVA diols, strong enough to facilitate incorporation into the multilayers, but also weak enough to be sustainably released and induce therapeutic effects. Further, since one of the BA-PAA has been reported to spontaneously form stable nanoparticles [34], the multilayers may also release bortezomib-

containing nanoparticles that may be easily internalized by cells. Further release of bortezomib from the ester can then be achieved through the acidic pH in the endosomal vesicles, while the BA-PAA provide the necessary endosomal escape mechanism [35-37].



Scheme 7.1 (A) Schematic PVA diol ester formation with BA-PAA and bortezomib, (B) Boronic acid-diol ester formation and Lewis acidity.

7.2 MATERIALS AND METHODS

Mowiol® 4-98 (PVA, ~27 kDa), sulfuric acid (H_2SO_4 , 95-98%), hydrogen peroxide (H_2O_2 , 30 wt% in H_2O), and alizarin red S (ARS) were purchased from Sigma-Aldrich (Zwijndrecht, The Netherlands). Sodium dihydrogen phosphate monohydrate ($\text{NaH}_2\text{PO}_4 \cdot \text{H}_2\text{O}$, 99.0-102.0%) and disodium hydrogen phosphate dihydrate ($\text{Na}_2\text{HPO}_4 \cdot 2\text{H}_2\text{O}$, 99.5%) were purchased from Merck (Darmstadt, Germany). Bortezomib (Bort, 99%) was purchased from LC Laboratories (Woburn, USA). Solvents were of reagent grade and used without further purification unless otherwise noted. Milli-Q water (18.2 $\text{M}\Omega \cdot \text{cm}$ at 25 °C) was obtained from a Synergy® water purification system (Millipore).

DAB-BA-PAA and ABOL-BA-PAA were synthesized as described previously in Chapter 5.

PBS buffer was prepared by dissolving 1.54 g of $\text{Na}_2\text{HPO}_4 \cdot 2\text{H}_2\text{O}$, 0.3 g of $\text{NaH}_2\text{PO}_4 \cdot \text{H}_2\text{O}$, and 8.2 g of NaCl into 1.0 L of Milli-Q water and adjusting the pH to 7.4.

UV characterization of multilayers was performed in the dry state using a UV-2401 PC (Shimadzu, 's-Hertogenbosch, The Netherlands) UV spectrophotometer. Each film fabricated on UV-transparent 7.5 x 37 x 1 mm quartz glass (Ted Pella, Redding, USA) was measured in three different arbitrary positions. Absorbance scan was carried out in the 200-400 nm wavelength range. All data points were then corrected for baseline offset by subtracting the absorbance value at 400 nm from each data point.

Poly-D-lysine-coated 96-well plates (PDL-TCPS) for multilayer build-up for cell culture and transfection experiments were purchased from Greiner (Alphen aan den Rijn, The Netherlands).

COS-7 cells (European Collection of Animal Cell Cultures (ECACC) Catalogue No. 87021302) were grown in DMEM containing 4.5 g/L glucose and GlutaMAX™ (Invitrogen, Breda, The Netherlands) supplemented with 2% (v/v) PennStrepp (Lonza, Breda, The Netherlands) and 10% (v/v) fetal bovine serum (Lonza, Breda, The Netherlands).

Fluorescence intensity measurement was carried out in an Infinite M200 PRO plate reader (Tecan, Giessen, The Netherlands). AlamarBlue for cell viability measurements was purchased from Invitrogen (Breda, The Netherlands).

7.2.1 MULTILAYERED THIN FILM CONSTRUCTION AND BUILD-UP PROFILES

Fresh BA-PAA solutions were prepared shortly before the start of multilayer build-up from the solid materials which had been re-lyophilized overnight to avoid weighing errors due to their hygroscopic properties. All BA-PAA solutions (2.0 mg/mL) were prepared in PBS buffer at pH 7.4 to avoid possible variations in pH.

Prior to the assembly, quartz (7.5 x 32 mm) substrates were etched for 30 minutes in piranha acid solution to activate the surface, rinsed with copious amounts of Milli-Q water, and dried under N_2 stream. These substrates were then dipped into DAB-BA-PAA or ABOL-BA-PAA solution (2.0 mg/mL in PBS buffer pH 7.4) for 5 min, transferred into washing solution containing PBS buffer for 1 min, transferred into PVA+ARS (2.0 mg/mL PVA mixed with 1300 μM Bort in PBS buffer pH 7.4) solution for 5 min, and finally dipped into the second washing solution containing PBS buffer for 1 min. This cycle was repeated to reach the desired number of bilayers. Drying under N_2 stream was performed either after every BA-PAA layer deposition. The resulting ensemble is denoted by BA-PAA-(PVA+Bort#BA-PAA)_n, where BA-PAA represents either DAB-BA-PAA or ABOL-BA-PAA and *n* represents the number of bilayers. The first BA-PAA layer is regarded as a precursor layer and therefore excluded from the bilayer number count. Typically, the ensemble consists of 10 bilayers with the BA-PAA polymer as the last layer. For every multilayered system, three samples were fabricated in parallel to give estimation for standard deviation. To study the build-up profiles, UV spectra were recorded after each drying step following BA-

PAA layer formation, throughout the 200-400 nm range. Every absorbance values were then corrected for baseline shift at 400 nm. Afterwards, the multilayers were dipped into PVA+Bort solution to continue multilayer build-up.

Multilayers for cell culture were fabricated directly in the wells of poly-D-lysine-coated 96-well plates (PDL-TCPS, Greiner) by alternately dispensing deposition (70 μ L) and washing (2x 100 μ L) solutions under sterile conditions inside the laminar flow hood (LFH). Deposition started with PVA+Bort (2.0 mg/mL ChS and various concentration of Bort in PBS buffer, 30 min for the first layer, 5 min next) as the first layer to a total of 10 bilayers ending with the BA-PAA layer. No intermediate drying steps were applied. At the end of the fabrication the plates were left inside the LFH briefly to dry the films. Coated plates were kept at 4 °C and used as soon as possible (typically overnight). These multilayered samples are designated as (PVA+Bort#BA-PAA)₁₀ without indicating the presence of a PDL layer as a precursor layer. Compared to multilayers built on quartz and silicon wafer substrates, these systems substitute the first BA-PAA layer with PDL layer inherent to the well plate surface.

7.2.2 KINETICS OF *IN VITRO* THERAPEUTIC EFFICACY OF BORTEZOMIB-CONTAINING MULTILAYERS

Optimization of COS-7 cell seeding density: the metabolic activity signal through AlamarBlue (AB) assay was first optimized for different cell seeding densities for multiple monitoring up to 73 h. Briefly, COS-7 cells from a confluent culture flask were trypsinized and resuspended into 3100 cells/well and serially diluted. After ~4h of culture in the incubator, AB was added to reach 10% final concentration in the cell culture medium. The fluorescence intensity of resorufin (i.e. metabolically-reduced resazurin in AB, $\lambda_{ex}/\lambda_{em}$ = 545/590 nm) was then monitored as 0 h culture duration. From time to time the fluorescence measurement was repeated using the same plate reader settings up to 73 h of total culture duration.

For the kinetic study of the effect of Bort-containing multilayers on cell metabolic activity, COS-7 cells were cultured on multilayer-covered wells at the optimal cell seeding density. Following 4 h of culture to let the cells to attach, AB was then added to reach 10% final concentration. From time to time the fluorescence measurement was carried out using the same plate reader settings up to 61 h of total culture duration.

7.2.3 END POINT METABOLIC ACTIVITY OF CELLS CULTURED ON MULTILAYERS

The effect of various multilayered surfaces on COS-7 cell metabolic activity was investigated via AB assay. Briefly, COS-7 cells were cultured at 20,000 cells/well seeding density. Following a specified cell culture duration, the culture medium was removed, replaced with 10% AB in fresh culture medium, and incubated in the incubator for another 6 h. The fluorescence intensity was then recorded using a plate reader. Metabolic activity was displayed as percentage of fluorescence intensity of cells cultured on PS wells.

7.2.4 BORTEZOMIB RELEASE INTO CELL CULTURE MEDIUM AND ITS EFFICACY

(PVA+325 μ M Bort#BA-PAA) multilayers were built at 2, 4, & 10 bilayers on PDL-TCPS. On top of these multilayers, cell culture medium was distributed at 200 μ L/well. The wells were then incubated in the incubator for ~24 h. COS-7 cells were seeded on untreated PS 96-well plates at 20,000 cells/well seeding density. Following 4 h of culture in the incubator to let the cells attach, the cell culture medium was replaced with the media which had been used to incubate the multilayers. The cells were further cultured for 2 d after which an end point AB assay was performed. Metabolic activity was displayed as percentage of fluorescence intensity of cells cultured on PS in regular cell culture medium.

7.3 RESULTS AND DISCUSSION

7.3.1 MULTILAYERED THIN FILM BUILD-UP

We have reported previously the syntheses of two randomly branched boronic acid- (BA-) functionalized poly(amido amine)s (BA-PAA)s (Chapter 5). The Degree of BA functionalization for the two BA-PAA)s were similar at ~50%, with branching estimated to be ~10 and ~30% for DAB-BA-PAA and ABOL-BA-PAA, respectively, and number average molecular weight of 12 and 14 kg/mol, respectively. Chemical structures of the two BA-PAA polymers, poly(vinyl alcohol) (PVA), and bortezomib utilized in this study are presented in Chart 7.1.

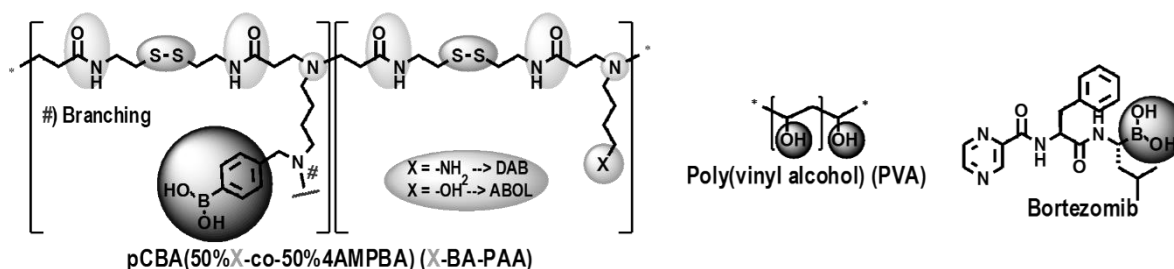


Chart 7.1 Chemical structures of DAB-BA-PAA, ABOL-BA-PAA, PVA, and bortezomib.

The incorporation of bortezomib in the multilayer was achieved during build-up of the layers by mixing bortezomib into the PVA deposition solution in PBS buffer pH 7.4. The PVA concentration in this deposition solution was 2.0 mg/mL, consistent with the previous experiment to prepare multilayered system without bortezomib (Chapter 5). At this PVA concentration we found that a final bortezomib concentration of 1300 μ M was achievable without visible aggregation or precipitation of the drug. It is expected that PVA may also help increase the solubility of bortezomib through the possible boronate ester formation. The boronate ester formation between the boronic acid (BA) of bortezomib and diol of PVA is represented in Scheme 7.1a. As previously indicated, the BA moieties in BA-PAA)s also form boronate ester with diols of PVA as the main driving force for multilayer formation. However, as the diol moiety in PVA is present in excess in the deposition solution, it was expected that multilayer build up could still proceed. The relatively high concentration of bortezomib in the deposition solution was chosen to statistically increase the possibility for incorporation.

Figure 7.1a shows build-up profiles of DAB-BA-PAA-(PVA+Bort#DAB-BA-PAA)₁₀ and ABOL-BA-PAA-(PVA+Bort#ABOL-BA-PAA)₁₀ based on the increase of absorbance values at 227 nm (attributed to the phenyl ring of BA-PAA). The build-up profiles of DAB-BA-PAA-(PVA#DAB-BA-PAA)₁₀ and ABOL-BA-PAA-(PVA#ABOL-BA-PAA)₁₀ (originally shown in Chapter 5) are also shown for reference. From this figure it can be seen that the build-up profiles were similar for systems with and without bortezomib in the PVA deposition solutions. Likewise, the UV spectra (Figure 7.1b, inset) of the 10-bl multilayers also show no significant difference between films with and without bortezomib. Nevertheless, the 20 times diluted (PVA+Bort) deposition solution clearly shows a distinctive absorption peak at 270 nm, with relatively on par extinction coefficient with the phenyl peak of BA-PAA at the respective deposition solution concentrations. The *molar* extinction coefficient of bortezomib itself is approximately twice that of BA-PAA. This indicates that the multilayer either did not contain bortezomib, or the bortezomib was present at low concentration not sensitive enough for UV spectroscopy measurements. Therefore, to further gain insights on the presence of bortezomib in the as prepared multilayers, 0.36 M alizarin red S (ARS) in phosphate buffer solution was used to incubate the films. ARS contains a catechol moiety and is known to form a strong boronate ester with boronic acid, which would in turn renders the boronate ester fluorescence [38]. Assuming that there is no significant difference in the amount of BA-PAA incorporated for 10 bl of films with and without bortezomib, a higher fluorescence intensity of the Bort-containing films would indicate presence of bortezomib in the films. Indeed, we found that non-bortezomib films showed lower fluorescence values (data not shown). The difference was statistically significant, but was not very pronounced, most likely

attributed to the generally low amount of bortezomib and the likely lower binding coefficient of ARS to bortezomib, as compared to phenylboronic acid in BA-PAA, for example.

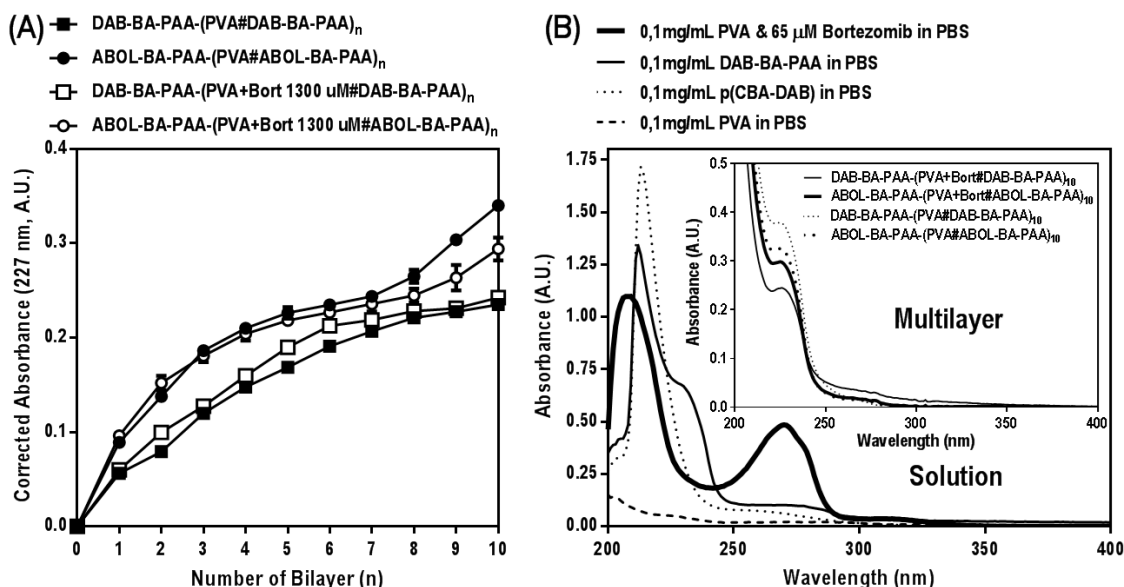


Figure 7.1 (A) Build-up profiles (left) and (B, inset, $n = 10$) UV spectra of DAB-BA-PAA-(PVA+Bort#DAB-BA-PAA)_n and ABOL-BA-PAA-(PVA+Bort#ABOL-BA-PAA)_n and respective non-Bort systems in the dry state based on the absorbance values at 227 nm. (B) Solution-state UV spectra of (relevant) multilayer components.

It needs to be noted that the bortezomib concentration used for the multilayer build-up is much higher than the concentrations used in other *in vitro* cell culture studies [39-42]. Indeed when it is assumed that the bortezomib concentration that is incorporated in the multilayer films is actually lowered down to nM range due to loss during the subsequent washing steps and dipping in the PVA polymer solution, it can be expected that the peak at 270 nm would not be visible anymore. Therefore, based on these considerations and the indications of bortezomib presence obtained from the ARS fluorescence studies, it was expected that there was a good possibility that bortezomib was still incorporated in a sufficient amount to exert a pharmacological effect. Other means of analytical determination of incorporated bortezomib need to be considered for future studies for more precise characterizations.

7.3.2 KINETICS OF *IN VITRO* THERAPEUTIC EFFICACY OF BORTEZOMIB-CONTAINING MULTILAYERS

As previously described, treatment of cells with bortezomib causes the cells to undergo apoptosis due to bortezomib inhibition of proteasome activity. This effect can be easily detected as a cessation in the metabolic activity of the cells cultured on the surface of the multilayers. To this purpose, we first followed the change in metabolic activity throughout a culture duration to determine a minimal treatment duration after which an end point measurement can be carried out. The non-toxic feature of AlamarBlue (AB) assay makes it possible to follow cells' metabolic activity without affecting or terminating cell growth. For a valid result, the assay needs to be optimized for the specific treatment, cell lines, and desired duration.



We intended to follow the cell metabolic activity for at least 3 days following one-time addition of AB reagent. Therefore, an optimal cell seeding density is needed where the cells would give an increasing response of fluorescence intensity, indicating stable growth throughout the 3 days of culture. Figure 7.2 shows the resorufin (metabolically reduced AB reagent) fluorescence intensity from COS-7 cells cultured at various cell seeding densities over 73 h duration. By maintaining the same instrument settings and AB content, it was found that ~400 cells/well was the optimal seeding density for cumulative increase in fluorescence intensity for 3 day-long culture duration.

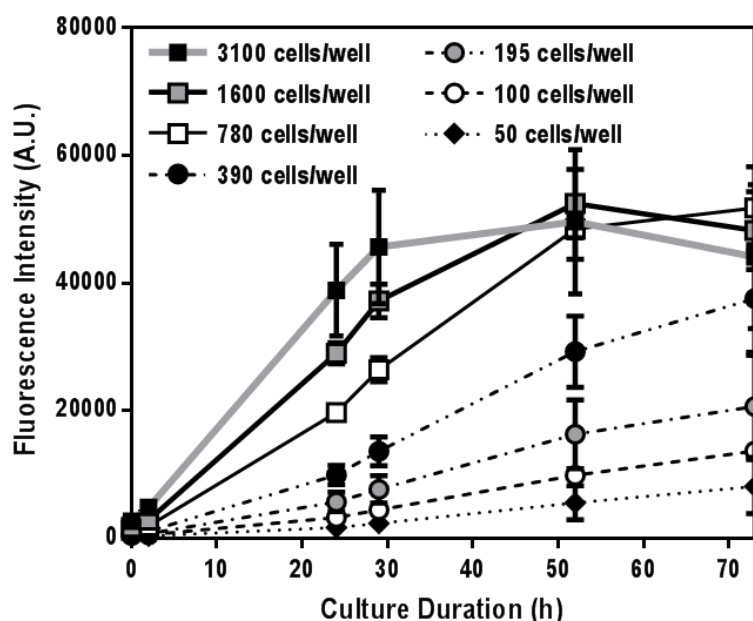


Figure 7.2 COS-7 cell seeding density optimization for repeated monitoring of metabolic activity up to 73 h of culture.

Next, using the optimal cell seeding density, COS-7 cells were cultured on the four multilayers, i.e. two BA-PAA, with and without 1300 μM bortezomib in the PVA deposition solutions. Figure 7.3 shows the cumulative changes in the amount of metabolically reduced AB reagent in the four different systems. The figure indicates that COS-7 cells cultured on non-Bort multilayers continuously grew throughout the 61 h culture duration. This result was in agreement with the results in Chapter 5 where the 10-bl (PVA#BA-PAA) multilayers were found to not show significant cytotoxic effect on cells growing on the surface. However, due to the very low seeding density used for this experiment, the cells were most likely in the lag phase of the growth profile as indicated by linear increase in metabolic activity over time. On the other hand, Bort-containing multilayered systems showed increasing fluorescence intensity only for the first 20 h of culture, where the increase was relatively similar to that of non-Bort systems. Following the first 20 h of culture, the increase declined significantly, indicating that most of the cells were no longer metabolically active, and so the fluorescence signal stayed relatively stable. Notably, at 22 h time point the metabolic activity of cells cultured on bortezomib-containing systems were roughly 86% of non-Bort multilayers', decreasing further to ~58% at 40 h data point and to ~42% at the end of the 61 h culture period. Figure 7.3 also shows that bortezomib was indeed present in the multilayers and that 2 d culture duration was sufficient to conduct end point measurements of metabolic activity. Following 2 d culture duration, the optimal therapeutic effect has been reached, relative to the controls.

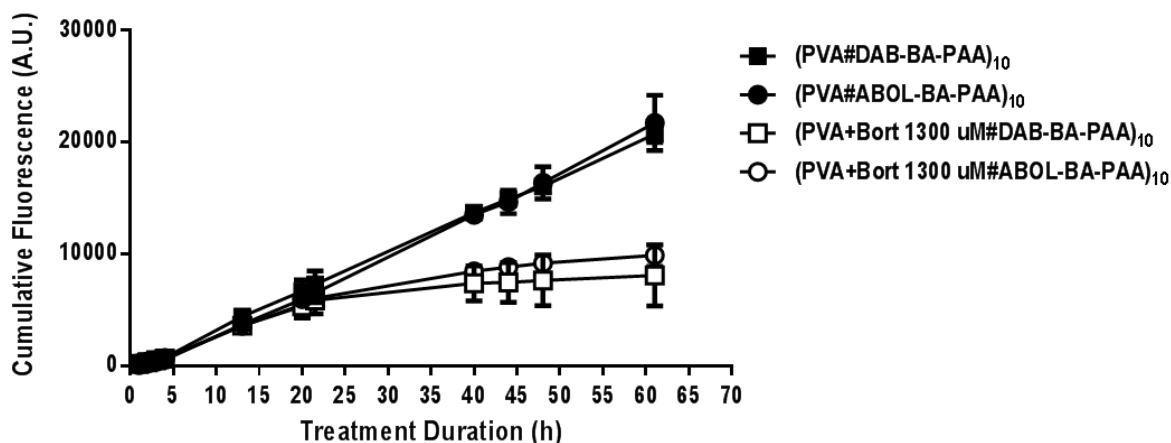


Figure 7.3 Cumulative metabolic activity changes of COS-7 cells cultured on multilayers with and without bortezomib.

To further confirm that the effect observed in Figure 7.3 was not due to the low seeding density, the experiment was repeated using the normal cell seeding density of 20,000 cells/well. Cells were cultured for 2 days after which the AB assay was applied for an end point metabolic activity measurement. For end point measurements, metabolic activity is shown as the percentage of fluorescence intensity of a sample relative to that of control cells cultured on untreated PS wells. Figure 7.4 confirms the result shown in Figure 7.3, where the metabolic activity of cells cultured on Bort-containing multilayers were significantly lower than the cells cultured on Bort-free multilayers.

From other controls in Figure 7.4, it can be seen that adding 1300 μM free bortezomib directly to cells cultured on non-Bort films resulted in a slightly lower bortezomib efficacy compared to when the same amount of bortezomib is added to cells without the presence of any multilayered system. This signifies the affinity of bortezomib for the multilayers. It needs to be noted that for these controls, bortezomib was added at the same concentration of the bortezomib in deposition solution. These controls represent the full extent of bortezomib efficacy should all of the bortezomib in the deposition solution be incorporated to and released from the films. As previously mentioned, this bortezomib concentration is much higher than those normally used for *in vitro* cell culture studies, giving the effect of complete inhibition of cell growth. It is also interesting to note, albeit still within the error bars, that the presence of free PVA in the Bort solution reduce its efficacy, signifying Bort-PVA interactions that affect Bort's pharmacological behavior.

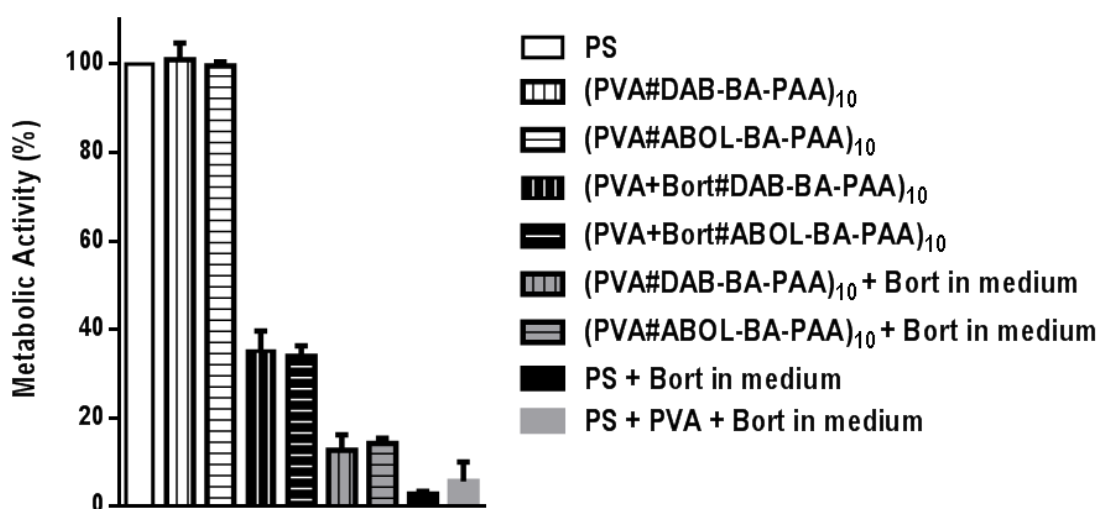


Figure 7.4 End point AB assay of cells cultured for 2 days with different treatment conditions.

Since the BA moiety in bortezomib is involved in its interaction to inhibit proteasome [25], it can be expected that at least the majority of released bortezomib has to be available in its free form without boronate ester formation with PVA to induce optimal therapeutic effects. From the obtained results, it is too early to speculate on the specific mechanism in which bortezomib is released from the films. However, it is worth mentioning that it has been reported previously that ABOL-BA-PAA may spontaneously form stable nanoparticles under physiological conditions that may facilitate cellular uptake of ARS (i.e. a reporter molecule bearing a catechol for strong boronate ester formation with BA moieties) [34]. Chapter 6 also demonstrates that the multilayers may release particles under physiological conditions which contain a boronate ester of BA-PAA and ARS. It can therefore be postulated that bortezomib may be released both in a complexed particle form through partial dissolution of the multilayered film and in free form through diffusion from the multilayers. The latter is also supported by the supposedly weaker binding constant of aliphatic BA of bortezomib to PVA diols. Subsequently, release of free bortezomib from these particles may be facilitated by the acidic endosomal pH which would dissociate the boronate ester anion into free bortezomib and trigonal boronic acid [19].

7.3.3 EFFECT OF DIFFERENT BORTEZOMIB CONCENTRATION

To understand whether the bortezomib concentration in the deposition solution has an effect on the therapeutic efficacy of the multilayers, multilayers were built with different bortezomib concentrations in the same PVA deposition solutions. COS-7 cells were then cultured at 20,000 cells/well seeding density for 2 days after which an end point metabolic activity measurement was carried out. Figure 7.5 shows that the multilayers more effectively reduce metabolic activity when the bortezomib concentration in the deposition solution is increased. This result indicates that bortezomib concentration in the deposition solution can be used to tune the efficacy of the multilayers.

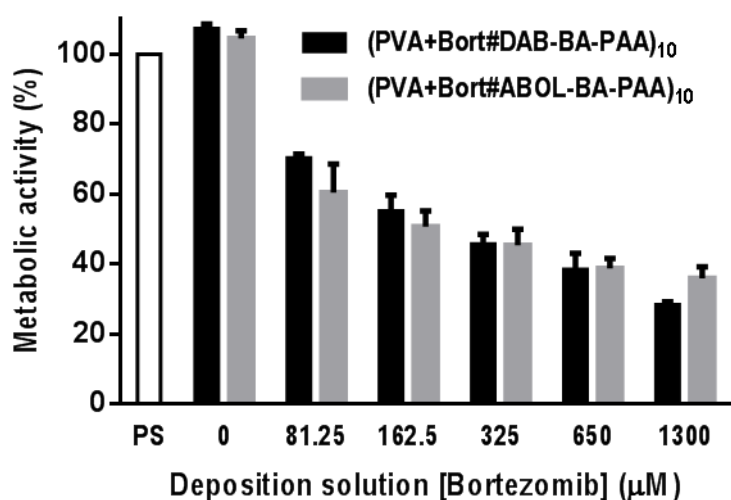


Figure 7.5 Effect of different bortezomib deposition concentrations on the therapeutic efficacy of the multilayers (metabolic activity).

7.3.4 EFFECT OF BILAYER NUMBERS

To investigate whether the number of bilayers may as well affect the efficacy of the film, 2, 5, 7, and 10-bilayered multilayers prepared using three different bortezomib concentrations (i.e. 81.25, 325, and 1300 μM) were used as substrates for COS-7 cell culture for 2 days after which an end point AB assay was performed. Figure 7.6 shows that for the three different bortezomib concentrations used, different numbers of bilayers did not significantly change the efficacy of the multilayers. In average, the metabolic activity decreases only by $\sim 13\%$ from 2 bl to 10 bl, with bigger effect observed for the lowest bortezomib concentration used. Although Figure 7.1 indicates that build up typically slows down after the fifth cycle of deposition, a 2-bilayered multilayer would still contain at least $\sim 60\%$ less materials than a 10-bilayered multilayer. Therefore, if bortezomib is released into cell culture medium proportionally to the bilayer number, a 2-bl multilayer should reduce significantly less metabolic activity compared to a 10-bl multilayer. The results therefore may indicate the pronounced effect of the surface instead of the total amount of incorporated bortezomib. Multilayers prepared with higher bortezomib concentration would have more bortezomib localized on every layer, including the surface than those prepared with lower bortezomib concentration. It seems that the majority of the multilayer therapeutic efficacy is provided by these surface-localized bortezomib, with diffusion playing very minor role, causing the slight increase in efficacy with increasing bilayer numbers.

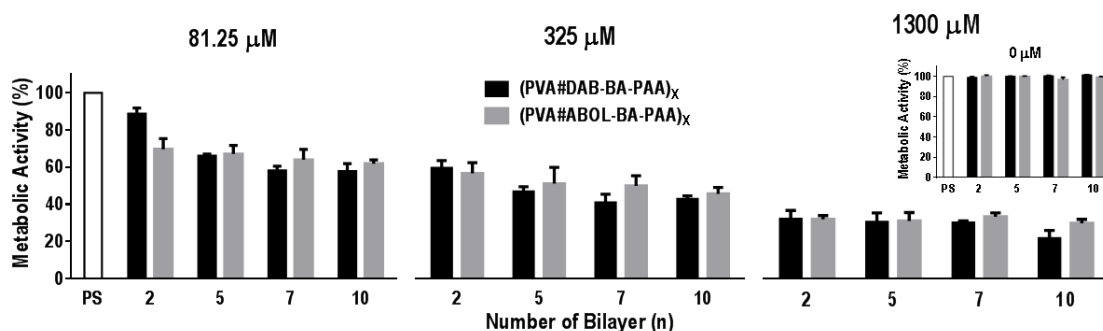


Figure 7.6 Effect of number of bilayers on multilayer efficacy, studied at 3 different bortezomib concentrations i.e. 81.25, 325, and 1300 μM , inset shows the control experiments for non-Bort systems.

7.3.5 BORTEZOMIB RELEASE INTO CELL CULTURE MEDIUM

To understand how the different Bort-containing multilayers induce cellular uptake of bortezomib that leads to decrease in metabolic activity, an experiment was carried out where cells cultured for 4 h on untreated PS wells (i.e. healthy cells) were treated with cell culture medium which had been exposed for 24 h in the cell culture incubator to Bort-containing multilayers. These media, further referred to as **release medi(a)um**, might contain bortezomib (either free or in complexed particle form) that were **released** from the multilayers. Figure 7.7 indicates that there is a clear dose response in the efficacy of the release medium based on the number of bilayers of multilayered system from which the release medium was obtained. The 10-bl release media induced significantly higher efficacy than the release media from 4-bl multilayers. The 2-bl release media, on the other hand, was not found to have enough active bortezomib to induce significant therapeutic effect.

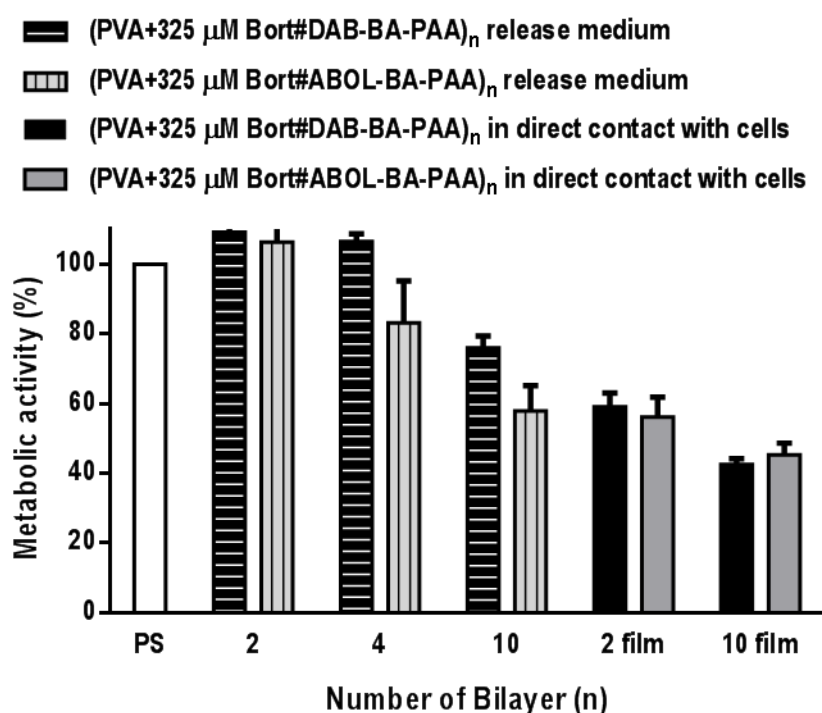


Figure 7.7 Therapeutic efficacy (metabolic activity) of bortezomib release media from various multilayers. White bar: negative control with cells cultured on untreated PS wells without film or bortezomib. Striped bars: relative metabolic activity of cells cultured as with negative controls and treated with release media from films of various bilayer numbers. Black and grey bars: metabolic activity of cells cultured directly on the multilayered surface at various bilayer numbers.

It is very interesting how different the efficacy of a Bort-multilayer can be depending on whether cells are put directly or indirectly in contact with the multilayers. As shown in Figure 7.7, when used in direct contact, a 2-bl multilayer induced very significant therapeutic effect not achievable using only the release medium. On the other hand, a 10-bl multilayers induced only slightly higher therapeutic effect than a 2-bl when used in direct contact, but provided much higher efficacy through the release medium. This phenomenon indicates that in addition to the very efficient cellular contact-uptake explained in the previous section, the multilayers can also be used to provide dose-responsive release of active materials for additional effect on cells located farther away from or not in direct contact with the multilayered surface.

The two modes of action of the multilayer-based therapy reported in this study are illustrated in Figure 7.8. Cells in direct contact with the multilayers may benefit more from the high localization of bortezomib on the surface. In this condition, the bortezomib also has higher chance of being released in boronate ester form with PVA and/or

BA-PAA. This is especially prominent when comparing the striking difference in efficacy of 2-bilayered multilayers when used in direct and indirect contact with the cells (Figure 7.7). Cells in direct contact receive the maximal therapeutic efficacy which mainly depends on the bortezomib concentration in the deposition solution, but not on the total amount of bortezomib incorporated in the film. If the enhanced efficacy of direct contact is provided solely through a concentration gradient of bortezomib during diffusion out of the multilayer, then the effect should also be significantly enhanced by higher number of bilayers. Thus, we hypothesize that direct contact facilitates more uptake of bound bortezomib which maximizes therapeutic efficacy, for example through electrostatic interaction of positively-charged bortezomib-polymer particle complexes which promote cellular uptake followed by facilitated endosomal escape [36, 37]. Polymer-complexed bortezomib may be released as a result of multilayer rearrangement and/or as a result of enzymatic activities on cellular membranes [6, 43].

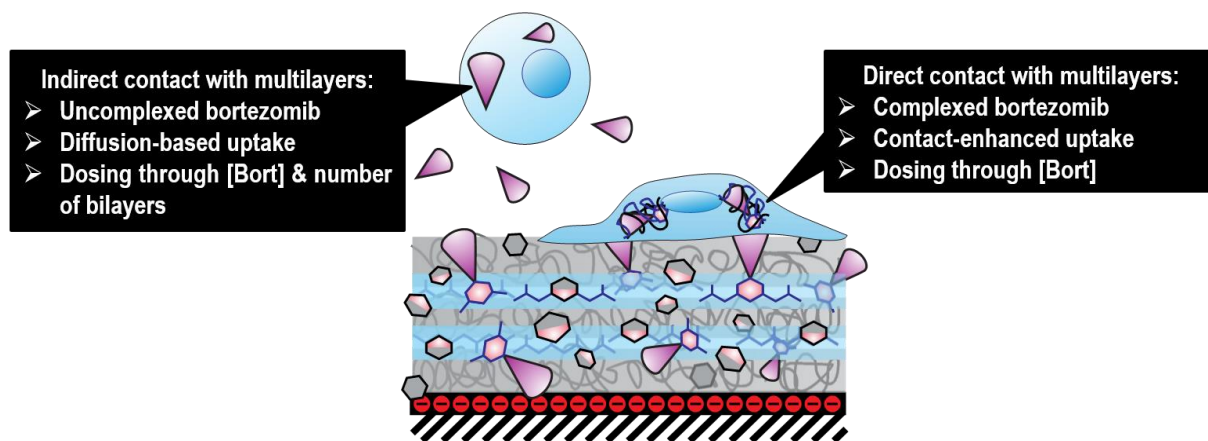


Figure 7.8 Illustration of bortezomib uptake by cells in indirect and direct contact with the multilayers.

Cells not in contact with the surface of the multilayers may only take up materials that are released from the multilayers. Although bortezomib may be released in particle-complexed form, these particles would have to travel longer distance and/or stay stable for longer period before being internalized by cells. Therefore, diffusion of free bortezomib can be expected to take place to higher extent, resulting in direct dependence of multilayer efficacy on the number of bilayers.

For a specific application, the multilayer can be designed in two separate ways. Firstly, through the concentration of therapeutic agent in the deposition solution which mainly govern the extent of therapeutic efficacy for cells directly in contact with the multilayer surface. And secondly, through the number bilayers which mainly governs the extent of therapeutic efficacy for cells farther away from the multilayer surface. One could also imagine that by adding additional barrier layers (i.e. multilayers without bortezomib), the cascade of release and their respective extent can also be tuned.

Regarding the two different BA-PAA, we have observed from the results that there is not much difference in the multilayer efficacy based on the types of BA-PAA used. Although the build-up profiles shown in Figure 7.1 indicated slightly higher deposition of DAB-BA-PAA multilayers, the build-up was characterized based on the amount of phenyl groups of BA-PAA deposited, and therefore did not signify the amount of incorporated bortezomib. More thorough investigation in the mechanism of cellular uptake, for example via fluorescence labeling of PVA, BA-PAA, and/or bortezomib is needed to further understand and optimize the efficacy of these multilayers.

7.4 CONCLUSIONS

Multilayers of branched copolymer of boronic acid-functionalized poly(amido amine)s (BA-PAA)s and poly(vinyl alcohol) (PVA) have been investigated to incorporate bortezomib through parallel loading with bortezomib mixed into PVA deposition solution. Based on UV spectroscopy, the build-up profiles showed no significant difference in multilayers with and without bortezomib, which likely signify the low amount of incorporated bortezomib into the multilayers.

To further investigate whether the multilayers did contain sufficient amounts of bortezomib to induce apoptosis as its therapeutic effect, AlamarBlue (AB) assay was performed where the change in metabolic activity was followed for up to 61 h of culture. COS-7 cells cultured directly on the surface of multilayers with and without bortezomib initially showed similar increase in metabolic activity for the initial 20 h. However, after this period the cells cultured on bortezomib-containing multilayers showed ceased metabolic activity, indicating that most of the cells had undergone apoptosis. On the other hand, metabolic activity of cells cultured on multilayers without bortezomib kept increasing linearly throughout the 61 h of culture duration. This result was confirmed not to be the effect of low cell seeding density used to maintain linear response of the AB reagent. In an end point experiment, COS-7 cells cultured at 20,000 cells/mL (i.e. optimal seeding density) on (PVA+1300 μ M Bort#BA-PAA)s₁₀ showed at least 80-90% less metabolic activity compared to those cultured on (PVA#BA-PAA)s₁₀ alone.

Furthermore, the multilayer efficacy was found to be dependent on the bortezomib concentration in the deposition solution, with higher efficacy at higher bortezomib concentration. This finding indicates that the amount of incorporated bortezomib in the layers directly correlates with the bortezomib concentration in the deposition solution. Remarkably, the bortezomib efficacy was found to be only slightly affected by the number of bilayers when cells were cultured directly on the multilayers. These led to the conclusion that the concentration of localized bortezomib molecules on the surface play a dominant role in the multilayer efficacy. The only slight effect of the number of bilayers indicates that diffusion of bortezomib out of the multilayers has the less pronounced effect. To further understand the effect of passive diffusive release of bortezomib from the multilayers, an experiment was carried out where cells were treated with release medium that had been used to incubate bortezomib-containing multilayers at various bilayer numbers. It was found that the efficacy of the release medium was dependent on the number of bilayers of the multilayer with which the medium had been incubated. Lower number of bilayers results in less decrease in metabolic activity, and vice versa. These results indicate the possibility of dual release mechanisms. Firstly, cells that are in contact with the multilayers receive highly localized treatment where the effective dose depends on the bortezomib concentration in the deposition solution. Secondly, cells farther away from the multilayered surface receive diffusive-like treatment where effective dose depends both on bortezomib concentration in deposition solutions and on the number of bilayers.

It was acknowledged that bortezomib needs to be in its free form to play its role to inhibit proteasome. Therefore, regarding the mechanism of release, it was also postulated that the multilayers may release bortezomib both in its particle-complexed form and in its free form through diffusion. Complexed bortezomib was hypothesized to be released in the lower pH of endosomal vesicles. Nevertheless, further studies in the release mechanism of bortezomib from the multilayers still need to be thoroughly investigated.

The results present a probability in developing a multilayered surface with dual tunable release profiles and dosages. Additionally, these multilayers are also responsive to pH, reducing agents, and other diol-containing molecules. These latter properties have not been investigated in the current study but may provide an exciting opportunity for various demanding biomedical applications.

7.5 REFERENCES

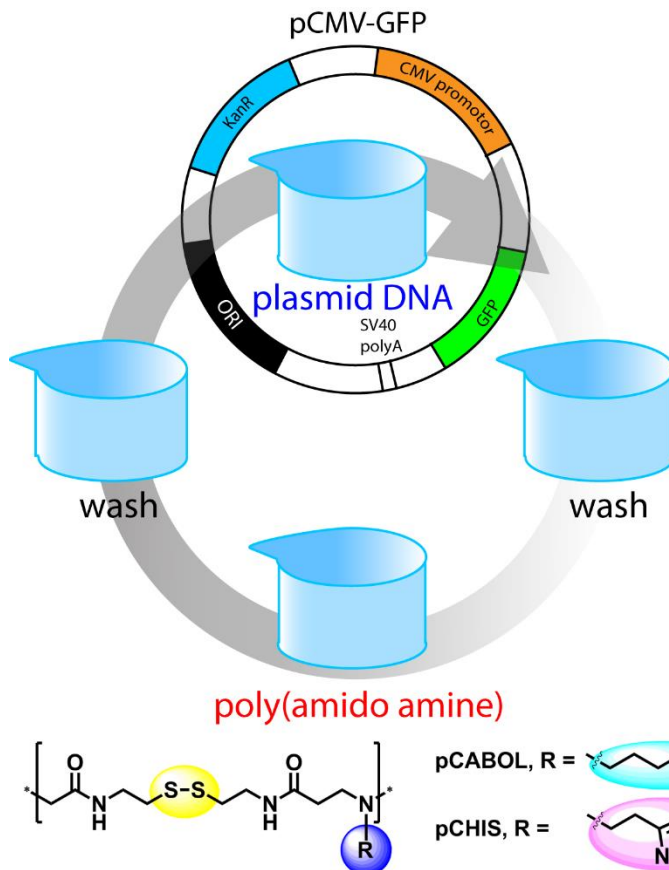
- [1] P.T. Hammond, Building biomedical materials layer-by-layer, *Mater Today*, 15 (2012) 196-206.
- [2] K. Ariga, Y. Yamauchi, G. Rydzek, Q. Ji, Y. Yonamine, K.C.W. Wu, J.P. Hill, Layer-by-layer Nanoarchitectonics: Invention, Innovation, and Evolution, *Chem. Lett.*, 43 (2014) 36-68.
- [3] J.A. Lichter, K.J. Van Vliet, M.F. Rubner, Design of Antibacterial Surfaces and Interfaces: Polyelectrolyte Multilayers as a Multifunctional Platform, *Macromolecules*, 42 (2009) 8573-8586.
- [4] E.M. Saurer, R.M. Flessner, S.P. Sullivan, M.R. Prausnitz, D.M. Lynn, Layer-by-Layer Assembly of DNA- and Protein-Containing Films on Microneedles for Drug Delivery to the Skin, *Biomacromolecules*, 11 (2010) 3136-3143.
- [5] D. Richard, I. Nguyen, C. Affolter, F. Meyer, P. Schaaf, J.C. Voegel, D. Bagnard, J. Ogier, Polyelectrolyte multilayer-mediated gene delivery for semaphorin signaling pathway control, *Small*, 6 (2010) 2405-2411.
- [6] J. Blacklock, Y.Z. You, Q.H. Zhou, G. Mao, D. Oupicky, Gene delivery in vitro and in vivo from bioreducible multilayered polyelectrolyte films of plasmid DNA, *Biomaterials*, 30 (2009) 939-950.
- [7] K.F. Ren, T. Cruzier, C. Roy, C. Picart, Polyelectrolyte multilayer films of controlled stiffness modulate myoblast cell differentiation, *Adv. Funct. Mater.*, 18 (2008) 1378-1389.
- [8] I.C. Lee, Y.-C. Wu, Assembly of Polyelectrolyte Multilayer Films on Supported Lipid Bilayers To Induce Neural Stem/Progenitor Cell Differentiation into Functional Neurons, *ACS Appl. Mater. Interfaces*, (2014).
- [9] P.-W. Fu, S.-Y. Wang, Y.-R. Chen, C.-M. Lo, Cardiomyocyte differentiation of mouse iPSCs regulated by polypeptide multilayer films (1180.21), *The FASEB Journal*, 28 (2014).
- [10] J. Hong, L. Alvarez, N. Shah, Y. Cho, B.-S. Kim, L. Griffith, K. Char, P. Hammond, Multilayer thin-film coatings capable of extended programmable drug release: application to human mesenchymal stem cell differentiation, *Drug Deliv. and Transl. Res.*, 2 (2012) 375-383.
- [11] I.C. Lee, Y.-C. Wu, Facilitating neural stem/progenitor cell niche calibration for neural lineage differentiation by polyelectrolyte multilayer films, *Colloids and Surfaces B: Biointerfaces*, 121 (2014) 54-65.
- [12] M.S. Niepel, D. Peschel, T. Groth, Controlling fibroblast adhesion with pH modified polyelectrolyte multilayers, *International Journal of Artificial Organs*, 34 (2011) 185-191.
- [13] L. Richert, F. Boulmedais, P. Lavallo, J. Mutterer, E. Ferreux, G. Decher, P. Schaaf, J.-C. Voegel, C. Picart, Improvement of Stability and Cell Adhesion Properties of Polyelectrolyte Multilayer Films by Chemical Cross-Linking, *Biomacromolecules*, 5 (2003) 284-294.
- [14] W.-B. Tsai, Y.-H. Chen, H.-W. Chien, Collaborative Cell-Resistant Properties of Polyelectrolyte Multilayer Films and Surface PEGylation on Reducing Cell Adhesion to Cytophilic Surfaces, *Journal of Biomaterials Science-Polymer Edition*, 20 (2009) 1611-1628.
- [15] K. Ren, L. Fourel, C.G. Rouvière, C. Albiges-Rizo, C. Picart, Manipulation of the adhesive behaviour of skeletal muscle cells on soft and stiff polyelectrolyte multilayers, *Acta Biomater.*, 6 (2010) 4238-4248.
- [16] V. Karagkiozaki, E. Vavoulidis, P.G. Karagiannidis, M. Gioti, D.G. Fatouros, I.S. Vizirianakis, S. Logothetidis, Development of a nanoporous and multilayer drug-delivery platform for medical implants, *Int. J. Nanomed.*, 7 (2012) 5327-5338.
- [17] R.C. Smith, M. Riollano, A. Leung, P.T. Hammond, Layer-by-Layer Platform Technology for Small-Molecule Delivery, *Angew. Chem. Int. Ed.*, 48 (2009) 8974-8977.
- [18] B. Thierry, P. Kujawa, C. Tkaczyk, F.M. Winnik, L. Bilodeau, M. Tabrizian, Delivery Platform for Hydrophobic Drugs: Prodrug Approach Combined with Self-Assembled Multilayers, *J. Am. Chem. Soc.*, 127 (2005) 1626-1627.
- [19] G. Springsteen, B. Wang, A detailed examination of boronic acid-diol complexation, *Tetrahedron*, 58 (2002) 5291-5300.
- [20] D.G. Hall, Structure, Properties, and Preparation of Boronic Acid Derivatives. Overview of Their Reactions and Applications, in: *Boronic Acids*, Wiley-VCH Verlag GmbH & Co. KGaA, 2006, pp. 1-99.
- [21] W.Q. Yang, X.M. Gao, B.H. Wang, Boronic acid compounds as potential pharmaceutical agents, *Medicinal Research Reviews*, 23 (2003) 346-368.
- [22] P.C. Trippier, C. McGuigan, Boronic acids in medicinal chemistry: anticancer, antibacterial and antiviral applications, *MedChemComm*, 1 (2010) 183-198.
- [23] B.A. Teicher, G. Ara, R. Herbst, V.J. Palombella, J. Adams, The proteasome inhibitor PS-341 in cancer therapy, *Clinical Cancer Research*, 5 (1999) 2638-2645.
- [24] P.G. Richardson, P. Sonneveld, M.W. Schuster, D. Irwin, E.A. Stadtmauer, T. Facon, J.-L. Harousseau, D. Ben-Yehuda, S. Lonial, H. Goldschmidt, D. Reece, J.F. San-Miguel, J. Bladé, M. Boccadoro, J. Cavenagh, W.S. Dalton, A.L. Boral, D.L. Esseltine, J.B. Porter, D. Schenkein, K.C. Anderson, Bortezomib or High-Dose Dexamethasone for Relapsed Multiple Myeloma, *New England Journal of Medicine*, 352 (2005) 2487-2498.
- [25] M. Groll, C.R. Berkers, H.L. Ploegh, H. Ova, Crystal Structure of the Boronic Acid-Based Proteasome Inhibitor Bortezomib in Complex with the Yeast 20S Proteasome, *Structure*, 14 (2006) 451-456.
- [26] Y. Wang, A.K. Rishi, V.T. Puliappadamba, S. Sharma, H.J. Yang, A. Tarca, Q.P. Dou, F. Lonardo, J.C. Ruckdeschel, H.I. Pass, A. Wali, Targeted proteasome inhibition by Velcade induces apoptosis in human mesothelioma and breast cancer cell lines, *Cancer Chemother. Pharmacol.*, 66 (2010) 455-466.

- [27] J. Adams, M. Behnke, S. Chen, A.A. Cruickshank, L.R. Dick, L. Grenier, J.M. Klunder, Y.-T. Ma, L. Plamondon, R.L. Stein, Potent and selective inhibitors of the proteasome: Dipeptidyl boronic acids, *Bioorg. Med. Chem. Lett.*, 8 (1998) 333-338.
- [28] T. Hideshima, P. Richardson, D. Chauhan, V.J. Palombella, P.J. Elliott, J. Adams, K.C. Anderson, The proteasome inhibitor PS-341 inhibits growth, induces apoptosis, and overcomes drug resistance in human multiple myeloma cells, *Cancer Res.*, 61 (2001) 3071-3076.
- [29] T. Hideshima, C. Mitsiades, M. Akiyama, T. Hayashi, D. Chauhan, P. Richardson, R. Schlossman, K. Podar, N.C. Munshi, N. Mitsiades, K.C. Anderson, Molecular mechanisms mediating antimyeloma activity of proteasome inhibitor PS-341, 2003.
- [30] E. Suzuki, S. Demo, E. Deu, J. Keats, S. Arastu-Kapur, P.L. Bergsagel, M.K. Bennett, C.J. Kirk, Molecular Mechanisms of Bortezomib Resistant Adenocarcinoma Cells, *Plos One*, 6 (2011).
- [31] S. Lu, J. Wang, The resistance mechanisms of proteasome inhibitor bortezomib, *Biomarker research*, 1 (2013) 13-13.
- [32] B. Piperdi, Y.-H. Ling, L. Liebes, F. Muggia, R. Perez-Soler, Bortezomib: Understanding the Mechanism of Action, *Molecular Cancer Therapeutics*, 10 (2011) 2029-2030.
- [33] FDA-CDER, Application Number: 21-602 Clinical Pharmacology and Biopharmaceutics Review(s), in, FDA Maryland, 2003.
- [34] M. Piest, M. Ankoné, J.F.J. Engbersen, Carbohydrate-interactive pDNA and siRNA gene vectors based on boronic acid functionalized poly(amido amine)s, *J Control Release*, 169 (2013) 266-275.
- [35] C.C. Scott, F. Vacca, J. Gruenberg, Endosome maturation, transport and functions, *Seminars in Cell & Developmental Biology*, 31 (2014) 2-10.
- [36] H.K. Shete, R.H. Prabhu, V.B. Patravale, Endosomal Escape: A Bottleneck in Intracellular Delivery, *J. Nanosci. Nanotechnol.*, 14 (2014) 460-474.
- [37] A.K. Varkouhi, M. Scholte, G. Storm, H.J. Haisma, Endosomal escape pathways for delivery of biologicals, *J Control Release*, 151 (2011) 220-228.
- [38] G. Springsteen, B.H. Wang, Alizarin Red S. as a general optical reporter for studying the binding of boronic acids with carbohydrates, *Chem. Commun.*, (2001) 1608-1609.
- [39] C. Li, Y. He, S. Nicolson, M. Hirsch, M.S. Weinberg, P. Zhang, T. Kafri, R.J. Samulski, Adeno-associated virus capsid antigen presentation is dependent on endosomal escape, *Journal of Clinical Investigation*, 123 (2013) 1390-1401.
- [40] E.G. Mimnaugh, W. Xu, M. Vos, X. Yuan, J.S. Isaacs, K.S. Bisht, D. Gius, L. Neckers, Simultaneous inhibition of hsp 90 and the proteasome promotes protein ubiquitination, causes endoplasmic reticulum-derived cytosolic vacuolization, and enhances antitumor activity, *Molecular cancer therapeutics*, 3 (2004) 551-566.
- [41] T.B. Shabaneh, S.L. Downey, A.L. Goddard, M. Screen, M.M. Lucas, A. Eastman, A.F. Kisselev, Molecular Basis of Differential Sensitivity of Myeloma Cells to Clinically Relevant Bolus Treatment with Bortezomib, *Plos One*, 8 (2013).
- [42] J. Codony-Servat, M.A. Tapia, M. Bosch, C. Oliva, J. Domingo-Domenech, B. Mellado, M. Rolfe, J.S. Ross, P. Gascon, A. Rovira, J. Albanell, Differential cellular and molecular effects of bortezomib, a proteasome inhibitor, in human breast cancer cells, *Molecular Cancer Therapeutics*, 5 (2006) 665-675.
- [43] L. Richert, A. Schneider, D. Vautier, C. Vodouhe, N. Jessel, E. Payan, P. Schaaf, J.-C. Voegel, C. Picart, Imaging cell interactions with native and crosslinked polyelectrolyte multilayers, *Cell Biochem Biophys*, 44 (2006) 273-285.

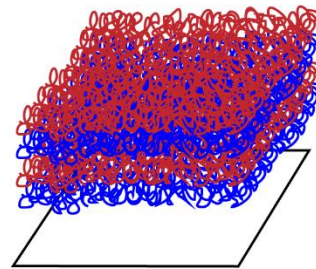
CHAPTER 8

Optimization of Poly(amido amine)-Based Multilayered Thin Films for Surface-Mediated Cell Transfection[‡]

ABSTRACT



Layer by Layer coating



Supports:

- Poly-D-lysine-coated polystyrene
- Poly(ε-caprolactone)
- Heparinized Poly(ε-caprolactone)
- Poly(lactic acid)



3D plotted scaffolds applicability

Multilayered thin films from two linear poly(amido amine)s (pCABOL and pCHIS) with functional plasmid DNA encoding for green fluorescence protein (pCMV-GFP) have been optimized for transfection efficiency of COS-7 cells cultured on top of these films. Out of the two polymers, pCABOL was found to be more superior in facilitating transfection, which was attributed to higher incorporation and release of the transfection agents from the multilayers. With pCABOL multilayers, transfection efficiency could be maintained at the optimal value throughout a wider range of seeding densities, and a higher amount of transfected cells can be obtained by simply seeding higher amount of cells. The pCABOL multilayers were further found to provide optimal transfection efficiency at 10 bilayers, where increasing number of bilayers further did not proportionally increase transfection efficiency. Using these optimal conditions, pCABOL multilayer were fabricated on poly(ε-caprolactone) (PCL), heparinized PCL (PCL-HEP), and poly(lactic acid) (PLA) disks as examples of common biomaterials. With all of the substrates investigated, transfection efficiency was found to be in the range of 25 – 50% transfected cells at the optimal seeding density and bilayer numbers. Moreover, the multilayers were found to completely mask the properties of the original substrates, with significant improvement in cell adhesion and cell shape, especially for PCL and PLA disks after multilayer coating. Finally, to demonstrate that the multilayers can be used to

[‡] Sry D. Hujaya, Giulia Marchioli, Karin Roelofs, Lorenzo Moroni, Aart A. van Apeldoorn, Jos M.J. Paulusse, Marcel Karperien, Johan F.J. Engbersen, submitted for publication.

conveniently add transfection capability to 3D scaffolds, 3D-printed fibers of PCL (with and without an additional covalent heparin layer) were utilized as substrates for multilayer formation. Scanning electron microscopy showed multilayer-coated scaffolds with a relatively thin layer conforming to the shape of the original substrates and covering smaller pores on the surface. Upon seeding of the cells into the scaffolds, significant improvement in cell adhesion was observed, especially for the PCL scaffold without heparin layer which showed very poor cell adhesion prior to the multilayer coating. Transfection was observed on both 3D PCL and PCL-HEP scaffolds, which signifies layer-by-layer dip-coating of pCABOL and functional DNA as a versatile and inexpensive method to easily add transfection capability to biomaterials of any nature and shape. This approach could be beneficial in various relevant biomedical and tissue engineering applications.

8.1 INTRODUCTION

The layer-by-layer (LbL) fabrication technique has emerged as a versatile way not only to modify or improve surface properties, but also to add extra functionalities to the surface of various biomaterials [1-4]. For example, a substantial development in tissue engineering relies on scaffolds for mechanical cell supports and many medical procedures rely on mechanical support devices such as stents, prostheses, and other implants that have specific shapes and sizes. Moreover, often these devices are made of specific biomaterials chosen for their mechanical strength and biodegradability, but does not really provide optimal performance in their interactions with cells, leading to various foreign body reactions [5]. For these instances, LbL assembly offers an option to coat various substrates with thin multilayers of functional macromolecules simply by dipping the substrates alternately between two all-aqueous solutions containing the desired macromolecules. The resulting surface can now promote or reduce cell adhesion [6-8], deliver small drugs [9-11] or therapeutic proteins [12-15], induce differentiation [16-19] and cell transfection [20-22]. Moreover, the extent and variety of material incorporation and release can be adjusted simply by adding or reducing the deposition cycles.

A promising application for LbL assembly that has recently received increasing attention is surface-mediated cell transfection [23]. As early as 1993, Lvov et al. reported the preparation of a multilayer using DNA as a building block [24]. Since then, several research groups have studied the potential of LbL-based multilayers to provide localized delivery of transcriptionally active DNA. The DNA may be deposited between the layers as it is [20, 25], or pre-complexed with polymers into polyplexes [26, 27]. Notably, surface-mediated cell transfection has been attempted on intravascular stents [28, 29], flexible stainless steel [20], poly(D-lactic acid) film [30], and microneedles [31] aimed for vaccination application [32, 33].

Multilayer coatings for surface-mediated transfection purposes on 3D scaffolds for tissue engineering have not been extensively reported. Attempts to introduce transfection capability to 3D scaffolds are mostly carried out before [34, 35] or after [36-38] seeding into the scaffolds, by loading the plasmid or polyplex into the matrix of the scaffolds [39, 40] or adsorbing on the surface [41-43]. Mineral coatings have also been reported, most notably CaP [44], which was incubated with lipoplexes to induce transfection upon cell seeding [45]. Compared to these techniques, LbL dipping technique offers the possibility to design more intricate multilayer design for prolonged or scheduled release [46] of multiple components. Moreover, the all-aqueous conditions for formation of the LbL films enable to preserve native structures of functional macromolecules. As a recent example, Holmes et al. reported multilayer coating of 3D scaffolds with multilayers of glycol-chitosan and hyaluronic acid. The multilayer-coated scaffolds were found to enhance tissue growth relative to non-coated scaffolds, and additional transfection capability could be observed by depositing a layer of DNA-containing lipoplexes [47]. Hammond and co-workers have reported the multilayer assembly on poly(lactic-co-glycolic acid) molded into microneedle arrays for transcutaneous delivery of plasmid DNA [31]. The multilayer-coated microneedles successfully induce transfection on mice *in vivo*.

To enable multilayer formation, a pair of macromolecules is needed that interact with each other. For negatively-charged DNA, a positively-charged biocompatible polymer may serve as a good counterpart. Poly(amido amine)s (PAA) are a class of peptidomimetic polymers synthesized via Michael-type addition polymerization of amines and bisacrylamides. Through the presence of amide bonds, PAAs are inherently biodegradable through hydrolysis. Moreover, through the availability of various building blocks, these polymers can also be designed to incorporate various moieties for added functionality such as charge-shift, bioreducibility, 'stealth' properties, targeting moieties, and more [48-50].

Previously, we have reported the fabrication and characterizations of multilayered thin films from linear PAAs and DNA (Chapter 3). Two PAAs, pCABOL which contains primary alcohol side chain and pCHIS with histamine side chain (see abstract figure) built up linearly with DNA into multilayers that spontaneously released polymer-DNA complexes in the presence of physiological salt concentration. The multilayers were both biocompatible and

capable to facilitate transfection on COS-7 cells cultured directly on the surface of multilayer-coated culture plates *in vitro*. In this Chapter, a study of optimization of the cell transfection efficiency of the multilayers is described, using flow cytometry as an analytical tool to determine transfection efficiency as a function of the PAA type, cell seeding density, and layer number. Finally, with the optimized conditions, surface-mediated cell transfection was attempted on poly(ϵ -caprolactone) (PCL), heparinized PCL (PCL-HEP), and poly(lactic acid) (PLA) substrates, both in 2D (disk shape) and 3D (fiber deposited PCL and PCL-HEP).

8.2 MATERIALS AND METHODS

8.2.1 CHEMICALS, SYNTHESSES AND CHARACTERIZATION

N,N'-Cystamine bisacrylamide (CBA, Polysciences), 4-amino-1-butanol (ABOL, Sigma-Aldrich, Zwijndrecht, The Netherlands), *N*-Boc-1,4-diaminobutane (NBDAB, Sigma-Aldrich, Zwijndrecht, The Netherlands), histamine dihydrochloride (HIS.2HCl, Sigma-Aldrich, Zwijndrecht, The Netherlands), calcium chloride (CaCl₂, Sigma-Aldrich, Zwijndrecht, The Netherlands), triethylamine (TEA, Sigma-Aldrich, Zwijndrecht, The Netherlands), *tert*-butylamine (*t*BA, Sigma-Aldrich, Zwijndrecht, The Netherlands), sodium dihydrogen phosphate monohydrate (NaH₂PO₄·H₂O, Merck, Darmstadt, Germany), disodium hydrogen phosphate dihydrate (Na₂HPO₄·2H₂O, Merck, Darmstadt, Germany), sodium chloride (NaCl, Sigma-Aldrich, Zwijndrecht, The Netherlands), dithiothreitol (DTT, Sigma-Aldrich, Zwijndrecht, The Netherlands), 4-(2-Hydroxyethyl)piperazine-1-ethanesulfonic acid (HEPES, Sigma-Aldrich, Zwijndrecht, The Netherlands) and glucose (Sigma-Aldrich, Zwijndrecht, The Netherlands) were purchased in the highest purity available and used as received. Solvents were of reagent grade and used without further purification unless otherwise noted. Milli-Q water was obtained from a Synergy® water purification system (Millipore). PBS buffer was prepared by dissolving 1.54 g of Na₂HPO₄·2H₂O, 0.3 g of NaH₂PO₄·H₂O, and 8.2 g of NaCl into 1 L of Milli-Q water and adjusting the pH to 7.4. HEPES buffered glucose (HBG) was prepared by dissolving 4.79 g of HEPES, and 50 g of glucose into 1 L of Milli-Q water and adjusting the pH to 7.4.

pCABOL and pCHIS were synthesized according to previous reports (Chapter 3). Briefly, *N,N'*-cystamine bisacrylamide and 4-amino-1-butanol or histamine dihydrochloride were mixed in a brown polymerization flask in an equimolar mixture using 1 mL of methanol/water 3/1 as solvent and containing 200 mM CaCl₂ as catalyst [51]. Polymerization was carried out under N₂ atmosphere for two days at 70 °C during which a gradual viscosity increase was observed. The polymerization was terminated by adding excess *tert*-butylamine into the mixture and stirring at 70 °C for two or three more days. After bringing the flask to room temperature, the solution was diluted and acidified to pH ~5 by addition of 4 M HCl and purified by ultrafiltration using a 1,000 Da MWCO membrane. The purified polymer solution was then freeze-dried leaving white transparent solid as the final product in its HCl-salt form at ~50% recovery. ¹H-NMR spectroscopy confirmed complete termination and allowed determination of the number-average MW based on the *tert*-butylamine end-group. ¹H-NMR spectra were recorded on an AVANCE III-400MHz NMR (Bruker, Wormer, The Netherlands) spectrometer. Gel permeation chromatograms were recorded on a Polymer Labs GPC 220 in 0.1 M NaOAc buffer pH 4 with 25% methanol as eluent and 0.7 mL/min flow rate against poly(ethylene glycol) (PEG) standards. pCABOL ¹H-NMR (D₂O) δ (ppm) = 1.35 (s, 9H, (CH₃)₃R); 1.60 (m, 2H, CH₂CH₂NR); 1.77 (m, 2H, CH₂CH₂OH); 2.74 (t, 4H, CH₂CONHRNHCOCH₂); 2.85 (t, 4H, CH₂SSCH₂); 3.22 (t, 2H, HO(CH₂)₃CH₂NR); 3.44 (t, 4H, NCOCH₂CH₂NRCH₂); 3.53 (t, 4H, CH₂CH₂SSCH₂CH₂); 3.62 (t, 2H, CH₂OH). ¹H-NMR end group analysis M_w = 9 kg/mol. GPC M_w = 3.8 kg/mol (M_w/M_n = 1.18). pCHIS ¹H-NMR (D₂O) δ (ppm) = 1.39 (s, 9H, (CH₃)₃R); 2.78 – 2.95 (m, 8H, CH₂CONHRNHCOCH₂ & CH₂SSCH₂); 3.23 (t, 2H, CCH₂); 3.48 – 3.80 (m, 10H, (CH₂)₃N & CH₂CH₂SSCH₂CH₂); 7.45 (s, 1H, NC=CH); 8.71 (s, 1H, N=CH). ¹H-NMR end group analysis M_w = 5.5 kg/mol. GPC M_w = 4.6 kg/mol (M_w/M_n = 1.26).

8.2.2 SUBSTRATE PREPARATION

Poly-D-lysine-coated 96-well plates (PDL-TCPS) for multilayer build-up for cell culture and transfection experiments were purchased from Greiner (Alphen aan den Rijn, The Netherlands).

Poly(lactic acid) (PLA) sheets 120 μm thick were kindly provided by Sidaplast (Ghent, Belgium) and cut in a 6 mm diameter disks with a biopsy puncher (Miltex, Rietheim - Weilheim, Germany)

Poly(ε-caprolactone) (PCL) M_w 45,000 was purchased from Sigma, (Zwijndrecht, the Netherlands). 2D disks were fabricated by placing the PCL grains in between two hydrophobic silica wafers and heating the PCL grains in a

press at 100 °C. Pressure was applied to the molten polymer. After cooling, the polymer sheet was removed from the press and disks of 6 mm in diameter were punched out from the polymer sheet with a biopsy puncher.

Poly(ϵ -caprolactone) 3D plotted scaffolds were fabricated using a rapid prototyping machine (sysENG, Germany). Scaffolds presented a toroidal shape and were 8 mm in the outer diameter and 4 mm in the inner diameter. The scaffold thickness was 1 mm. Fiber spacing was 600 μ m.

Covalent immobilization of heparin (HEP) on the PCL sheets and 3D printed PCL was performed by dissolving 1% (w/v) heparin (Sigma, Zwijndrecht, the Netherlands) in 0.05 M 2-(N-morpholino)ethanesulfonic acid (MES) buffer (Sigma, Zwijndrecht, the Netherlands) at pH 5.5. 1-Ethyl-3-(3-dimethylaminopropyl)carbodiimide (EDC) and N-Hydroxysuccinimide (NHS) (Sigma, Zwijndrecht, the Netherlands) were added at a concentration of 0.5 M to the heparin solution, vigorously stirred and added to the PCL disks. After 15 h reaction at room temperature, the disks were extensively washed with water [52, 53].

8.2.3 MULTILAYER CONSTRUCTION

Multilayers for cell culture were fabricated directly in the wells of poly-D-lysine-coated 96-well plates (PDL-TCPS, Greiner) by alternately dispensing 70 μ L of plasmid DNA (1.0 mg/mL in sterile water) and poly(amido amine) (PAA) (2.0 mg/mL in PBS pH 7.4) with washing solutions in between which consisted of the solvents of the respective deposition solutions (2x 150 μ L). The layer-by-layer (LbL) deposition was performed under sterile conditions. The DNA used to induce cell transfection was plasmidic DNA pCMV-GFP (PlasmidFactory, Bielefeld, Germany) at 1.0 mg/mL concentration in sterile water. The resulting ensemble is denoted by (pCMV-GFP#PAA)_n, where PAA represents the identity of the poly(amido amine) used and **n** represents the number of bilayer. Typically, the ensemble consists of 10 bilayer with the plasmid DNA as first layer. Deposition started with pCMV-GFP (30 min for the first layer, 10 min next) to a total of 10 bilayers, ending with the PAA layer. No intermediate drying steps were applied. At the end of the fabrication process, the plates were briefly left inside the laminar flow hood to allow the films to dry. Coated plates were kept at 4 °C and used as soon as possible (typically overnight).

LbL assembly on the 2D disks and 3D plotted constructs was carried out by alternate dipping of the PCL and PCL-HEP constructs in sufficient volume of 2.0 mg/mL pCABOL and 1.0 mg/mL pCMV-GFP solutions. Unlike for multilayer fabrication on PDL-TCPS, deposition on 2D and 3D constructs started with pCABOL layer as a precursor layer with 30 min deposition duration. Next deposition steps were 10 minutes long followed by two washing steps for 1 minutes each. Typical multilayer on 2D and 3D constructs is denoted by pCABOL-(pCMV-GFP#pCABOL)₁₀ to indicate the presence of a pCABOL layer as a precursor layer that is excluded from the bilayer count. Multilayer-coated 2D disks were glued on the bottom of regular polystyrene 96-well plates using silicone glue. For 3D scaffolds, three scaffolds were simultaneously coated in the same 48-well as the container. The constructs were left to dry in the laminar flow hood or with nitrogen stream at the end of the assembly and kept at 4 °C until use.

Scanning electron microscopy (SEM) of the 3D plotted PCL scaffolds and heparin-coated PCL plotted scaffolds, with or without multilayers were carried out following gold sputtering of samples (Cressington sputter coater 108 auto) on a Philips – XL 30 ESEM-FEG. SEM images were taken with an accelerating voltage of 5 kV.

8.2.4 CELL CULTURE, TRANSFECTION AND METABOLIC ACTIVITY

COS-7 cells (European Collection of Animal Cell Cultures (ECACC) Catalogue No. 87021302) were grown in DMEM containing 4.5 g/L glucose and GlutaMAX™ (Invitrogen, Breda, The Netherlands) supplemented with 1% (v/v) Pen/Strep (Lonza, Breda, The Netherlands) and 10% (v/v) fetal bovine serum (Lonza, Breda, The Netherlands). Cells were cultured at 37 °C, in a 5% CO₂ incubator and trypsinized at about 80% confluency. Unless otherwise specified, cells were seeded in a 96-well plate at a density of 7,360, 24,000 or 44,800 cells/well.

On the 3D plotted constructs, cells were seeded at a density of 320,000 cells/construct in four small droplets of 80 μL each.

Cell imaging was performed using an EVOS digital inverted microscope (EMS, Wageningen, The Netherlands) equipped with a 4X objective and an EVOS light cube (EMS, Wageningen, The Netherlands) for GFP imaging.

Presto blue assay for the measurement of cells metabolic activity was purchased from Invitrogen (Breda, the Netherlands) and used according to the manufacturer's instructions. Fluorescence intensity was measured at 535-560/590-615 ex/em using an Infinite M200 PRO plate reader (Tecan, Giessen, The Netherlands). As positive controls, cells were also seeded on uncoated TC-treated polystyrene well plates (TCPS). All fluorescence intensities were corrected by subtracting the values with those of their respective no-cell control wells. Metabolic activity was calculated as the percentage of fluorescence intensity of the samples relative to cells cultured on TCPS (100% metabolic activity). Experiments were done in triplicates.

8.2.5 DETERMINATION OF TRANSFECTION EFFICIENCY BY FLOW CYTOMETRY

After 48 h culturing, COS-7 cells on multilayer-coated PDL-TCPS and on the polymer disks were trypsinized (100 μL of 0.25% trypsin solution, Invitrogen, Breda, the Netherlands). Cell suspensions were then centrifuged (5 min, 300 g , 1200 rpm) and the pellets were then resuspended into 100 μL of medium. Cells were kept on ice until measurement by the FACSCalibur (Becton-Dickinson, Breda, The Netherlands). Excitation of expressed GFP was performed at 488 nm and emission was detected via a 530 nm band-pass filter. At least 4,000 and 10,000 events were measured for samples with lower and higher seeding density, respectively. Data analysis was performed using the FACS Cellquest Software. The gate setting was equal for all samples within the same experiment. Dot plot was applied to separate live cell population from dead cells and film residues. From the histogram obtained, marker was drawn to identify cells as live GFP-positive cells or GFP-negative cells.

8.2.6 PICOGREEN ASSAY AND AGAROSE GEL ELECTROPHORESIS

PicoGreen assay was performed to estimate the amount of DNA in the multilayers. Multilayered samples were prepared as described in Section 8.2.3. At the end of the multilayer formation, pCMV-GFP and PAA deposition solutions were collected and diluted 500 times in sterile water. For calibration curve, clean unused pCMV-GFP solution of known concentration was first diluted 500 times in sterile water and then serially diluted. Finally, 10 μL of diluted solutions were transferred into black 96-well plate containing 90 μL of 1X picogreen solution in TE buffer, incubated for 5 min at RT in the dark and read for fluorescence intensity (485/520 ex/em) using the Infinite M200 PRO plate reader (Tecan, Giessen, The Netherlands). Direct method for pCMV-GFP concentration determination was carried out similarly, but each sample solution was retrieved from multilayer-coated well which had been incubated for 1 h in 200 μL of 4.0 mM DTT in either PBS or HBG at pH 7.4 in the incubator.

For agarose gel electrophoresis, 200 μL of complete cell culture medium was added directly on top of multilayer-coated culture wells (prepared as described in Section 8.2.3) and incubated for 1 h in the incubator. Following the incubation, 21 μL of incubation medium was collected from each samples, mixed with 4 μL of loading buffer and loaded into a 1.5 wt% agarose gel (Bio-Rad) containing 1X SYBR Safe (Invitrogen). Electrophoresis was run for 90 min at 90 V in TAE running buffer (40 mM tris(hydroxymethyl)aminomethane, 20 mM acetic acid, 1.0 mM EDTA, pH 8.2). Pictures were taken on a FluorChem M (ProteinSimple, Westburg, Leusden, the Netherlands) under UV illumination.

8.3 RESULTS AND DISCUSSION

We have reported previously the fabrication and characterizations of multilayers from linear poly(amido amine)s (PAAs) and DNA (Chapter 3). When functional reporter plasmid DNA (pCMV-GFP) was used as the DNA constituent, these multilayers were found to provide transfection on COS-7 cells cultured on the multilayered surface. The mechanism of release of DNA from the multilayer was deduced to occur by a thermodynamically driven rearrangement of the multilayers which resulted in release of electrostatic polymer-DNA complexes or polyplexes which were then internalized by the cells. This rearrangement/release was found to take place rapidly within one hour of incubation under physiological salt conditions. In this report, effects of cell seeding density, type of PAA, and number of bilayers were investigated to optimize the transfection efficiency of the multilayered systems. Subsequently, the optimized conditions were used to build multilayers on several common biomaterials, both in 2D and 3D, to demonstrate the possibility to add cell transfection capabilities to these materials.

8.3.1 EFFECTS OF TYPE OF PAA AND SEEDING DENSITY

Previously, it was reported that multilayers from pCABOL and pCHIS (see abstract figure for structures) with pCMV-GFP may be used to provide cell transfection by simply culturing the cells on the multilayer-covered surface (Chapter 3). Under the conditions used, the two multilayers were found to be biocompatible, since these cells showed metabolic activities similar to those cultured on regular PS. Moreover, fluorescence microscopy showed that the two PAAs provide about similar transfection efficiency.

To investigate if cell seeding density may influence the result of cell transfection efficiency, COS-7 cells were seeded at three seeding densities, i.e. 7,360 cells/well (23,000 cells/cm²), 24,000 cells/well (70,000 cells/cm²), and 44,800 cells/well (140,000 cells/cm²). Transfection efficiency increased slightly going from 1 d to 2 d of culture along with the increase in cell number, but no further significant increase was observed upon longer culture duration (data not shown). Thus 2 d was found to be the optimal culture duration for transfection efficiency. Overlaid brightfield and GFP images of COS-7 cells cultured on three different seeding densities on (pCMV-GFP#pCABOL)₁₀ and (pCMV-GFP#pCHIS)₁₀ multilayers after 2 d of culture are shown in Figure 8.1a. In accordance to the previous results (Chapter 3), Figure 8.1a shows good cell attachment on both multilayers. After the 2 d of culture cells at the lowest seeding density have just reached confluency. Cells at the middle seeding density were notably more crowded, while cells at the highest seeding density were overconfluent with significantly more detached dead cells observed. The similar confluency on both multilayers indicates that the differences in the PAAs have no influence on the cell proliferation rate. Figure 8.1a also indicates qualitatively that the transfection efficiencies achieved by the two different multilayers depend on the seeding density of the cells on top of the multilayered films. For (pCMV-GFP#pCABOL)₁₀, an optimum in transfection efficiency is observed at the intermediate seeding density while for (pCMV-GFP#pCHIS)₁₀, the highest transfection efficiency is seen at the lowest seeding density. Note that the lowest seeding density (7,360 cells/well) used here is almost twice the seeding density used in Chapter 3, where the transfection efficiency was found to be comparable for the pCABOL and pCHIS multilayers. Given the impression from the results in Figure 8.1a that the transfection efficiencies of the two PAAs converge at lower seeding density, the results described in Chapter 3 are in good agreement with the current findings.

To get a quantitative estimation of the transfection efficiency on all of the studied samples, flow cytometry was employed to count GFP-positive cells from the rest of the cell population. Figure 8.1b shows the plot of percentage of transfected cells in the total cell population in each sample. This graph agrees with the qualitative observation in Figure 8.1a that at all different seeding densities used here, the pCABOL-multilayer provides higher transfection efficiency than the pCHIS-multilayer. Furthermore, the pCABOL-multilayer provides the highest transfection efficiency at intermediate seeding density (i.e. 24,000 cells/well), while pCHIS-multilayer provides highest transfection efficiency at the lowest seeding density (i.e. 7,360 cells/well).

Figure 8.1c shows transfection efficiency from a different point of view, i.e. this figure gives the absolute number of transfected cells that are produced on the two multilayers at the three cell seeding densities. This graph shows that to obtain maximal amount of transfected cells, the best conditions are to use the pCABOL-multilayer at the highest seeding density. On the other hand, pCHIS-multilayer is best utilized at low to middle seeding density, where more transfected cells will be obtained as opposed to highest seeding density.

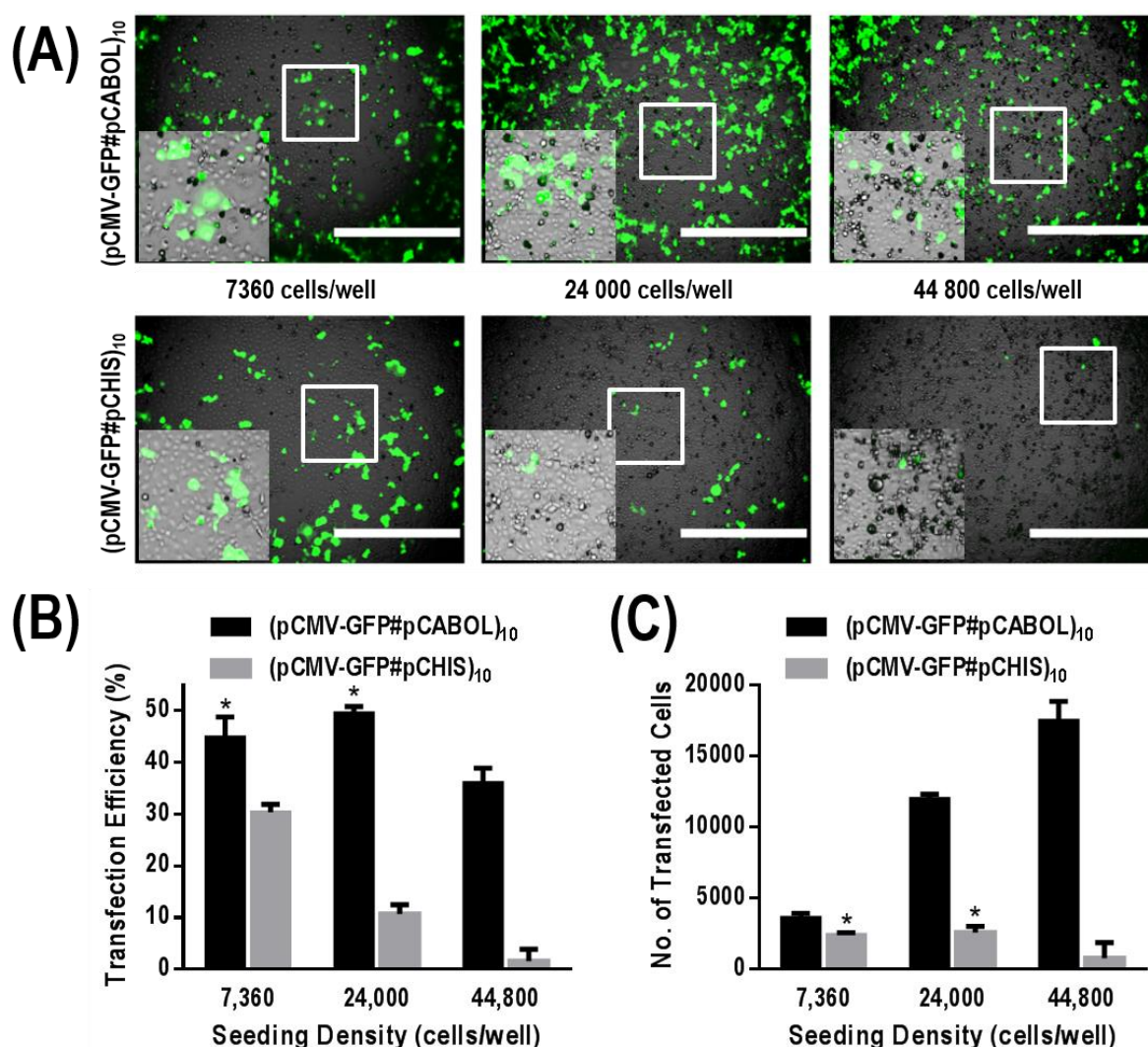


Figure 8.1 (A) Overlaid brightfield and GFP images of COS-7 cells 48 h after being cultured on (pCMV-GFP#pCABOL)₁₀ (top) and (pCMV-GFP#pCHIS)₁₀ (bottom) at 7,360 (left), 24,000 (middle), and 44,800 (right) cells/well seeding densities (bars = 1,000 μ m). Insets show the higher magnification to reveal the general cell morphology and confluency. (B) Transfection efficiency in percentage of total live cell population, and (C) absolute number of transfected cells irrespective to the total cell population. *) Not significantly different from each other ($p > 0.05$).

In relation to cell growth phase, optimal transfection efficiency is normally reached when the cells are in the log phase [54]. Therefore, the lowest seeding density which leads to ~95% confluency after 2 d of culture can be expected to provide highest transfection efficiency, as is observed for the pCHIS system. Higher seeding density may lead to stationary or even death phase, where proliferation and subsequently production of GFP protein is no longer optimal.

Unlike the pCHIS system, pCABOL multilayers maintain optimal transfection efficiency up to the intermediate seeding density, before finally declining at the highest seeding density (Figure 8.1b). The ability of pCABOL system to provide both higher transfection efficiency than pCHIS, and to maintain it up to the intermediate



seeding density may be related to previous findings that pCABOL provides higher transfection efficiency than pCHIS when used as polyplex at the same polymer/DNA ratio [55]. Thus, pCABOL acts as a better transfection agent for DNA than pCHIS under the same conditions.

However, in a layer-by-layer multilayered thin film system, the ratio of polymer/DNA in a multilayer is largely determined by specific interactions between a given polymer-DNA pair. In a previous study based on UV absorbance measurements at 260 nm (see Chapter 3) we have shown that for 10-bilayered films, both pCABOL and pCHIS facilitated the deposition of approximately similar amount of DNA. The pCHIS multilayer, however, contained significantly more polymer than the pCABOL multilayer, as could be seen from the significantly higher thickness based on AFM. Thus, at the same number of bilayers, the pCHIS system contains a higher polymer/DNA ratio compared to the pCABOL system. This difference may further influence DNA packing and/or transfection capability of the multilayers. Therefore, in order to gain better insights into the amount of incorporated pCMV-GFP in the two multilayered systems and to qualitatively observe differences in the release of polyplex into cell culture medium, PicoGreen assay and agarose gel electrophoresis were employed, respectively.

The PicoGreen assay was utilized to estimate the amount of incorporated pCMV-GFP in the multilayers by comparing the decrease in pCMV-GFP concentration in the deposition solution before and after multilayer formation (Figure 8.2a). From the assay, it was estimated that (pCMV-GFP#pCABOL)₁₀ and (pCMV-GFP#pCHIS)₁₀ multilayers coated on the surface of a 96-well contained 2.37 ± 0.13 and 1.96 ± 0.06 μg of pCMV-GFP, respectively. This leads to ~ 650 , and ~ 540 $\text{ng}/\text{cm}^2/\text{layer}$, respectively, which fall within a broad range of reported values of DNA-containing multilayers [20, 28, 46, 56]. It needs to be noted that this indirect method is based on the assumption that there is no change in the solution volume before and after the 10-bilayer deposition, and that there is no significant loss in pCMV-GFP during the washing steps. Nevertheless, the values indicate that pCABOL leads to deposition of slightly more pCMV-GFP than pCHIS which is quite in agreement with the previous qualitative UV spectroscopy results (Chapter 3).

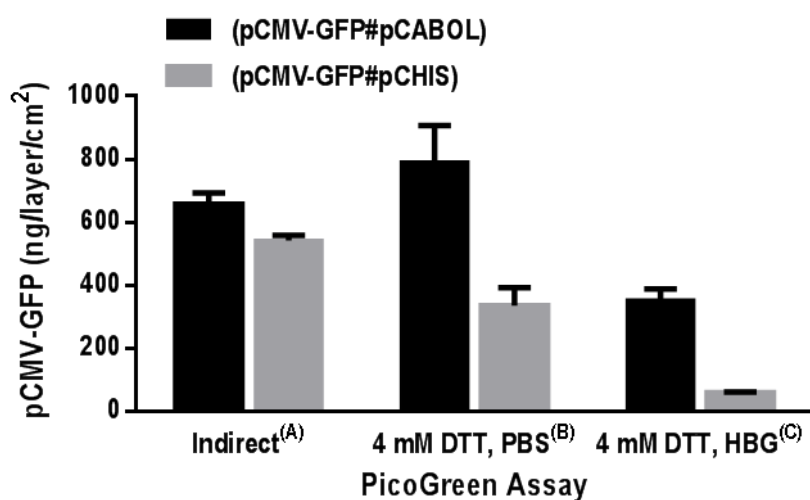


Figure 8.2 pCMV-GFP quantification by determination of the concentration differences in the deposition solution before and after multilayer build-up (A), and by PicoGreen assay after multilayer degradation for 1 h in 4.0 mM DTT in PBS (B) or HBG (C).

In an attempt to get more direct estimation of pCMV-GFP content, 4.0 mM DTT was employed to degrade the layers for 1 h and the degradation solution was analyzed on DNA content by PicoGreen assay (Figure 8.2b and c). We observed different values depending on the type of buffer used for the degradation solution (i.e. PBS or HEPES buffered glucose (HBG) pH 7.4), indicating possible differences in degradation efficiencies in the two different buffers, notably in the presence of salt where PBS contains salt while HBG does not. Interestingly, using

this approach the pCABOL multilayers were found to **release** at least twice as much pCMV-GFP than pCHIS multilayers. We have previously observed that upon multilayer dissolution or disassembly under physiological salt conditions or in the presence of DTT, multilayers of pCHIS release DNA more slowly than pCABOL multilayers which may indicate a stronger binding of DNA to pCHIS (possibly due to higher pCHIS/DNA ratio and possible intercalation of the histamine's imidazole ring into the DNA double helix [57] (see Chapter 3)). Thus, the much lower values of DNA content upon pCHIS multilayer degradation may be an underestimation due to less release of DNA in this case. In the future, additional analytical methods for the determination of the amount of incorporated and released DNA need to be used to obtain complementary results, such as quantitative PCR, or quartz crystal microbalance.

Next, to gain more insights into the pCMV-GFP released into cell culture medium, multilayer-coated wells were incubated with cell culture medium for 1 h in the incubator after which the incubation solutions were loaded into a gel for electrophoresis. Free pCMV-GFP in water and in medium were used as controls. The digital photograph of the gel under UV illumination is shown in Figure 8.3. The agarose gel confirms the dissolution of multilayers upon only 1 h of contact with physiological salt concentration, as reported previously (Chapter 3). Longer incubation of 5 h did not lead to significant difference in the band location and intensities (data not shown). Notably, it was observed from lanes 1 and 2 that pCABOL and pCHIS multilayers disassemble into transcriptionally-active free pCMV-GFP mostly present in its open circular conformation. This finding is in agreement with the report from Zhang et al. [25] which also showed the preference for open circular pDNA that is released from the multilayer. The absence of supercoiled pCMV-GFP may indicate the preferred state of pDNA during deposition on the surface. Indeed, an open circular conformation may lead to more multivalent electrostatic binding with the oppositely-charged surface, leading to stronger attachment. The visible bands in the wells of the gel also shows the presence of possible polymer-bound pCMV-GFP. This band appears brighter for pCABOL than for pCHIS multilayers. As controls, we show that a similar band is not observed for pCMV-GFP dissolved in the cell culture medium, indicating that any possible DNA retardation has been due to the PAA and not to the various plasma proteins in the cell culture medium. We note that for a typical polyplex system, stronger complexation, for example through higher polymer/DNA ratio, usually leads to less visible bands in the gel wells due to the lower accessibility of the dye to intercalate into the condensed DNA [55]. This may suggest stronger complexation of pCMV-GFP with pCHIS relative to pCABOL, in line with the previous discussions. In this particular case, however, the weaker but sufficient interaction between pCABOL and pCMV-GFP for internalization by cells may lead to more efficient unpacking of the pCMV-GFP cargo within the cytoplasm, resulting in better transfection [58].

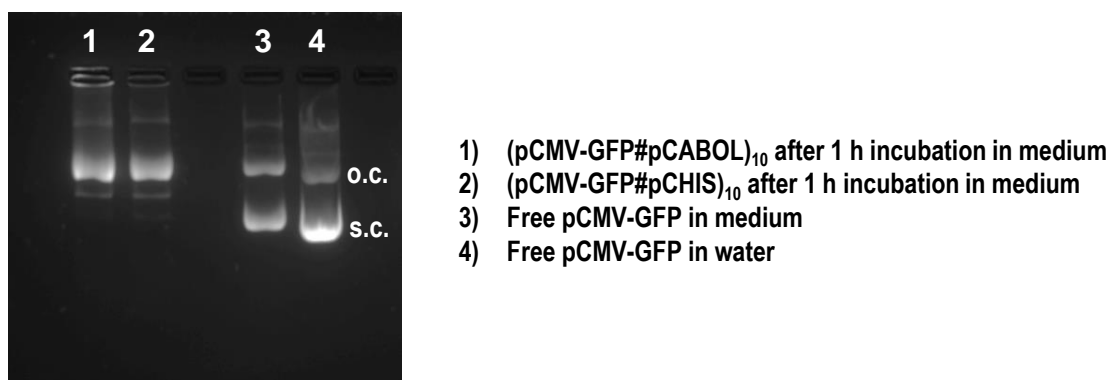


Figure 8.3 Agarose gel electrophoresis of cell culture media used to incubate the 10-bilayered pCABOL and pCHIS multilayers (lane 1 & 2, respectively) and pCMV-GFP solutions in both water (lane 3) and cell culture medium (lane 4) as controls. O.c. = open circular, s.c. = supercoiled.

From the PicoGreen assay and agarose gel electrophoresis, it can be postulated that the difference in transfection capability between the two multilayers is due to the fact that the pCABOL multilayers contain and



release more pCMV-GFP, and that the polyelectrolyte complex between pCABOL and pCMV-GFP is likely more efficient in inducing transfection. Since the pCABOL multilayers deliver more transfection agents, transfection efficiency can be maintained over higher cell seeding density (Figure 8.1b) and so higher initial amount of cells leads to higher amount of transfected cells (Figure 8.1c). At the highest cell seeding density, the absolute amount of transfected cells increased steadily (Figure 8.1c) but the significant growth of non-transfected cells in relation to the transfection speed causes the overall transfection efficiency to decrease (Figure 8.1b). On the other hand, for pCHIS multilayers, less amount of effective transfection agent leads to a lower amount of transfected cells which does not increase further with higher seeding density (Figure 8.1c). In fact, increasing the initial amount of cells cultured leads to a dominating growth of non-transfected cells which leads to a decrease in the percentage of transfected cells (Figure 8.1b). It can therefore be concluded that pCABOL-based multilayers are more efficient than pCHIS-multilayers in facilitating surface-mediated cell transfections.

8.3.2 BILAYER NUMBER OPTIMIZATION AND METABOLIC ACTIVITY

Based on the previous results, the number of bilayers necessary for optimal cell transfection was examined for the (pCMV-GFP#pCABOL)₁₀ system, using the intermediate seeding density of 24,000 cells/well. Cells were seeded on multilayers composed of 5, 7, 9.5, 10 and 15 bilayers and the percentage of transfected cells was quantified accordingly (Figure 8.4a and b). Cell transfection efficiency increases with increasing bilayer number and reaches its optimal, plateau value at 10 to 15 bilayers (Figure 8.4b). This indicates that transfection efficiency depends on the amount of transfection agent provided by the multilayers.

Previously it has been found that build-up of the pCABOL and pCHIS multilayers proceeds linearly with increasing bilayer (bl) numbers (Chapter 3). Therefore, it can be expected that a 5-bl multilayer would contain and eventually release half of the amount of materials contained in a 10-bl multilayer. Figure 8.4b shows, however, that a 5-bl multilayer leads to only ~15% transfection efficiency of that achieved by a 10-bl multilayer. Moreover, increasing the bl number from 10 to 15 leads only to very small increase in transfection efficiency. This indicates that other factors may play a role in the relation between bl number and transfection efficiency. Lower bilayer numbers probably lead to less optimal release [59]. On the other hand, higher bilayer number needs to compete with the cellular life cycle, where cells are constantly replicating into new cells that are yet to be transfected, resulting in a plateau value.

Figure 8.4b also shows a significant difference ($p < 0.05$) in transfection efficiency between 9.5 and 10 bilayers, i.e. multilayers ending with pCMV-GFP and pCABOL layer, respectively. However, the difference is not tremendous which indicates that the absence of pCABOL topmost layer does not significantly hamper transfection. Cells were still growing and transfected albeit with slightly lower transfection efficiency. This result is in agreement with various other reports on DNA-based coatings which suggest a low-immunogenic behavior of DNA [60, 61]. Nevertheless, this result also indicates that the transfection is most conveniently achieved when the last layer is a polymer layer (10 bl). Additional polymer layer in general increases the polymer/DNA ratio and therefore may provide more efficient transfection agents.

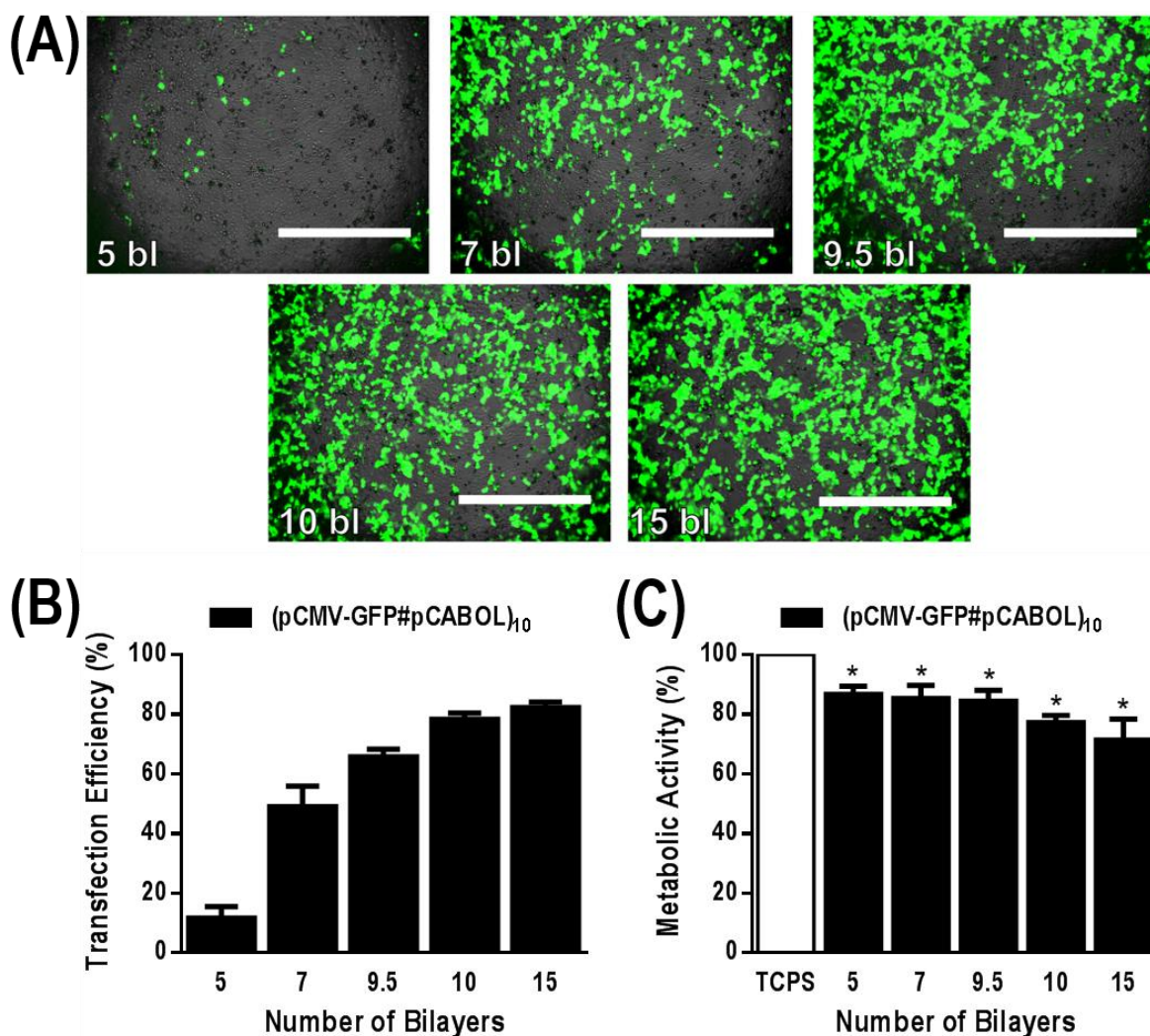


Figure 8.4 (A) Overlaid brightfield and GFP images of COS-7 cells 46 h after being cultured on (pCMV-GFP#pCABOL)₁₀ multilayers with various bilayer numbers at 24,000 cells/well seeding density. Bars = 1,000 μm. (B) Transfection efficiency and (C) cell metabolic activity relative to the number of bilayers. *) Not significantly different from one another (p>0.05).

Cell metabolic activity in relation to the bilayer number was also analyzed and expressed as a percentage of the metabolic activity of cells seeded on tissue culture plastic (TCPS) (Figure 8.4c). A significant difference was observed between TCPS control and cells seeded on multilayers, but the number of bilayers used had no influence on cell metabolic activity. Further, cells maintained similar shapes throughout the various bilayer numbers studied that are comparable to those cultured on TCPS. As already proved in other studies, PAAs are not toxic to cells [55]. The decrease in the metabolic activity of COS-7 cells seeded on substrates with increasing bilayer numbers can be accounted more to a sustained transfection rate and GFP production than to a toxic effect of the polymer (Figure 8.4c). It is generally accepted that transfection causes cells to allocate more efforts towards biosynthesis of the recombinant proteins which further leads to decreased metabolic activity [54].

8.3.3 TRANSFECTION EFFICIENCY OF MULTILAYERS ASSEMBLED ON VARIOUS SUBSTRATES

To test the applicability of the (pCMV-GFP#pCABOL)₁₀ multilayer to add cell transfecting capability to several common biomaterials, these multilayers were assembled on poly(ϵ -caprolactone) (PCL), heparinized poly(ϵ -caprolactone) (PCL-HEP), and poly(lactic acid) (PLA) (Figure 8.5a), in a similar way as was previously done with poly-D-lysine (PDL)-coated 96-well plates (PDL-TCPS) (see Section 8.2.3), but with pCABOL as the precursor layer instead of PDL. The transfection efficiency of COS-7 cells, seeded at a density of 24,000 cells/well and cultured for 48 h on the coated disks is shown in Figure 8.5b. The transfection efficiency was found to be slightly higher for PLA disks than for PCL-based disks, and was about similar to the values obtained for PDL-TCPS substrates (Figure 8.1b). Despite the increased surface roughness and the presence of a negatively charged surface underneath the multilayer due to the heparin coating, these differences have little effect on the transfection efficiency. The results indicate that the multilayers were formed to a similar extent on the three different substrates and completely mask the properties of the underlying surface at the 10-bl utilized. The masking of the underlying substrate was notably very prominent for PCL and PLA disks where cell attachment and cell shape were found to be significantly improved after multilayer coating compared to uncoated substrates (data not shown). It is therefore believed that the reported multilayers may not only add cell transfecting capability, but can also improve cell adhesion for poor cell-adhering biomaterials.

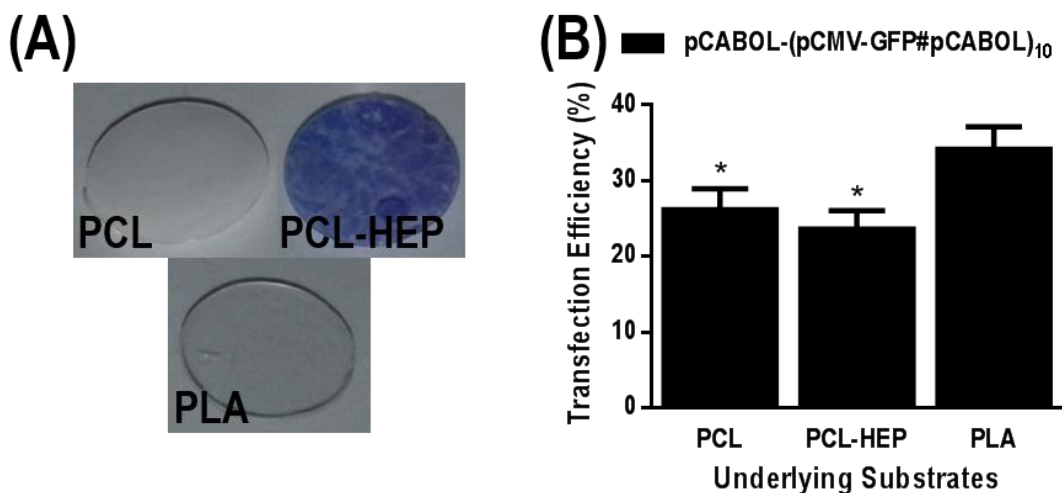


Figure 8.5 (A) Digital photograph of the three disks: PCL (white opaque), PCL-HEP (stained with Azure A), and PLA (transparent). (B) Transfection efficiency of COS-7 cells cultured on multilayer-coated disks after 48 h of culture. *) Not significantly different from each other ($p > 0.05$).

8.3.4 3D PLOTTED SCAFFOLD APPLICATION

To further demonstrate the versatility of the multilayer coating to provide new functionality to various scaffolds and supports for tissue engineering applications, we fabricated (pCMV-GFP#pCABOL)₁₀ multilayer on 3D fiber deposited PCL and PCL-HEP scaffolds. Using this approach, for example, cells can be transfected right at the spot of the implantation site.

3D fiber deposition technique was used for the fabrication of three-dimensional PCL scaffolds, which were subsequently heparinized (for PCL-HEP) and coated with multilayers (Figure 8.6). Covalent attachment of heparin already caused a change in the scaffold topography, making the smooth PCL surface topography look rougher. This has been previously reported to facilitate cell adhesion on the material, both because of the increased nano-scaled topography, providing anchor points to cells and also because heparin increases protein adsorption on the surface [53].

Higher magnification SEM images confirmed multilayer coating both on PCL and heparinized PCL, where slight changes can be observed in the scaffold topography with and without multilayer (Figure 8.6). The multilayer

which has been reported to be about 100 nm thick (Chapter 3), conforms to the topography of the original substrates, thus, maintaining the rough feature of heparinized surface, but covering up smaller pores observed on the surface of the substrates.

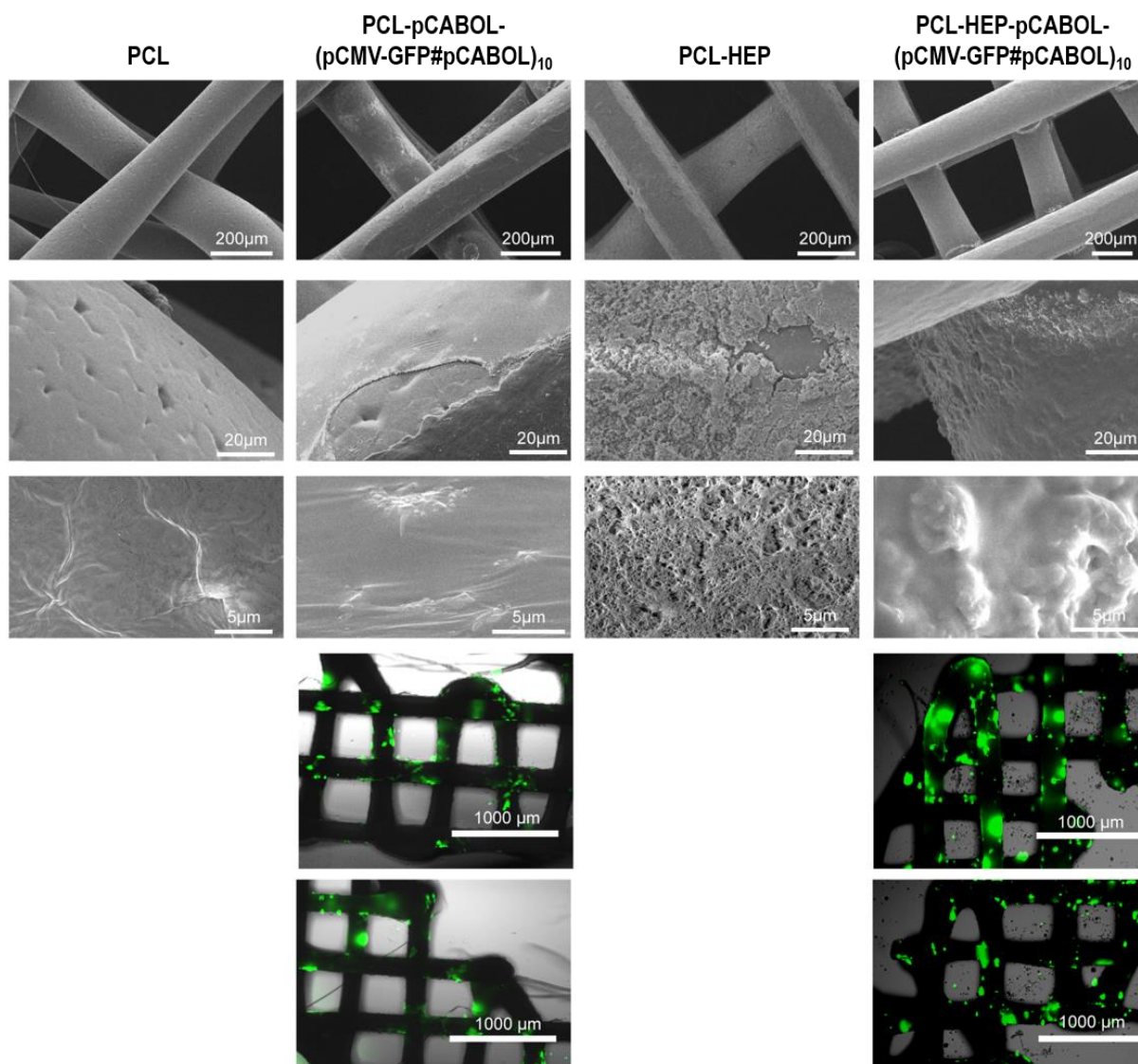


Figure 8.6 First three rows: SEM images of 3D fiber PCL and PCL-HEP scaffolds with and without multilayer coating at various magnifications. Two bottom rows: Overlaid brightfield and fluorescence microscopy images of COS-7 cells cultured on the multilayer-coated scaffolds.

When multilayer-covered scaffolds were seeded with COS-7 cells, transfection was observed to occur both on PCL and heparinized PCL scaffolds. As also observed for the flat disk substrates, cell adhesion on multilayer-coated substrates was considerably improved with respect to uncoated PCL where cells in general show very limited adhesion on the surface (data not shown). The positive transfection observed on the 3D scaffolds were confirmed through the co-localization of GFP-producing cells with the opaque scaffolds. We did observe that due to the relatively wide fiber spacing ($\sim 600 \mu\text{m}$), a lot of cells fell through the spaces/pores during seeding and subsequently attached and proliferated on the well surface. Some of these cells were also successfully transfected through the transfection agent released into the cell culture medium (data not shown). It is postulated that by decreasing the fiber spacing of the 3D scaffolds, higher and more efficient seeding density can be obtained, possibly leading to even higher transfection efficiency.



8.4 CONCLUSIONS

Layer-by-layer assembly through dip coating technique has been shown as a versatile and inexpensive method to add biofunctionality to various biomaterials in various shapes and sizes. In this report, pCABOL and pCHIS, two peptidomimetic linear poly(amido amine)s differing in the type of side group of the polymers have been used to form multilayers with pCMV-GFP as a reporter plasmid. These multilayers were optimized for their capability in facilitating transfection of cells cultured directly on the surface of the multilayers. Initially, multilayers were fabricated directly on the surface of poly-D-lysine-coated 96-well plate (PDL-TCPS) at 10 bilayers. On these multilayers, COS-7 cells were seeded at three different seeding densities, i.e. 7,360, 24,000, and 44,800 cells/well. It was found that transfection efficiency depends on the initial cell seeding density. For pCABOL-based multilayers, highest percentage of transfected cells was observed at the low and middle seeding densities, however, the absolute amount of transfected cells kept increasing up to the highest seeding density. For pCHIS-based multilayers, the highest percentage of transfected cells was observed at the lowest seeding density, which progressively decreased at higher seeding densities, while the absolute amount of transfected cells were found to be optimal only at lowest and intermediate seeding densities. To complement these findings, a PicoGreen assay was carried out to obtain information about the amount of DNA present in the multilayers. It was found that pCABOL multilayers contained and released more pCMV-GFP than pCHIS multilayers. Furthermore, agarose gel electrophoresis revealed the presence of transcriptionally active pCMV-GFP in open circular conformation, likely indicating the preferred conformation of the plasmid during layer deposition. The gel also revealed the possibility of stronger electrostatic polymer-DNA complexes from pCHIS multilayers, relative to pCABOL, which was likely due to the higher polymer/DNA ratio in the multilayer. The weaker but sufficient electrostatic interactions between pCABOL and pCMV-GFP were postulated to lead to higher transfection capability as compared to pCHIS, in addition to the generally higher content and release of pCMV-GFP from the pCABOL multilayers. In conclusion, pCABOL multilayers provide a greater amount of more efficient transfection species compared to the pCHIS multilayers. This leads to increase in transfection efficiency upon increase of seeding densities until the seeding density becomes too high that growth of non-transfected cells dominates over the rate of transfection, causing the overall percentage of transfected cells (i.e. transfection efficiency) to decrease. This was also verified by calculating the absolute amount of transfected cells which showed to have been increased even at the highest cell seeding density. For pCHIS multilayers, the lower amount of available transfection species leads to transfection efficiencies that are highest when there are a relatively low amount of cells to be transfected. As with the pCABOL multilayers, at higher seeding densities the number of transfected cells is overrun by the more dominating growth of non-transfected cells.

The effect of the number of bilayers was further examined with pCABOL multilayers with a cell seeding density of 24,000 cells/well. This system proved to be the most optimal for transfection efficiency in the previous experiments. Transfection efficiency was found to increase with increasing layer number, but not in a linear manner as was expected from the build-up profile indicating steady increase in the amount of incorporated DNA. In addition, the transfection efficiency reached a plateau level at 10 – 15 bilayers where no significant increase in transfection efficiency was observed upon increasing the bilayer numbers. The initial increase is explained by a sub-optimal release of the amount of polymer-DNA complex at lower number of bilayers, and a saturation of cellular uptake (at 80% transfection efficiency) of polymer-DNA complex to maintain stable proliferation at higher number of bilayers. Indeed, although it can be considered as statistically insignificant ($p > 0.05$), the metabolic activity was found to steadily decrease slightly with increasing bilayer number, consistently with a higher transfection rate and production of GFP. No pronounced cytotoxic effect was found under the conditions investigated. From these results, it can be concluded that 10 bilayer is the optimal bilayer number for pCABOL multilayers to obtain maximal transfection efficiency while maintaining metabolic activity. A topmost layer of pCMV-GFP was found to still facilitate cell attachment and proliferation, but with slightly less transfection efficiency than a pCABOL top layer.

To demonstrate the multilayer ability to add transfection capability to several common biomaterials, PCL, heparinized PCL, and PLA disks were coated with (pCMV-GFP#pCABOL)₁₀ multilayers and used to culture COS-7 cells at the optimal seeding density. Transfection was found to be equally efficient as when using PDL-TCPS as substrates, ranging from 25 – 50% transfected cells regardless of the type of substrates used. Notably, multilayer formation gave significant improvement of cell attachment for PCL and PLA disks which were initially found to give poor cell attachment prior to multilayer coating.

Finally, to demonstrate that the multilayers may be utilized to coat complex 3D structures, 3D fiber deposited PCL and heparinized PCL scaffolds were utilized as substrates for multilayer assembly. SEM revealed positive layer formation where a thin film could be observed to conform to the topography of the original surface, and cover smaller pores. These multilayer-coated scaffolds successfully transfected COS-7 cells cultured on the surface. It is believed that transfection efficiency in such scaffolds can be further improved by reducing the fiber spacing of the 3D substrates to facilitate better cell seeding and attachment.

These results demonstrate the versatility of pCABOL-based multilayers with functional DNA to add transfection capability to biomaterials, implants, and scaffolds of various nature and shapes. Such surface-mediated transfection may prove beneficial in various biomedical and tissue engineering applications.

8.5 REFERENCES

- [1] B.M. Wohl, J.F.J. Engbersen, Responsive layer-by-layer materials for drug delivery, *J Control Release*, 158 (2012) 2-14.
- [2] Y. Jang, S. Park, K. Char, Functionalization of polymer multilayer thin films for novel biomedical applications, *Korean J. Chem. Eng.*, 28 (2011) 1149-1160.
- [3] H. Kerdjoudj, N. Berthelemy, F. Boulmedais, J.F. Stoltz, P. Menu, J.C. Voegel, Multilayered polyelectrolyte films: a tool for arteries and vessel repair, *Soft Matter*, 6 (2010) 3722-3734.
- [4] P.T. Hammond, Building biomedical materials layer-by-layer, *Mater Today*, 15 (2012) 196-206.
- [5] J.M. Anderson, A. Rodriguez, D.T. Chang, Foreign body reaction to biomaterials, *Semin. Immunol.*, 20 (2008) 86-100.
- [6] Y.X. Sun, K.F. Ren, J.L. Wan, G.X. Chang, J. Ji, Electrochemically Controlled Stiffness of Multilayers for Manipulation of Cell Adhesion, *ACS Appl. Mater. Interfaces*, 5 (2013) 4597-4602.
- [7] N. Aggarwal, N. Altgarde, S. Svedhem, G. Michanetzis, Y. Missirlis, T. Groth, Tuning Cell Adhesion and Growth on Biomimetic Polyelectrolyte Multilayers by Variation of pH During Layer-by-Layer Assembly, *Macromol. Biosci.*, 13 (2013) 1327-1338.
- [8] W.-B. Tsai, Y.-H. Chen, H.-W. Chien, Collaborative Cell-Resistant Properties of Polyelectrolyte Multilayer Films and Surface PEGylation on Reducing Cell Adhesion to Cytophilic Surfaces, *Journal of Biomaterials Science-Polymer Edition*, 20 (2009) 1611-1628.
- [9] V. Karagkiozaki, E. Vavoulidis, P.G. Karagiannidis, M. Gioti, D.G. Fatouros, I.S. Vizirianakis, S. Logothetidis, Development of a nanoporous and multilayer drug-delivery platform for medical implants, *Int. J. Nanomed.*, 7 (2012) 5327-5338.
- [10] R.C. Smith, M. Riollano, A. Leung, P.T. Hammond, Layer-by-Layer Platform Technology for Small-Molecule Delivery, *Angew. Chem. Int. Ed.*, 48 (2009) 8974-8977.
- [11] B. Thierry, P. Kujawa, C. Tkaczyk, F.M. Winnik, L. Bilodeau, M. Tabrizian, Delivery Platform for Hydrophobic Drugs: Prodrug Approach Combined with Self-Assembled Multilayers, *J. Am. Chem. Soc.*, 127 (2005) 1626-1627.
- [12] S. Anandhakumar, A.M. Raichur, Polyelectrolyte/silver nanocomposite multilayer films as multifunctional thin film platforms for remote activated protein and drug delivery, *Acta Biomater*, 9 (2013) 8864-8874.
- [13] X. Su, B.-S. Kim, S.R. Kim, P.T. Hammond, D.J. Irvine, Layer-by-Layer-Assembled Multilayer Films for Transcutaneous Drug and Vaccine Delivery, *Acs Nano*, 3 (2009) 3719-3729.
- [14] M. Keeney, M. Mathur, E. Cheng, X. Tong, F. Yang, Effects of Polymer End-Group Chemistry and Order of Deposition on Controlled Protein Delivery from Layer-by-Layer Assembly, *Biomacromolecules*, 14 (2013) 794-800.
- [15] M.L. Macdonald, R.E. Samuel, N.J. Shah, R.F. Padera, Y.M. Beben, P.T. Hammond, Tissue integration of growth factor-eluting layer-by-layer polyelectrolyte multilayer coated implants, *Biomaterials*, 32 (2011) 1446-1453.
- [16] I.C. Lee, Y.-C. Wu, Facilitating neural stem/progenitor cell niche calibration for neural lineage differentiation by polyelectrolyte multilayer films, *Colloids and Surfaces B: Biointerfaces*, 121 (2014) 54-65.
- [17] P.-W. Fu, S.-Y. Wang, Y.-R. Chen, C.-M. Lo, Cardiomyocyte differentiation of mouse iPSCs regulated by polypeptide multilayer films (1180.21), *The FASEB Journal*, 28 (2014).
- [18] J. Hong, L. Alvarez, N. Shah, Y. Cho, B.-S. Kim, L. Griffith, K. Char, P. Hammond, Multilayer thin-film coatings capable of extended programmable drug release: application to human mesenchymal stem cell differentiation, *Drug Deliv. and Transl. Res.*, 2 (2012) 375-383.
- [19] K.F. Ren, T. Crouzier, C. Roy, C. Picart, Polyelectrolyte multilayer films of controlled stiffness modulate myoblast cell differentiation, *Adv. Funct. Mater.*, 18 (2008) 1378-1389.
- [20] J. Blacklock, Y.Z. You, Q.H. Zhou, G. Mao, D. Oupicky, Gene delivery in vitro and in vivo from bioreducible multilayered polyelectrolyte films of plasmid DNA, *Biomaterials*, 30 (2009) 939-950.
- [21] D. Richard, I. Nguyen, C. Affolter, F. Meyer, P. Schaaf, J.C. Voegel, D. Bagnard, J. Ogier, Polyelectrolyte multilayer-mediated gene delivery for semaphorin signaling pathway control, *Small*, 6 (2010) 2405-2411.
- [22] E.M. Saurer, R.M. Flessner, S.P. Sullivan, M.R. Prausnitz, D.M. Lynn, Layer-by-Layer Assembly of DNA- and Protein-Containing Films on Microneedles for Drug Delivery to the Skin, *Biomacromolecules*, 11 (2010) 3136-3143.
- [23] C.M. Jewell, D.M. Lynn, Multilayered polyelectrolyte assemblies as platforms for the delivery of DNA and other nucleic acid-based therapeutics, *Adv Drug Deliver Rev*, 60 (2008) 979-999.
- [24] Y. Lvov, G. Decher, G. Sukhorukov, Assembly of thin films by means of successive deposition of alternate layers of DNA and poly(allylamine), *Macromolecules*, 26 (1993) 5396-5399.
- [25] J.T. Zhang, L.S. Chua, D.M. Lynn, Multilayered thin films that sustain the release of functional DNA under physiological conditions, *Langmuir*, 20 (2004) 8015-8021.
- [26] F. Meyer, V. Ball, P. Schaaf, J.C. Voegel, J. Ogier, Polyplex-embedding in polyelectrolyte multilayers for gene delivery, *Biochimica et Biophysica Acta (BBA) - Biomembranes*, 1758 (2006) 419-422.
- [27] J.K. Sun, K.F. Ren, L.Z. Zhu, J. Ji, Multilayers based on cationic nanocomplexes for co-delivery of doxorubicin and DNA, *Colloid Surface B*, 112 (2013) 67-73.
- [28] C.M. Jewell, J. Zhang, N.J. Fredin, M.R. Wolff, T.A. Hacker, D.M. Lynn, Release of plasmid DNA from intravascular stents coated with ultrathin multilayered polyelectrolyte films, *Biomacromolecules*, 7 (2006) 2483-2491.
- [29] E.M. Saurer, C.M. Jewell, D.A. Roenneburg, S.L. Bechler, J.R. Torrealba, T.A. Hacker, D.M. Lynn, Polyelectrolyte Multilayers Promote Stent-Mediated Delivery of DNA to Vascular Tissue, *Biomacromolecules*, 14 (2013) 1696-1704.

- [30] Y. Hu, K. Cai, Z. Luo, C. Chen, H. Dong, J. Hao, L. Yang, L. Deng, Fabrication of Galactosylated Polyethylenimine and Plasmid DNA Multilayers on poly (D,L-lactic acid) Films for in situ Targeted Gene Transfection, *Adv. Eng. Mater.*, 11 (2009) B30-B34.
- [31] P.C. DeMuth, X. Su, R.E. Samuel, P.T. Hammond, D.J. Irvine, Nano-Layered Microneedles for Transcutaneous Delivery of Polymer Nanoparticles and Plasmid DNA, *Adv. Mater.*, 22 (2010) 4851-4856.
- [32] N.W. Kim, M.S. Lee, K.R. Kim, J.E. Lee, K. Lee, J.S. Park, Y. Matsumoto, D.G. Jo, H. Lee, D.S. Lee, J.H. Jeong, Polyplex-releasing microneedles for enhanced cutaneous delivery of DNA vaccine, *J Control Release*, 179 (2014) 11-17.
- [33] P.C. DeMuth, A.V. Li, P. Abbink, J. Liu, H. Li, K.A. Stanley, K.M. Smith, C.L. Lavine, M.S. Seaman, J.A. Kramer, A.D. Miller, W. Abraham, H. Suh, J. Elkhader, P.T. Hammond, D.H. Barouch, D.J. Irvine, Vaccine delivery with microneedle skin patches in nonhuman primates, *Nat Biotechnol*, 31 (2013) 1082-1085.
- [34] X. Guo, Q.X. Zheng, I. Kulbatski, Q. Yuan, S.H. Yang, Z.W. Shao, H. Wang, B.J. Xiao, Z.Q. Pan, S. Tang, Bone regeneration with active angiogenesis by basic fibroblast growth factor gene transfected mesenchymal stem cells seeded on porous beta-TCP ceramic scaffolds, *Biomed. Mater.*, 1 (2006) 93-99.
- [35] B.A. Borden, J. Yockman, S.W. Kim, Thermoresponsive Hydrogel as a Delivery Scaffold for Transfected Rat Mesenchymal Stem Cells, *Molecular Pharmaceutics*, 7 (2010) 963-968.
- [36] W.W. Thein-Han, J. Saikhun, C. Pholpramoo, R.D.K. Misra, Y. Kitiyanant, Chitosan-gelatin scaffolds for tissue engineering: Physico-chemical properties and biological response of buffalo embryonic stem cells and transfectant of GFP-buffalo embryonic stem cells, *Acta Biomater*, 5 (2009) 3453-3466.
- [37] Y.B. Xie, S.T. Yang, D.A. Kniss, Three-dimensional cell-scaffold constructs promote efficient gene transfection: Implications for cell-based gene therapy, *Tissue Eng.*, 7 (2001) 585-598.
- [38] C. Sapet, C. Formosa, F. Sicard, E. Bertasio, O. Zelphati, N. Laurent, 3D-fection: cell transfection within 3D scaffolds and hydrogels, *Therapeutic delivery*, 4 (2013) 673-685.
- [39] J.H. Jang, C.B. Rives, L.D. Shea, Plasmid delivery in vivo from porous tissue-engineering scaffolds: Transgene expression and cellular Transfection, *Mol. Ther.*, 12 (2005) 475-483.
- [40] Y. Yang, X. Li, L. Cheng, S. He, J. Zou, F. Chen, Z. Zhang, Core-sheath structured fibers with pDNA polyplex loadings for the optimal release profile and transfection efficiency as potential tissue engineering scaffolds, *Acta Biomater*, 7 (2011) 2533-2543.
- [41] X. Zhao, D. Komatsu, M. Hadjiargyrou, BMP-2 Delivery using Electrospun PLLA/Collagen I Scaffolds with Surface Adsorbed plasmid DNA/Transfection Complexes, *J. Bone Miner. Res.*, 28 (2013) 2.
- [42] Y. Kido, J.-i. Jo, Y. Tabata, A gene transfection for rat mesenchymal stromal cells in biodegradable gelatin scaffolds containing cationized polysaccharides, *Biomaterials*, 32 (2011) 919-925.
- [43] H.D. Lu, L.L. Lv, Y.H. Dai, G. Wu, H.Q. Zhao, F.C. Zhang, Porous Chitosan Scaffolds with Embedded Hyaluronic Acid/Chitosan/Plasmid-DNA Nanoparticles Encoding TGF-beta 1 Induce DNA Controlled Release, Transfected Chondrocytes, and Promoted Cell Proliferation, *Plos One*, 8 (2013) 13.
- [44] M. Keeney, J. van den Beucken, P.M. van der Kraan, J.A. Jansen, A. Pandit, The ability of a collagen/calcium phosphate scaffold to act as its own vector for gene delivery and to promote bone formation via transfection with VEGF(165), *Biomaterials*, 31 (2010) 2893-2902.
- [45] X. Yu, W.L. Murphy, 3-D Scaffold Platform for Optimized Non-viral Transfection of Multipotent Stem Cells, *Journal of Materials Chemistry B*, (2014).
- [46] N. Jessel, M. Oulad-Abdelghani, F. Meyer, P. Lavalle, Y. Haïkel, P. Schaaf, J.-C. Voegel, Multiple and time-scheduled in situ DNA delivery mediated by β -cyclodextrin embedded in a polyelectrolyte multilayer, *Proceedings of the National Academy of Sciences*, 103 (2006) 8618-8621.
- [47] C. Holmes, J. Daoud, P.O. Bagnaninchi, M. Tabrizian, Polyelectrolyte Multilayer Coating of 3D Scaffolds Enhances Tissue Growth and Gene Delivery: Non-Invasive and Label-Free Assessment, *Adv. Healthc. Mater.*, 3 (2014) 572-580.
- [48] P. Vader, L. van der Aa, J.J. Engbersen, G. Storm, R. Schiffelers, Physicochemical and Biological Evaluation of siRNA Polyplexes Based on PEGylated Poly(amido amine)s, *Pharm. Res.*, 29 (2012) 352-361.
- [49] G. Coué, C. Freese, R.E. Unger, C. James Kirkpatrick, J.F.J. Engbersen, Bioresponsive poly(amidoamine)s designed for intracellular protein delivery, *Acta Biomater*, 9 (2013) 6062-6074.
- [50] M. Piest, J.F.J. Engbersen, Effects of charge density and hydrophobicity of poly(amido amine)s for non-viral gene delivery, *J Control Release*, 148 (2010) 83-90.
- [51] A. Zintchenko, L.J. van der Aa, J.F. Engbersen, Improved synthesis strategy of poly(amidoamine)s for biomedical applications: catalysis by "green" biocompatible earth alkaline metal salts, *Macromol. Rapid Commun.*, 32 (2011) 321-325.
- [52] S. Singh, B.M. Wu, J.C.Y. Dunn, Accelerating Vascularization in Polycaprolactone Scaffolds by Endothelial Progenitor Cells, *Tissue Engineering Part A*, 17 (2011) 1819-1830.
- [53] S. Singh, B.M. Wu, J.C.Y. Dunn, The enhancement of VEGF-mediated angiogenesis by polycaprolactone scaffolds with surface cross-linked heparin, *Biomaterials*, 32 (2011) 2059-2069.
- [54] C.Y.M. Hsu, H. Uludag, A simple and rapid nonviral approach to efficiently transfect primary tissue-derived cells using polyethylenimine, *Nat. Protocols*, 7 (2012) 935-945.
- [55] C. Lin, Z. Zhong, M.C. Lok, X. Jiang, W.E. Hennink, J. Feijen, J.F.J. Engbersen, Novel Bio-reducible Poly(amido amine)s for Highly Efficient Gene Delivery, *Bioconjugate Chem.*, 18 (2006) 138-145.

- [56] J.J.J.P. van den Beucken, M.R.J. Vos, P.C. Thüne, T. Hayakawa, T. Fukushima, Y. Okahata, X.F. Walboomers, N.A.J.M. Sommerdijk, R.J.M. Nolte, J.A. Jansen, Fabrication, characterization, and biological assessment of multilayered DNA-coatings for biomaterial purposes, *Biomaterials*, 27 (2006) 691-701.
- [57] A.J. Ruiz-Chica, A. Soriano, I. Tunon, F.M. Sanchez-Jimenez, E. Silla, F.J. Ramirez, FT-Raman and QM/MM study of the interaction between histamine and DNA, *Chem Phys*, 324 (2006) 579-590.
- [58] D.V. Schaffer, N.A. Fidelman, N. Dan, D.A. Lauffenburger, Vector unpacking as a potential barrier for receptor-mediated polyplex gene delivery, *Biotechnol. Bioeng.*, 67 (2000) 598-606.
- [59] S.S. Ono, G. Decher, Preparation of Ultrathin Self-Standing Polyelectrolyte Multilayer Membranes at Physiological Conditions Using pH-Responsive Film Segments as Sacrificial Layers, *Nano Lett.*, 6 (2006) 592-598.
- [60] J.J. van den Beucken, X.F. Walboomers, M.R. Vos, N.A. Sommerdijk, R.J. Nolte, J.A. Jansen, Biological responses to multilayered DNA-coatings, *Journal of biomedical materials research. Part B, Applied biomaterials*, 81 (2007) 231-238.
- [61] T. Fukushima, Y. Inoue, T. Hayakawa, K. Taniguchi, K. Miyazaki, Y. Okahata, Preparation of and tissue response to DNA-lipid films, *Journal of Dental Research*, 80 (2001) 1772-1776.

This thesis described the development of multilayered thin films from poly(amido amine)s (PAAs) for surface functionalization of various biomaterials. Structure-function relationships of various PAAs are discussed in detail both in relation to multilayer build-up capability and the applicability of the resulting multilayers. Two potential applications of the multilayers were more specifically addressed, i.e. surface-mediated gene delivery, and drug-releasing surfaces.

In **Chapter 1**, a general background and overview with regard to the studies described in this thesis was depicted. **Chapter 2** presented a literature review on the physicochemical aspects of layer-by-layer (LbL) assembly and its development for biomedical applications.

In **Chapter 3**, the first research was focused on the straightforward translation of a series of linear PAAs previously established as promising non-viral vectors for gene delivery. The series consisted of PAAs with increasing positive charges under physiological conditions. The expectations was that the charge differences would result in different capabilities of each PAA in building multilayers with DNA. It was found that PAA with higher positive charges facilitated less deposition of DNA at the same fabrication conditions. However, the resulting multilayers were more stable under physiological conditions. The least positively-charged PAA, pCABOL, provided highest incorporation of DNA per deposition cycle, but the resulting multilayer readily rearranged and released more than half of the DNA content within one hour of incubation under physiological conditions. While the most positively-charged PAA (pCDAB) showed significant cytotoxicity, the two other PAAs, pCHIS and pCABOL were biocompatible and could facilitate surface-mediated cell transfection *in vitro*. The attempts to increase the multilayer stability and provide more controlled release of transfection agent were described in **Chapter 4**. A series of linear PAA random copolymers of pCDAB and pCABOL was synthesized to study the effect of additional positive charges on the stability of the multilayers. 90%ABOL copolymer provided higher stability than pCABOL homopolymer, but at the expense of less DNA incorporation. To further increase the multilayer stability, multilayer of 90%ABOL copolymer was covalently crosslinked with glutaraldehyde (GA), which increased multilayer stability tremendously. It was found that the multilayer-mediated cell transfection decreased in the order of pCABOL homopolymer > 90%ABOL copolymer > GA-crosslinked 90%ABOL copolymer, signifying the importance of a release mechanism for successful multilayer-mediated cell transfection.

Chapter 5 described the syntheses of two randomly branched copolymers of boronic acid (BA)-functionalized PAAs (BA-PAAs) to form multilayers with diol-containing macromolecules via the more specific and dynamic boronic ester formation. Multilayers formed with poly(vinyl alcohol) (PVA) were thin, highly responsive to acidic pH and to glucose. On the other hand, multilayers formed with chondroitin sulfate (ChS) were thicker, non-responsive to glucose, and showed more complicated behavior at acidic pH. It was proposed that boronic ester formation is the major driving force for PVA-based multilayer build-up, while electrostatic interaction is the major driving force for ChS-based multilayer build-up. Thus, it was proposed that ChS-based multilayers might be used as delivery system for diol-containing drugs, while PVA-based multilayers might be used as delivery system for boronic acid-containing drugs. The *in vitro* cell culture study showed that all of the investigated multilayers were able to facilitate cell proliferation to the same extent as polystyrene control. **Chapter 6** described the utilization of ChS-based multilayers as delivery system for alizarin red S (ARS), a model for catechol amine drugs. The multilayers successfully incorporated ARS with amount controllable through the number of deposition cycle. The loaded multilayers displayed ARS release profiles that are responsive to reducing agents and pH. The multilayers successfully facilitated release and cellular uptake of ARS not only in its free form, but as boronic ester with the BA-PAAs, as observed through the specific fluorescence of the boronic ester. Further, confocal microscopy confirmed the colocalization of fluorescent particles in the nuclei of the treated cells. In **Chapter 7**, the PVA-based multilayers were parallel-loaded with bortezomib, a proteasome inhibitor used for treatment of multiple myeloma. The therapeutic efficacy of the multilayers was optimized by varying the bortezomib concentration in the deposition solution, and the layer number. It was proposed that bortezomib-loaded multilayers displayed dual-release profiles depending on the spatial aspects of the target cells. Cells that

were in direct contact with the multilayers experienced the maximal efficacy of the drug-loaded surface and thus higher dose was obtained through higher bortezomib concentration in the deposition solution that translated directly to the surface-localized concentration. Cells that were not in direct contact with the multilayers were less affected by the high concentration of surface-bound bortezomib, but more by the amount of bortezomib released from the multilayers. Thus, higher dose was obtained through the higher amount of deposited layers that translated directly to the total amount of incorporated bortezomib in the whole multilayered construct.

Chapter 8 described the optimization of pCHIS and pCABOL-based multilayers previously reported in Chapter 3 for surface-mediated cell transfection. The optimization was carried out by varying the cell seeding density on the surface, and by studying the efficacy of each PAA to promote maximal transfection. For both PAA, the intermediate seeding density provided the highest transfection efficiency. pCABOL was much more effective than pCHIS which was attributed to the former's ability to incorporate and release more plasmid DNA (pDNA) and its better overall performance as a gene carrier. The optimal conditions were applied to coat poly(ϵ -caprolactone) (PCL), heparinized PCL (PCL-HEP), and poly(lactic acid) (PLA) both in 2D and 3D. Multilayers were successfully formed on the selected biomaterials and facilitated cell transfection of up to 50%. Moreover, on PCL and PLA, significant improvement in cellular attachment was observed after multilayer coating. Transfection was also successful on 3D PCL and PCL-HEP scaffolds, demonstrating the possibility of attaining functionalized cell-transfecting scaffolds.

In conclusion, poly(amido amine)-based multilayered thin films are promising for the development of cell-transfecting and drug-eluting surfaces. The PAAs facilitate controlled incorporation of materials into thin multilayered structures that conform to any size and shape of the substrates. Functional DNA can be incorporated and released without denaturation, and small drugs can be incorporated and released in a highly localized manner to avoid affecting non-target cells. The multilayers are also biocompatible in general, and may provide improved cell-surface interactions.

Dit proefschrift beschrijft de ontwikkeling van coatings bestaande uit dunne multilagen gebaseerd op poly(amidoamine)s (PAAs) voor het functionaliseren van oppervlakten van verschillende soorten biomaterialen. De relatie tussen structuur en functie van verschillende PAAs wordt in detail besproken met betrekking tot het vermogen multilagen op te bouwen en de mogelijkheden de verkregen multilagen toe te passen voor gecontroleerde afgifte. Twee potentiële toepassingen van de ontwikkelde multilagen zijn verder uitgewerkt, nl. de afgifte van nucleotiden voor gen-transfectie en de afgifte van laag-moleculaire bioactieve stoffen.

Hoofdstuk 1 geeft een algemene inleiding over het onderwerp van dit proefschrift en een overzicht van het in dit proefschrift beschreven onderzoek. In **Hoofdstuk 2** wordt een literatuurstudie beschreven die de fysicochemische eigenschappen en mogelijke biomedische toepassingen van laag-voor-laag (LbL) opgebouwde multilagen behandelt.

In **Hoofdstuk 3** beschrijft de eerste studies om LbL multilagen te maken van enkele lineaire PAAs waarvan is gebleken dat ze veelbelovende niet-virale vectoren voor genterapie zijn. De serie bestond uit PAAs met toenemende positieve lading onder fysiologische omstandigheden. Het uitgangspunt daarbij was dat de ladingsverschillen tussen de PAAs zullen resulteren in verschillen in het vermogen om met DNA een multilaag coating te vormen. De experimenten lieten zien dat PAAs met hoge positieve lading met DNA multilagen vormen waarin minder DNA is opgenomen dan de multilagen gevormd met minder positief geladen PAA. De multilagen met de hoog positieve PAAs zijn echter wel stabiel onder fysiologische omstandigheden. Vorming van LbL multilagen met het minst positief geladen PAA, pCABOL, geeft in de hoogste incorporatie van DNA per depositie cyclus, maar de resulterende coating verandert snel van structuur en verlies meer dan de helft van het DNA-gehalte binnen een uur onder fysiologische omstandigheden. Het meest positief geladen PAA (pCDAB) blijkt duidelijk cytotoxische eigenschappen te hebben, maar de beide andere PAAs, pCHIS en pCABOL bleken goed biocompatibel te zijn en in staat om cellen in vitro via het oppervlak van de multilagen te transfecteren. Pogingen om de stabiliteit van de LbL multilagen te vergroten en de afgifte van het transfectie agent te controleren zijn beschreven in **Hoofdstuk 4**. Een serie van lineaire copolymeren met variabele hoeveelheid pCDAB en pCABOL werd gesynthetiseerd om het effect van extra positieve lading op stabiliteit van de meerlaagse coating te bestuderen. Een multilaag van pCDAB/pCABOL met 90% ABOL geeft een hogere stabiliteit dan die van het pCABOL homopolymeer, maar bevat minder ingebouwd DNA. Om de stabiliteit van deze multilaag verder te vergroten werd deze covalent gecrosslinked met glutaraldehyde (GA), waardoor de stabiliteit van de multilaag sterk toeneemt. Vergelijking van de transfectie capaciteit van de verschillende multilagen laat zien dat deze afneemt in de volgorde pCABOL homopolymeer > 90% ABOL copolymeer > GA gecrosslinkte 90% ABOL copolymeer. Deze volgorde is een belangrijke indicatie dat de mogelijkheid DNA (als polymeercomplex) af te geven uit de multilagen een belangrijke factor is om effectieve celtransfectie vanuit de LbL multilagen te verkrijgen.

In **Hoofdstuk 5** wordt de synthese van twee willekeurig vertakte copolymeren van boorzuur (BA) gefunctionaliseerde PAAs (BA-PAAs) beschreven, alsmede de vorming van multilagen van deze copolymeren met de diol-bevattende macromoleculen poly(vinyl alcohol) (PVA) en chondroitin sulfaat (ChS). De boorzuurgroepen in de BA-PAAs vormen een reversibele binding met de diolgroepen van respectievelijk PVA en ChS onder vorming van een boorzure ester groep waardoor er een dynamische (reversibele) interactie tussen de twee types lagen ontstaat. Multilagen opgebouwd uit BA-PAAs met PVA waren relatief dun en erg gevoelig voor zure pH en glucose in oplossing. Multilagen met ChS waren dikker en reageerden niet op de aanwezigheid van glucose in oplossing terwijl de respons op pH verlaging een gecompliceerd patroon liet zien. De verschillen kunnen verklaard worden door aan te nemen dat voor de BA-PAA/PVA multilagen de boorzure ester vorming de belangrijkste kracht is om de lagen bij elkaar houden, terwijl dit voor de BA-PAA/ChS multilagen de electrostatische interacties zijn tussen het positief geladen BA-PAA en het negatief geladen ChS. Hieruit werd geconcludeerd dat de ChS gebaseerde multilagen nog vrije boorzuurgroepen bevatten die gebruikt zouden kunnen worden om een afgiftesysteem te ontwikkelen voor bioactieve moleculen die een diol groep bevatten, terwijl de op PVA gebaseerde multilagen geschikt zouden kunnen zijn voor de afgifte van boorzuur bevattende verbindingen. In vitro celcultuur studies lieten zien dat op alle

multilagen goede celgroei plaatsvindt, gelijk aan die op polystyreen oppervlakken. **Hoofdstuk 6** beschrijft de toepassing van op ChS gebaseerde multilagen als afgiftesysteem voor alizarine S (ARS), dat dient als model voor catecholamine medicijnen. Het blijkt mogelijk om tijdens de opbouw van de multilagen bij elke depositie cyclus ARS in gecontroleerde hoeveelheden mede op te nemen. De ARS beladen multilagen zijn responsief op aanwezigheid van reducerende agentia en verlaging van pH en geven ARS af dat zowel in vrije vorm als in de vorm van BA-PAA gebonden boorzure ester door de aanwezige cellen wordt opgenomen. De laatste vorm is zichtbaar in de cellen vanwege de specifieke fluorescentie van de boorzure ester. Door middel van confocale microscopie was ook zichtbaar dat er fluorescente deeltjes in de kern van de cellen aanwezig waren. In **Hoofdstuk 7** worden experimenten beschreven waarbij multilagen gebaseerd op PVA met BA-PAA worden beladen met bortezomib, een proteasoom-remmer die gebruikt wordt bij de behandeling van multipel myeloom. De therapeutische effectiviteit van de multilagen werd geoptimaliseerd door variatie van de bortezomib concentratie in de depositie oplossing en door variatie van het aantal lagen in het multilaag systeem. Uit de resultaten blijkt dat de bortezomib beladen multilagen een duaal afgifte profiel vertonen waarbij bortezomib opname door de cellen afhankelijk is van de directe omgeving waarin de cellen zich bevinden. De hoogste dosis bortezomib wordt opgenomen door cellen die in direct contact zijn met het bortezomib beladen oppervlak van de multilagen. Cellen die niet in direct contact met de multilagen zijn nemen bortezomib op via het medium waaraan het bortezomib uit de multilagen wordt afgegeven. In dit laatste geval is het aantal lagen waaruit het multilaag systeem is opgebouwd van directe invloed omdat dit dienst doet als depot voor bortezomib.

Hoofdstuk 8 beschrijft de optimalisatie van de eerder in Hoofdstuk 3 beschreven pCHIS en pCABOL gebaseerde multilagen voor oppervlakte-gemedieerde cel transfectie. Variatie in de zaaidichtheid van de cellen op het oppervlak van de multilagen en het effect van elk PAA op de transfectie-efficiëntie is daarbij onderzocht. Voor beide PAAs blijkt een gemiddelde zaaidichtheid van de cellen op het oppervlak de beste transfectie resultaten te geven. pCABOL is daarbij meer effectief dan pCHIS, wat wordt toegeschreven aan het vermogen van de pCABOL multilagen om meer plasmid DNA op te nemen en de doorgaans betere transfectie die met pCABOL/DNA complexen wordt verkregen. De gevonden optimale condities werden daarna toegepast voor 2D en 3D coating van poly(ϵ -caprolacton) (PCL), ge-hepariniseerd PCL (PCL-HEP), en polymelkzuur (PLA) oppervlakken. Hierop konden met succes multilagen worden aangebracht en cellen op deze materialen werden tot 50% getransfecteerd.

Daarbij bleek tevens dat na coating met een multilaag op de PCL en PLA materialen aanzienlijke verbetering van de cel aanhechting optrad. Transfectie verliep ook succesvol op 3D PCL en PCL-HEP materialen voorzien van multilagen, hetgeen de mogelijk opent om op deze wijze gefunctionaliseerde materialen te ontwikkelen die gecontroleerd bioactieve stoffen aan cellen afgeven in contact met deze materialen.

ACKNOWLEDGEMENT

With a four-year long study coming to a close, it is my pleasure to express my profound gratitude to those who have helped make this thesis possible.

First and foremost, I would like to thank my supervisor, Prof. Johan Engbersen, for the invaluable opportunity to become part of your research group both as a master and a PhD student. I remember the lessons I had in your Controlled Drug Delivery course as very inspiring. The field of knowledge was a new one for me, yet as a student with a background in chemistry, it felt familiar and exciting. Even to this moment, your critical chemical view on biomaterials for drug and gene delivery remains an aspiration of mine. Thank you for all of your supervision, guidance, patience, understanding, and support to help me finish this PhD project. I am very honored to have you as my supervisor.

I would also like to thank my co-supervisor, Dr. Jos Paulusse for your scientific advices and suggestions. There were quite a handful of technical difficulties during my study and your views and suggestions helped me learn to be creative in looking for possible solutions. I am also very grateful for your help with GPC, for providing me with a lot of reading materials, and for helping me out with the manuscripts.

I would also like to thank my collaborators, Giulia Marchioli, Dr. Aart van Apeldoorn, and Prof. Marcel Karperien for making the study in Chapter 8 possible. Thank you for all the hours spent in the lab together, Giulia! It was not always a smooth sailing, but I am very pleased it worked out well in the end. Thank you very much for your input in cell biology, both in practice and theory. And finally, thanks for being my paranymph! It was a pleasure working with you and I wish you the best for the remaining of your study as well.

My gratitude goes to all of my committee members: Prof. Wim Hennink, Prof. Gert Storm, Prof. Bart Ravoo, Prof. Jurriaan Huskens, Prof. Marcel Karperien and Dr. Aart van Apeldoorn for taking the time to read this thesis and share your invaluable scientific insights.

I gratefully acknowledge the financial support from the Netherlands Institute of Regenerative Medicine (NIRM).

A lot of other people have also helped me along the way. You may think that it was not much, but for me they were all significant and I can't be thankful enough. Karin Roelofs, my deepest gratitude for all your help with the FACS, the electrophoresis, the cell cultures, and the *samenvatting*. Your enthusiasm was always refreshing, even when my results were not very satisfying. Hetty ten Hoppen, thank you very much for your efforts in collecting all of the AFM data presented in this thesis. I know that the number of samples was not in any way small, and it must have taken a lot of your time. To my former students: Guoying, Tony, and Arantxa, thank you for the work together that have paved the way to the studies presented in this thesis. Tony, thanks also for the mass spectrometry measurements you did for me. To my former tutor, Martin, thanks for a first hands-on experience in biomaterial science. *Mba* Dwi, thanks for the countless little helps and stimulating discussions we have had together. Also thanks for being my paranymph! *Aku doakan sukses, Mba!* Karin (Hendriks), thanks for all the help you've provided me since the start of my master project in the group. You've been so kind to answer all the small little questions I would otherwise know not who to ask. Zlata, thanks for all the time spent flipping through order forms, checking catalogs and delivery status. Thanks for making sure no experiment get delayed due to chemicals and equipment. Lydia, you and Hetty had always made sure the cell culture lab was organized and fully stocked. Thank you. Marc, thanks for maintaining the best lab environment and the freeze dryer, thanks also

for providing me with an introduction to the SEM. Anita, thank you for always being very friendly! It's always nice chatting with you!

I would also like to thank the rest of the former and present members of BMC, CDD and BST groups who have directly or indirectly provided support and help throughout the last five years: Prof. Jan Feijen, Prof. Dirk Gripma, Prof. Piet Dijkstra, Dr. André Poot, Suvi, Hans, Grégory, Arkady, Leony, Peter, Mery, Maria, René, Niels, Sanne, Ruchi, Jai, Iris, Karin, Praneeth, Acarilla, Bade, Aga, Rachel, Sebastian, Erwin, Bas, and Fritz.

I would also like to thank some people from other groups: *Ibu* Megawati Santoso, my former supervisor back in Indonesia, Rik Akse and Ben Betlem for facilitating my first arrival to the Netherlands, Herbert Wormeester for the help with ellipsometry, Ron Gill for the collaboration on the incorporation of gold nanoparticles in multilayered thin films, Himanshu Chaudhary for the help with confocal microscopy, Jacqueline Plass for the training on bacterial transformation and DNA isolation.

I would also like to give my thanks and regards to former and present members of PPI (*Persatuan Pelajar Indonesia*) Enschede who have provided me with information when I was still a new research student and did not know much about The Netherlands. To know that I have your support here is like having a second family in The Netherlands. Siti and May, thanks for all the good time together.

Finally, as always, many thanks to *papa*, *mama*, and Yuni back home in Indonesia, who I have not seen in four years, and to my husband, Charles, thank you for the love, understanding and continuous support.

Dewi

October 2014

Enschede

CURRICULUM VITAE

Sry Dewi Hujaya was born on October 23rd, 1986 in Medan, North Sumatra, Indonesia. In 2004 she enrolled in the Department of Chemistry in Bandung Institute of Technology (ITB) in Bandung, Indonesia, where she received a scholarship for a fast track and Master's double degree programs. In 2008 she obtained her Bachelor's degree of Science (SSi), while completing half of her Master's degree program in ITB, majoring in Organic Chemistry. On January 2009, she continued her Master's study in the Department of Chemical Engineering in the University of Twente in Enschede, The Netherlands. She obtained her Master of Science degree (MSc) on January 2010, after completing a six-month Master project entitled "Water-Soluble Hydrogels from Boronated Poly(ethylene glycol)-Linkers with Poly(vinyl alcohol)" in the research group of Prof. Dr. Johan Engbersen under the daily supervision of Dr. Martin Piest. She returned to Indonesia to obtain her second Master's degree title (MSi) on April 2010 before returning to the same research group in the University of Twente on July 2010 to start her PhD research on "Multilayered Thin Films from Poly(amido amine)s for Controlled Delivery". The results of her PhD research are described in this thesis.